ISBN 0-315-54823-1

Canada

Theory of Guided Waves for Cylindrical Structures Embedded in Stratified Media

by

Gregory Ernest John Bridges

A thesis
presented to the University of Manitoba
in partial fulfillment of the
requirements for the degree of
Doctor of Philosophy
in
Electrical Engineering

Winnipeg, Manitoba, 1989

THEORY OF GUIDED WAVES FOR CYLINDRICAL STRUCTURES EMBEDDED IN STRATIFIED MEDIA

BY

GREGORY ERNEST JOHN BRIDGES

A thesis submitted to the Faculty of Graduate Studies of the University of Manitoba in partial fulfillment of the requirements of the degree of

DOCTOR OF PHILOSOPHY

I hereby declare that I am the sole author of this thesis.

I authorize the University of Manitoba to lend this thesis to other institutions or individuals for the purpose of scholarly research.

Greg E.J. Bridges

I further authorize the University of Manitoba to reproduce this thesis by photocopying or by other means, in total or in part, at the request of other institutions or individuals for the purpose of scholarly research.

Greg E.J. Bridges

The University of Manitoba requires the signatures of all persons using or photocopying this thesis. Please sign below and give address and date.

Abstract

An examination of the guided waves supported by cylindrical structures embedded in a plane layered media is presented. A theory for general cylindrical structures, both open and closed, is developed using a hybrid Green's function-integral equation approach. A spectral-domain analysis is utilized in the infinite axial dimension of the structure, with an integral equation formulated over the remaining transverse dimensions. Appropriate Green's functions are developed to account for the infinite stratified supporting medium and a method of moments technique is then used to solve the resulting set of spectral-domain integral equations. Once the guided wave geometry has been formulated, the wave properties characteristic to these structures are examined. This leads to the identification of various commonly used approximation methods, with specific attention being paid to the use of only the discrete mode contributions to represent the electromagnetic quantities. To this extent, a method of solving for the propagation constants and a new definition of the characteristic impedances of the discrete modes for open guided wave structures is presented.

The remainder of the work is devoted to the discussion of various problems which can be modeled using the geometry under consideration. Excitation of and propagation along infinite thin-wire transmission lines located above a lossy half-space is examined, with numerical results presented for the discrete mode propagation constants and the currents excited by external dipole and delta function voltage sources. The validity of using the transmission line approximation in the near field and the saddle point method in the far field are discussed. Analytical expressions for the propagation constants and characteristic impedances of a single thin-wire conductor are formulated using the proposed techniques. These results are compared to the expressions generated using the definitions currently available in the literature. Finally, the case of an arbitrary shaped conductor, which can be located near or at the lossy planar interface is examined.

The appendices provide formulations and evaluation techniques for the Green's functions of planar sources embedded in a stratified medium. Special emphasis is placed on formulating the homogeneous half-space geometry. The resulting Green's functions present themselves in single or double infinite integral form, with analytical expressions usually not available making them difficult to evaluate. To this extent, existing approximation methods and some new closed form expressions are presented for their evaluation. As well, a technique for their numerical integration is proposed, which has the advantage that it accounts for a possible highly oscillatory nature in the integrand.

Acknowledgements

The author wishes to express his appreciation to Prof. L. Shafai of the Electrical Engineering Department, University of Manitoba, for his supervision and encouragement throughout the course of this work.

Thanks is extended to my fellow colleagues for helpful advice during the preparation of this thesis and for the many discussions on mutual topics of interest.

Financial support from the Natural Science and Engineering Research Council of Canada and the Province of Manitoba, in the form of Scholarships, and through the University of Manitoba, in the form of a University Fellowship, are appreciated.

" 'Let's consider your age to begin with - how old are you?'

'I'm seven and a half, exactly.'

'You needn't say "exactually," ' the Queen remarked. 'I can believe it without that.' "

Lewis Carroll, *Through the Looking-Glass*

Table of Contents

List of Figures

Chapter 1
Introduction

1.1. OBJECTIVES AND MOTIVATION

This thesis presents a theory of guided waves for cylindrical structures which are embedded in a plane layered media. In this context, the term cylindrical describes a geometry which is infinite in one spacial dimension and bounded in the remaining two other dimensions, this also including the problem of multiple unconnected cylindrical bodies. The guiding structure may be comprised of a conducting, dielectric, or in the most general case an inhomogeneous material. A solution is developed to handle any of these cases to the extent that appropriate Green's functions can be derived for each region of the geometry, however, specific applications in this thesis will be for homogeneous conducting structures. The geometry under consideration is first formulated as a general three-dimensional scattering problem. The formulation is then specialized to the case of a cylindrical (two-dimensional bounded) guided wave structure, where the material properties of the cylindrical structure as well as the infinite medium in which it is embedded are arbitrary. The characterization of and wave properties related to this geometry are then discussed. Building upon this basis, the problem of a cylindrical structure which is embedded in a layered supporting medium is then formulated. The layered media may consist of any finite number of isotropic homogeneous planar regions, with the electrical properties of each region being arbitrary. Even though the formulation of the problem is general to any number of layered regions, most of the applications studied in the thesis are for a single planar interface. The combination of the two types of geometries, cylindrical and planar, has been chosen since it can be used to represent a large number of practical problems. Each type of geometry alone is capable of supporting its own class of wave phenomena, while the solution of their combination will exhibit the properties of both as well as some new phenomena; these including radiation, surface wave, and discrete modal contributions. The discussion of a large number of examples will be presented in order to study some of the basic properties associated with this chosen problem. To this extent, a detailed examination of thin-wire guided wave structures located over a lossy half-space will be made, various approximation methods will be deduced, and their validity will be studied by comparison with the exact solution. The commonly utilized transmission line approximation requires the determination of the propagation constants and characteristic

impedances of the discrete guided modes supported by the structure. A new definition for the characteristic impedance of open guided wave structures will be presented, and the justification for its use will be discussed. As well, arbitrary shaped guided wave structures which are located near or touching an interface will be studied.

The motivation behind this work is mainly in the understanding of the guided wave properties of open cylindrical structures. The incorporation of a layered supporting media adds new wave phenomena and lends itself to many practical applications since open guiding structures are not usually located in free space, but must be supported by some means; and in many cases the supporting medium is a planar structure. The geometry can be used to describe transmission lines over an earth for purposes of studying wave propagation, electromagnetic interference, and remote sensing problems. As well, modern antenna and computer design utilize microstrip, MMIC, and printed circuit board technologies, which can all be analyzed by this geometry.

1.2. THESIS OUTLINE AND CONTRIBUTIONS

Chapter two of the thesis is devoted to the presentation of a theory of guided waves supported by cylindrical structures, as developed from a general scattering approach. The properties of these structures are discussed and then the formulation is specialized to the case of a stratified supporting medium. One of the oldest methods of solving scattering problems is through a Green's function approach, where the fields due to specified sources in the presence of the chosen geometry are determined by directly solving the wave equation and satisfying the boundary conditions. Results of many different source configurations, for the excitation of cylindrical structures as well as stratified media, can be found in the literature using this approach [Stratton, Harrington1, Wait13, Felsen]. On the other hand, the integral equation formulation of cylindrical structure geometries, whose solution is usually obtained using a method of moments technique, are newer but also abundant in the literature [Harrington2, Harrington3, Mittra1, Mittra2]. The solution of the geometry being studied in this thesis combines the integral equation approach for modeling the cylindrical scattering geometry with the Green's function approach for modeling the effects of the stratified supporting media in which it is embedded. An overview of this hybrid Green's function-integral equation approach for the solution of many scattering problems has been discussed by Newman [Newman2]. Once the guided wave problem has been formulated, and solved using the method of moments, chapter two then examines the wave properties characteristic to these structures. The development of the properties of guided wave structures is based on the work of Collin, Schelkunoff and Marcuvitz [Collin, Schelkunoff2, Marcuvitz], who presented a general modal theory for the analysis of closed cylindrical geometries. A discussion of the wave properties of open structures is discussed to some extent in [Collin] with a detailed analysis of layered geometries given by Felsen and Marcuvitz [Felsen], and the use of the method of steepest descent for a far field evaluation and subsequent identification of the various

wave components is presented thoroughly by [Collin, Felsen] and others [Tamir1, Tamir2, Hessel]. Chapter two next examines the use of only the discrete mode contributions to represent the structure currents and fields. The use of the discrete modes allows a much simplified transmission line approach to the formulation of many antenna and scattering problems, and the application of many useful network and modal solution techniques. Special emphasis is paid to the characterization of *open* guided wave structures, and to this extent, a method of solving for the propagation constants and a new definition of the characteristic impedance of the discrete modes are presented. An attempt has been made to make the formulations and discussions up to this point as general as possible so that the presented theory is applicable to arbitrary guided wave structures (both open and closed, and independent of material properties to the extent that appropriate Green's functions can be derived). The last part of chapter two is devoted to specializing the geometry so that the guided wave structure is embedded in a stratified supporting media. This requires the modification of the integral equation formulation and the specification of the required wave equations that must be solved for in each of the planar layers. The corresponding Green's functions for sources embedded in a layered geometry are derived in appendix A. The last section in chapter two discusses the wave properties supported by the combination of the cylindrical and planar geometries.

The remaining parts of the thesis are devoted to the discussion of various problems which can be modeled using the cylindrical/planar geometry chosen. Chapter three addresses one of the earliest applications of this geometry type, that of excitation of and wave propagation along infinite thin-wire transmission lines located over a lossy earth. Early solutions of this problem were based on a circuit approach, where the currents behaved according to the telegrapher's equations [Carson, Pollaczek, Wise], these being valid only at lower frequencies. Formulation of single conductor [Wait5, dosSantos, Chang3, Kuester2, Chiba, Wedepohl] and multiple conductor [Wait9, Kuester4] systems, based on an exact solution of Maxwell's equations, have since extended the validity to a much higher frequency range. Many studies of the wave properties of this geometry have been undertaken [Chang3, Kuester4, Olsen5], of specific interest being the extraction of the discrete guided wave modes. As the exact solution involves the evaluation of difficult integrals, these similar to that developed by Sommerfeld [Sommerfeld2] for dipole sources over a lossy interface, many approximation techniques have been examined [Kaidanov, Kikuchi, Carpentier1, Shen3], the most utilized being the low frequency quasi-TEM approximation [Carson, King1, Olsen7]. Finally, the excitation of the infinite transmission line by various source types has also been of interest, of specific importance being the excitation by a dipole source [Chang3, Kuester2, King4, Hill] for application in antenna problems, and the excitation by an incident plane wave source [Olsen1, Scharfman, Fontaine, Bridges6] for application in electromagnetic interference and electromagnetic pulse problems. In chapter three, the solution of the multiple thin-wire over lossy earth case is extracted directly

from the general integral equation formulation presented in chapter two. The resulting formulation is valid for an arbitrary source excitation, and thus can handle a wide variety of applications. Next, the wave properties associated with this specific geometry are delineated and are then used to deduce various approximate evaluation techniques to simplify the infinite integrals involved in the exact solution. A numerical study of various transmission line geometries for typical earth electrical properties is presented at the end of the chapter. Specific attention is paid to the characterization of the discrete modal properties of the structure, since additional guided wave modes exist in addition to the traditional quasi-TEM modes. Also, of specific importance is the validity of the various approximation techniques often used in practice, which can only be fully understood by referring back to the exact solution from which they were obtained. This task is thus also examined at the end of chapter three. Even though many of the specific applications discussed in this chapter have been previously addressed throughout the literature, the purpose of this work is to present a detailed and coherent theory of the transmission line above earth problem. Indeed, this topic can be considered as one of the most widely published areas in the electromagnetic and power engineering fields over the last century.

Chapter four examines the problem of defining an appropriate characteristic impedance for the discrete modes of propagation supported by open guided wave structures. A discussion of the properties of guided wave structures is initially developed from the theory presented for closed waveguides [Collin, Marcuvitz, Schelkunoff2, Kerns2]. For the analysis of these structures using a transmission line approach, the two required parameters are the propagation constants and the characteristic impedances of the discrete guided modes. The definition and solution of the propagation constants is straight forward as there is a direct physical relationship with the electromagnetic quantities. The definition of the characteristic impedances, however, is somewhat arbitrary since there is no direct relationship between the electromagnetic quantities and the circuit quantities modeling the structure except in the TEM limit. Various definitions for closed waveguide structures have been used in the literature [Marcuvitz, Schelkunoff3, Kerns1], and the harder problem of a definition for open structures has also been addressed [Getsinger, Brews2, Fache2, Jansen2]. In chapter four, an alternative definition of the characteristic impedance of guided wave structures is proposed. The definition follows directly from the hybrid Green's function-integral equation solution of the structure and collapses to the TEM result in the quasi-static limit. As an example, the specific case of a thin-wire conductor located over a lossy half-space is then addressed, where the results of the proposed definition are compared to the results generated using the other definitions currently available in the literature. As a by-product of this study, a closed form solution for the axially directed power of the discrete modes supported by a conducting strip embedded in a stratified media is formulated, as presented in appendix C.

Even though the formulations developed in chapters three and four apply to general guided wave structures, the numerical results presented have mainly been for circular thin-wire systems, where a uniform and axially directed current distribution on the conductors has been assumed. Chapter five examines the case of an arbitrary shaped conductor which can be located *near* or *at* a lossy planar interface. In the past almost all theories have treated the conductor over earth problem assuming a thin-wire approximation to model the conductor. When the conductor is either located well above or buried well below the interface, the propagation constants of the discrete guided modes will be close to the wavenumber of the medium in which it is embedded and the approximation is valid. This is not the case, however, when the conductor is located near or at the interface, where a more accurate model must then be used to take into account a non-uniform current distribution. Various techniques have been proposed in the literature to examine this problem, but either a thin-wire or uniform current assumption is still made [Coleman, Wait4, Chang1, Olsen7] or the formulation is not valid when the conductor becomes very near (touching) the interface [Pogorzelski]. Chapter five presents an exact formulation of the problem, which is valid even when the conductor is in contact with the interface. Results for the case of a circular conductor located over an earth having typical electrical properties are given and a comparison is made to the various other approximation methods which have been utilized throughout the literature.

The derivation of the Green's functions for sources which are embedded in a stratified media geometry are presented in appendix A. These are primarily based on the formulations in the literature for sources over a layered earth [Kuester4, Wait3, Wait11] and for microstrip geometries [Jansen2, Itoh, Das, Fukuoka]. The derivation of specialized formulations for the case of a single homogeneous half-space is emphasised. These Green's functions are usually in integral form, requiring either a single or double infinite integration for their evaluation. Appendix B presents various techniques for the evaluation of these infinite integrals, commonly known as Sommerfeld integrals. Exact analytical solution of the integrals is usually difficult due to the presence of singularities and branch cuts in their integrands. The appendix discusses some of the approximate techniques commonly used for their evaluation, and some new closed form expressions are developed for the integrals arising in the special case of a lossy half-space. In general however, for an accurate evaluation of the integrals, and to extract the proper behaviour of all the wave components (surface waves etc.), numerical techniques must be employed. To this extent, a technique for the numerical integration of the infinite integrals is also presented in the appendix. The proposed method has the advantage that it accounts for the possible highly oscillatory nature of the integrand when evaluated in the far field region.

Chapter 2
Guided Wave Structures

This chapter provides the general framework for the analysis of cylindrical guided wave structures. The formulation of the guided wave geometry will be in terms of a hybrid Green's function-integral equation approach, which is general to the extent that appropriate Green's functions can be developed for each region of the structure. The characterization of the wave properties of open and closed guiding structures is presented, with emphasis on the accurate definition of the propagation constants and characteristic impedances of the discrete modes. The formulation of structures which are embedded in a stratified supporting medium is then addressed, and the guided wave properties of this geometry are then examined. The method of presenting the results of this chapter may appear in non-standard form at many times, however, this is mainly due to the attempt to keep the theory as concise and general as possible. Various applications, which can be modeled using special cases of the geometry considered, will be presented in the remaining chapters of the thesis.

2.1. SOLUTION METHODOLOGY

Any scattering problem can be formulated from Maxwell's equations, in terms of a wave equation, along with appropriate boundary conditions, which must be satisfied at all points in the region under study. For the most general case, where the region is comprised of a complex inhomogeneous media, the solution of the wave equation must be performed directly in its differential form. A discretization of the region into a finite number of spacial cells, in which the material can be considered constant, is the most common solution methodology. Fortunately however, in most scattering problems, the material inhomogeneities occur at discrete boundaries inside the problem region. These bounding surfaces define the geometry of the scattering structure to be studied. Structures may be of various types; bounded in three dimensions defining a finite scatterer, bounded in two dimensions defining an infinite guiding wave structure, or bounded in only one dimension defining a stratified media, with each structure type having its own particular characteristics and wave properties associated with it. As defined by the discrete boundaries, the region under study can be partitioned into subregions, where internal to each subregion the media is homogeneous. The problem then requires the solution of the wave equation in each homogeneous subregion along with the satisfaction of the boundary conditions at all their interfaces.

For geometries where the media discontinuities conform to a known coordinate system, the solution of the wave equation and satisfaction of the boundary conditions at their interfaces can be performed using a transformation approach for the *entire* problem region. Here, a solution to the differential equations are usually found by expanding the fields in terms of a set of orthogonal eigenfunctions particular to the chosen coordinate system, with the unknown expansion coefficients then determined from the application of the boundary conditions. For open (infinite) structures, the eigenfunctions are continuous and the transform is in integral form; for closed (finite) structures, the eigenfunctions are discrete (periodic) and the transform is a summation. This solution methodology can be referred to as a Green's function approach and is an exact solution to the extent that the eigenfunction basis used in the transform is complete. However, this method works well, and is the most appropriate, only when the geometry of the scattering structure coincides with a known orthogonal coordinate system. For solutions of complex scattering geometries, this approach becomes impractical or impossible.

For complex scattering geometries, the solution of the wave equation in each *individual* homogeneous subregion can easily be found using a transformation approach, usually in terms of an integral over the subregion volume. Then, the Green's theorem can be used to transform the volume integral into a set of surface integrals over the boundaries defining the subregions. The kernel of the integral operator for each subregion will contain the appropriate homogeneous space Green's function, with the field discontinuities at the subregion boundaries usually being identified with equivalent sources. This approach is referred to as an integral equation method, where a solution requires the determination of the unknown equivalent sources in the integrand by utilizing the boundary conditions at the subregion interfaces. Once the currents are determined, a second step is then required to yield the resulting fields in each subregion. Using this method, the solution of arbitrary shaped scattering structures is easily facilitated by expanding the equivalent surface currents in terms of a suitable basis set, usually spacially discrete for irregular geometries. Solution of the integral equation in this manner is termed a method of moments solution (boundary element method). Even though this method is general and applicable to complex geometries, the results are approximate and sensitive to the choice of basis functions. Further, if one or more of the structure surfaces is infinite in extent, as in the case of a planar layered media, the unknown sources must be determined over an infinite interval, making this solution technique impracticable.

A compromise between these two solution techniques is to solve part of the problem using a Green's function approach and part using an integral equation formulation. This means incorporating the effects of as many media discontinuities as possible into the Green's function, and then expanding only the boundaries that do not coincide with a specific orthogonal coordinate system in terms of unknown equivalent sources. Thus, the surface integral equation will be over only the irregular geometrical surfaces,

regular material discontinuities being incorporated into an appropriate Green's function. This approach is referred to as a hybrid Green's function-integral equation method and combines the flexibility of the integral equation formulation for modeling scatterers of complex geometry with the exactness of the Green's function solution. This approach is used in this thesis to solve the problem of cylindrical guided wave structures embedded in a stratified media.

The purpose of this section is to formulate the general surface integral equation solution to the wave equation for a bounded region having arbitrarily defined material properties. To this extent, the standard problem in electromagnetics of determining the fields at any point in a bounded region V due to specified electric and magnetic sources, $\bar{J}_s$ and $\bar{M}_s$, is discussed. The electric $\bar{E}$ and magnetic $\bar{H}$ fields must be solutions of Maxwell's equations in the region as well as satisfy any boundary conditions at the region boundary S, where S defines the surface bounding the region V. Assuming an $e^{-j\omega t}$ time dependence, the time-harmonic solution of the fields can be described in terms of the set of partial differential equations in the region as [Stratton,p.464]

$$[\nabla^2+k^2(\bar{r})]\,\bar{E}(\bar{r}) = -j\omega\mu(\bar{J}_s(\bar{r})+\frac{1}{k^2}\nabla\nabla\cdot\bar{J}_s(\bar{r})) + \nabla\times\bar{M}_s(\bar{r}) \quad , \bar{r}\in V \tag{2.1a}$$

$$[\nabla^2+k^2(\bar{r})]\,\bar{H}(\bar{r}) = -j\omega\varepsilon'(\bar{M}_s(\bar{r})+\frac{1}{k^2}\nabla\nabla\cdot\bar{M}_s(\bar{r})) - \nabla\times\bar{J}_s(\bar{r}) \quad , \bar{r}\in V \tag{2.1b}$$

$$k^2(\bar{r}) = \omega^2\mu\varepsilon' \quad , \quad \varepsilon' = \varepsilon + j\sigma/\omega$$

where $\bar{r}$ defines a point in the region V, $k(\bar{r})$ is the wavenumber at this point, and μ, ε, σ define the electrical properties of the medium which can in general also be functions of position $\bar{r}$.

For further discussion, (2.1) will be described in the form of an operator equation, where the inverse operator determines the fields in the region due to the specified sources. Thus, defining $\bar{f}(\bar{r})=(\bar{E}(\bar{r}),\bar{H}(\bar{r}))^t$ and $\bar{g}_s(\bar{r})=(\bar{J}_s(\bar{r}),\bar{M}_s(\bar{r}))^t$ where t denotes the transpose,

$$[\nabla^2 + k^2(\bar{r})]\,\bar{f}(\bar{r}) = \mathrm{F}\{\bar{g}_s(\bar{r})\} \qquad , \bar{r}\in V \tag{2.2}$$

$$\bar{f}(\bar{r}) = \mathrm{L}^{-1}\{\bar{g}_s(\bar{r})\} = \iiint_V \bar{\bar{\Gamma}}(\bar{r},\bar{r}')\bar{g}_s(\bar{r}')d\bar{r}' \tag{2.3}$$

where F is a function of the source terms as defined in (2.1). Here $\bar{\bar{\Gamma}}(\bar{r},\bar{r}')$ is an appropriate Green's function which satisfies the set of p.d.e.'s of the form (2.2) when the source is considered a delta function located at $\bar{r}'$. $\bar{\bar{\Gamma}}(\bar{r},\bar{r}')$ *also* takes into account the region external to V (this including sources external to V). The derivation of $\bar{\bar{\Gamma}}(\bar{r},\bar{r}')$ satisfying all these requirements can pose a formidable task. To simplify this problem, the Green's Theorem [Harrington1, Stratton] is used, so that (2.3) can be

determined as a sum of a volume integral representing the field $\bar{f}^{inc}(\bar{r})$ due to the sources $\bar{g}_s(\bar{r})$, plus a surface integral term $\bar{f}^{scat}(\bar{r})$ accounting for the effect of the region external to the boundary S as

$$\bar{f}(\bar{r}) = \bar{f}^{inc}(\bar{r}) + \bar{f}^{scat}(\bar{r}) \tag{2.4}$$

$$\bar{f}^{inc}(\bar{r}) = \iiint_V \bar{\bar{G}}(\bar{r},\bar{r}')\bar{g}_s(\bar{r}')\,d\bar{r}' \qquad ,\bar{r},\bar{r}' \in V \tag{2.5}$$

$$\bar{f}^{scat}(\bar{r}) = \iint_S \bar{\bar{G}}(\bar{r},\bar{r}')\bar{g}(\bar{r}')\,d\bar{r}' \qquad ,\bar{r} \in V \;\; , \;\; \bar{r}' \in S \tag{2.6}$$

where $\bar{g}(\bar{r})$ is an equivalent surface current modeling the fields and sources exterior to the region V ($\bar{g}(\bar{r})$ are additional sources to $\bar{g}_s(\bar{r})$). The Green's function $\bar{\bar{G}}(\bar{r},\bar{r}')$ is now required to satisfy only the set of delta source p.d.e.'s of the form (2.2) in the region V *only*, and is thus much simpler to formulate in general than the Green's function $\bar{\bar{\Gamma}}(\bar{r},\bar{r}')$.

The specific geometry under study in this thesis consists of an arbitrary shaped cylindrical guiding structure, bounded in two spacial dimensions and infinite in one dimension. The cylindrical structure is allowed to be embedded in a stratified supporting medium, infinite in two spacial dimensions, with planar material discontinuities specified in the remaining dimension. Following the hybrid solution methodology, the boundary surface defining the cylindrical guiding structure is modeled by equivalent sources, with an integral equation developed over this surface. The Green's function kernel of the integral is then formulated to incorporate the effect of the stratified supporting media. The integral equation formulation part of this problem is similar to that found in the literature for arbitrary cylindrical structures in free space, except the Green's function in this case is not the simple free space Green's function, but contains the added complexity of a plane layered media. Felsen and Marcuvitz [Felsen] derive Green's functions as well as discuss the wave properties for many material configurations. The Green's functions utilized throughout this thesis are derived and discussed in detail in appendix A.

2.2. GUIDED WAVES FOR TWO-DIMENSIONAL BOUNDED (CYLINDRICAL) STRUCTURES

In this section, the solution of two-dimensional bounded (cylindrical) guided wave structures will be presented. The formulation is developed using a hybrid integral equation-Green's function approach where an integral equation is developed over the surface of the cylindrical structure. The solution is general to arbitrarily shaped cylindrical structures with internal media and a supporting medium that may be inhomogeneous to the extent that appropriate Green's functions can be derived. A description of the geometry for a general scattering structure is given in figure 2.1a. The region $V=V_0+\Sigma V_i$ contains N distinct subregions V_i which define the scatterer, these

subregions being embedded in the remaining infinite supporting region V_0. The boundaries of the subregions are defined by the surface $S=\Sigma S_i$. For cylindrical guided wave structures, the N subregions are chosen to be of infinite extent in the z-dimension, their surfaces being defined by the generating curves C_i in the x-y plane; $(\bar{\rho}=\rho(x,y), -\infty<z<\infty) \in S_i$, $\bar{\rho} \in C_i$, $i=1,2,...,N$ as shown in figure 2.1b. When a planar layered supporting medium V_0 is considered, the stratification is chosen to be symmetric in the x-z dimensions, the interface planes at specified values along the y-axis. Appropriate Green's functions are required to represent the fields in each of the defined subregions V_i. For the specific case of cylindrical structures embedded in a layered media, the effect of the stratification is incorporated into the Green's function for the region V_0.

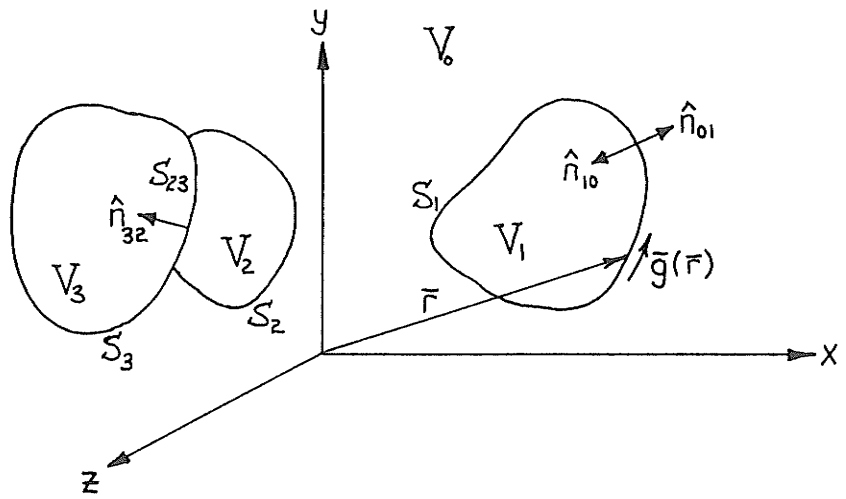

Figure 2.1a: General scattering geometry.

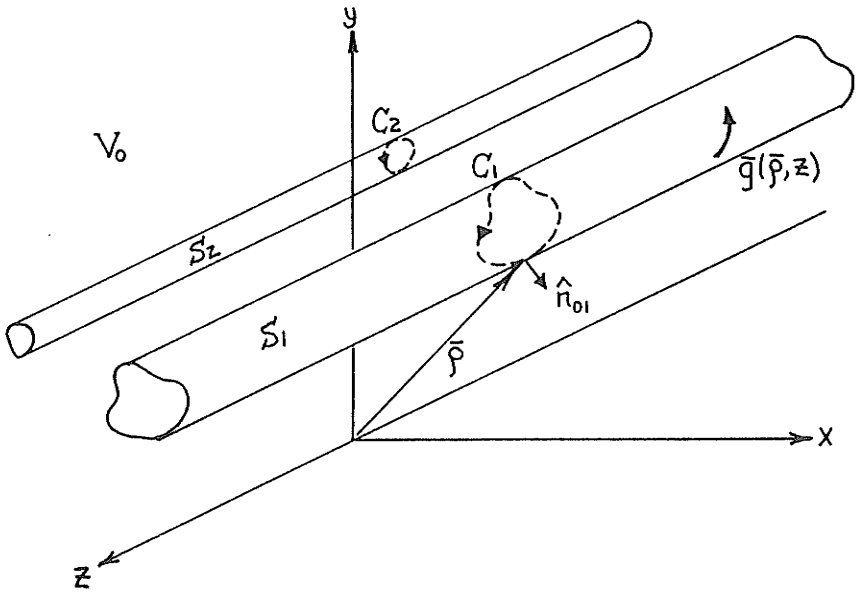

Figure 2.1b: Cylindrical guided wave structure.

Using the Green's theorem, the volume integral (2.3) developed in section 2.1, giving the fields in the region V in terms of specified internal sources, had been transformed into a surface integral (2.6). Using this formulation, the fields in a defined subregion V_i can be determined as

$$\bar{f}_i(\bar{r}) = \bar{f}_i^{inc}(\bar{r}) + \mathrm{L}_i^{-1}\{\bar{g}(\bar{r})\} \quad ; \bar{r}\in V_i \tag{2.7}$$

$$\mathrm{L}_i^{-1}\{\bar{g}(\bar{r})\} = \iint_{S_i} \bar{\bar{G}}_i(\bar{r},\bar{r}')\bar{g}(\bar{r}')d\bar{r}' = \bar{f}_i^{scat}(\bar{r}) \tag{2.8}$$

where $\bar{f}_i^{inc}(\bar{r})$ are the fields due to sources interior to only the region V_i. The integral term over the surface S_i yields the scattered fields due to coupling through the aperture, which are modeled as equivalent surface currents $\bar{g}(\bar{r})$ on the boundary. The appropriate tensor Green's function $\bar{\bar{G}}_i(\bar{r},\bar{r}')$ for the region V_i is determined so that the wave equation

$$[\nabla^2 + k_i^2(\bar{r})]\bar{f}_i^{scat}(\bar{r}) = \mathrm{F}\{\bar{g}(\bar{r})\delta(\bar{r}-\bar{r}')\} \quad ; \bar{r}\in V_i \ , \bar{r}'\in S_i \tag{2.9}$$

is satisfied along with all required boundary conditions at material discontinuities internal to the region V_i. F is a function of the source terms as given in (2.1). Thus, the operator L_i^{-1} gives the scattered field due to the equivalent sources $\bar{g}(\bar{r})$ on the surface S_i. The determination of the unknown equivalent currents $\bar{g}(\bar{r})$ at the surfaces $S=\Sigma S_i$ bounding all the subregions is facilitated by satisfying the continuity of tangential fields at their interfaces. Thus, utilizing these boundary conditions on all surfaces

$$\hat{n}_{ij}(\bar{r})\times\bar{f}_i(\bar{r}) + \hat{n}_{ji}(\bar{r})\times\bar{f}_j(\bar{r}) = 0 \quad ; \bar{r}\in S_{ij} \tag{2.10}$$
$$\hat{n}_{ij} = -\hat{n}_{ji} \quad , \quad S_{ij} = S_{ji} = S_i \cap S_j$$

where $\hat{n}_{ij}$ is the inward unit normal vector to the region V_i at the interface surface $S_{ij}=S_i\cap S_j$ between the two regions V_i and V_j. Satisfying (2.10) for every subregion, a set of integral equations over all the surfaces can then be developed as [Harrington2, Mittra1]

$$\hat{n}_{ij}(\bar{r}) \times \left[\bar{f}_i^{inc}(\bar{r}) + \mathrm{L}_i^{-1}\{\bar{g}(\bar{r})\} - f_j^{inc}(\bar{r}) - \mathrm{L}_j^{-1}\{\bar{g}(\bar{r})\} \right] = 0 \tag{2.11}$$
$$; \bar{r}\in S_{ij} \quad , \ i=0,1,...,N \quad , \ j=0,1,...,N$$

The solution of this set of integral equations will yield the unknown equivalent surface currents $\bar{g}(\bar{r})$, after which the fields interior to each region can be determined from (2.6). The currents and fields formulated by the preceding integral equation solution are general to arbitrary scattering objects; three-dimensional bounded finite structures, as well as two-dimensional bounded cylindrical structures. The geometries of interest in this thesis, are cylindrical guiding structures, where the surfaces S_i defining the scatterer are infinite in one dimension and bounded in the remaining two dimensions.

Since the physical geometry of the problem is symmetric in one dimension, a solution will be obtained utilizing the infinite Fourier transform pair

$$\tilde{\bar{x}}(\bar{\rho}) = \tilde{\bar{x}}(\bar{\rho},k_z) = \Gamma_z\{\bar{x}(\bar{r})\} = \int_{-\infty}^{\infty} \bar{x}(\bar{\rho},z)e^{-jk_z z}\,dz \tag{2.12a}$$

$$\bar{x}(\bar{r}) = \bar{x}(\bar{\rho},z) = \Gamma_z^{-1}\{\tilde{\bar{x}}(\bar{\rho})\} = \frac{1}{2\pi}\int_{-\infty}^{\infty} \tilde{\bar{x}}(\bar{\rho},k_z)e^{+jk_z z}\,dk_z \tag{2.12b}$$

where the cylindrical structure has been chosen to be invariant in the z-dimension. Using (2.12), the integral equation over the surface S in (2.11) can be reduced to one over the generating curve C as

$$\hat{h}_{ij}(\bar{\rho}) \times \left[\tilde{\bar{f}}_i^{inc}(\bar{\rho}) + \tilde{L}_i^{-1}\{\tilde{\bar{g}}(\bar{\rho})\} - \tilde{\bar{f}}_j^{inc}(\bar{\rho}) - \tilde{L}_j^{-1}\{\tilde{\bar{g}}(\bar{\rho})\} \right] = 0 \tag{2.13}$$

$$; \bar{\rho} \in C_{ij} = C_i \cap C_j \quad , i=0,1,...,N \quad , j=0,1,...,N \quad , -\infty < k_z < \infty$$

$$\tilde{L}_i^{-1}\{\tilde{\bar{g}}(\bar{\rho})\} = \int_{C_i} \tilde{\bar{\bar{G}}}(\bar{\rho},\bar{\rho}')\tilde{\bar{g}}(\bar{\rho}')\,d\bar{\rho}' = \tilde{\bar{f}}_i^{scat}(\bar{\rho}) \tag{2.14}$$

The solution of the integral equation, as well as the determination of the Green's functions for each region has been simplified to a two-dimensional problem. Note that the transformed two-dimensional quantities now contain only a subset of the wave properties characteristic to the region they describe, the complete set being recovered upon the inverse transformation. The final solution of the fields then requires the inverse transformation since the sources $\bar{f}_i^{inc}(\bar{r})$ are not in general invariant in the z-dimension.

For simplicity, the set of integral equations (2.13) will be written in the general form

$$\hat{h}(\bar{\rho}) \times \tilde{L}^{-1}\{\tilde{\bar{g}}(\bar{\rho})\} = \hat{h}(\bar{\rho}) \times \tilde{\bar{f}}^{inc}(\bar{\rho}) \quad ; \bar{\rho} \in C \quad , -\infty < k_z < \infty \tag{2.15}$$

where $\hat{h}(\bar{\rho})$ is the unit normal to the contour C with $\tilde{\bar{f}}^{inc}(\bar{\rho})$ and $\tilde{L}^{-1}$ dependent on which part of the contour $\bar{\rho}$ falls. Since the generating contour C of the guiding wave structure is bounded in two dimensions, any infinite discrete (periodic) set of complete basis functions can be chosen to represent the unknown currents $\tilde{\bar{g}}(\bar{\rho})$ [Harrington2]. In terms of the chosen basis, the currents will be expanded as

$$\tilde{\bar{g}}(\bar{\rho},k_z) = \sum_{n=1}^{N} x_n(\bar{\rho})\bar{I}_n(k_z) = [x(\bar{\rho})]^t[\bar{I}(k_z)] \tag{2.16}$$

where $x_n(\bar{\rho})$ is one basis function of the set and $\bar{I}_n$ is a scalar constant. The basis $\{x_n(\bar{\rho})\,; n=1,2,...,N\}$ is usually chosen to be linearly independent over the contour C and is then complete if $N \to \infty$. Note that all vector components of the equivalent current $\tilde{\bar{g}}(\bar{\rho})$ are expanded using the same basis set in (2.16). By chosing a suitable

inner product $<,>$, and an arbitrary set of weighting functions $w_m(\bar{\rho})$, which also form a complete basis, the integral equation (2.15) can be discretized as

$$< w_m(\bar{\rho}) , \hat{h}(\bar{\rho}) \times \tilde{L}^{-1} \left\{ \sum_{n=1}^{N} x_n(\bar{\rho}) \bar{I}_n(k_z) \right\} > = < w_m(\bar{\rho}) , \hat{h}(\bar{\rho}) \times \bar{\bar{f}}^{inc}(\bar{\rho}) > \quad ; m=1,2,...,M \tag{2.17}$$

where the inner product is defined as

$$< a(\bar{\rho}) , b(\bar{\rho}) > = \int_C a(\bar{\rho}') b(\bar{\rho}') \, d\bar{\rho}' \tag{2.18}$$

The general form (2.17) is referred to as a method of moments solution (boundary element), with the particular choice of the weighting set $w_n(\bar{\rho}) = x_n(\bar{\rho})$ being defined as Galerkin's method [Harrington2]. A unique solution of (2.17) can be obtained for a finite number of basis functions $M=N$, with the resulting set of linear equations then solved in matrix form as

$$[\bar{\bar{Z}}(k_z)][\bar{I}(k_z)] = [\bar{F}^{inc}(k_z)] \quad ; -\infty < k_z < \infty \tag{2.19}$$

where

$$\bar{F}_m^{inc}(k_z) = < w_m(\bar{\rho}) , \hat{h}(\bar{\rho}) \times \bar{\bar{f}}^{inc}(\bar{\rho}) > \tag{2.20}$$

$$\bar{\bar{Z}}_{mn}(k_z) = < w_m(\bar{\rho}) , \hat{h}(\bar{\rho}) \times \tilde{L}^{-1}\{x_n(\bar{\rho})\} > = < w_m(\bar{\rho}) , \hat{h}(\bar{\rho}) \times \int_C \bar{\bar{G}}(\bar{\rho},\bar{\rho}') x_n(\bar{\rho}') \, d\bar{\rho}' > \tag{2.21}$$

since

$$< w_m(\bar{\rho}) , \hat{h}(\bar{\rho}) \times L^{-1} \left\{ \sum_{n=1}^{N} x_n(\bar{\rho}) \bar{I}_n(k_z) \right\} > = \sum_{n=1}^{N} < w_m(\bar{\rho}) , \hat{h}(\bar{\rho}) \times \int_C \bar{\bar{G}}(\bar{\rho},\bar{\rho}') x_n(\bar{\rho}') \, d\bar{\rho}' > \bar{I}_n(k_z) \tag{2.22}$$

The interaction (impedance) matrix $\bar{\bar{Z}}(k_z)$ will be diagonal for the special case where the expansion functions $x_n(\bar{\rho})$ are chosen as the eigenfunctions of $\tilde{L}^{-1}$. When the boundary C of the cylindrical structure coincides with some orthogonal coordinate system, the determination of a basis in terms of known functions which diagonalize $\bar{\bar{Z}}(k_z)$ is usually possible and should be utilized. However, in the general case of an arbitrary generating contour C, or if the Green's function in the kernel of $\tilde{L}^{-1}$ describes a complicated medium, $\bar{\bar{Z}}(k_z)$ will not be diagonal. For the general case, a transform can be found to diagonalize $\bar{\bar{Z}}(k_z)$ which is determined from the eigenvalue problem

$$[\bar{\bar{Z}}(k_z) - \lambda_i(k_z)][\bar{p}_i(k_z)] = 0 \quad ; i=1,2,...,N \tag{2.23}$$

where $\lambda_i(k_z)$ are the resulting eigenvalues and $\overline{p}_i(k_z)$ are the corresponding eigenvectors. By utilizing all eigenvectors, a transform $\overline{P}(k_z)$ can be determined which can be used to diagonalize $\overline{\overline{Z}}(k_z)$ and solve for the scalar quantities $\overline{I}(k_z)$ as

$$[\overline{I}(k_z)] = [\overline{\overline{Z}}(k_z)]^{-1}[\overline{F}^{inc}(k_z)] \quad \text{or} \quad [\overline{\mathrm{i}}] = [\overline{\overline{\mathrm{z}}}_D]^{-1}[\overline{\mathrm{f}}^{inc}] \tag{2.24}$$

where

$$[\overline{I}(k_z)] = [\overline{P}(k_z)][\overline{\mathrm{i}}] \quad , \quad [\overline{F}^{inc}(k_z)] = [\overline{P}(k_z)][\overline{\mathrm{f}}^{inc}] \tag{2.25}$$

$$[\overline{\overline{\mathrm{z}}}_D] = [\overline{P}(k_z)]^{-1}[\overline{\overline{Z}}(k_z)][\overline{P}(k_z)] \tag{2.26}$$

$$\left[\overline{P}(k_z)\right] = \left[\left[\overline{p}_1(k_z)\right]\left[\overline{p}_2(k_z)\right]\cdots\left[\overline{p}_N(k_z)\right]\right] \tag{2.27}$$

and $\overline{\overline{\mathrm{z}}}_D$ is diagonal. The vectors $\overline{\mathrm{i}}$ and $\overline{\mathrm{f}}^{inc}$ are the resulting eigencurrents and eigenfields, respectively, for the specified guiding structure. The elements of $\overline{\overline{\mathrm{z}}}_D$ are the impedance values relating the equivalent eigencurrents to the excitation at the boundary surface C. In general $\overline{P}(k_z)$ as well as $\overline{\mathrm{i}}$, $\overline{\mathrm{f}}^{inc}$, and $\overline{\overline{\mathrm{z}}}_D$ are functions of the transform variable k_z. Special cases do arise, however, where $\overline{P}(k_z)$ is constant and independent of k_z [2.1].

The general solution of the integral equation (2.15), for an arbitrary source excitation is found using the inverse transform (2.12) as

$$\overline{g}(\overline{r}) = \Gamma_z^{-1}\{\overline{\tilde{g}}(\overline{\rho},k_z)\} \tag{2.28}$$

$$\overline{\tilde{g}}(\overline{\rho},k_z) = [x(\overline{\rho})]^t[\overline{I}(k_z)]$$

$$= [x(\overline{\rho})]^t[\overline{\overline{Z}}(k_z)]^{-1}[\overline{F}^{inc}(k_z)] = [x(\overline{\rho})]^t[\overline{P}(k_z)][\overline{\mathrm{i}}] \tag{2.29}$$

The scattered fields $\overline{f}_i^{scat}(\overline{r})$ and thus the total field at any point in the region V_i can be determined using (2.14) as

$$\overline{f}_i^{scat}(\overline{r}) = \mathrm{L}_i^{-1}\{\overline{g}(\overline{r})\} = \Gamma_z^{-1}\left\{\tilde{\mathrm{L}}_i^{-1}\{\overline{\tilde{g}}(\overline{\rho},k_z)\}\right\}$$

$$= \Gamma_z^{-1}\left\{\tilde{\mathrm{L}}_i^{-1}\{[x(\overline{\rho})]^t[\overline{I}(k_z)]\}\right\}$$

2.1 The transform $\overline{P}(k_z)$ will be independent of k_z for the special condition that the structure geometry is symmetrical (and a corresponding set of symmetric basis functions is chosen). An example may be a symmetric two conductor thin-wire transmission line, where $p_1 = [\,1/\sqrt{2}\,,\ 1/\sqrt{2}\,]$, $p_2 = [\,1/\sqrt{2}\,,\ -1/\sqrt{2}\,]$ independent of k_z. Under these physical conditions, $\overline{\overline{Z}}$ will be symmetric and all elements $\overline{Z}_{ii}$ will be equal.

$$= \Gamma_z^{-1}\left\{ \tilde{L}_i^{-1}\{[x(\bar{\rho})]^t\}[\bar{\bar{Z}}(k_z)]^{-1}[\bar{F}^{inc}(k_z)] \right\}$$

$$= \Gamma_z^{-1}\left\{ [\tilde{L}_i^{-1}\{x_n(\bar{\rho})\}]^t [< w_m(\bar{\rho}) , \hat{n}(\bar{\rho}) \times \tilde{L}^{-1}\{x_n(\bar{\rho})\} >]^{-1} \right.$$

$$\left. \cdot [< w_m(\bar{\rho}) , \hat{n}(\bar{\rho}) \times \bar{\bar{f}}^{inc}(\bar{\rho}) >] \right\} \qquad (2.30)$$

The solution of the guided wave problem has been formulated using a Fourier transform for the axially invariant structure dimension and a discrete (periodic) transformation for the remaining two transverse dimensions. The axial transform was in terms of the infinite set of eigenfunctions $\{\exp(+jk_z z)\}$, with the discrete transform developed using an arbitrary set of basis functions and an appropriate inner product. The diagonalization of the transverse dimension transform yielded a solution in terms of the eigenfunctions for that particular structure. Unlike the axial eigenfunctions however, the eigenfunctions for the transverse dimensions do not necessarily correspond to known analytical functions since the structure boundary does not coincide with a known orthogonal coordinate system in the general case. The diagonalization of the problem in terms of its eigenfunctions, is useful since simplified solutions in terms of only the dominant modes can be developed. Thus, the inverse transform of only these dominant ones are required.

2.3. DISCRETE MODE ANALYSIS

The formulation of the induced currents and scattered fields for a cylindrical guided wave structure was formulated in the last section. The solution to the problem was developed in terms of a one-dimensional transform as

$$\bar{f}^{scat}(\bar{\rho},z) = \Gamma_z^{-1}\left\{ \tilde{L}^{-1}\{\bar{\bar{g}}(\bar{\rho},k_z)\} \right\} \qquad (2.31)$$

$$\bar{g}(\bar{\rho},z) = \Gamma_z^{-1}\left\{ [x(\bar{\rho})]^t [\bar{\bar{Z}}(k_z)]^{-1}[\bar{F}^{inc}(k_z)] \right\} \qquad (2.32)$$

The solution to (2.31,2.32) is exact to the extent that a complete basis $x(\bar{\rho})$ is used. The formulation of the problem using a complete set of transform functions will include contributions from all the wave properties of the structure, the individual contributions being identified by examination of the poles and branch cuts that may be present in the complex k_z plane [Felsen]. Each type of material discontinuity (one, two, or three dimensional) in the region V will contribute to the possible variety of wave phenomena present. For cylindrical structures (bounded in two dimensions) there will be a double set of poles in the complex k_z plane, these corresponding to the

homogeneous solutions of the integral equation (2.11,2.15) ie: $(\bar{f}^{inc}(\bar{r})=0)$. The location of the poles are determined from the zeros of the impedance matrix $\bar{\bar{Z}}(k_z)$ and their contribution to the integral transforms (2.31,2.32) represents a set of discrete propagating modes guided along the cylindrical structure. As well as the wave properties due to the two-dimensional bounded structure, there will be phenomena due to any other types of material discontinuities present in the individual subregions V_i , $i=0,1,2,...,N$. These are incorporated into the Green's functions $\bar{\bar{G}}_i(\bar{r},\bar{r}')$ for each medium, and are represented by branch cuts and singularities of various orders in the complex k_z plane. Instead of discrete propagating modes, the branch cuts represent a continuous spectrum of modes. For open (infinite) region problems, there is at least one second order branch cut present in the k_z plane representing radiated fields. For a stratified exterior region, their will be two second order branch cuts representing radiated fields into the most upper and lower media, as well as first order branch cuts representing surface waves trapped by the layered media. The wave properties for the specific case of cylindrical guiding structures embedded in a stratified media will be discussed in section 2.6.

In this section we will examine the discrete guided wave contributions to the fields and currents for a general cylindrical structure [Collin,ch.5]. The discrete mode solutions are determined from the eigenvalues of the homogeneous case of (2.15), with the corresponding eigenvectors giving the current distribution on the surface boundary S for each mode. The properties of the modes are characterized by the resulting eigenvalues (propagation constants) k_z^p , $p=1,2,...,P$ and by the magnitude of their associated residue contributions in (2.31) and (2.32), which indicates their relative excitation by a given source. For closed structures (the supporting medium V_0 is surrounded by perfect conductor), the discrete mode contributions of the inverse transform in (2.32) form an infinite discrete set of eigenfunctions which are a complete basis, and no branch cut contributions are present. For open structures (the supporting medium V_0 extends to infinity), the set of discrete eigenfunctions is finite and does not form a complete basis. If open structures are considered, the complete set of basis functions requires the inclusion of a continuous spectra of modes, these represented as the branch cuts in the complex k_z plane. However, for many problems of interest, the major contribution is due to the discrete mode subset, and even though it does not form a complete basis, the approximate results are very acceptable. The use of only the discrete mode contributions to represent the structure currents in (2.32) allows a much simplified transmission line approach to the formulation of many antenna and scattering problems. Also, the many useful network properties and modal solution techniques developed for transmission line and closed waveguide problems can then be applied [Marcuvitz, Kerns2, Schwinger, Tripathi1]. The use of this approximation in the solution of a large class of problems will be the topic of section 2.4.

To this extent, consider the contribution to the current in (2.32) due to the finite set of discrete modes only

$$\bar{g}(\bar{\rho},z) \approx +j\sum_{p=1}^{P}\lim_{k_z\to k_z^p}\left\{ (k_z-k_z^p)[x(\bar{\rho})]^t[\bar{\bar{Z}}(k_z)]^{-1}[\bar{F}^{inc}(k_z)]e^{+jk_z|z|} \right\} \quad (2.33)$$

where for discussion purposes, the source is considered finite and located at $z=0$. The propagation constants k_z^p are determined from the solution of the homogeneous integral equation (2.19). For this purpose, a mode equation can be developed from the general eigenvalue problem (2.23) with $\lambda(k_z)=0$ as

$$\left.\begin{aligned} &\left|[\bar{\bar{Z}}(k_z)]\right| = 0 \;\rightarrow\; k_z^p \\ &[\bar{\bar{Z}}(k_z^p)][\bar{v}^p] = 0 \end{aligned}\right\} \quad ; p=1,2,...,P \quad (2.34)$$

giving rise to P eigenvalues (propagation constants) and their corresponding eigenvectors $\bar{v}^p$. Using the determined eigenvectors, the pth term in the mode expansion (2.33) can be diagonalized into the form

$$\bar{g}_p(\bar{\rho},z) = [x(\bar{\rho})]^t[\bar{v}^p]\frac{1}{2\bar{\bar{Z}}_{Cp}}[\bar{q}^p]^t[\bar{F}^{inc}(k_z^p)]e^{+jk_z^p|z|} \quad (2.35)$$

$$\bar{\bar{Z}}_{Cp} = -\frac{j}{2}\frac{1}{\bar{N}_v^p\,\bar{N}_q^p}\frac{\partial}{\partial k_z}\left\{|\bar{\bar{Z}}(k_z)|\right\}_{k_z=k_z^p} \quad (2.36)$$

where $\bar{\bar{Z}}_{Cp}$ is defined here to be the characteristic impedance of the pth mode for the guiding wave structure. This definition is valid for all general guided wave structures, both open and closed. The transform vectors $\bar{v}^p$, $\bar{q}^p$ and the normalization constants $\bar{N}_v^p$, $\bar{N}_q^p$ are given by

$$\begin{aligned} \bar{v}_j^p &= \mathrm{cof}_{1j}\{\bar{\bar{Z}}(k_z^p)\}/\bar{N}_v^p \quad ; j=1,2,...,N \\ \bar{q}_i^p &= \frac{\mathrm{cof}_{i1}\{\bar{\bar{Z}}(k_z^p)\}}{\mathrm{cof}_{11}\{\bar{\bar{Z}}(k_z^p)\}}/\bar{N}_q^p \quad ; i=1,2,...,N \\ \bar{N}_v^p &= \left[\sum_{i=1}^{N}\bar{v}_i^p\right]^{1/2}, \qquad \bar{N}_q^p = \left[\sum_{i=1}^{N}\bar{q}_i^p\right]^{1/2} \end{aligned} \quad (2.37)$$

Note that if $\bar{\bar{Z}}(k_z^p)$ is symmetric, then $[\bar{q}^p]=[\bar{v}^p]$ and accordingly $\bar{N}_q^p=\bar{N}_v^p$. The function $\mathrm{cof}_{ij}\{Z\}$ gives the cofactor of the ijth element of the matrix Z. Using the expression (2.35) for each of the P modes, a transformation can be developed to solve (2.33) in matrix form as

$$\bar{g}(\bar{\rho},z) = [x(\bar{\rho})]^t[\bar{T}][2\bar{\bar{Z}}_C]^{-1}[\bar{\bar{D}}(z)][\bar{Q}]^{-1}[\bar{F}^{inc}(k_z^p)]$$

$$= [x(\bar{\rho})]^t[\bar{T}][\bar{i}(z)] \tag{2.38}$$

which can more easily be defined using

$$[\bar{i}(z)] = [2\bar{\bar{Z}}_C]^{-1}[\bar{\bar{D}}(z)][\bar{f}^{inc}] \tag{2.39}$$

$$\bar{f}_p^{inc} = \sum_{j=1}^{N} \bar{Q}_{jp}\, \bar{F}_j^{inc}(k_z^p) \qquad ; p=1,2,...,P \tag{2.40}$$

$$\bar{\bar{D}}_{ij}(z) = \begin{cases} e^{+jk_z^p|z|} & , i=j=p \\ 0 & , i\neq j \end{cases} \tag{2.41}$$

where $\bar{\bar{D}}(z)$ and $\bar{\bar{Z}}_C$ are diagonal matrices describing the propagation and impedance characteristics, respectively, of the structure. The vectors $\bar{i}$ and $\bar{f}^{inc}$ are the strengths of the corresponding current and incident field eigenfunctions for the structure. The transformations are determined from the eigenvectors $\bar{v}^p$ and $\bar{q}^p$ as

$$\begin{aligned} [\bar{T}] &= \left[[\bar{v}^1][\bar{v}^2] \cdots [\bar{v}^P] \right] \\ [\bar{Q}] &= \left[[\bar{q}^1][\bar{q}^2] \cdots [\bar{q}^P] \right] \end{aligned} \tag{2.42}$$

Note that $\bar{Q}^{-1}=\bar{T}^t$ for the case of $\bar{\bar{Z}}(k_z^p)$, $p=1,2,...,P$ being symmetric. Once the currents $\bar{g}_p(\bar{\rho},z)$ due to each of the discrete modes are determined, the corresponding fields can be deduced as

$$\bar{f}_p^{scat}(\bar{\rho},z) = \Gamma_z^{-1}\left\{ \tilde{L}^{-1}\{\tilde{\bar{g}}_p(\bar{\rho},k_z^p)\} \right\}$$

$$= \int_C \tilde{\bar{\bar{G}}}(\bar{\rho},\bar{\rho}',k_z^p)\tilde{\bar{g}}_p(\bar{\rho}',k_z^p)\, d\bar{\rho}'\, e^{+jk_z^p|z|} \tag{2.43}$$

2.4. TRANSMISSION LINE APPROACH AND QUASI-TEM APPROXIMATION

As discussed in section 2.3, the use of only the discrete mode contributions to represent the currents and scattered fields for a cylindrical guiding structure allows the utilization of many transmission line and network theory techniques, greatly expanding the number of practical problems that can be solved. In utilizing the transmission line approach, the currents induced on the cylindrical structure can be formulated in terms of an infinite set of localized delta function sources along the length of the structure, the magnitude of the sources being proportional to the incident fields at the surface of the structure [King3]. A formulation in this manner can be developed directly from the exact solution (2.28) by utilizing the convolution theorem to represent the incident

fields as

$$\bar{g}(\bar{\rho},z) = \Gamma_z^{-1}\left\{ [x(\bar{\rho})]^t [\bar{\bar{Z}}(k_z)]^{-1} [\bar{F}^{inc}(k_z)] \right\} \tag{2.44}$$

$$\bar{F}_m^{inc}(k_z) = < w_m(\bar{\rho}) , \hat{h}(\bar{\rho}) \times \bar{\tilde{f}}^{inc}(\bar{\rho},k_z) > \tag{2.45}$$

$$\bar{\tilde{f}}^{inc}(\bar{\rho},k_z) = \Gamma_z \{\bar{f}^{inc}(\bar{\rho},z)\} = \int_{-\infty}^{\infty}\int_{-\infty}^{\infty} \delta(z-z')e^{-jk_z z}\, dz\ \bar{f}^{inc}(\bar{\rho},z')\, dz' \tag{2.46}$$

Thus,

$$\bar{g}(\rho,z) = \int_{-\infty}^{\infty} [x(\bar{\rho})]^t [\bar{\bar{K}}_\infty(z,z')][\bar{F}^{inc}(z')]\, dz' \tag{2.47}$$

$$\bar{\bar{K}}_\infty(z,z') = \Gamma_z^{-1}\left\{ [\bar{\bar{Z}}(k_z)]^{-1} e^{-jk_z z'} \right\} \tag{2.48}$$

$$\bar{F}_m^{inc}(z') = < w_m(\bar{\rho}) , \hat{h}(\bar{\rho}) \times \bar{f}^{inc}(\bar{\rho},z') > \tag{2.49}$$

For an infinite structure, the convolution operator $\bar{\bar{K}}_\infty(z,z')$ determines the current at the observation point z due to a delta function source of strength $\bar{f}^{inc}(\bar{\rho},z')$ at the location z'. The formulation of the problem using the convolution integral is still exact as long as the representation of the delta source kernel $\bar{\bar{K}}_\infty(z,z')$ includes the complete mode properties of the structure, these being the discrete mode contributions as well as the continuous mode spectra. However, the transmission line theory assumes that all currents on the cylindrical structure can be represented in terms of forward and reverse exponential traveling waves only, the continuous mode spectra required for a complete solution being neglected. Thus, using the theory developed in section 2.3, the convolution operator $\bar{\bar{K}}_\infty(z,z')$ will be approximated as

$$\bar{\bar{K}}_\infty(z,z') = [\bar{T}][2\bar{\bar{Z}}_C]^{-1}[\bar{\bar{D}}(z,z')][\bar{Q}]^{-1} \tag{2.50}$$

where the transforms $\bar{T}$ and $\bar{Q}$ were given in (2.37,2.42), and the characteristic impedances of the guided wave structure $\bar{\bar{Z}}_C$ were given by (2.36). The diagonal matrix $\bar{\bar{D}}(z,z')$ is given as

$$\bar{\bar{D}}_{ij}(z,z') = \begin{cases} e^{+jk_z^p |\, z-z'\,|} & , i=j=p \\ 0 & , i\neq j \end{cases} \tag{2.51}$$

where k_z^p , $p=1,2,...,P$ are the possible characteristic propagating modes of the two-dimensional structure. The solution of the equivalent currents using (2.47) is more complete than the form (2.38) of the previous section. In (2.38), only the discrete mode contributions of the source $\bar{\tilde{f}}^{inc}$ is considered, whereas (2.47) allows the full

spectral representation of the source, with only the resulting induced currents assumed to have an exponential behaviour. The scattered fields can be determined using (2.30), or as in the previous section for only the discrete mode contribution using (2.43).

The formulation presented in (2.47-2.51) can be generalized to a transmission line configuration of finite length and with arbitrary boundary conditions at its terminals. If the propagation constants k_z^p and the characteristic impedances $\overline{\overline{Z}}_C$ of the structure are known, this is accomplished by modifying the the convolution operator $\overline{\overline{K}}_\infty(z,z')$ to the specific finite transmission line considered and formulating the convolution integral as

$$\overline{g}(\overline{\rho},z) = \int_L [x(\overline{\rho})]^t [\,\overline{\overline{K}}_L(z,z')\,][\,\overline{F}^{inc}(z')\,]\,dz' \quad ; z \in L \tag{2.52}$$

where the path L is along the axial length of the structure and $\overline{\overline{K}}_L(z,z')$ is the modified convolution operator. Using (2.6) and (2.52), the fields can also be determined for the structure. Once the currents are formulated for all guiding structures in a larger problem, they can be embedded into a network of interconnected transmission lines and the whole problem solved simultaneously [Legro, King4, Kami]. As mentioned in section 2.3, the presented transmission line theory, which assumes only the discrete mode contributions, will be an exact formulation for closed guiding structures, and also a very accurate approximation in many cases of open guiding structures.

2.4.1. Quasi-TEM Approximation

The formulation of the transmission line approach presented by (2.47-2.52) determined the currents and fields in terms of the full set of discrete exponential modes for the structure. The propagation constants k_z^p were solutions of the exact two-dimensional wave equations which were satisfied in each region V_i of the problem geometry and were determined from the eigenvalues of the homogeneous mode equation (2.34). The solution of the mode equation yielded the full set of all possible discrete modes, which may consist of TEM, TM, TE, and hybrid forms. In general however, solution of the exact mode equation (2.34) may be difficult to evaluate, and for many problems, the use of a smaller subset of the full set of discrete modes may be adequate to represent the problem. This chosen smaller subset will usually consist of only the dominant modes of the structure, for many cases of guided wave structures these being the TEM transmission line modes.

In the quasi-TEM approximation, the propagation constants k_z^p and the characteristic impedances $\overline{\overline{Z}}_{Cp}$ are determined from the equivalent circuit parameters of the transmission line. These per unit length circuit parameters are then derived by assuming the axial variation of the fields in the solution of the wave equations (2.9) is equal to the wavenumber of the medium in which the guiding structure is embedded ($k_z \approx k_i$) [Coleman, Olsen7]. In this manner, the fields in the supporting medium will be a solution of the two-dimensional Laplace equation. The quasi-TEM approximation is

applicable where the dimensions of the guiding structure are much less than the wavelength of the medium in which it is embedded.

2.5. INTEGRAL EQUATION FORMULATION FOR CYLINDRICAL GUIDING STRUCTURES EMBEDDED IN A LAYERED MEDIA

In this section, an integral equation will be developed to determine the currents induced on and the fields scattered by an infinite cylindrical guiding structure embedded in a stratified media. The integral equation is developed from the formulation presented in section 2.2 for general cylindrical guided wave structures. The geometry of the problem under consideration, as shown in figure 2.2, consists of a two-dimensional bounded scatterer representing the infinite cylindrical guiding structure.

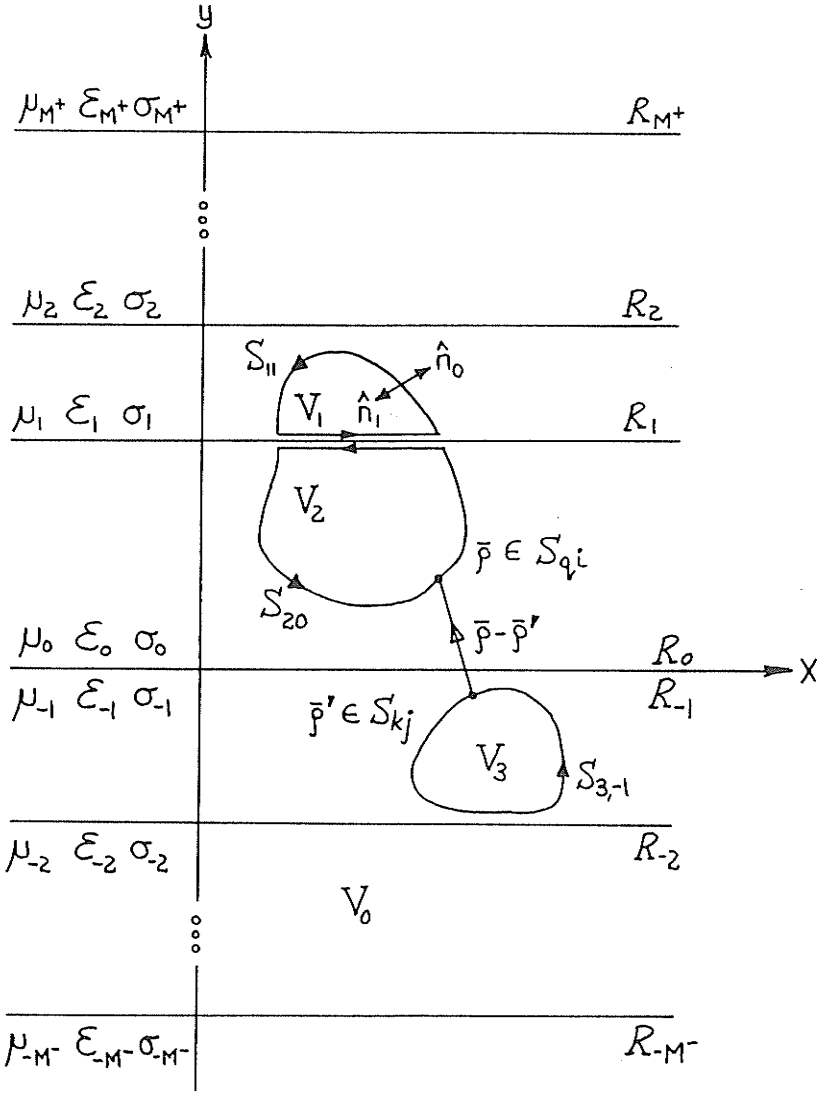

Figure 2.2: Scattering structure embedded in a stratified media.

The problem is divided into $N+1$ regions, the exterior infinite region V_0 and N distinct unconnected subregions V_i. The surface S defining the scattering structure then

consists of N surfaces S_i for each subregion. For cylindrical guiding structures, the N scattering subregions are infinite in extent and chosen to be invariant in the z-dimension. The surfaces S_i of the structure are then defined by the generating curves C_i in the x-y plane as $(\bar{\rho}=\rho(x,y), -\infty<z<\infty)\in S_i$, $\bar{\rho}\in C_i$; $i=1,2,...,N$. The external region V_0 is defined as a layered supporting medium, the stratification being chosen as x-z planes so that the cylindrical guiding structure is parallel to the planar interfaces. The layered media is made up of $M^+ + M^- + 1$ planar regions R_j , $-M^- \le j \le M^+$, where the upper most region R_{M^+} is a half-space and the lower most region R_{M^-} is a half-space. Each layer R_j is characterized by the material electrical constants μ_j, ε_j, σ_j. The defining surface S is divided into distinct subsurfaces, each unique to both a scattering region V_i and a layered region R_j as

$$S = \sum_{i=1}^{N} S_i = \sum_{i=1}^{N} \sum_{j=-M^-}^{M^+} S_{ij} \tag{2.53}$$

Using the formulation developed in section 2.2, the fields in each subregion V_i , $i=0,1,2,...,N$ can be determined using the surface integral equation (2.11) for the region $\bar{r}\in V_i$ as

$$\bar{E}_i(\bar{r}) = \bar{E}_i^{inc}(\bar{r}) + \iint_{S_i} \bar{\bar{G}}_i^{ee}(\bar{r},\bar{r}')\bar{J}(\bar{r}') + \bar{\bar{G}}_i^{em}(\bar{r},\bar{r}')\bar{M}(\bar{r}')\, d\bar{r}' \tag{2.54a}$$

$$\bar{H}_i(\bar{r}) = \bar{H}_i^{inc}(\bar{r}) + \iint_{S_i} \bar{\bar{G}}_i^{me}(\bar{r},\bar{r}')\bar{J}(\bar{r}') + \bar{\bar{G}}_i^{mm}(\bar{r},\bar{r}')\bar{M}(\bar{r}')\, d\bar{r}' \tag{2.54b}$$

where in (2.54) the fields and currents are defined as

$$\bar{f}(\bar{r}) = (\bar{E}(\bar{r}),\bar{H}(\bar{r}))^t \quad , \quad \bar{g}(\bar{r}) = (\bar{J}(\bar{r}),\bar{M}(\bar{r}))^t \tag{2.55}$$

At the surfaces $\bar{r}\in S_i$

$$\bar{J}(\bar{r}) = \hat{n}_i(\bar{r})\times\bar{H}_i(\bar{r}) \quad , \quad \bar{M}(\bar{r}) = -\hat{n}_i(\bar{r})\times\bar{E}_i(\bar{r}) \tag{2.56}$$

are the equivalent electric and magnetic surface currents representing the tangential components of the fields at the boundary of the region V_i, with $\hat{n}_i(\bar{r})$ being the inward unit normal vector at the boundary. The tensor Green's functions $\bar{\bar{G}}_i(\bar{r},\bar{r}')$ for each region V_i are appropriately chosen so that the wave equation is satisfied and all fields are continuous across internal media discontinuities. Formulating the fields in terms of the electric $\bar{\Pi}_i^e$ and magnetic $\bar{\Pi}_i^m$ Hertz vector potentials, The Green's functions can be deduced by solving the set of differential equations

$$[\nabla^2 + k_i^2(\bar{r})]\,\bar{\Pi}_i^e(\bar{r}) = \frac{-j\omega\mu_i}{k_i^2}\bar{J}(\bar{r})\delta(\bar{r}-\bar{r}') \quad ; \bar{r}\in V_i \ , \ \bar{r}'\in S_i \tag{2.57a}$$

$$[\nabla^2 + k_i^2(\bar{r})]\,\bar{\Pi}_i^m(\bar{r}) = \frac{-j\omega\varepsilon_i'}{k_i^2}\bar{M}(\bar{r})\delta(\bar{r}-\bar{r}') \quad ; \bar{r}\in V_i \ , \ \bar{r}'\in S_i \tag{2.57b}$$

$$\bar{E}_i(\bar{r}) = \nabla\nabla\cdot\bar{\Pi}_i^e(\bar{r}) + k_i^2\bar{\Pi}_i^e(\bar{r}) + \frac{k_i^2}{-j\omega\varepsilon_i'}\nabla\times\bar{\Pi}_i^m(\bar{r}) \tag{2.58a}$$

$$\bar{H}_i(\bar{r}) = \nabla\nabla\cdot\bar{\Pi}_i^m(\bar{r}) + k_i^2\bar{\Pi}_i^m(\bar{r}) + \frac{k_i^2}{+j\omega\mu_i}\nabla\times\bar{\Pi}_i^e(\bar{r}) \tag{2.58b}$$

as discussed in appendix A. The wavenumber $k_i = \omega\sqrt{\mu_i\varepsilon_i'}$ in each region V_i is defined by the permeability μ_i and a complex permittivity $\varepsilon_i' = \varepsilon_i + j\sigma_i/\omega$ In general, each region V_i may be inhomogeneous, but if the material discontinuities are regular and coincide with a known orthogonal coordinate system, the solution of (2.57) can be found in a closed or integral form. Such is the case with a planar layered media as the supporting region V_0. Since the geometry of the cylindrical guiding structure is invariant in the z-dimension and the layered supporting media is invariant in the x-z dimensions, the two-dimensional cartesian integral transform will be utilized for the the solution of (2.57) as

$$x(\bar{r},\bar{r}') = \Gamma_z^{-1}\Gamma_x^{-1}\{\{\tilde{\bar{x}}(k_x,y,y',k_z)\}\} \tag{2.59}$$

Details are discussed in appendix A, with the solution for various geometry types described in appendix B.

Matching the boundary conditions at the interfaces between the external region V_0 and the N cylindrical scatterers yields a set of integral equations in terms of the unknown equivalent currents. Using the general form (2.11), a set of integral equations determining the currents $(\bar{J}(\bar{r}),\bar{M}(\bar{r}))^t$ are given as

$$\hat{n}_0(\bar{r})\times\left[(\bar{E}_0^{inc}(\bar{r}),\bar{H}_0^{inc}(\bar{r}))^t + \sum_{k=1}^{N}\sum_{j=-M^-}^{M^+}\iint_{S_{kj}}\bar{\bar{G}}_0^{ij}(\bar{r},\bar{r}')(\bar{J}(\bar{r}'),\bar{M}(\bar{r}'))^t\,d\bar{r}'\right]$$
$$= \hat{n}_0(\bar{r})\times\left[(\bar{E}_q^{inc}(\bar{r}),\bar{H}_q^{inc}(\bar{r}))^t + \iint_{S_q}\bar{\bar{G}}_q^{ij}(\bar{r},\bar{r}')(\bar{J}(\bar{r}'),\bar{M}(\bar{r}'))^t\,d\bar{r}'\right] \tag{2.60}$$
$$; \bar{r}\in S_{qi} \quad , -M^-\le i\le M^+ \quad , q=1,2,...,N$$

The set of integral equations is enough to uniquely define the unknown surface currents. As well, since the incident field quantities $\bar{E}_i^{inc}(\bar{r})$ and $\bar{H}_i^{inc}(\bar{r})$ are not independent, chosing different linear combinations of the sets of equations is possible, and useful near resonant conditions. For bodies S_q which are perfectly conducting, the tangential electric field and equivalent magnetic surface currents are zero; $-\hat{n}_0\times\bar{E}(\bar{r}) = +\bar{M}(\bar{r}) = 0\ ;\bar{r}\in S_q$, yielding two separate sets of equations that can be solved.

In the integral equation (2.60), the Green's functions $\bar{\bar{G}}_q(\bar{r},\bar{r}')\ , q=1,2,...,N$ satisfy the differential equations (2.57) for the internal regions V_q. For homogeneous scatterers, $\bar{\bar{G}}_q(\bar{r},\bar{r}')$ can be deduced from the primary fields derived in appendix A,

this being the free space dyadic Green's function [Harrington1,p.120]. For complex inhomogeneous media, an alternative solution is required. In the external plane layered media V_0, the appropriate Green's function $\overline{\overline{G}}_0^{ij}(\bar{r},\bar{r}')\,;\bar{r}\in R_i\ ,\bar{r}'\in R_j$, represents the fields in the region R_i due to a source located in the region R_j. In the integral equation (2.60), this corresponds specifically to $\bar{r}\in S_{qi}$ and $\bar{r}'\in S_{kj}$. The tensor Green's function is derived by solving the wave equations (2.57) in each layered region in terms of the electric and magnetic Hertz potential vectors as

$$\overline{\overline{G}}_0^{ij}(\bar{r},\bar{r}') = \begin{bmatrix} \overline{\overline{G}}^{ij(ee)}(\bar{r},\bar{r}') & \overline{\overline{G}}^{ij(em)}(\bar{r},\bar{r}') \\ \overline{\overline{G}}^{ij(me)}(\bar{r},\bar{r}') & \overline{\overline{G}}^{ij(mm)}(\bar{r},\bar{r}') \end{bmatrix} = \mathrm{F}_i\left\{\overline{\Pi}_i^e(\bar{r}),\overline{\Pi}_i^m(\bar{r})\right\} \quad (2.61)$$

where $\bar{r}\in R_i$ and $\bar{r}'\in R_j$ for $-M^-\le i,j\le M^+$. The individual elements of the tensor (2.61) are given as

$$\begin{aligned} G_{\alpha\beta}^{ij(ee)}(\bar{r},\bar{r}') &= \left[\ \nabla\nabla\cdot\overline{\Pi}_i^e(\bar{r}) + k_i^2\overline{\Pi}_i^e(\bar{r})\ \right]\cdot\hat{u}_\alpha \\ G_{\alpha\beta}^{ij(em)}(\bar{r},\bar{r}') &= \left[\ \frac{+j\omega\mu_i}{k_i^2}\nabla\times\overline{\Pi}_i^m(\bar{r})\ \right]\cdot\hat{u}_\alpha \\ G_{\alpha\beta}^{ij(me)}(\bar{r},\bar{r}') &= \left[\ \frac{-j\omega\varepsilon_i'}{k_i^2}\nabla\times\overline{\Pi}_i^e(\bar{r})\ \right]\cdot\hat{u}_\alpha \\ G_{\alpha\beta}^{ij(mm)}(\bar{r},\bar{r}') &= \left[\ \nabla\nabla\cdot\overline{\Pi}_i^m(\bar{r}) + k_i^2\overline{\Pi}_i^m(\bar{r})\ \right]\cdot\hat{u}_\alpha \end{aligned} \quad (2.62)$$

for all $\alpha\in(x,y,z)$ and $\beta\in(x,y,z)$. $\overline{\Pi}_i^e(\bar{r})$ and $\overline{\Pi}_i^m(\bar{r})$ are solutions of the set of wave equations for $\bar{r}'\in R_j$

$$\left.\begin{aligned} [\nabla^2+k_i^2]\,\overline{\Pi}_i^e(\bar{r}) &= \frac{-j\omega\mu_j}{k_j^2}\delta(\bar{r}-\bar{r}')\hat{u}_\beta \\ [\nabla^2+k_i^2]\,\overline{\Pi}_i^m(\bar{r}) &= \frac{-j\omega\varepsilon_j'}{k_j^2}\delta(\bar{r}-\bar{r}')\hat{u}_\beta \end{aligned}\right\};\ \bar{r}\in R_i\ ,\ -M^-\le i\le M^+ \quad (2.63)$$

subject to the appropriate boundary conditions at the interfaces between the regions. Note that the source terms in (2.63) are zero if $i\neq j$. A solution to the set of partial differential equations (2.63) is given in appendix A, along with the resulting Green's functions for a layered supporting medium. The formulations presented are valid for both finite and two-dimensional bounded scattering objects embedded in a layered medium. For cylindrical guiding structures, the geometry of both the external stratified medium and the guiding structure are invariant in one dimension. Utilizing the Fourier transform pair defined in section 2.2 (2.12), the set of surface integral equations (2.60) can be transformed into a set of contour integral equations as done in (2.13). Thus, the set of integral equations for cylindrical guiding structures can be solved in the transformed domain as

$$\hat{h}_T(\bar{\rho})\times\Big[\ (\bar{\bar{E}}_0^{inc}(\bar{\rho},k_z),\bar{\bar{H}}_0^{inc}(\bar{\rho},k_z))^t + \sum_{k=1}^{N}\sum_{j=-M^-}^{M^+}\int_{C_{kj}}\bar{\bar{\bar{G}}}_0^{ij}(\bar{\rho},\bar{\rho}',k_z)(\bar{\bar{J}}(\bar{\rho}',k_z),\bar{\bar{M}}(\bar{\rho}',k_z))^t\ d\bar{\rho}'\ \Big]$$
$$= \hat{h}_T(\bar{\rho})\times\Big[\ (\bar{\bar{E}}_q^{inc}(\bar{\rho},k_z),\bar{\bar{H}}_q^{inc}(\bar{\rho},k_z))^t + \int_{C_q}\bar{\bar{\bar{G}}}_q^{ij}(\bar{\rho},\bar{\rho}',k_z)(\bar{\bar{J}}(\bar{\rho}',k_z),\bar{\bar{M}}(\bar{\rho}',k_z))^t\ d\bar{\rho}'\ \Big] \qquad (2.64)$$
$$;\ \bar{\rho}\in C_{qi}\quad,\ -M^-\le i\le M^+\ ,\ q=1,2,...,N\quad,\quad -\infty<k_z<\infty$$

where the contour of integration is defined by the generating curve $C\in\bar{\rho}$ and $\hat{h}_T$ is the unit inward normal to the region V_0 along C and transverse to the z-axis. All fields and currents have an $\exp\{+jk_z z\}$ dependence in the axial dimension, with the resulting set of wave equations (2.63) now being defined in two-dimensional form for $\bar{\rho}'\in R_j$ as

$$\left.\begin{aligned}[\nabla_T^2-(k_z^2-k_i^2)]\,\bar{\bar{\Pi}}_i^e(\bar{\rho},k_z) &= \frac{-j\omega\mu_j}{k_j^2}\delta(\bar{\rho}-\bar{\rho}')\hat{u}_\beta\\ [\nabla_T^2-(k_z^2-k_i^2)]\,\bar{\bar{\Pi}}_i^m(\bar{\rho},k_z) &= \frac{-j\omega\varepsilon_j'}{k_j^2}\delta(\bar{\rho}-\bar{\rho}')\hat{u}_\beta\end{aligned}\right\};\ \bar{\rho}\in R_i\ ,\ -M^-\le i\le M^+ \qquad (2.65)$$

where ∇_T is the transverse differential operator. Solutions to the set of wave equations in (2.65) are given in appendix A.

2.6. WAVE PROPERTIES OF CYLINDRICAL GUIDED WAVE STRUCTURES EMBEDDED IN A STRATIFIED MEDIUM

The specific geometries considered in this thesis consist of a planar layered media (symmetric in two dimensions) in which a guiding wave structure (symmetric in one dimension) is embedded. One of the symmetry dimensions of the planar media is chosen to coincide with that of the guiding structure, so that the entire problem geometry is invariant in one dimension. Chosing the invariant dimension to be along the z-axis, the fields $\bar{f}(\bar{r})$ and currents $\bar{g}(\bar{r})$ were determined using the Fourier transformation as

$$\bar{g}(\bar{r}) = \Gamma_z^{-1}\left\{\bar{\tilde{g}}(\bar{\rho},k_z)\right\} = \Gamma_z^{-1}\left\{[x(\bar{\rho})]^t[\bar{\bar{Z}}(k_z)]^{-1}[\bar{F}^{inc}(k_z)]\right\} \qquad (2.66)$$

$$\bar{f}_i(\bar{r}) = L_i^{-1}\left\{\bar{g}(\bar{r})\right\} = \Gamma_z^{-1}\left\{\tilde{L}_i^{-1}\{\bar{\tilde{g}}(\bar{\rho},k_z)\}\right\} \qquad (2.67)$$

where the transform pair Γ_z , Γ_z^{-1} was defined in (2.12). Thus, the equivalent currents induced on the guiding structure surface depends on the excitation by a specified source $\bar{F}^{inc}(k_z)$ and the effect of the geometry of the structure, which is represented

through $\overline{\overline{Z}}(k_z)$. Both the incident fields due to the source $\overline{g}_s(\overline{r})$ as well as the scattered fields due to the surface currents $\overline{g}(\overline{r})$ are determined from the form (2.67). Each of the problem geometry types is capable of supporting its own class of wave properties, their combination exhibiting the properties of both as well as some new ones. These wave properties will present themselves in the transforms (2.66,2.67) through branch cuts and poles in the complex spectral domain. A detailed discussion is given in chapter three with regards to thin-wire structures over a single lossy interface [Chang3, Kuester4], as well as in appendix B, which concentrates on the evaluation techniques of these transforms. Also, Examination of the far field behaviour of the fields will give insight into their wave properties [Collin, Felsen].

The specific wave properties present in the structures studied can be discussed by examining the spectral domain for each geometry type. In cartesian coordinates, the field or current quantities can be described as a weighted sum of plane waves having a dependence $\exp[+j\overline{k}_R\cdot\overline{R}] = \exp[+jk_x x + jk_y y + jk_z z]$ where $|\overline{k}_R| = \sqrt{k_x^2+k_y^2+k_z^2} = k_i$ is the wavenumber in the medium i. The inverse transformations (2.66), with respect to k_z, will contain several sets of branch cuts as well as a set of poles in the complex k_z plane as shown in figure 2.3. The contributions from the branch cuts arise from two sources. The first is due to the enforcement of the radiation condition, where the fields must decay as $|\overline{R}| \to \infty$. For a planar layered geometry, this specifies that the fields must decay in the upper most half-space k_{+M^+} for $y \to +\infty$, $|x| \to \infty$, and in the lower most half-space k_{-M^-} for $y \to -\infty$, $|x| \to \infty$, thus defining the irrationals $\mathrm{Im}[\sqrt{k_x^2+k_y^2}] = \mathrm{Re}[\sqrt{k_z^2-k_{\pm M^{+-}}^2}] \geq 0$. This results in the branch cuts in the k_z plane emanating from $k_z = \pm k_{+M^+}, \pm k_{-M^-}$ representing the spectrum of radiated fields.

The remaining branch cuts arise from the TM and TE surface waves which can be supported by the layered geometry. Representing the fields and currents in terms of radial waves along the interface as $\exp[\overline{k}_R\cdot\overline{R}] = \exp[\overline{\lambda}\cdot\overline{\rho}]\exp[+jk_y y]$ where $|\overline{\lambda}| = \sqrt{k_x^2+k_z^2}$, the surface waves are found for specific values of the radial wavenumber λ_{Bs} ; $s=1,2,...,S$. For each surface wave, the propagation constant in the direction perpendicular to the layered media is fixed $k_{yBs} = +j\sqrt{\lambda_{Bs}-k_i^2}$. Since the surface waves must decay in the radial direction $|x| \to \infty$, a set of branch cuts, due to the irrationals $\mathrm{Im}[k_{xBs}] = \mathrm{Re}[\sqrt{k_z^2-\lambda_{Bs}^2}] \geq 0$, in the k_z plane emanating from $k_z = \pm\lambda_{Bs}$ represents the spectrum of surface waves.

Finally, a set of poles is present in the k_z plane, indicated as k_z^p ; $p=1,2,...,P$. The poles represent the characteristic propagating modes supported by the guiding wave structure and are found from the homogeneous solutions ($\overline{f}^{inc}=0$) of the two-dimensional integral equation (2.15), these also being the zeros of $\overline{\overline{Z}}(k_z)$ in (2.34) ($|\overline{\overline{Z}}(k_z^p)| = 0$). As well as the presence of the surface wave branch cuts and poles on the proper Riemann surfaces defined for fields decaying as $|\overline{R}| \to \infty$, there may also be surface wave branch cuts and poles on any of the improper Riemann surfaces.

Their contributions give rise to leaky wave fields which can be extracted in the far field analysis of the geometry as discussed in appendix B [Felsen, Tamir1].

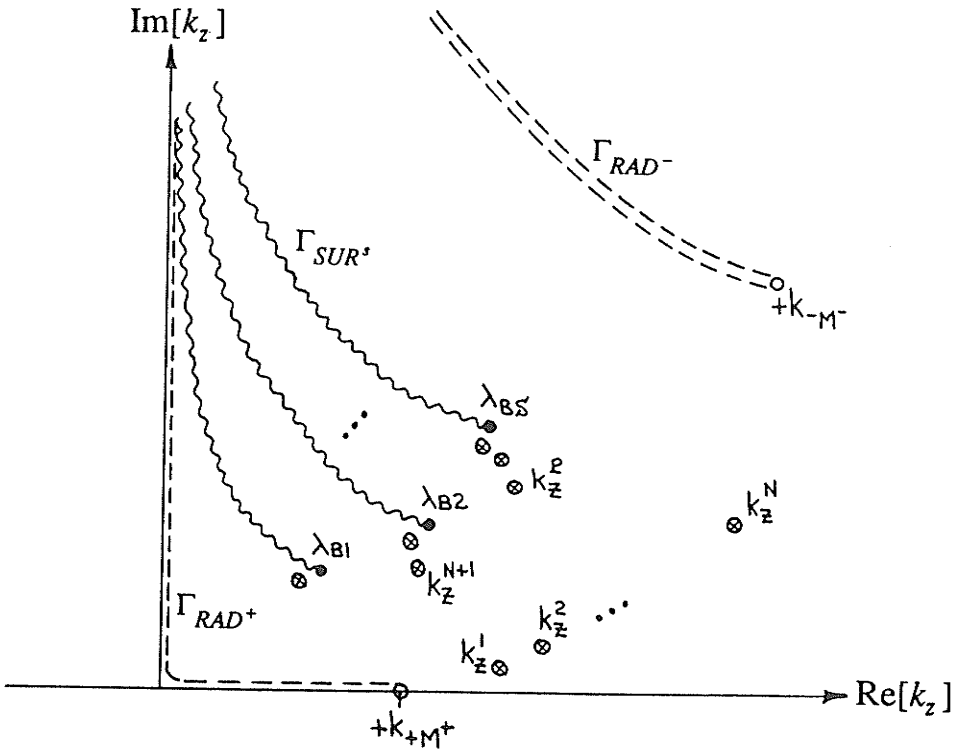

Figure 2.3: Branch cuts and poles in the complex k_z domain.

Chapter 3
Excitation of Multiple Conductor Structures Above a Lossy Half-Space

In this chapter, problems associated with thin-wire multiple conductor systems (transmission lines) located over a homogeneous lossy earth are studied. This is a special case of the general problem of an arbitrary shaped cylindrical structure embedded in a stratified media, as presented in section 2.5. The study of this special case has many applications in power transmission, electromagnetic compatibility and remote sensing studies, and antenna design. To this extent, *circular* conductors which adhere to the thin-wire condition, as well as being assumed to be good conductors at all the frequencies considered will be concentrated on in this chapter. The problem will be formulated directly from the general solution presented in chapter 2, which was based on a spectral domain approach. The final solution will thus be in terms of an integral transform. The excitation of the structure by arbitrarily oriented electric or magnetic dipole sources located in the upper half-space as well as by delta function voltage sources located along the conductor axis are considered. This makes the formulation applicable to many desired excitations. Next, the wave properties supported by this geometry will be presented, and from this discussion, various methods of approximating the integral transform will be deduced.

A numerical study of various transmission line geometries for typical earth electrical properties is then presented. Special attention is paid to the characterization of the discrete mode properties of the structure and to the validity of various far field and near field approximation methods. Some interesting features regarding additional discrete modes of propagation, in addition to the traditional quasi-TEM type modes, are identified, and the use of an improved small-argument approximation for the mode equation is discussed. As well, conditions are specified under which the discrete mode and saddle point approximation methods are valid. The latter is especially important in electromagnetic pulse studies, where the incident field due to the Compton electron source region is usually modeled as a plane wave.

Since the geometry tackled in this chapter has been under investigation for decades, many of the specific applications presented have previously been addressed throughout the literature. The purpose of this work is to present a unified approach to the solution of all possible cases encountered in wire over half-space problems. To this extent, all formulations, both exact and approximate, can be traced directly back to

Maxwell's equations, allowing their physical significance to be examined. As well, the approximate methods are compared to the results of the exact solution in all cases. The properties and techniques developed in this chapter for evaluating the single interface case can then be applied to more general situations, such as multiple layered media, and arbitrary shaped conductors which do not adhere to the thin-wire conditions.

3.1. INTEGRAL EQUATION FORMULATION

Consider a set of N infinite conductors of arbitrary shape located above and parallel to a lossy homogeneous interface as shown in figure 3.1. The region $y>0$ is considered to be free space, characterized by a permittivity ε_e and a permeability μ_e. The region $y<0$ is designated as the lossy earth, characterized by a permittivity ε_g, a permeability μ_g, and a conductivity σ_g. The N conductor geometries are defined by the generating contours $C_n(\bar{\rho})$; $n=1,2,...N$ which are chosen to be invariant in the z-dimension, this then creating the surface $S = \Sigma S_n$. The electrical properties of each of the conductors are characterized by a permittivity ε_n, a permeability μ_n, and a conductivity σ_n. It is required to determine the induced currents on the transmission line structure due to a specified excitation, which can be located exterior to the conductors in the upper medium, or internal to the conductors.

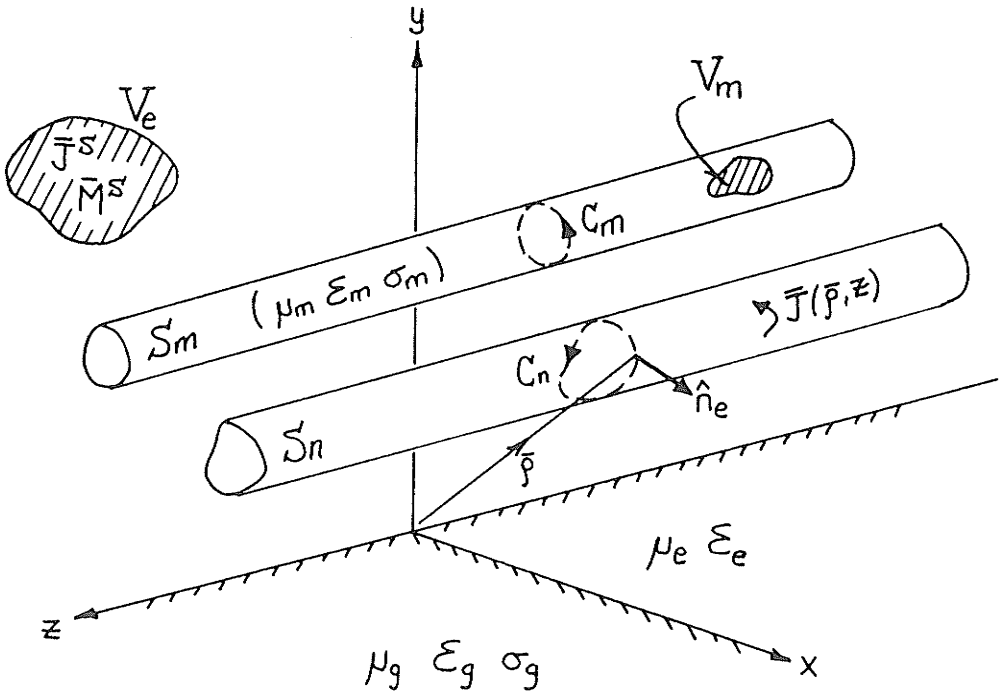

Figure 3.1: Transmission line structure above a lossy half-space.

The solution of the problem is facilitated by solving the wave equation in each media region (the conductors and upper and lower half-spaces) and satisfying the boundary conditions at their interfaces. The problem considered is a special case of the general multiple stratified media geometry formulated in section 2.5, where the number of layers is given as $M^{+}=0$ and $M^{-}=1$, with the region $i=0$ corresponding to the air medium (e) and the region $i=-1$ corresponding to the earth medium (g). A solution can thus be determined from the integral equation form (2.64). If the conductors of the transmission line structure are all considered to be good conductors $(\sigma_n \gg \omega\varepsilon_n)$, the electric current $\bar{J}$ on the surface S will dominate the contribution to the fields. Further, since all the conductors of the structure are located in the upper half-space, only the Green's function $\bar{\bar{G}}_e=\bar{\bar{G}}_e^{ee(ee)}$ is required. A solution can then be determined in terms of the integral equation (2.60) by matching the tangential fields at the N conductor surfaces as

$$\hat{h}_e(\bar{r})\times\left[\bar{E}_e^{inc}(\bar{r})+\sum_{n=1}^{N}\iint_{S_n}\bar{\bar{G}}_e(\bar{r},\bar{r}')\bar{J}(\bar{r}')d\bar{r}'\right] \tag{3.1}$$

$$=\hat{h}_e(\bar{r})\times\left[\bar{E}_m^{inc}(\bar{r})+\iint_{S_m}\bar{\bar{G}}_m(\bar{r},\bar{r}')\bar{J}(\bar{r}')d\bar{r}'\right] \quad ;\bar{r}\in S_m \quad ;m=1,2,...N$$

where $\hat{h}_e(\bar{r})$ is the unit normal to the surface S at $\bar{r}$. This is simply the electric field integral equation which must be satisfied over the infinite length of the conductor[3.1]. $\bar{J}(\bar{r})$ is the induced electric current on the surface of the structure which is to be determined by solving the integral equation. The Green's function $\bar{\bar{G}}_e(\bar{r},\bar{r}')$ is formulated to take into account the effect of the lossy planar interface and is defined in appendix A from the fields of an arbitrarily oriented current element (A.86-A.88). The Green's function $\bar{\bar{G}}_m(\bar{r},\bar{r}')$ is simply the homogeneous space Green's function incorporating the appropriate electrical characteristics of the mth conductor medium. $\bar{E}_e^{inc}(\bar{r})$ is the incident field defined at the conductor surfaces S due to external sources located in the upper half-space and $\bar{E}_m^{inc}(\bar{r})$ is the incident field at the conductor surface S_m due to sources internal to the conductor m. The incident fields are determined from the given volume source distributions V_e, V_m as

$$\bar{E}_e^{inc}(\bar{r})=\int_{V_e}\bar{\bar{G}}_e^{(ee)}(\bar{r},\bar{r}')\bar{J}^S(\bar{r}')+\bar{\bar{G}}_e^{(em)}(\bar{r},\bar{r}')\bar{M}^S(\bar{r}')d\bar{r}' \quad ;\bar{r}\in S\ ,\bar{r}'\in V_e \tag{3.2a}$$

$$\bar{E}_m^{inc}(\bar{r})=\int_{V_m}\bar{\bar{G}}_m^{(ee)}(\bar{r},\bar{r}')\bar{J}^S(\bar{r}')+\bar{\bar{G}}_m^{(em)}(\bar{r},\bar{r}')\bar{M}^S(\bar{r}')d\bar{r}' \quad ;\bar{r}\in S_m\ ,\bar{r}'\in V_m \tag{3.2b}$$

Thus, the incident field is determined through a sum of elementary delta function

3.1 For a general guiding structure consisting of conductors having arbitrary material properties, both electric and magnetic equivalent surface currents are required to satisfy the continuity of fields at the conductor-supporting media interface. This requirement will partially be fulfilled by satisfying the continuity of the *primary* fields of the thin-wire conductor in the half-space problem as discussed in section 3.2.1.

sources weighted by the current distribution.

As in section 2.5, when the physical geometry of the conductor-half-space problem is invariant with respect to the z-dimension, a solution to the integral equation can be obtained in the spectral domain by utilizing the spacial Fourier transform pair

$$f(k_z) = \int_{-\infty}^{\infty} \mathrm{f}(z) e^{-jk_z z}\, dz \quad , \quad \mathrm{f}(z) = \frac{1}{2\pi} \int_{-\infty}^{\infty} f(k_z) e^{+jk_z z}\, dk_z \tag{3.3}$$

The integral equation (3.1) can then be solved as a two-dimensional problem as

$$\hat{n}_e(\bar{\rho}) \times \left[\bar{\bar{E}}_e^{inc}(\bar{\rho},k_z) + \sum_{n=1}^{N} \int_{C_n} \bar{\bar{G}}_e(\bar{\rho},\bar{\rho}',k_z) \bar{J}(\bar{\rho}',k_z) d\bar{\rho}' \right]$$

$$= \hat{n}_e(\bar{\rho}) \times \left[\bar{\bar{E}}_m^{inc}(\bar{\rho},k_z) + \int_{C_m} \bar{\bar{G}}_m(\bar{\rho},\bar{\rho}',k_z) \bar{J}(\bar{\rho}',k_z) d\bar{\rho}' \right] \tag{3.4}$$

$$; \bar{\rho} \in C_m \quad ; \quad m=1,2,...N \quad , \quad -\infty < k_z < \infty$$

where all fields and currents are now assumed to have an axial dependence of the form $e^{+jk_z z - j\omega t}$. The path of integration in the integral equation (3.4) is now over the generating curve C.

3.2. THIN-WIRE APPROXIMATION

A solution to the integral equation (3.4) determining the induced surface current $\bar{J}(\bar{\rho},k_z)$ can be obtained using a standard method of moments approach as described in section 2.2. In this manner, the current on the structure is expanded in terms of some chosen basis as

$$\bar{J}(\bar{\rho},k_z) = \sum_{n=1}^{N} x_n(\bar{\rho}) \bar{I}_n(k_z) \tag{3.5}$$

where $x_n(\bar{\rho})$ is the nth basis function and $\bar{I}_n$ is a scalar constant to be determined. An approximate solution is then obtained by defining a suitable inner product and some testing basis as developed in (2.17-2.22). For the general case of arbitrary shaped conductors, the solution can become complicated considering the evaluation of the Green's functions for the half-space. To simplify the solution, the thin-wire approximation is usually assumed in the majority of engineering problems dealing with wire structures. In the thin-wire approximation, the azimuthal current distribution around the circumference of the conductors is assumed to be uniform and only an axial current component is considered (azimuthal components are assumed negligible). This approximation is valid when the transverse dimensions of the conductors are small compared to the wavelength in the medium in which they are embedded and if the distance from all other discontinuities (such as the air-earth interface or other conductors) is large compared to each of the conductor dimensions. This approximation has been the basis of almost all the previous works in solving conductor above half-space problems. Its

validity has been examined in [Chang1, Pogorzelski, Bridges7] and will be the subject of Chapter 5 of this thesis.

The thin-wire approximation will be applied to the general integral equation by specifying the expansion functions in (3.5) to be equivalent to the conductor generating contours $x_n(\bar{\rho}) \alpha C_n$, such that the scalar constants $\bar{I}_n = I_n \hat{z}$ will represent the total axially directed current in each conductor. Since only an axially directed current is assumed $\bar{J}(\bar{\rho}) = J_z(\bar{\rho})\hat{z}$, continuity of only the tangential $\hat{z}$ component of the electric field on the surface S is required and thus only the Green's function component $G_{ezz}(\bar{\rho},\bar{\rho}')$ is used. Using this chosen basis, the integral equation (3.4) can be solved for the E_z component as

$$< w_m(\bar{\rho}), \left[E_{ez}^{inc}(\bar{\rho},k_z) + \sum_{n=1}^{N} \int_{C_n} G_{ezz}(\bar{\rho},\bar{\rho}',k_z) x_n(\bar{\rho}') d\bar{\rho}' I_n(k_z) \right] > \tag{3.6}$$

$$= < w_m(\bar{\rho}), \left[E_{mz}^{inc}(\bar{\rho},k_z) + \int_{C_m} G_{ezz}(\bar{\rho},\bar{\rho}',k_z) x_m(\bar{\rho}') d\bar{\rho}' I_m(k_z) \right] > \quad ; m=1,2,...,N$$

where the basis and testing functions are defined as

$$x_m(\bar{\rho}) = w_m(\bar{\rho}) = \frac{C_m}{\int_{C_m} d\bar{\rho}'} = \frac{C_m}{2\pi a_m} \tag{3.7}$$

and where the last term in (3.7) has been normalized for the special case of a *circular* conductor of radius a_m. Since the basis and weighting function magnitudes are independent of $\bar{\rho}$, the inner product $<w_m, f>$ will now define the *average* value of the quantity f over the transverse dimensions of the conductor m as

$$<f(\bar{\rho},k_z)>_m = < w_m(\bar{\rho}), f(\bar{\rho},k_z) > = \frac{1}{\int_{C_m} d\rho'} \int_{C_m} f(\bar{\rho}',k_z) d\bar{\rho}' \tag{3.8}$$

The set of linear equations resulting from (3.6) can be solved in matrix from as

$$[Z(k_z)][I(k_z)] = [<E_z^S(k_z)>] \tag{3.9}$$

$$[Z(k_z)] = [Z^w(k_z) - Z^e(k_z)] \tag{3.10}$$

$$[<E_z^S(k_z)>] = [<E_z^{ext}(k_z)>] - [<E_z^{int}(k_z)>] \tag{3.11}$$

where $[I(k_z)]$ is the column vector giving the induced current on the conductors. The impedance matrix (3.10) consists of two terms, an external impedance term $[Z^e(k_z)]$ representing the mutual coupling between the conductors (the integral over C_n in (3.6)), and a self impedance term $[Z^w(k_z)]$ representing the conductors surface impedance (the integral over C_m in (3.6)). The incident field $[<E_z^S(k_z)>]$ gives the contributions from the sources in the external region (upper half-space) and from the

sources internal to each conductor.

The current induced on the transmission line can now be determined by solving (3.9) and performing the inverse transform (3.3). Once the currents are determined, the scattered fields can also be calculated as described in section 2.2 (2.30). Thus, the induced currents and scattered fields in the upper half-space are given as

$$[\,I(z)\,] = \frac{1}{2\pi}\int_{-\infty}^{\infty} [\,Z(k_z)\,]^{-1}[<E_z^S(k_z)>]e^{+jk_z z}\,dk_z \tag{3.12}$$

$$\overline{E}_e(\overline{r}) = \overline{E}_e^{inc}(\overline{r}) + \overline{E}_e^{scat}(\overline{r}) \tag{3.13}$$

$$\begin{aligned}\overline{E}_e^{scat}(\overline{r}) &= \frac{1}{2\pi}\int_{-\infty}^{\infty}\sum_{n=1}^{N}\int_{C_n}\overline{\overline{G}}_e(\overline{\rho},\overline{\rho}',k_z)x_n(\overline{\rho}')I_n(k_z)\hat{z}\,d\overline{\rho}'\,e^{+jk_z z}\,dk_z \\ &= \frac{1}{2\pi}\int_{-\infty}^{\infty}[<\overline{G}_{ez}(\overline{\rho},k_z)>][\,Z(k_z)\,]^{-1}[<E_z^S(k_z)>]\,e^{+jk_z z}\,dk_z\end{aligned} \tag{3.14}$$

$$<\overline{G}_{ez}(\overline{\rho},k_z)>_m = \frac{1}{\int_{C_m} d\overline{\rho}'}\int_{C_m}\overline{\overline{G}}_e(\overline{\rho},\overline{\rho}',k_z)\hat{z}\,d\overline{\rho}' \tag{3.15}$$

where the elements of the Green's function $G_{e\alpha z}$; $\alpha\in\{x,y,z\}$ can be deduced from the fields derived in appendix A (A.82-A.84).

3.2.1. Solution for Multiple Conductor Structures

The specific case of a system of N thin circular conductors will be derived as shown in figure 3.2, where a_n is the radius of the conductors, $\overline{\rho}_{mn}$ is the vector from the center of the nth conductor to the mth conductor, and $\overline{\rho}_{mn}^{*}$ is the vector from the nth conductor image to the mth conductor. The derivation of the impedance matrix elements $Z_{mn}^{e}(k_z)$ and $Z_{mn}^{w}(k_z)$, is accomplished by determining the fields external and internal to the nth conductor, which carries a current $I_n(k_z)$. Assuming an axial dependence of the form $e^{+jk_z z}$, the fields can be deduced by solving the two-dimensional wave equation in each of the air and earth half-spaces and inside the conductor region. These can be determined in terms of potential vectors [Stratton] as

$$\begin{aligned}
[\nabla^2 - (k_z^2-k_e^2)]\,\overline{\Pi}^e &= \frac{-j\omega\mu_e}{k_e^2}\frac{I_n(k_z)}{2\pi a_n}\delta(\overline{\rho}-\overline{\rho}')\hat{z} && ;\ y>0\ ,\ |\,\overline{\rho}\,|>a_n \\
[\nabla^2 - (k_z^2-k_g^2)]\,\overline{\Pi}^g &= 0 && ;\ y<0 \\
[\nabla^2 - (k_z^2-k_n^2)]\,\overline{\Pi}^n &= \frac{-j\omega\mu_n}{k_n^2}\frac{I_n(k_z)}{2\pi a_n}\delta(\overline{\rho}-\overline{\rho}')\hat{z} && ;\ y>0\ ,\ |\,\overline{\rho}\,|<a_n
\end{aligned} \tag{3.16}$$

where $\bar{\Pi}^e$, $\bar{\Pi}^g$ and $\bar{\Pi}^n$ are the two-dimensional Hertz vector potentials in the air, earth and conductor regions, respectively. Here $k_e = \sqrt{\omega^2 \mu_e \varepsilon_e}$ is the propagation constant in the air medium, $k_g = \sqrt{\omega^2 \mu_g \varepsilon_g + j\omega\mu_g \sigma_g}$ is the propagation constant in the ground medium, and $k_n = \sqrt{\omega^2 \mu_n \varepsilon_n + j\omega\mu_n \sigma_n}$ is the propagation constant internal to the nth conductor. The associated fields, and thus the Green's functions required for the integral equation (3.6), are determined from

$$\bar{E} = \nabla\nabla\cdot\bar{\Pi} + k^2\bar{\Pi} \quad , \quad \bar{H} = \frac{k^2}{j\omega\mu}\nabla\times\bar{\Pi} \tag{3.17}$$

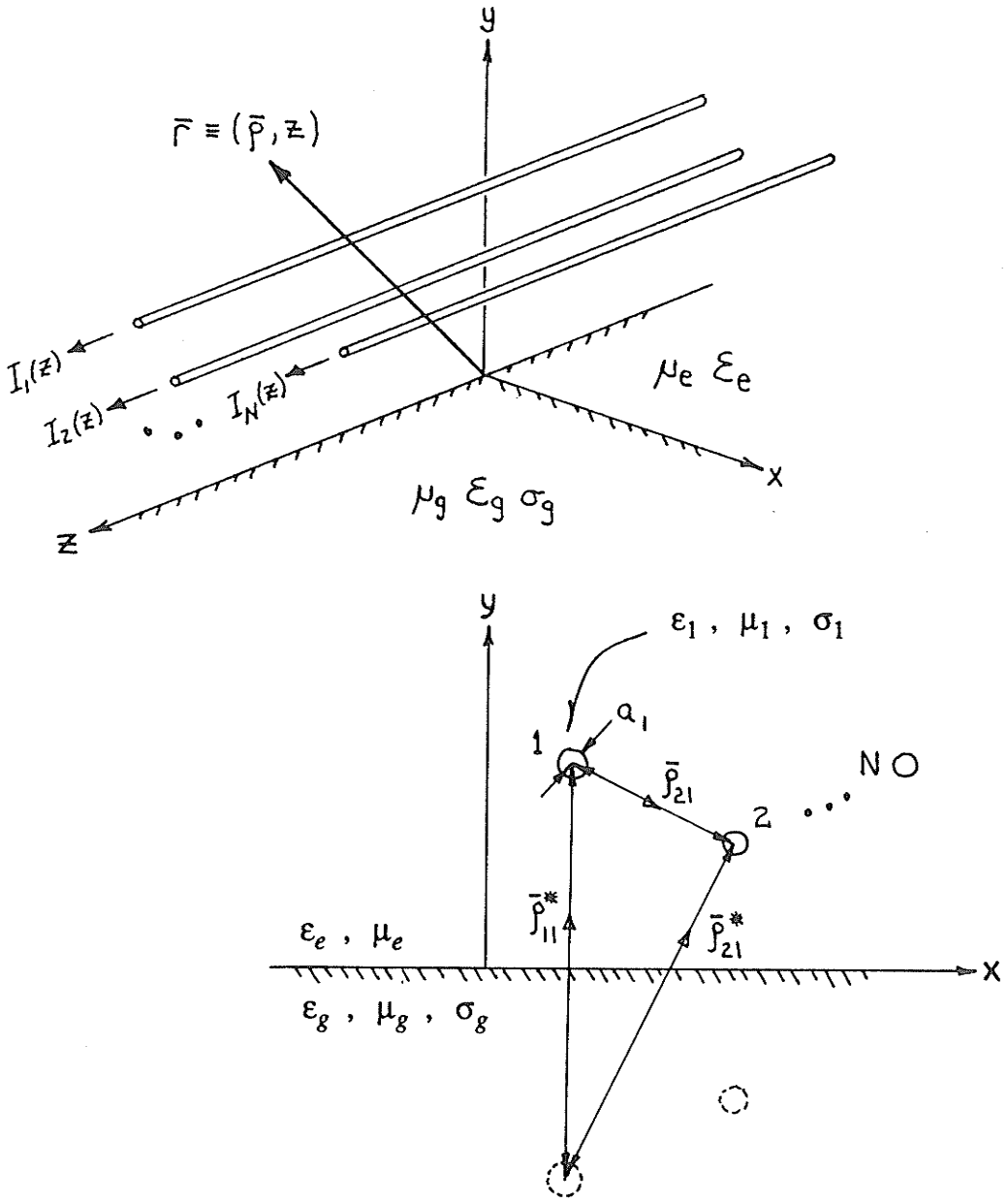

Figure 3.2: Circular thin-wire N-conductor geometry.

A solution to (3.16) is obtained using the usual transform techniques and then satisfying the boundary conditions at the air-earth interface as discussed in appendix A [Wait3, Wait5, Kuester4], as well as at the air-conductor interface [Stratton]. The fields for an electric current source over a half-space are derived in appendix A (A.80-A.85). In the formulation given below, an exact solution of the boundary conditions at the air-conductor interface for the primary fields is derived. Thus, instead of matching only E_z at the conductor surface as done in (3.6), all primary fields of the general TM case are considered. For the secondary fields (reflected off the air-earth interface), only coupling from the E_z component is assumed important. Thus, many different conductor types, not just perfect conductors, can be handled with the formulation by specifying an appropriate surface impedance as detailed latter. In the case of equal air and ground permeabilities ($\mu_g=\mu_e$), the external impedance matrix elements Z^e_{mn} are determined as

$$Z^e_{mn}(k_z) = \begin{cases} A_n \left[\tau_e^2 K_0(\tau_e a_m) - I_0(\tau_e a_m) B_{mn} \right] & , m=n \\ A_n I_0(\tau_e a_m) \left[\tau_e^2 K_0(\tau_e \mid \overline{\rho}_{mn} \mid) - B_{mn} \right] & , m \neq n \end{cases} \tag{3.18}$$

$$A_n = \left[\frac{-j\omega\mu_e}{2\pi k_e^2} \right] \frac{1}{(\tau_e a_n) K_1(\tau_e a_n)}$$

$$B_{mn} = \left[\tau_e^2 K_0(\tau_e \mid \overline{\rho}^*_{mn} \mid) + k_e^2 \mathbf{J}(\tau_e, \overline{\rho}^*_{mn}) - k_z^2 \mathbf{G}(\tau_e, \overline{\rho}^*_{mn}) \right]$$

$$\mathbf{J}(\tau_e, \overline{\rho}^*_{mn}) = \int_{-\infty}^{\infty} \frac{1}{U_e + U_g} e^{-U_e \mid y_n + y_m \mid + j\lambda(x_n - x_m)} \, d\lambda \tag{3.19a}$$

$$\mathbf{G}(\tau_e, \overline{\rho}^*_{mn}) = \int_{-\infty}^{\infty} \frac{1}{n^2 U_e + U_g} e^{-U_e \mid y_n + y_m \mid + j\lambda(x_n - x_m)} \, d\lambda \tag{3.19b}$$

$$U_e = \sqrt{\lambda^2 + \tau_e^2} \quad , \quad U_g = \sqrt{\lambda^2 + \tau_g^2} \quad , \quad \mathrm{Re}[U_e, U_g] \geq 0$$

where $\mid \overline{\rho}_{mn} \mid = \sqrt{(x_n - x_m)^2 + (y_n - y_m)^2}$ and $\mid \overline{\rho}^*_{mn} \mid = \sqrt{(x_n - x_m)^2 + (y_n + y_m)^2}$. Here $\tau_e = \sqrt{k_z^2 - k_e^2}$ and $\tau_g = \sqrt{k_z^2 - k_g^2}$ are the transverse propagation constants in the air and earth media, respectively. The real parts of the irrationals $\mathrm{Re}[U_e, U_g] \geq 0$ and $\mathrm{Re}[\tau_e, \tau_g] \geq 0$ have been chosen to retain a positive value on the correct Riemann sheet. These branch cuts have been defined to ensure that the currents and fields decay at infinity. $I_0(z)$, $K_0(z)$, $K_1(z)$ are modified Bessel functions of complex argument and n is the refractive index of the air-earth interface. In the derivation of (3.18), the terms involving $K_0(\tau_e \mid \overline{\rho}_{mn} \mid)$ are due to the primary field of the current source, and the terms involving $K_0(\tau_e \mid \overline{\rho}^*_{mn} \mid)$ are due to its image as if the earth were perfectly conducting. The remaining terms in integral form, (3.19a) and (3.19b), are the corrections due to the imperfectly conducting earth.

The internal impedance matrix elements Z^w_{mn} can easily be determined for various conductor types such as solid conductors, Goubau lines, wrapped conductors, etc., by specifying the surface impedance for the desired geometry [Wait7, Vance]. For thin solid conductors the internal impedance matrix is defined as [Stratton]

$$Z^w_{mn}(k_z) = \delta_{mn}\left[\frac{+j\omega\mu_n}{2\pi k_n^2}\right]\frac{\tau_n^2 I_0(\tau_n a_n)}{(\tau_n a_n) I_1(\tau_n a_n)} \quad , \quad \delta_{mn} = \begin{cases} 1 & , m=n \\ 0 & , m\neq n \end{cases} \tag{3.20}$$

where $\tau_n = \sqrt{k_z^2 - k_n^2}$ with $k_n = \sqrt{\omega^2\mu_n\varepsilon_n + j\omega\mu_n\sigma_n}$ and $\mu_n, \varepsilon_n, \sigma_n$ are the electrical parameters characterizing the nth conductor. $I_0(z)$, $I_1(z)$ are the modified Bessel functions. If a perfect conductor is assumed, so that the integral equation (3.6) is exact, then the $1/(\tau_e a)K_1(\tau_e a)$ term in (3.18) is replaced by $I_1(\tau_e a)$ and consequently $Z^w = 0$.

The modified Bessel function terms $I_0(\tau_e a_m)$ in (3.18) account for the average circumferential value of the fields over the conductor surfaces as employed in accordance with the thin-wire approximation. Thus, the quantities in brackets $<>$ in (3.11), which denoted the average value of the fields over the transverse dimensions of the conductors, is determined analytically for *circular* conductors from (3.8) as [Abramowitz, Harrington1]

$$<f(\bar{\rho}, k_z)>_m = \frac{1}{2\pi a_m}\int_{C_m} f(\bar{\rho}', k_z)\, d\bar{\rho}' = I_0(\sqrt{k_z^2 - k_e^2}\, a_m) f(\bar{\rho}_m, k_z) \tag{3.21}$$

where a_m is the radius of the mth conductor and $\bar{\rho}_m$ is the position at its center. k_e was defined as the wavenumber in the upper half-space. The induced currents are now given using (3.12) as

$$[\mathrm{I}(z)] = \frac{1}{2\pi}\int_{-\infty}^{\infty} [Z(k_z)]^{-1}[\bar{I}(k_z)][E_z^S(k_z)] e^{+jk_z z}\, dk_z \tag{3.22}$$

$$\bar{I}_{mn}(k_z) = \begin{cases} I_0(\sqrt{k_z^2 - k_e^2}\, a_n) & ; m=n \\ 0 & ; m\neq n \end{cases}$$

As defined by (3.2), the incident field $[E_z^S(k_z)]$ is determined from the integration of the specified volume source distributions V_e, V_m. The source region $V_S = V_e \cup V_m$, combining the external and internal source regions, produce a current

$$[\mathrm{I}(z)] = \int_{V_S}\frac{1}{2\pi}\int_{-\infty}^{\infty} [Z(k_z)]^{-1}[\bar{I}(k_z)][E_z^S(\bar{\rho}_s, k_z)] e^{+jk_z(z-z_s)} dk_z\, d\bar{r}_s \tag{3.23}$$

$$E^S_{zm}(\bar{\rho}_s, k_z) = \left[\bar{\bar{G}}_e^{(ee)}(\bar{\rho}_m, \bar{\rho}_s, k_z)\bar{J}^S(\bar{\rho}_s, z_s) + \bar{\bar{G}}_e^{(em)}(\bar{\rho}_m, \bar{\rho}_s, k_z)\bar{M}^S(\bar{\rho}_s, z_s)\right]\cdot\hat{z}$$
$$- \left[\bar{\bar{G}}_m^{(ee)}(\bar{\rho}_m, \bar{\rho}_s, k_z)\bar{J}^S(\bar{\rho}_s, z_s) + \bar{\bar{G}}_m^{(em)}(\bar{\rho}_m, \bar{\rho}_s, k_z)\bar{M}^S(\bar{\rho}_s, z_s)\right]\cdot\hat{z} \tag{3.24}$$

The Green's function $\overline{\overline{G}}_e(\overline{\rho}_m,\overline{\rho}_s,k_z)$ defines the electric field at the center of the mth conductor $\overline{\rho}_m$ due to the sources $\overline{J}^S$, $\overline{M}^S$ located at $(\overline{\rho}_s,z_s)$ in V_e. The Green's functions $\overline{\overline{G}}_m(\overline{\rho}_m,\overline{\rho}_s,k_z)$ perform the same task for sources internal to the mth conductor V_m. For the system of thin circular conductors considered in this section, the source terms internal to the conductors represent elementary delta function sources given as

$$V_m^S(z_s) = \frac{1}{I_0(\tau_e a_m)}\left[\overline{\overline{G}}_m^{(ee)}(\overline{\rho}_m,\overline{\rho}_s,k_z)J_z^S(z_s)\hat{z}\right]\cdot\hat{z} \tag{3.25a}$$

$$U_m^S(z_s) = \frac{1}{I_0(\tau_e a_m)}\left[\overline{\overline{G}}_m^{(em)}(\overline{\rho}_m,\overline{\rho}_s,k_z)M_z^S(z_s)\hat{z}\right]\cdot\hat{z} \tag{3.25b}$$

where $V_m^S(z_s)$ represents a delta function voltage source exciting the mth conductor at $z=z_s$, and $U_m^S(z_s)$ represents a delta function current loop source around the periphery of the mth conductor at $z=z_s$.

3.2.2. VED, VMD and Voltage Source Excitation

In this section the special cases of excitation of the transmission line system by a vertical electric dipole (VED), vertical magnetic dipole (VMD), and a delta function voltage source will be considered. All problems can be formulated in terms of these three cases, as a combination of these source types can be used to represent any desired excitation. As discussed in appendix A, the VED and VMD sources are the conventional TM and TE components for which the fields of an arbitrarily oriented electric or magnetic dipole located exterior to the conductors can be represented. Sources located interior to the conductors can be modeled as a sum of delta function voltage sources or current loop sources along the conductor axis as given by (3.25). A general study of the excitation of a single conductor above a lossy earth was presented by Kuester et. al. [Kuester2]. They considered these three source types and formulated the problem in an integral form. The current induced on a transmission line due to a vertical electric dipole in the presence of a lossy half-space has been previously formulated by Wait and others [Wait8, Wait9, Olsen4], also in an integral form. Calculated results for the special case of a perfectly conducting earth have been given for purposes of determining the depolarizing effects of transmission lines [Hill], and results for a two conductor system above a perfectly conducting earth were presented by Olsen [Olsen6]. The exact solution of the latter case was compared to two limiting techniques; the steepest descent approximation and the transmission line approximation. For the case of a single wire over a lossy half-space, Olsen and Usta also used the steepest descent approximation [Olsen4]. The excitation of an infinite thin-wire transmission line located in free space by a delta function voltage source has been studied by numerous researchers [Schelkunoff1, Shen2], with the excitation of the transmission line when located over a lossy half-space being examined by Chang and Olsen [Chang3]. In the latter case, an examination of the contributions of the modal components to the induced currents and to the input impedance was made. The use of

the leaky wave modes to represent the radiated fields of a transmission line excited by a delta function source has also been considered [Carpentier1, Carpentier3, Leviatan].

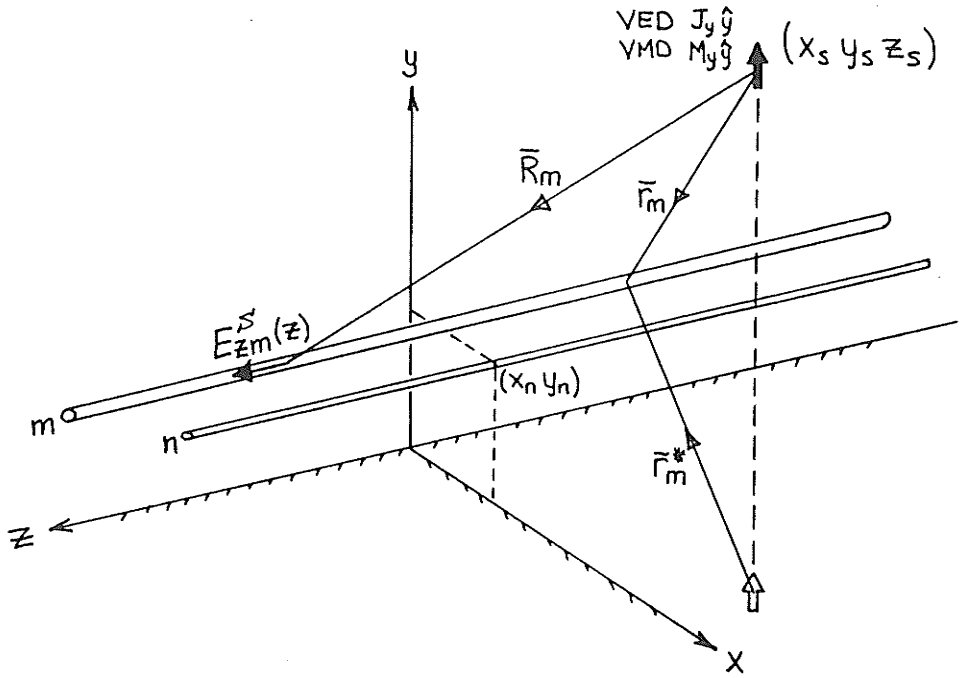

Figure 3.3: VED/VMD excitation of a transmission line.

Consider the current induced on a transmission line due to a VED or VMD as shown in figure 3.3. The dipole is located in the upper half-space at (x_s, y_s, z_s), with a moment $J_y\hat{y}$ for the VED, and $M_y\hat{y}$ for the VMD. The axial component of the imposed electric field $[E^S_z(k_z)]$ at the conductors is given in the spectral domain, as formulated in appendix A (A.86,A.89), as

$$E^S_{zm}(k_z) = \frac{-j\omega\mu_e}{2\pi k_e^2} J_y(+jk_z)\left\{\frac{\tau_e(y_m - y_s)}{|\bar{r}_m|}K_1(\tau_e|\bar{r}_m|) - \frac{\tau_e(y_m + y_s)}{|\bar{r}^*_m|}K_1(\tau_e|\bar{r}^*_m|) - n^2\frac{\partial}{\partial y}\mathbf{G}(\tau_e,\bar{r}^*)\right]_{y=y_m}\Bigg\} e^{-jk_z z_s} \quad (3.26)$$

$$E^S_{zm}(k_z) = \frac{1}{2\pi} M_y\left\{\frac{\tau_e(x_m - x_s)}{|\bar{r}_m|}K_1(\tau_e|\bar{r}_m|) - \frac{\tau_e(x_m - x_s)}{|\bar{r}^*_m|}K_1(\tau_e|\bar{r}^*_m|) - n^2\frac{\partial}{\partial x}\mathbf{J}(\tau_e,\bar{r}^*)\right]_{x=x_m}\Bigg\} e^{-jk_z z_s} \quad (3.27)$$

for the VED and VMD, respectively. The distances $|\bar{r}_m| = \sqrt{(x_m - x_s)^2 + (y_m - y_s)^2}$ and $|\bar{r}_m^*| = \sqrt{(x_m - x_s)^2 + (y_m + y_s)^2}$ are defined for the mth conductor of the transmission line which is located at (x_m, y_m). $K_1(z)$ and $I_0(z)$ are modified Bessel functions and the functions $\mathbf{G}(\tau_e, \bar{r}^*)$ and $\mathbf{J}(\tau_e, \bar{r}^*)$ were previously defined by (3.19). The axial component of the electric field due to an arbitrarily oriented electric or magnetic dipole source can then be determined as a combination of (3.26,3.27) by specifying J_y and M_y using the transformations defined in appendix A (A.32).

The evaluation of the fields of a dipole source over a lossy half-space has received much attention in the literature [Stratton, Felsen, Kuester3, Rahmat-Samii, Parhami2], with the work of Sommerfeld [Sommerfeld2, Sommerfeld3] and Banos [Banos] probably being the most referred to. The exact solution requires the evaluation of infinite integrals, these being described to some degree in appendix B. To simplify these integrals, many adequate approximation techniques have also been formulated for the near field and the far field regions [Bannister4, Wait3, King5, Felsen].

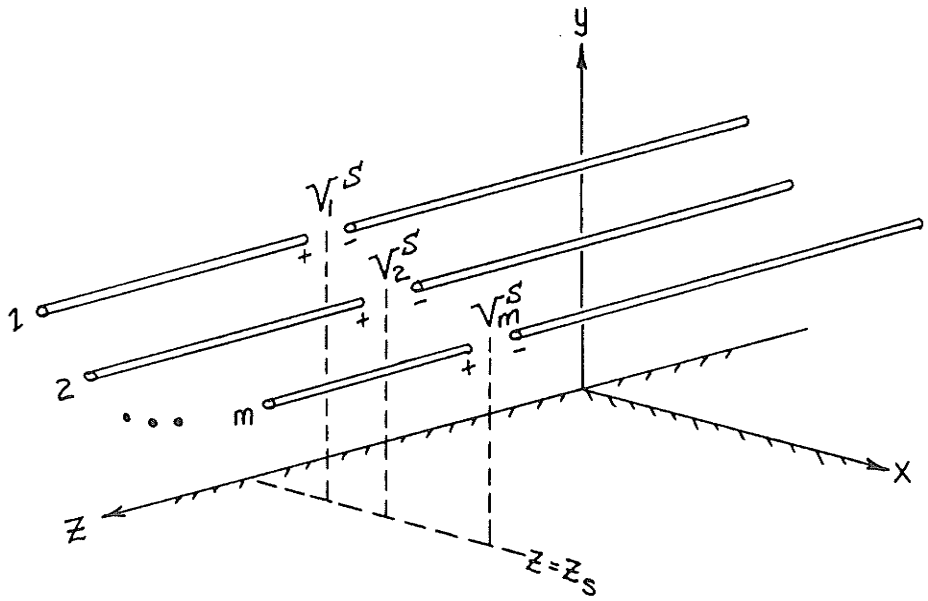

Figure 3.4: Delta function voltage source excitation.

Next, the excitation of the transmission line by a delta function voltage source $[V^S(z_s)]$ will be considered as shown in figure 3.4. The axial components of the imposed electric field $[E^S(k_z)]$ in this case is given from (3.3) as

$$V_m^S(z_s) = -\int_{-\infty}^{\infty} <E_z^{int}(z)>_m \delta(z - z_s)dz$$

$$E_{zm}^S(k_z) = -E_{zm}^{int}(k_z) = \frac{1}{I_0(\tau_e a_m)} V_m^S(z_s) e^{-jk_z z_s} \tag{3.28}$$

where $[V^S(z_s)]$ defines the magnitudes of the voltage sources on the N conductors at

the axial location z_s. Note that the input impedance for the structure can also be determined from the current at the source point [I($z=z_s$)], as calculated using (3.22), such that

$$[\,I(z=z_s)\,] = [\,Y_{in}\,][\,V^S(z_s)\,]$$

$$[\,Y_{in}\,] = [\,Z_{in}\,]^{-1} = \frac{1}{2\pi}\int_{-\infty}^{\infty}[\,Z(k_z)\,]^{-1}\,dk_z \tag{3.29}$$

where the diagonal terms in $[Z_{in}]$ give the self impedance for each conductor, and the off diagonal terms give the mutual impedances between conductors.

The scattered fields for the thin-wire structure can be determined from (3.14) as

$$\overline{E}_e^{scat}(\overline{r}) = \frac{1}{2\pi}\int_{-\infty}^{\infty}[<\overline{G}_{ez}(\overline{\rho},k_z)>][\,Z(k_z)\,]^{-1}[\,\overline{I}(k_z)\,][\,E_z^S(k_z)\,]e^{+jk_z(z-z_s)}dk_z \tag{3.30}$$

where the components of $[<\overline{G}_{ez}(\overline{\rho},k_z)>]$ can be determined from the fields (3.17) and the Green's functions derived in appendix A, in a similar manner as $[Z(k_z)]$ was derived. Thus, the components of the scattered fields $\overline{E}_e^{scat}(\overline{r})$ are given from

$$<G_{exz}(\overline{\rho},k_z)>_m = A_m(+jk_z)\left[\frac{\tau_e(x-x')}{|\,\overline{\rho}_D\,|}K_1(\tau_e\,|\,\overline{\rho}_D\,|) - \frac{\tau_e(x-x')}{|\,\overline{\rho}_D^*\,|}K_1(\tau_e\,|\,\overline{\rho}_D^*\,|) - \frac{\partial}{\partial x}\mathbf{G}(\tau_e,|\,\overline{\rho}_D^*\,|)\right] \tag{3.31}$$

$$<G_{eyz}(\overline{\rho},k_z)>_m = A_m(+jk_z)\left[\frac{\tau_e(y-y')}{|\,\overline{\rho}_D\,|}K_1(\tau_e\,|\,\overline{\rho}_D\,|) - \frac{\tau_e(y+y')}{|\,\overline{\rho}_D^*\,|}K_1(\tau_e\,|\,\overline{\rho}_D^*\,|) - \frac{\partial}{\partial y}\mathbf{G}(\tau_e,|\,\overline{\rho}_D^*\,|) + k_e^2\int\mathbf{J}(\tau_e,|\,\overline{\rho}_D^*\,|) - \mathbf{G}(\tau_e,|\,\overline{\rho}_D^*\,|)\,dy\right] \tag{3.32}$$

$$<G_{ezz}(\overline{\rho},k_z)>_m = A_m\left[\tau_e^2[K_0(\tau_e\,|\,\overline{\rho}_D\,|) - K_0(\tau_e\,|\,\overline{\rho}_D^*\,|)] + k_e^2\mathbf{J}(\tau_e,|\,\overline{\rho}_D^*\,|) - k_z^2\mathbf{G}(\tau_e,|\,\overline{\rho}_D^*\,|)\right] \tag{3.33}$$

$$A_m = \left[\frac{-j\omega\mu_e}{2\pi k_e^2}\right]\frac{1}{(\tau_e a_m)K_1(\tau_e a_m)}$$

$$|\,\overline{\rho}_D\,| = \sqrt{(x-x_m)^2+(y-y_m)^2}\quad,\quad \angle\overline{\rho}_D = \tan^{-1}\left[(y-y_m)/(x-x_m)\right]$$

$$|\,\overline{\rho}_D^*\,| = \sqrt{(x-x_m)^2+(y+y_m)^2}\quad,\quad \angle\overline{\rho}_D^* = \tan^{-1}\left[(y+y_m)/(x-x_m)\right]$$

where the functions $\mathbf{J}(\tau_e,\overline{\rho})$ and $\mathbf{G}(\tau_e,\overline{\rho})$ were defined in (3.19) as infinite integrals.

3.3. WAVE PROPERTIES AND LIMITING CASES

As discussed in section 2.6, the inverse transformation (3.22) determining the conductor currents on the structure will contain several sets of branch cuts as well as a set of poles located in the k_z plane as shown in figure 3.5 (even though only the upper half of the complex k_z plane is shown, the poles and branch cuts appear as complex pairs, with the corresponding counterparts symmetrically located about the origin). The poles, indicated as k_z^p; $p=1,2,...,P$, arise from the singularities of the impedance matrix $[Z(k_z)]$, which can be determined from the solution of the mode equation $\det[Z(k_z)] = |[Z(k_z)]| = 0$. Their contribution to the integral transform represents a set of discrete propagating modes for the structure. These currents have fields which decay exponentially in the axial direction from the source as $\exp(+jk_z^p|z-z_s|)$, where $\mathrm{Im}[k_z]\geq 0$ is defined when the contour of integration is deformed from the real axis to encompass the poles. The associated fields in the upper half-space for the discrete modes decay asymptotically in the radial direction away from the conductor axis as

$$\frac{e^{-\tau_e^p \rho_T}}{\sqrt{\rho_T}} e^{+jk_z^p|z-z_s|} \quad , \quad \rho_T = \sqrt{(x-x')^2+(y-y')^2} \tag{3.34}$$

where ρ_T is the transverse direction to the conductor axis, located at (x',y'), and $\tau_e^p=\sqrt{(k_z^p)^2-k_e^2}$; $\mathrm{Re}[\tau_e^p]\geq 0$ is the respective transverse propagation constant. For lossy structures, energy propagates into the conductors if they are finitely conducting and into the lossy half-space. The location of the poles is highly dependent on the geometry of the transmission line structure.

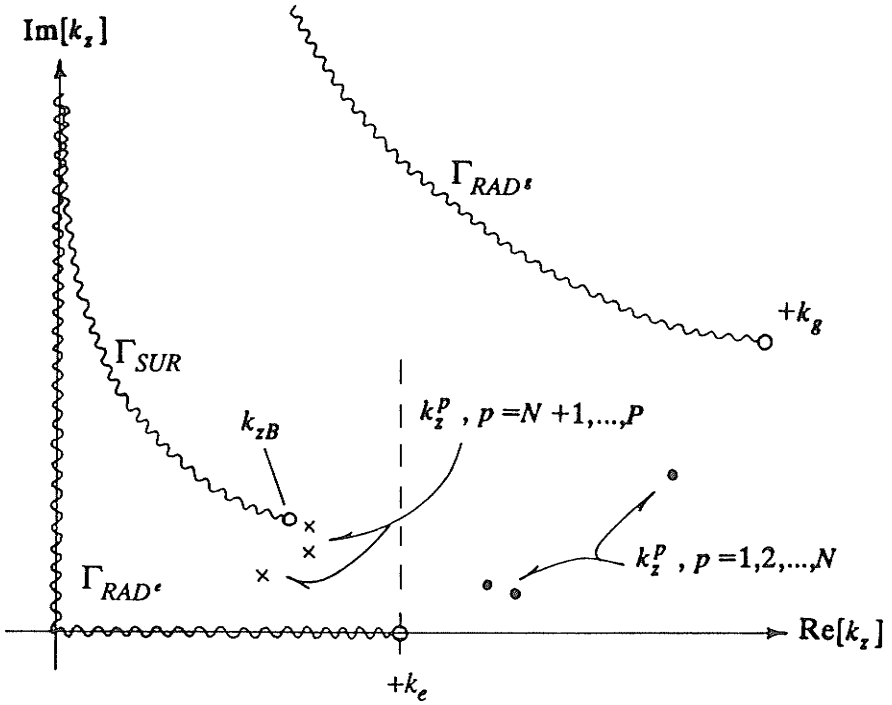

Figure 3.5: Location of the P poles and the three branch cuts in the upper half of the complex k_z plane.

The contribution due to the branch cuts appearing in the k_z plane arise from two sources. The first is due to the requirement on the irrationals $\mathrm{Re}[U_e, U_g] \geq 0$ defined so that the fields decay as $|y| \to \infty$ in the upper and lower half-spaces. These branch cuts, emanating from the points $k_z = \pm k_e, \pm k_g$, represent a spectrum of modes radiating into the air and earth half-spaces, respectively. These fields decay asymptotically as

$$\int_{\Gamma_{RAD^{e/g}}} I(k_z) \frac{e^{-\tau_{e/g}\rho_T}}{\sqrt{\rho_T}} e^{+jk_z|z-z_s|}\, dk_z \tag{3.35}$$

where $\mathrm{Re}[\tau_{e/g}] = \mathrm{Re}[\sqrt{k_z^2 - k_{e/g}^2}] \geq 0$ defines the branch cut $\Gamma_{RAD^{e/g}}$. Note that if the lower half-space is a good conductor, then the corresponding branch point $\pm k_g \approx \pm\sqrt{j\omega\mu_g\sigma_g}$ is located far off the real axis and the contribution to the current from this radiation mode is negligible. Secondly, an additional branch cut emanating from the branch point $k_z = \pm k_{zB} = \pm\lambda_B = \pm k_g/\sqrt{n^2+1}$, arises from the singularity in the denominator of the integral $\mathbf{G}(\tau_e, \overline{\rho}^*)$ in (3.19b). This branch cut represents a spectrum of TM surface waves supported by the interface and results from the requirement that the fields must decay as $|x| \to \infty$. They can be related to the Zenneck surface wave resulting from a dipole source over a half–space[3.2] [Zenneck]. The respective fields for the surface wave behaves asymptotically as

$$\int_{\Gamma_{SUR}} I(k_z) e^{-U_{eB}|y+y'| + jk_{xB}|x-x'|} e^{+jk_z|z-z_s|}\, dk_z \tag{3.36}$$

where $U_{eB} = \sqrt{\lambda_B^2 - k_e^2} = +jk_e/\sqrt{n^2+1}$ is the propagation constant of the surface wave in the direction perpendicular to the interface. λ_B (and thus U_{eB}) are strictly functions of only the electrical properties of the two half-spaces. The surface wave pole has no cut-off frequency and is thus always present. $\mathrm{Im}[k_{xB}] = \mathrm{Re}[\sqrt{k_z^2 - \lambda_B^2}] \geq 0$ defines the branch cut Γ_{SUR} and the branch point $\pm k_{zB}$ in the complex k_z plane. The continuous mode spectra associated with the surface wave and radiation branch cuts are not affected strongly by the conductor geometry, and may have a large contribution to the currents under certain conditions.

Further examination of the discrete modes, shows that the number of poles for the structure may be greater than the number of conductors ($P \geq N$). N of the discrete modes arise from the solutions of $|[Z(k_z)]| = 0$ in the region where typically all the terms of the matrix are slowly varying functions of the argument k_z. These can be considered as the dominant modes of the structure and are usually the major

3.2 The Zenneck surface wave is the pole contribution extracted from the transform (3.22) [Sommerfeld3, Stratton], and is a solution of the wave equation. This should not be confused with Norton's far field surface wave term which is distinct from the Zenneck surface wave [Norton, Wait3]. What Norton identified as the surface wave part is the additional correction terms to the standard geometrical optics approximation arising when the steepest descent path crosses the k_g branch cut and from the contribution of the TM surface wave pole which is in close proximity to the saddle point at low frequencies. The recent results presented by King [King5, King6] for the fields of dipole sources near an interface are based on Norton's work.

contribution to the current. As shown in figure 3.5, the remaining P-N solutions occur *near* the singularity in the impedance matrix due to the TM surface wave pole supported by the lossy half-space, which was identified by the branch point $+k_{zB}$ in the k_z plane. Excitation of these modes is usually very small for typical sources, and thus only the first N modes are usually important. Since the poles are located near $+k_{zB}$, a close approximation of the asymptotic behavior of the fields for these modes is given as

$$\frac{e^{-\tau_e^p \rho_T}}{\sqrt{\rho_T}} e^{+jk_{zB}|z-z_s|} \qquad ; p=N+1,\ldots, P \tag{3.37}$$

where $\tau_e^p \approx \sqrt{k_{zB}^2 - k_e^2} = U_{eB}$. At low frequencies, k_{zB} is found near k_e and thus, the modes are similar to plane waves propagating in the axial direction with a magnitude decaying as $\sqrt{\rho_T}$ in the transverse direction, the transverse exponential decay being very small. Excitation of modes of this type are difficult to realize for typical sources, and thus usually only the first N discrete propagating modes are important. However, as will be seen in latter sections, the contribution of these modes becomes important at higher frequencies and in other special cases.

The path of integration in the complex k_z plane can be deformed to separate the contributions due to each of the poles and branch cuts giving some insight to the behavior of the structure currents. The integral transform (3.22) can thus be constructed as a sum of discrete propagating modes as well as a spectrum of continuous modes as

$$[I(z)] = \sum_{p=1}^{P} [I_p(z)] + [I_{RAD^{e}}(z) + I_{RAD^{g}}(z)] + [I_{SUR}(z)] \tag{3.38}$$

$$[I_p(z)] = +j \lim_{k_z \to k_z^p} \left\{ (k_z - k_z^p)[Z(k_z)]^{-1}[\bar{I}(k_z)][E_z^S(k_z)] e^{+jk_z|z-z_s|} \right\} \tag{3.39}$$

$$[I_{RAD^{e/g}}(z)] = \frac{1}{2\pi} \int_{\Gamma_{RAD^{e/g}}} [Z(k_z)]^{-1}[\bar{I}(k_z)][E_z^S(k_z)] e^{+jk_z|z-z_s|} dk_z \tag{3.40}$$

$$[I_{SUR}(z)] = \frac{1}{2\pi} \int_{\Gamma_{SUR}} [Z(k_z)]^{-1}[\bar{I}(k_z)][E_z^S(k_z)] e^{+jk_z|z-z_s|} dk_z \tag{3.41}$$

where $\Gamma_{RAD^{e/g}}$ are the branch cuts emanating from $+k_{e/g}$ and Γ_{SUR} are the branch cuts emanating from $+k_{zB}$. The contribution from some of the integral terms in (3.38) is negligible in many problems. When the earth behaves as a good conductor, the contribution to the current due to the integral along the $\Gamma_{RAD^{g}}$ branch cut can be neglected [Chang3]. The dominance of the poles or remaining branch cuts then depends on the electrical distance of the source from the transmission line as well as the electrical

distance from the source to the observation point along the axis of the structure. Two limiting cases which are often used in practical applications will be examined in the next sections. In one extreme, when the source is electrically near the structure, the commonly utilized transmission line approximation can be used. In the other extreme, when the source is electrically far from the structure, the geometrical optics approximation will predominate (the source can be modeled as an incident plane wave).

3.3.1. Transmission Line Approximation

In this section, the formulation of the structure currents using a transmission line theory will be presented. The theory assumes that the currents on the transmission line structure can be completely represented by only the discrete mode contributions of (3.38). These modes take the form of exponential traveling waves $I_p \exp\{\pm jk_z^p z\}$, where k_z^p is one of the possible characteristic propagating modes of the structure. The representation of the current in this manner neglects the radiation and surface wave contributions, as given by the branch cuts present in the complete solution. The separate contributions to the structure currents due to the branch cuts and the discrete modes has been studied by Chang and Olsen [Chang3] and the properties of the discrete modes has also been extensively examined [Kuester4, Efthymiadis, Olsen5, Courbet, Bridges3]. It is expected that the discrete modes will be the dominant contribution to the current when the source is electrically near the transmission line. However, in the *immediate* neighborhood of the source as well as at *extremely* large distances, the radiation and surface wave spectra are expected to be significant and should not in general be neglected, since the continuous mode spectra decays algebraically whereas the discrete modes decay as $\exp(+jk_z^p \mid z-z_s \mid)$, and $\mathrm{Im}[k_z^p]$ can be substantially small. The use of only the discrete modes to represent the structure currents also allows a much simplified transmission line approach to the solution of (3.22) and the formulation of many antenna and scattering problems.

In this section the transmission line approximation is derived from the exact form given by (3.22). This approach is different from that usually taken in the literature where a two-dimensional form to the geometry and thus the wave equation (3.16) is assumed from the start. In utilizing the transmission line approach, the current on the structure is generated by an infinite set of delta function voltage sources distributed along the length of the conductors, with the magnitude of the sources proportional to the axial component of the imposed electric field. The current due to each localized source is then assumed to be of exponential form only, the branch cut contributions being neglected. The formulation of the problem in this manner, directly from (3.22), can be developed by utilizing the convolution theorem to represent the source as

$$[E_z^S(k_z)] = \int_{-\infty}^{\infty} [E_z^S(z_s)] \int_{-\infty}^{\infty} \delta(z-z_s) e^{-jk_z z}\, dz\, dz_s \tag{3.42}$$

Thus, using the expression (3.22) for the current and replacing the source term using (3.42),

$$[\,I(z)\,] = \int_{-\infty}^{\infty} [\,I(z\,,\,z_s)\,][\,E_z^S(z_s)\,]\;dz_s \tag{3.43}$$

$$[\,I(z\,,\,z_s)\,] = \frac{1}{2\pi} \int_{-\infty}^{\infty} [Z(k_z)]^{-1}[\overline{I}(k_z)]e^{+jk_z(z-z_s)}\;dk_z \tag{3.44}$$

Here $[I(z\,,\,z_s)]$ is the current at the observation point z due to a delta function voltage source of strength $[E_z^S(z_s)]$ located at z_s. This is now equivalent to the form developed for a delta function voltage source excitation, where now the sources are weighted by the axial component of the imposed electric field. The current formulated as in (3.43,3.44) is still an exact solution even though its evaluation in this form would be inappropriate.

In utilizing the transmission line approximation, we are only concerned with the contribution to the structure currents due to the discrete modes as defined in (3.39). The properties of these modes are characterized by the propagation constants k_z^p; $p=1,2,...,\,P$ and by the magnitude of their associated residue contribution, which determines their relative excitation by a given source. Considering the contribution to the currents due to the discrete modes only, the total induced current on the structure is derived as

$$[\,I(z)\,] \approx \int_{-\infty}^{\infty} j \sum_{p=1}^{P} \lim_{k_z \to k_z^p} \left\{ (k_z - k_z^p)[Z(k_z)]^{-1}[\overline{I}(k_z)]e^{+jk_z\,|\,z-z_s\,|} \right\} [\,E_z^S(z_s)\,]\;dz_s \tag{3.45}$$

This form for the induced currents is quite different from the discrete mode contribution considered in (3.39). In (3.45), the imposed source $[E_z^S(z_s)]$ does *not* have to behave as the discrete modes, but can give an exact representation of the source fields. Only the resulting current excited by the distributed source functions along the conductor axis are assumed to be dominated by the discrete mode contribution. Thus, in this form there are no restrictions placed on the source function. In the form (3.39), the source must be in the near field region for the discrete mode contribution to be dominant.

3.3.2. Modal Formulation of the Induced Currents

As discussed in section 3.3, the currents on the transmission line can be represented in terms of the characteristic modal current quantities for the structure. Unlike the representation in terms of the total conductor currents, the modal currents are orthogonal, with the relative distribution of currents and resulting field configuration being scale invariant with respect to the amplitude of a particular mode. A transformation, allowing the description of the currents in terms of modal quantities, is determined from the eigenvectors of the impedance matrix as

$$\lim_{k_z \to k_z^p} \left\{ [Z(k_z)][v^p] \right\} = 0 \quad , \; p=1,2,\ldots, P \tag{3.46}$$

$$[T] = \left[\left[v^1\right]\left[v^2\right] \cdots \left[v^P\right] \right] \quad , \quad [Q] = \left[\left[q^1\right]\left[q^2\right] \cdots \left[q^P\right] \right] \tag{3.47}$$

$$v_j^p = \mathrm{cof}_{1j}\{Z(k_z^p)\}/N_v^p \quad , \quad q_j^p = \frac{\mathrm{cof}_{j1}\{Z(k_z^p)\}}{\mathrm{cof}_{11}\{Z(k_z^p)\}}/N_q^p \quad ; \; j=1,2,\ldots,N$$

$$N_v^p = \left[\sum_{i=1}^{N} v_i^p \right]^{1/2} \quad , \quad N_q^p = \left[\sum_{i=1}^{N} q_i^p \right]^{1/2}$$

Here $[v^p]_{1xN}$ is the eigenvector corresponding to the pth eigenvalue k_z^p of the impedance matrix $[Z(k_z)]$. The transformation matrix $[T]_{NxP}$ is formed from the resulting P eigenvectors. The function $\mathrm{cof}_{ij}\{Z\}$ gives the cofactor of the ijth element of Z, and N_v^p, N_q^p are normalization constants. Also note that if $Z(k_z^p)$ is symmetric (as in the case when all conductors are the same, or if the quasi-TEM assumption is used), then $[Q]^{-1}=[T]^t$ and accordingly $N_q^p=N_v^p$. Note that the number of discrete modes is not necessarily equal to the number of conductors $P \geq N$ and thus, $[Q]$ and $[T]$ are not diagonal in general, with $\mathrm{rank}[Z_C] \geq \mathrm{rank}[Z(k_z^p)]$. Using the developed transformations, the transmission line currents (3.44) can be formulated in terms of modal quantities as

$$\begin{aligned}[\mathrm{I}(z,z_s)] &= [T][2Z_C]^{-1}[D(z,z_s)][Q]^{-1}[\overline{I}(k_z^p)][\mathrm{E}_z^S(z_s)] \\ &= [T][\mathrm{i}(z)]\end{aligned} \tag{3.48}$$

$$[\mathrm{i}(z)] = [2Z_C]^{-1}[D(z,z_s)][<\mathrm{e}_z(z_s)>] \tag{3.49}$$

$$<\mathrm{e}_z(z_s)>_p = \sum_{j=1}^{N} Q_{jp}\overline{I}_{jj}(k_z^p)\mathrm{E}_{zj}^S(z_s) \quad ; \; p=1,2,\ldots,P \tag{3.50}$$

$$D_{ij}(z,\, z_s) = \begin{cases} e^{+jk_z^p \,|\, z-z_s \,|} & , \; i=j=p \\ 0 & , \; i \neq j \end{cases} \tag{3.51}$$

$$Z_{Cij} = Z_{Cp} = \begin{cases} -\dfrac{j}{2}\dfrac{1}{N_v^p N_q^p}\dfrac{\partial}{\partial k_z}\left\{ \,|\, Z(k_z) \,|\, \right\}_{k_z=k_z^p} \\ \qquad = -\dfrac{j}{2}\displaystyle\sum_{q=1}^{N}(T_{qp})\sum_{k=1}^{N}(T_{kp})\frac{\partial}{\partial k_z}Z_{qk}(k_z^p) & , \; i=j=p \\ 0 & , \; i \neq j \end{cases} \tag{3.52}$$

where the second equality in (3.52) for Z_{Cp} is valid only if $Z(k_z)$ is symmetric

($[Q]^{-1}=[T]^t$). Here $[D(z, z_s)]$ and $[Z_C]$ are diagonal matrices describing the propagation and impedance characteristics, respectively, of the structure. The vectors $[i(z)]$ and $[<e_z>]$ are the strengths of the modal currents and exciting fields, respectively. The eigenvector v^p gives the distribution of current between the N conductors for the pth mode, and q^p gives the corresponding field distribution. Finally, the resulting impedance matrix for the *individual* conductors can be formed in terms of the discrete modes as

$$[\, I(z=z_s)\,] = 2[\, Y_{char}\,][\, V^S(z_s)/2\,]$$

$$[\, Y_{char}\,] = [\, Z_{char}\,]^{-1} = [\, T\,][\, Z_C\,]^{-1}[\, Q\,]^{-1} \tag{3.53}$$

where $[I(z=z_s)]$ is the current at the source location driven by the set of delta function voltage sources $[V^S(z_s)]$ as described in section 3.2.2. When the discrete modes dominate the currents, the characteristic impedance matrix (3.53) is a good approximation to the input impedance $[Z_{in}] \approx 2[Z_{char}]$, where $[Z_{in}]$ was defined using the complete spectral transform (3.29).

3.3.3. Quasi-TEM Approximation

Most studies determining the induced currents on transmission lines when the dimensions of the structure are much less than the free space wavelength rely mainly on the use of a quasi-TEM transmission line theory. The theory is an approximation to the exact discrete mode theory presented in sections 3.3.1 and 3.3.2, and still assumes that the currents on the transmission line structure take the form of exponential traveling waves $I_p \exp\{\pm jk_z^p z\}$. In the quasi-TEM theory, however, the propagation constants are determined from the transmission line circuit parameters [King1, Shen3, King4, Sunde, Chen], the approach being basically the same as that obtained by Carson and Pollaczek in 1926 [Carson, Pollaczek]. The per unit length circuit parameters are derived by applying the TEM assumption directly to the wave equation (setting $\tau_e=0$ in (3.16)). The validity of this approximation has been studied [King1, Sorbello, Bridges3, Carpentier2, Degauque1], and the basic observations for reliable application of the quasi-TEM transmission line approach is that the dimensions of the transmission line structure should be much less than the wavelength of the medium in which it is embedded ($|\,\bar{\rho}_{mn}\,|$, $|\,\bar{\rho}^*_{mn}\,| \ll \lambda_e$) as well as the refractive index at the air-earth interface should be large ($|\,n\,| \gg 1$).

The formulation presented in the last two sections can appropriately be denoted as a transmission line solution since only the discrete exponential current modes are used to represent the current on the structure. The values used for the propagation constants k_z^p are solutions of $|\,[Z(k_z)]\,| = 0$ as determined using the exact expressions (3.18-3.20) and thus, the resulting fields are solutions of the wave equation (3.16). The solution of the mode equation in this form can be considered a generalized eigenvalue problem

where an explicit expression can not be derived since the elements are complicated functions of the unknown eigenvalues and as such is difficult to evaluate. A useful approach in viewing the problem is to cast the mode equation into the form of a generalized transmission line equation

$$-\frac{\partial}{\partial z}[\,\mathrm{I}(z)\,] = [\,Y^{sh}\,][\,\mathrm{V}(z)\,] \tag{3.54a}$$

$$-\frac{\partial}{\partial z}[\,\mathrm{V}(z)\,] = [\,Z^{ser}\,][\,\mathrm{I}(z)\,] \tag{3.54b}$$

$$|\,[Z(k_z)]\,| = |\,[Z^{ser}] - [(jk_z)^2][Y^{sh}]^{-1}\,| = 0 \tag{3.55}$$

$$(Y^{sh})^{-1}_{mn} = \frac{1}{-j\,\omega\varepsilon_e 2\pi}\frac{1}{(\tau_e a_n)K_1(\tau_e a_n)} \cdot \left[K_0(\tau_e\,|\,\overline{\rho}_{mn}\,|) - I_0(\tau_e a_m)[K_0(\tau_e\,|\,\overline{\rho}^{*}_{mn}\,|) - \mathbf{G}(\tau_e,\overline{\rho}^{*}_{mn})]\right] \tag{3.56}$$

$$Z^{ser}_{mn} = Z^{w}_{mn} - \frac{j\,\omega\mu_e}{2\pi}\frac{1}{(\tau_e a_n)K_1(\tau_e a_n)} \cdot \left[K_0(\tau_e\,|\,\overline{\rho}_{mn}\,|) - I_0(\tau_e a_m)[K_0(\tau_e\,|\,\overline{\rho}^{*}_{mn}\,|) - \mathbf{J}(\tau_e,\overline{\rho}^{*}_{mn})]\right] \tag{3.57}$$

where Z^{ser}_{mn} are the series impedance and Y^{sh}_{mn} are the shunt admittance terms for the structure and $[(jk_z)^2]$ is diagonal. A common approach to simplifying the eigenvalue problem is to assume that the axial variation of the fields is equal to the free space value ($k_z \approx k_e$) when evaluating the mode equation. In this manner, the fields in the upper half-space will be solutions of the two-dimensional Laplace equation. This approach is denoted as the quasi-TEM transmission line approximation and is reasonable if the terms **J**, **G**, and K_0 involved in the calculation of the matrix elements in (3.55) are slowly varying functions of their argument ($\tau_e = \sqrt{k_z^2 - k_e^2}$) and the axial propagation constant for the structure is near k_e. This approximation is the one utilized by Carson [Carson] and is valid at low frequencies and high earth conductivities, but has been even used for studies in the higher frequency regions. Applying this approach by assuming $\tau_e \to 0$ in the arguments of I_0, K_0 and **J** in (3.56,3.57), an explicit expression for the transmission line parameters will then be given as

$$(Y^{sh})^{-1}_{mn} \approx \frac{1}{-j\,\omega\varepsilon_e 2\pi}\ln\left(\frac{|\,\overline{\rho}^{*}_{mn}\,|}{|\,\overline{\rho}_{mn}\,|}\right) \tag{3.58}$$

$$Z^{ser}_{mn} \approx Z^{w}_{mn} - \frac{j\,\omega\mu_e}{2\pi}\left[\ln\left(\frac{|\,\overline{\rho}^{*}_{mn}\,|}{|\,\overline{\rho}_{mn}\,|}\right) + \mathbf{J}_c(\overline{\rho}^{*}_{mn})\right] \tag{3.59}$$

$$Z_{mn}^{w} \approx \delta_{mn} \left[\frac{+j\omega\mu_n}{2\pi a_n k_n} \right] \frac{J_0(k_n a_n)}{J_1(k_n a_n)} \tag{3.60}$$

$$\mathbf{G}(\tau_e=0,\overline{\rho}_{mn}^{*}) \equiv 0 \quad , \quad \mathbf{J}(\tau_e=0,\overline{\rho}_{mn}^{*}) \rightarrow \mathbf{J}_c(\overline{\rho}_{mn}^{*})$$

$$\mathbf{J}_c(\overline{\rho}_{mn}^{*}) = \frac{2}{n^2-1} \int_0^{\infty} \left[u - \sqrt{u^2-(n^2-1)} \right] e^{-uk_e(y_m+y_n)} \cos(uk_e \mid x_m - x_n \mid) \, du \tag{3.61}$$

The solution of (3.55) under the quasi-TEM assumption is now a standard eigenvalue problem which yields the values of the propagation constants. The logarithmic terms in (3.58) and (3.59) represent the field due to the conductor and its image under the conditions of a perfectly conducting earth. The integral term $\mathbf{J}_c(\overline{\rho}_{mn}^{*})$ represents the conduction losses in the earth and the contribution of the integral $\mathbf{G}(\tau_e,\overline{\rho}_{mn}^{*})$, representing displacement current losses in the earth, has been neglected completely. A good approximation to the terms of the shunt admittance matrix is thus obtained using image theory under static conditions. Many expressions for evaluating the integral $\mathbf{J}_c(\overline{\rho}_{mn}^{*})$ are found in the literature as discussed in appendix B. Once the transmission line parameters are determined using the quasi-TEM approximation, the induced currents on the structure can be found through (3.43,3.48). Note that the quasi-TEM approximation yields only N solutions to the mode equation (3.55).

3.3.4. Steepest Descent Evaluation

When the source region is located electrically far from the transmission line, a geometrical optics approximation can be used to model the source. The approximation is applied by considering the steepest descent contribution from the source terms in the integral (3.22) derived in section 3.2.1. In this section, elementary vertical electric dipole (VED) and vertical magnetic dipole (VMD) sources will only be considered since, as discussed in appendix A, a combination of these two source types can be used to represent any possible source. It will also be shown that the saddle point contribution of the integral transform yields the plane wave incident model for the source. This result is of importance in many engineering applications for the modeling of source interactions with transmission lines. Usta and Olsen used the steepest descent approximation to determine the current induced on a single wire above a lossy interface at non-grazing angles of incidence [Olsen4]. The validity of the approximation in the grazing angle region was examined by studying the case of a two wire system over a perfectly conducting earth [Olsen6], and by a single wire system over a lossy earth [Bridges6]. The validity of modeling an incident electromagnetic pulse as an incident plane wave was specifically considered in the latter case. The radiated fields in the VHF/UHF region from corona discharge sources (modeled as VED sources at the conductor surfaces) was also recently determined using a steepest descent approach [Olsen8].

Consider the current induced on a transmission line due to a VED or VMD as shown in figure 3.6. Similar to the case discussed in section 3.2.2, the dipole is located in the upper half-space at (x_s,y_s,z_s), with a moment $J_y\hat{y}$, $M_y\hat{y}$, respectively. The distance $r_s=\sqrt{x_s^2+y_s^2}$ is the transverse distance from the dipole to the z-axis and $R_s=\sqrt{x_s^2+y_s^2+(z-z_s)^2}$ is the distance from the dipole to some observation point along the z-axis. The angles θ,ψ; $0<\theta<+\pi/2$, $-\pi<\psi<+\pi$ define the incident angle the source makes with the conductor axis and the earth. The angles $\phi=\tan^{-1}(y_s/x_s)$ and $\gamma=\tan^{-1}(r_s/(z-z_s))$ are used for defining the steepest descent paths ($\cos\theta\cos\psi=\cos\gamma$).

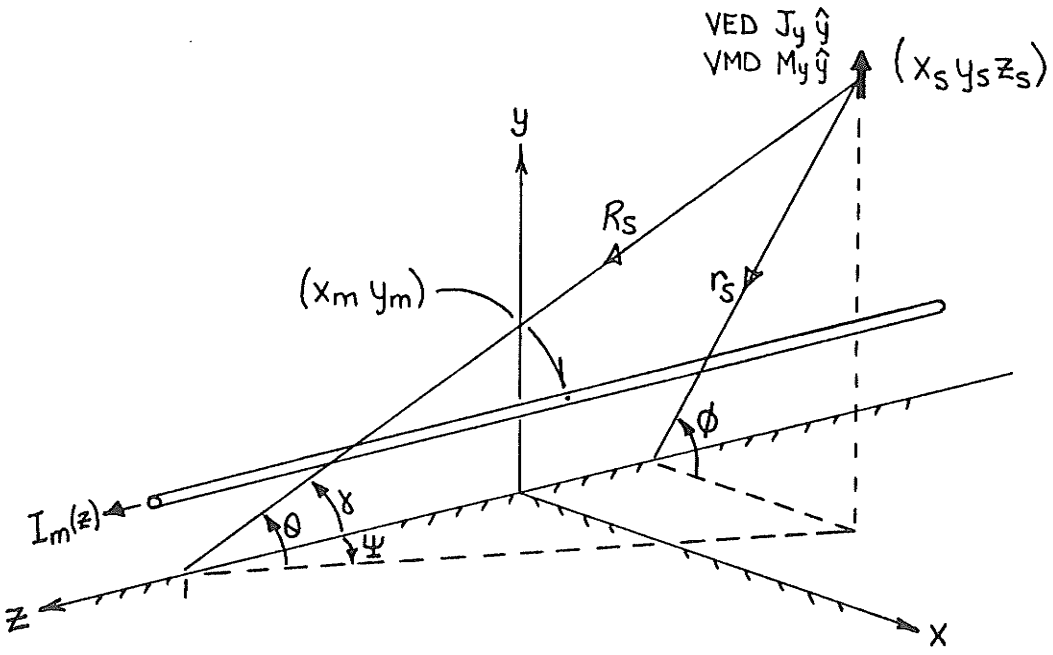

Figure 3.6: Steepest descent coordinates for VED/VMD excitation.

The exact expression for the induced current is derived using the general transform (3.22), where the axial component of the imposed electric field $[E_z^S(k_z)]$ is given in the spectral domain as formulated in appendix A and from (3.26,3.27) as

$$E_{zm}^S(k_z)=\frac{+j\omega\mu_e}{2\pi k_e^2}J_y\frac{\partial^2}{\partial z\,\partial y}\int_{-\infty}^{\infty}\left[\frac{e^{-U_e|y_m-y_s|}}{2U_e}+r_{eg}^e\frac{e^{-U_e(y_m+y_s)}}{2U_e}\right]e^{+jk_x(x_m-x_s)}dk_x\,e^{-jk_z z_s}$$

$$=\frac{-j\omega\mu_e}{2\pi k_e^2}J_y(+jk_z)\left\{\frac{\tau_e(y_m-y_s)}{|\bar{r}_m|}K_1(\tau_e|\bar{r}_m|)\right.$$

$$\left.-\frac{\tau_e(y_m+y_s)}{|\bar{r}_m^*|}K_1(\tau_e|\bar{r}_m^*|)-n^2\frac{\partial}{\partial y}G(\tau_e,\bar{r}^*)\right]_{y=y_m}\Bigg\}e^{-jk_z z_s} \qquad (3.62)$$

$$E_{zm}^{S}(k_z) = -\frac{1}{2\pi}M_y \frac{\partial}{\partial x}\int_{-\infty}^{\infty}\left[\frac{e^{-U_e|y_m-y_s|}}{2U_e} + r_{eg}^{m}\frac{e^{-U_e(y_m+y_s)}}{2U_e}\right]e^{+jk_x(x_m-x_s)}dk_x e^{-jk_z z_s}$$

$$= \frac{1}{2\pi}M_y\left\{\frac{\tau_e(x_m-x_s)}{|\bar{r}_m|}K_1(\tau_e|\bar{r}_m|)\right.$$

$$\left. - \frac{\tau_e(x_m-x_s)}{|\bar{r}_m^*|}K_1(\tau_e|\bar{r}_m^*|) - n^2\frac{\partial}{\partial x}\mathbf{J}(\tau_e,\bar{r}^*)\right]_{x=x_m}\Bigg\}e^{-jk_z z_s} \qquad (3.63)$$

$$r_{eg}^{e} = \frac{n^2U_e-U_g}{n^2U_e+U_g} \quad , \quad r_{eg}^{m} = \frac{U_e-U_g}{U_e+U_g}$$

for a VED and VMD, respectively. The distances $|\bar{r}_m| = \sqrt{(x_m-x_s)^2+(y_m-y_s)^2}$ and $|\bar{r}_m^*| = \sqrt{(x_m-x_s)^2+(y_m+y_s)^2}$ are defined for the mth conductor of the transmission line which is located at (x_m, y_m). $K_1(z)$ and $I_0(z)$ are modified Bessel functions and the functions $\mathbf{G}(\tau_e,\bar{r}^*)$ and $\mathbf{J}(\tau_e,\bar{r}^*)$ were previously defined by (3.19).

If the dipole is located electrically far from the transmission line, and far from the air-earth interface, the imposed electric field due to the VED or VMD can be determined through the method of steepest descent [Olsen4, Bridges6]. Unlike the usual steepest descent evaluation of these integrals [Felsen, Collin], however, the evaluation of (3.22) requires a two step approach, one for the k_x spectral domain and one for the k_z spectral domain. Also, the contribution of any branch cuts and surface wave poles must be considered. The two spectral domains considered are shown in figure 3.7, with the steepest descent paths given for various angles of incidence ϕ,γ. The associated saddle points are defined from the formulation developed in appendix B as

$$k_{zS} = +k_e\cos\gamma \qquad (3.64a)$$

$$k_{xS} = +j\tau_e\cos\phi = +k_e\sin\gamma\cos\phi \qquad (3.64b)$$

The radiation branch cuts in the two spectral domains are defined from the branch points $\pm k_e$, $\pm k_g$ in the k_z plane and $\pm j\tau_e$, $\pm j\tau_g$ in the k_x plane. The surface wave branch cut in the k_z plane is defined by the branch point $k_{zB}=+\lambda_B=+k_g/\sqrt{n^2+1}$. The position of the associated surface wave pole $k_{xB}=\sqrt{\lambda_B^2-k_z^2}$ is shown in the k_x plane as evaluated for various values of the saddle point k_{zS}, where

$$k_{xB}\Big]_{k_z=k_{zS}} = \sqrt{\lambda_B^2-k_{zS}^2} = +k_e\sin\gamma\left(\frac{n^2-\cot^2\gamma}{n^2+1}\right)^{1/2} \qquad (3.65)$$

The guided wave poles k_z^p are present only in the k_z plane. Note these poles are due to the singularities in the impedance matrix $[Z(k_z)]$ and not the source $[E_z^S(k_z)]$.

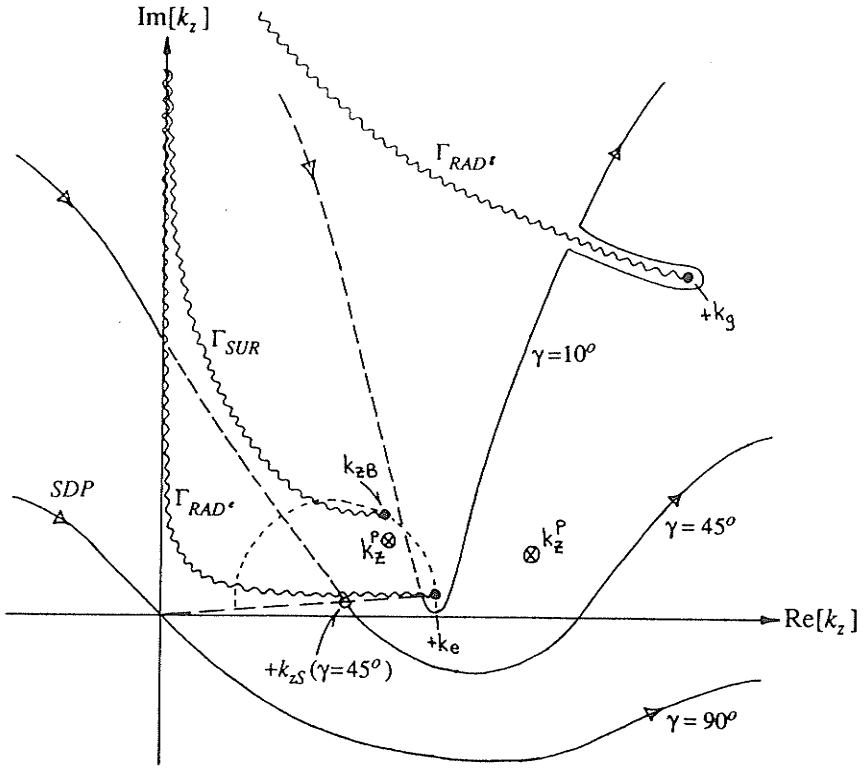

Figure 3.7a: Steepest descent paths in the complex k_z plane for various incident angles γ.

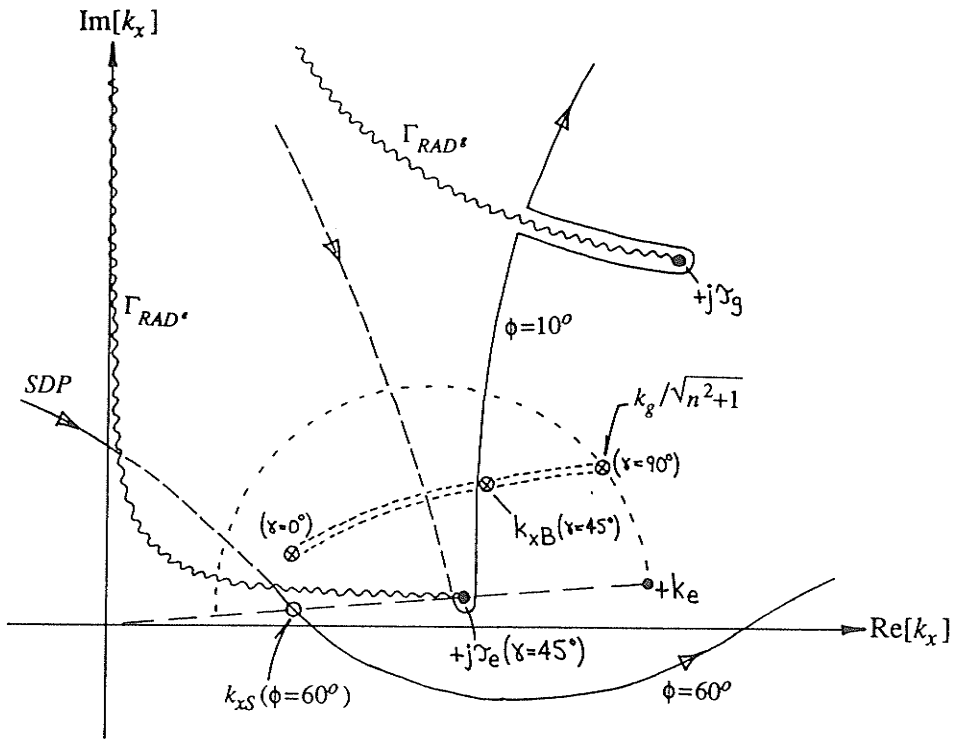

Figure 3.7b: Steepest descent paths in the complex k_x plane for γ=45^o and various angles ϕ. The possible locations of the pole k_{xB} are also given.

Examination of the steepest descent paths in the two complex spectral domains, as given in figure 3.7, shows that either of the lower half-space radiation branch cuts $\pm k_g$ or $\pm j\tau_g$ may be crossed for grazing angles of incidence with respect to the earth $\phi,\gamma\rightarrow 0$ (or $\theta\rightarrow 0$ since $\sin\theta=\sin\phi\sin\gamma$). The contribution from their inclusion is in the form of a *lateral* wave and can be determined from an evaluation at the branch point [Felsen]. The surface wave branch point k_{zB} is never crossed in the complex k_z plane for all angles of incidence γ (since $\mathrm{Re}[k_e]>\mathrm{Re}[k_{zB}]$ for all possible earth electrical properties), whereas the associated surface wave pole k_{xB} in the complex k_x plane moves to a location that can be crossed as $\gamma\rightarrow 0,\phi\rightarrow 0$. Even though this branch cut is never crossed in the k_z plane, its effect on the saddle point contribution is considerable due to its close proximity, especially at low frequencies. Its contribution is in the form of a surface wave that can be extracted by adding the effect of the pole contribution to the saddle point [Felsen]. Finally, it is also possible to excite the guided wave modes k_z^p for grazing angles of incidence with respect to the conductor axis $\gamma\rightarrow 0$, as also shown in figure 3.7 [3.3].

The first step in the steepest descent solution of (3.22) requires the steepest descent evaluation of the integrals (3.62) and (3.63) in the k_x plane. Under the far field conditions $|\tau_e\bar{r}_m|$, $|\tau_e\bar{r}_m^*|\gg 1$, where $\tau_e=\sqrt{k_z^2-k_e^2}$ is the transverse wave number, the modified Bessel function terms $K_1(z)$ can be evaluated using their asymptotic expressions [Abramowitz]. There are no surface wave poles or branch cuts present for these terms. The remaining integral terms can be evaluated using their steepest descent contributions as outlined in appendix B, these containing the surface wave and branch cut contributions. In the far field it will be assumed that $|\bar{r}_m|\approx|\bar{r}_m^*|\approx r_s$ and $(y_m-y_s)/|\bar{r}_m|\approx(y_m+y_s)/|\bar{r}_m^*|\approx-\sin\phi$, $(x_m-x_s)/|\bar{r}_m|\approx(x_m-x_s)/|\bar{r}_m^*|\approx-\cos\phi$. This assumption is valid at non-grazing angles $\phi\neq 0$ and approaches the plane wave incidence case as $|r_s|\rightarrow\infty$. Thus, the saddle point contribution to the remaining terms in (3.62) and (3.63) can be calculated so that the asymptotic evaluation of the incident fields is given by

$$E_{zm}^S(k_z)=\frac{-j\omega\mu_e}{2\pi k_e^2}J_y(+jk_z)\left[e^{-\tau_e(-y_m\sin\phi-x_m\cos\phi)}-R_E e^{-\tau_e(+y_m\sin\phi-x_m\cos\phi)}\right]\sqrt{\frac{\pi\tau_e}{2r_s}}\sin\phi e^{-\tau_e r_s} \tag{3.66}$$

3.3 A set of poles, located on the improper Riemann sheet $\mathrm{Re}[\tau_e]<0$, also exist in the complex k_z plane [Carpentier3]. Since the steepest descent path crosses over onto the improper Riemann sheet, for grazing angles of incidence with respect to the conductor axis $\gamma\rightarrow 0$, these poles may also be crossed leading to leaky wave mode contributions to the current. The use of the leaky wave pole contributions to represent the radiation branch cut spectra has been examined by Leviatan for the case of a wire located in free space [Leviatan]. Poles may also exist on the improper Riemann surface with respect to the surface wave branch cut as will be demonstrated in the results presented in section 3.4.1.

$$E_{zm}^{S}(k_z) = \frac{1}{2\pi} M_y \left[e^{-\tau_e(-y_m \sin\phi - x_m \cos\phi)} - R_H e^{-\tau_e(+y_m \sin\phi - x_m \cos\phi)} \right] \sqrt{\frac{\pi\tau_e}{2r_s}} \cos\phi e^{-\tau_e r_s} \tag{3.67}$$

$$R_E = r_{eg}^{e}\Big]_{k_x=k_{xs}} = \frac{n^2\tau_e \sin\phi - \sqrt{\tau_e^2 \sin^2\phi - k_e^2(n^2-1)}}{n^2\tau_e \sin\phi + \sqrt{\tau_e^2 \sin^2\phi - k_e^2(n^2-1)}}$$

$$R_H = r_{eg}^{m}\Big]_{k_x=k_{xs}} = \frac{\tau_e \sin\phi - \sqrt{\tau_e^2 \sin^2\phi - k_e^2(n^2-1)}}{\tau_e \sin\phi + \sqrt{\tau_e^2 \sin^2\phi - k_e^2(n^2-1)}}$$

for a VED and VMD, respectively. Note that the term $[\bar{I}(k_z)]$ and all the terms in the impedance matrix $[Z(k_z)]$ in (3.22) can not be evaluated in the same manner since their arguments are not in the asymptotic region. The surface wave poles and radiation branch cut contributions when $\phi \rightarrow 0$ are not included in (3.66,3.67).

The next step in the solution requires the steepest descent evaluation of (3.22) in the k_z plane, with the excitation $[E_z^S(k_z)]$ replaced by its asymptotic form (3.66,3.67). Under the far field condition $|k_e R_s| \gg 1$, the induced current can then be determined using the method of steepest descent as

$$[I(z)] = [Z(k_e \cos\gamma)]^{-1} [\bar{I}(k_e \cos\gamma)] [E_z^{inc}(\theta,\psi)] \tag{3.68}$$

$$E_{zm}^{inc}(\theta,\psi) = \Big\{ [E_\theta \sin\theta\cos\psi + E_\psi \sin\psi] e^{+jk_e[-y_m \sin\theta - x_m \cos\theta \sin\psi]} - [E_\theta \Gamma_E \sin\theta\cos\psi - E_\psi \Gamma_H \sin\psi] e^{+jk_e[+y_m \sin\theta - x_m \cos\theta \sin\psi]} \Big\} \tag{3.69}$$

$$\Gamma_E = \frac{n^2\sin\theta - \sqrt{n^2 - \cos^2\theta}}{n^2\sin\theta + \sqrt{n^2 - \cos^2\theta}} \quad , \quad \Gamma_H = \frac{\sin\theta - \sqrt{n^2 - \cos^2\theta}}{\sin\theta + \sqrt{n^2 - \cos^2\theta}}$$

where Γ_E and Γ_H are the plane wave TM and TE Fresnel reflection coefficients at the air-earth interface. Note that (3.68) is the same expression as that which would have been derived for an assumed incident plane wave, except the incident field E_θ, E_ψ is now modified by the far field factor of the VED,VMD dipoles in free space

$$E_\theta = \left(\frac{+jZ_0 k_e}{4\pi} J_y \right) \left(\frac{\cos\theta}{R_s} \right) e^{+jk_e R_s} \tag{3.70a}$$

$$E_\psi = \left(\frac{+jk_e}{4\pi} M_y \right) \left(\frac{\cos\theta}{R_s} \right) e^{+jk_e R_s} \tag{3.70b}$$

3.4. A STUDY OF THIN-WIRE STRUCTURES

The following sections present and discuss numerical results for the excitation of and wave propagation along a system of conductors located over a lossy half-space. As explained in section 3.3, the total current induced on the system of conductors due to a finite source will consist of a sum of discrete propagating modes as well as contributions from a continuous spectrum of radiating modes and a spectrum of surface wave modes. Under limiting conditions, many useful approximations to the exact inverse transform solution (3.22), which incorporates all these contributions, can be utilized. The dominance of the poles or branch cuts depends on the electrical distance of the source from the transmission line as well as the electrical distance from the source to the observation point along the axis of the structure. In one extreme, when the source is electrically near the structure, a transmission line approach can be used, where the pole contributions are dominant. In the other extreme, when the source is electrically far from the structure, a geometrical optics approximation can be used (the source can be modeled as an incident plane wave), where the upper half-space radiation branch cut will provide the dominant contribution. The next section will briefly characterize the discrete modes of propagation which a multiple thin-wire transmission line can support. This will then be followed by an examination of the validity of the transmission line and plane wave incidence models. For all the cases discussed, particular attention is paid to the validity of the quasi-TEM approximation.

3.4.1. Properties of Discrete Modes

This section is concerned with accurately characterizing the discrete propagating modes supported by a thin-wire transmission line structure. They are considered to be the dominant contributions to the current when the source is electrically near the transmission line and when the structure dimensions are small compared to the free space wavelength. The use of only the discrete modes to represent the currents allows a much simplified transmission line approach to the formulation of many antenna and scattering problems, and thus the determination and characterization of the modes as well as conditions for which approximating formulas are valid is important. The solution of the discrete modes of propagation along a multiple conductor transmission line over a lossy earth, based on the telegrapher's equations, has been successfully applied in power engineering problems for many decades. In 1926, Carson [Carson] took the finite conductivity of the earth into account by applying Maxwell's equations as well as some circuit concepts. This quasi-static theory, however, is valid only at low frequencies where distances are small compared to the free space wavelength and the earth conductivity is high enough so that displacement currents can be neglected. An exact formulation of the boundary value problem is obtained by using Maxwell's equations and satisfying the boundary condition at the air-earth interface, as presented in section 3.2.1 [Wait5, dosSantos]. The resulting formulation however, requires the solution of the Sommerfeld type Fourier integrals (3.19), whose accurate evaluation is

difficult. Recent investigations [Chang3, Olsen5] have given various solutions using numerical or analytical techniques, however, most of these studies have been aimed at single conductor systems only. Wait [Wait9] formulated the problem of a multiple conductor system over a layered earth and gave a solution in terms of integral expressions, and Kuester and Chang [Kuester4] gave numerical results for a symmetric two conductor system over a homogeneous earth.

The discrete modes of propagation are determined from the solutions of the homogeneous integral equation (3.4). For thin-wire structures, the exact solutions can be obtained from the eigenvalues of the impedance matrix (3.46), which is defined as the mode equation. The evaluation of the impedance matrix elements (3.18-3.20), is discussed in appendix B. It will be shown that the accurate evaluation of the Sommerfeld integrals (3.19) becomes imperative at higher frequencies. As well, since the integrand of one of these integrals (3.19b) contains a pole k_{xB} in its integrand, due to the TM surface wave supported by the half-space geometry, additional discrete modal solutions become mathematically feasible in the neighbourhood of this pole. An extensive parametric study of the discrete propagating modes supported by various conductor configurations and for typical earth properties is addressed in [Bridges3], where a comparison to the quasi-TEM and an alternative small argument approximation is also made. Only two specific conductor configurations will be discussed in this section, with comparisons to the quasi-TEM results in some cases. The quasi-TEM approximation was discussed in section 3.3.3, where the discrete modes were found from the solution of the standard eigenvalue equation (3.55). The evaluation of the matrix elements (3.58,3.59) in the quasi-TEM case is much simpler than those of the exact solution (3.56,3.57), with the only remaining integral (3.61) fully discussed in appendix B.

The solution of the mode equation (3.46) for the case of a single conductor above a lossy earth is considered first. Referring to figure 3.2, a copper wire of radius a_1=2.5mm is situated at a height $h=|\,\overline{\rho}_{11}^{*}/2\,|=1.0m$ above an earth having electrical properties $\varepsilon_{rg}=15$, $\sigma_g=0.01$. Figure 3.8 shows the result of evaluating the magnitude of the mode equation abs{ $|\,Z(k_z)\,|$ } over the normalized τ_e/k_e plane, where τ_e was defined as the radial wavenumber. Note that the desired propagation constant $k_z^p = k_e\sqrt{1-(\tau_e^p/k_e)^2}$ is defined such that the proper solutions of the mode equation occur in the quadrant $\mathrm{Re}[\tau_e^p/k_e]$, $\mathrm{Im}[\tau_e^p/k_e]\geq 0$. A frequency of f=30$MHz$ has been chosen making the refractive index of the interface n=3.95+j0.76. Figure 3.8 indicates two possible solutions of the mode equation in the normalized τ_e/k_e plane. One solution occurs in the region where the quasi-TEM solution is found ($\tau_e \rightarrow \tau^{TEM}$). The other occurs in the region near the TM surface wave pole λ_B ($\tau_e \rightarrow U_{eB}$). As derived in section 3.3, the surface wave pole presents itself as a singularity in the integral $\mathbf{G}(\tau_e, 2h\hat{y})$, its position in the complex τ_e/k_e plane being strictly a function of the half-space electrical properties $U_{eB}/k_e = +j/\sqrt{n^2+1}$. Figure 3.9 gives the normalized

solutions of the mode equation τ_e^p/k_e over the entire frequency spectrum. The results of the quasi-TEM approximation ($h \ll \lambda_e$) in one extreme as well as the solution of the corresponding Sommerfeld line in free space ($h \gg \lambda_e$) in the other extreme [Sommerfeld1] are shown for comparison. The solution which most closely adheres to the quasi-TEM result will be designated as the structure attached or "transmission line" mode (k_z^{TL}). The solution found near the pole U_{eB} will be designated the surface attached or "fast-wave" mode (k_z^{FW}) since the phase velocity for this mode is usually less than the free space value $\mathrm{Re}[k_z^{FW}] < k_e$. Figure 3.10 gives the corresponding values of the normalized propagation constants k_z^p/k_e as a function of frequency. The results are compared to those of Olsen [Olsen5], as well as to the quasi-TEM approximation. The quasi-TEM result is a good approximation to the exact solution at low frequencies ($|n| \gg 1$, $h/\lambda_e \ll 1$) where the dominant terms of the mode equation (3.46) are Z^w, $K_0(\tau_e a) - K_0(\tau_e 2h)$, and $\mathbf{J}(\tau_e, 2h\hat{y})$. In the high frequency range the solution converges to that of a conductor in free space [Stratton] where the dominant terms in the mode equation are Z^w and $K_0(\tau_e a)$. Note that the attenuation of the fast wave mode $\mathrm{Im}[k_z^{FW}]$ is considerably less than that of the transmission line mode $\mathrm{Im}[k_z^{TL}]$ over most of the frequency spectrum. However, the excitation of this mode, as determined by its residue contribution to the current in (3.39), is usually small. Only at very large distances from the source would the decay of the transmission line mode be enough for the fast wave mode to become important. In this range, however, the branch cut contributions (3.40,3.41) would also be important.

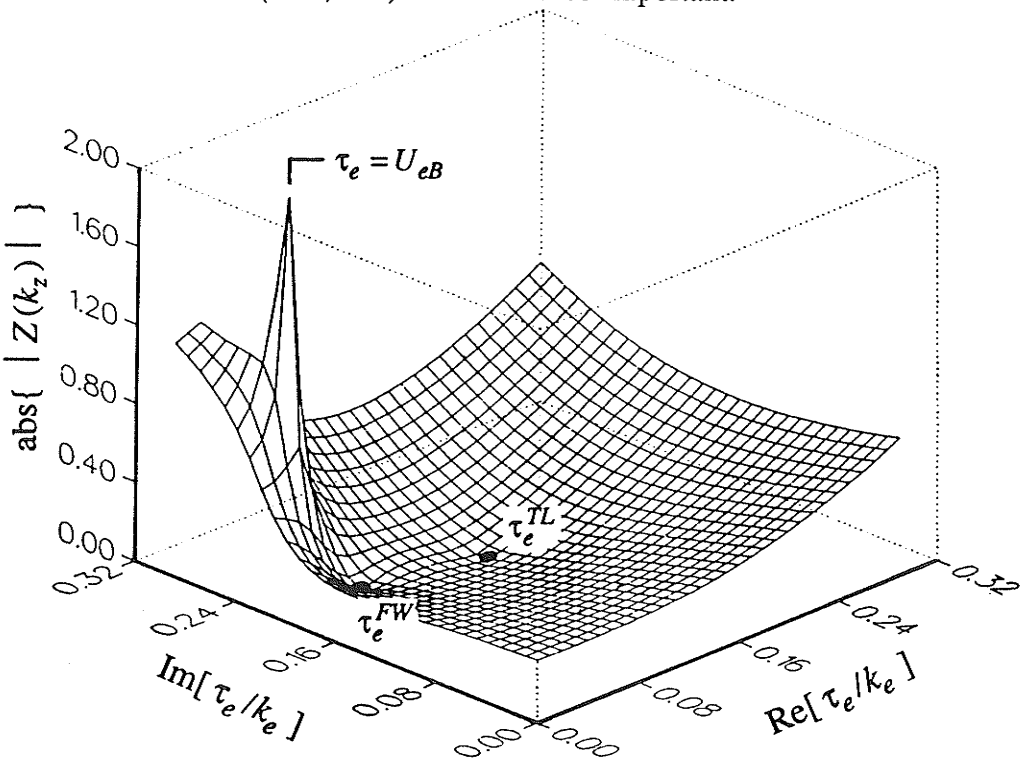

Figure 3.8: Evaluation of the mode equation $|Z(k_z = \sqrt{\tau_e^2 + k_e^2})|$ over the complex τ_e/k_e plane for a single conductor system.

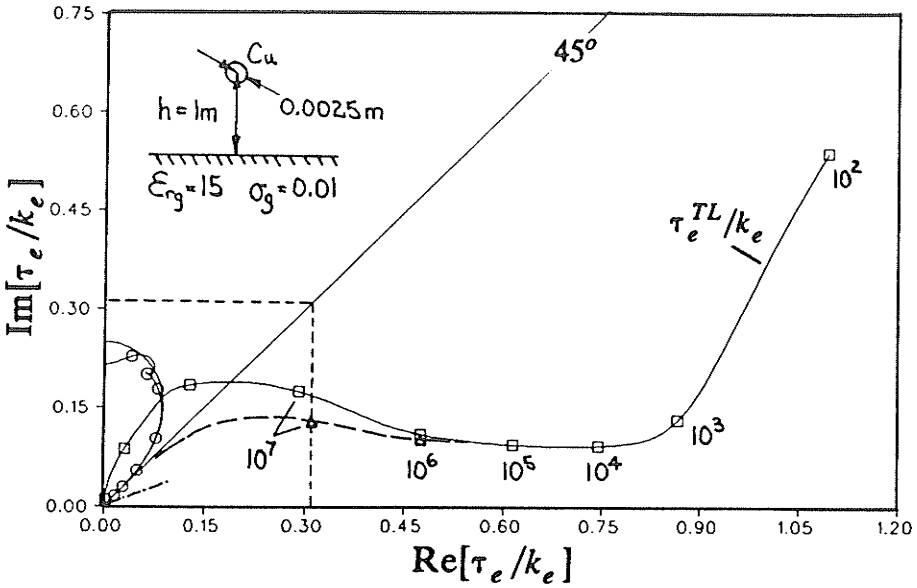

Figure 3.9a: Discrete mode solutions τ_e^p/k_e as a function of frequency.

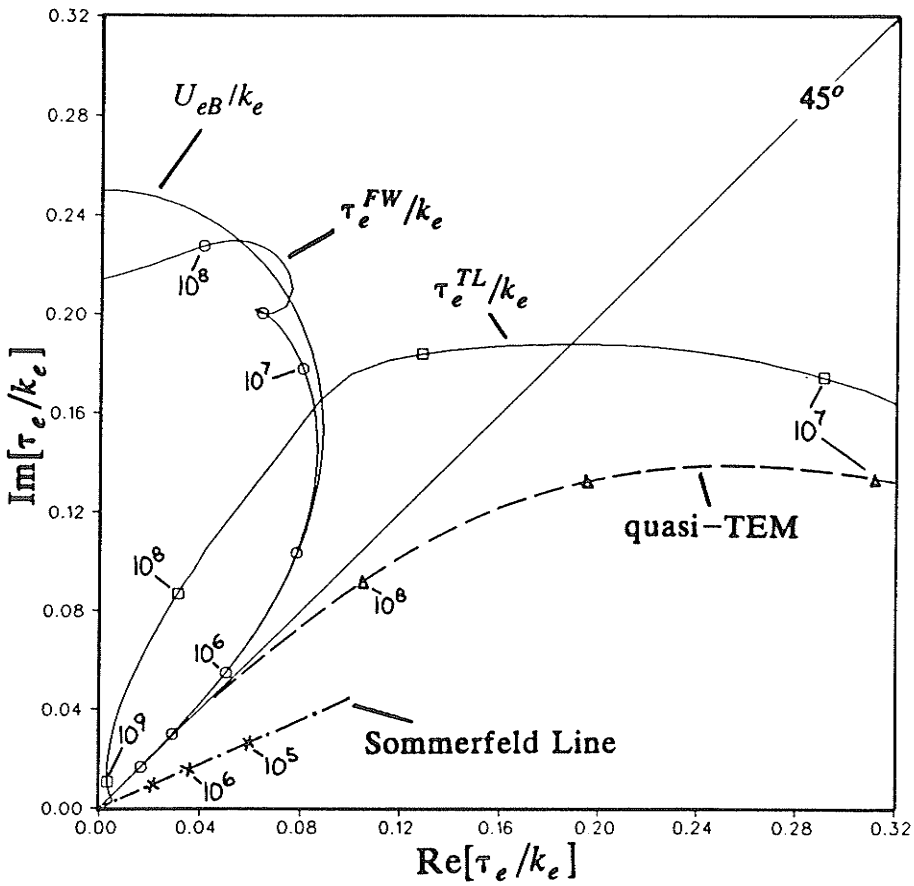

Figure 3.9b: Discrete mode solutions τ_e^p/k_e as a function of frequency. Enlarged high frequency region of figure 3.9a.

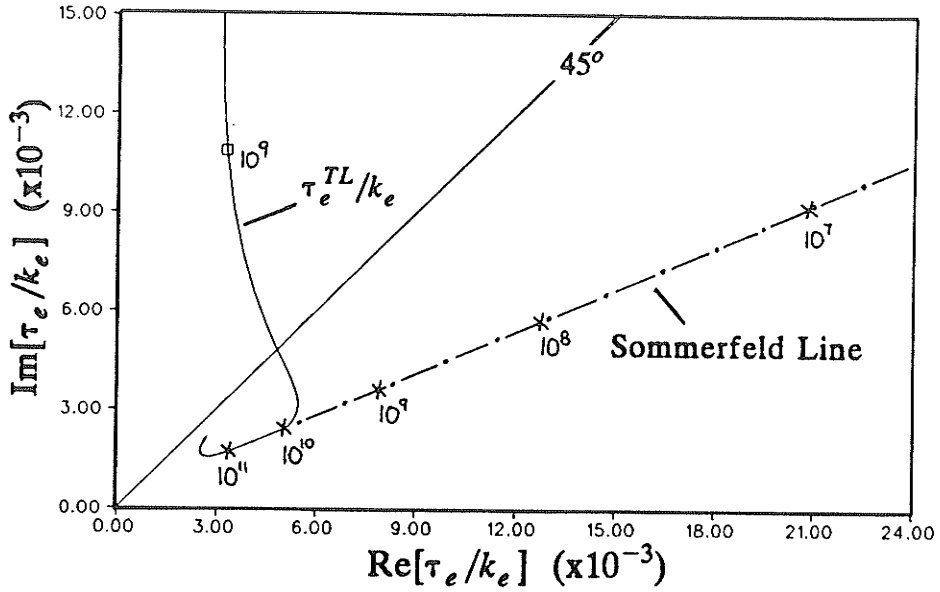

Figure 3.9c: Discrete mode solutions τ_e^p/k_e as a function of frequency. High frequency portion of figure 3.9a showing Sommerfeld line mode.

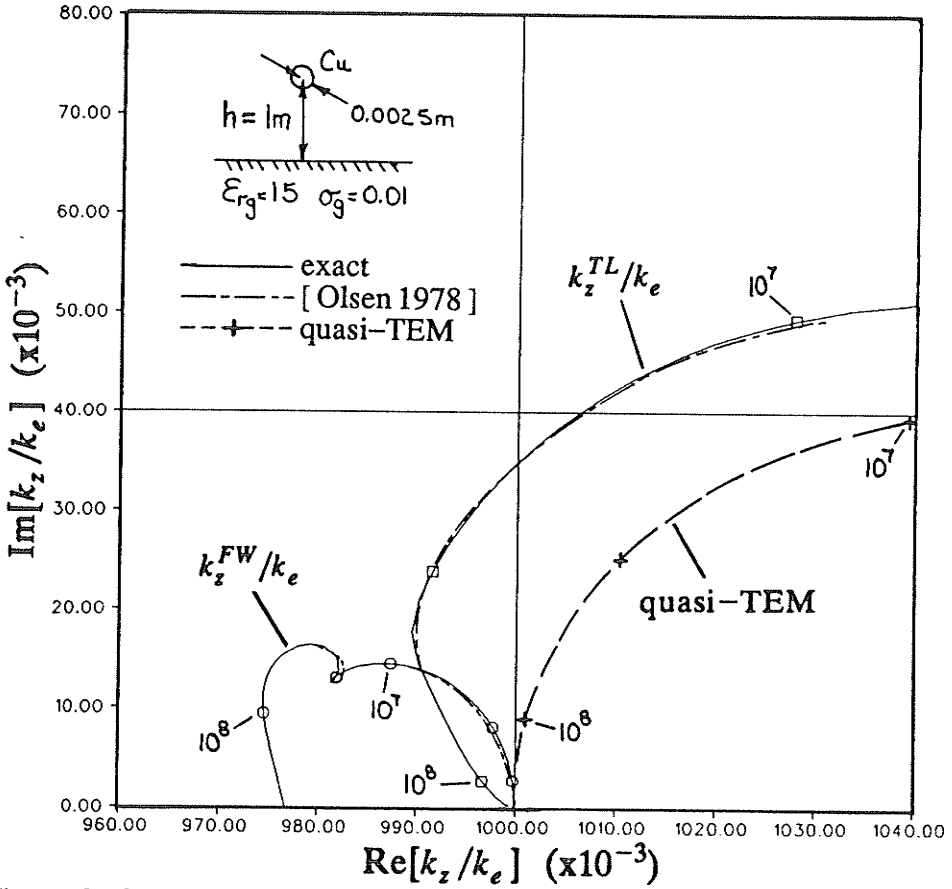

Figure 3.10: Normalized propagation constants k_z^p/k_e as a function of frequency corresponding to the results of figure 3.9.

In Figure 3.11, the normalized values of τ_e^p/k_e as a function of frequency are calculated for different conductor heights; h=1.0m→10.0m. Earth electrical parameters are the same as in Figure 3.9. Again, there are two possible solutions to the mode equation for each case. At small conductor heights, the fast-wave solution remains near the pole U_{eB} and the transmission line solution remains near the quasi-TEM result over the whole frequency range. However, for large conductor heights, the fast-wave solution moves into the region near the quasi-TEM result and similarly the transmission line solution moves into the region near the pole as frequency increases. Figure 3.11 shows that it is possible to find a specific height and frequency such that the fast-wave and transmission line solutions coincide $\tau_e^{TL} = \tau_e^{FW}$. For the case being studied, this situation occurs at h≈1.6m and f≈22MHz. The discrete modal fields for each solution become identical in this situation, the double root to the mode equation known as *modal degeneration* [Olsen5].

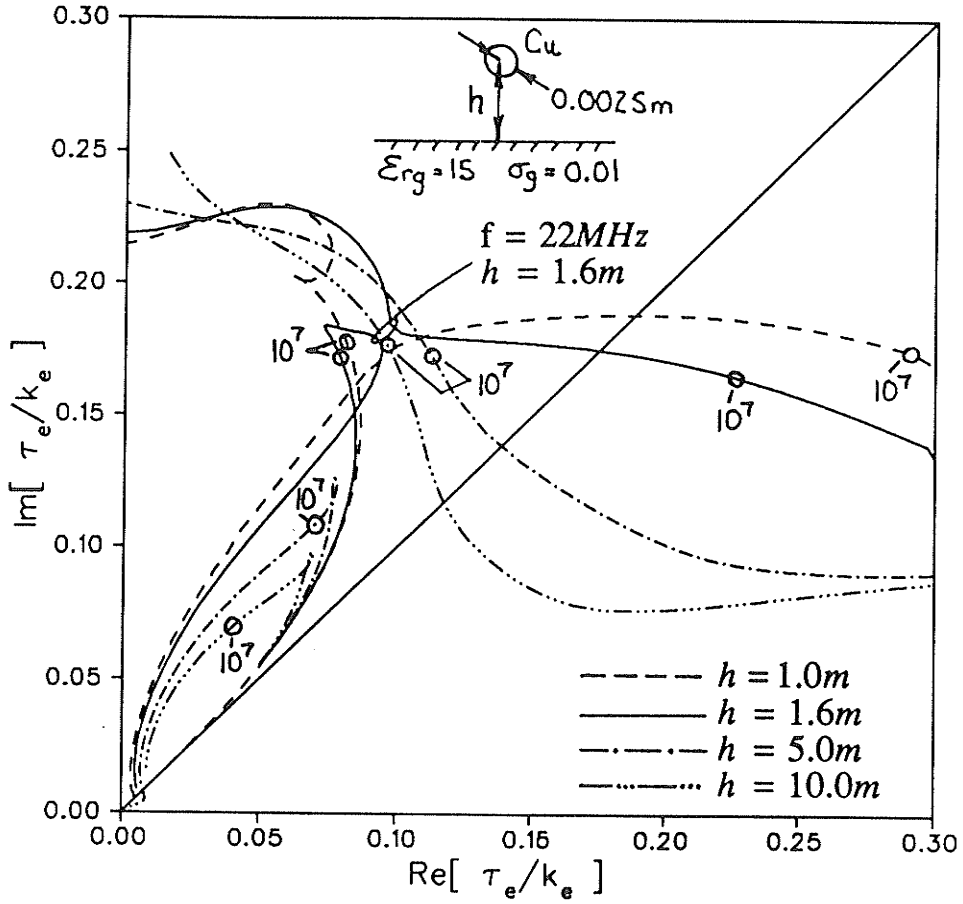

Figure 3.11: τ_e^p/k_e as a function of frequency for different conductor heights. The solid curve at f≈22MHz indicates the double root.

Figure 3.12 shows the result of evaluating the magnitude of the mode equation abs{ $|Z(k_z)|$ } over the normalized τ_e/k_e plane when a two conductor system is considered. Two copper conductors, both of radius $a_1=a_2=2.5mm$, are located at a distance $d=2.0m$ apart and a height $h=5.0m$ above an earth with electrical properties $\varepsilon_{rg}=15$, $\sigma_g=0.01$. There are four possible solutions to the mode equation for this case. Two of the solutions correspond to the normal transmission line modes, one symmetric (or ground mode), and one antisymmetric (or metallic mode). The remaining two solutions are found in the region of the pole singularity U_{eB}. Figure 3.13 gives the normalized solutions of the mode equation τ_e^p/k_e as a function of frequency, with figure 3.14 giving the corresponding results for k_z^p/k_e. One of the modes in the region of the pole is a proper solution over only a small portion of the frequency spectrum, and otherwise crosses onto an improper Riemann sheet as a result of the branch cut $|\mathrm{Re}[s]|>1$ as defined in the evaluation of the integral $\mathbf{G}(\tau_e,\bar{\rho}^*)$ in appendix B (B.20). The residue of this pole in (3.39) does not make a significant contribution to the current.

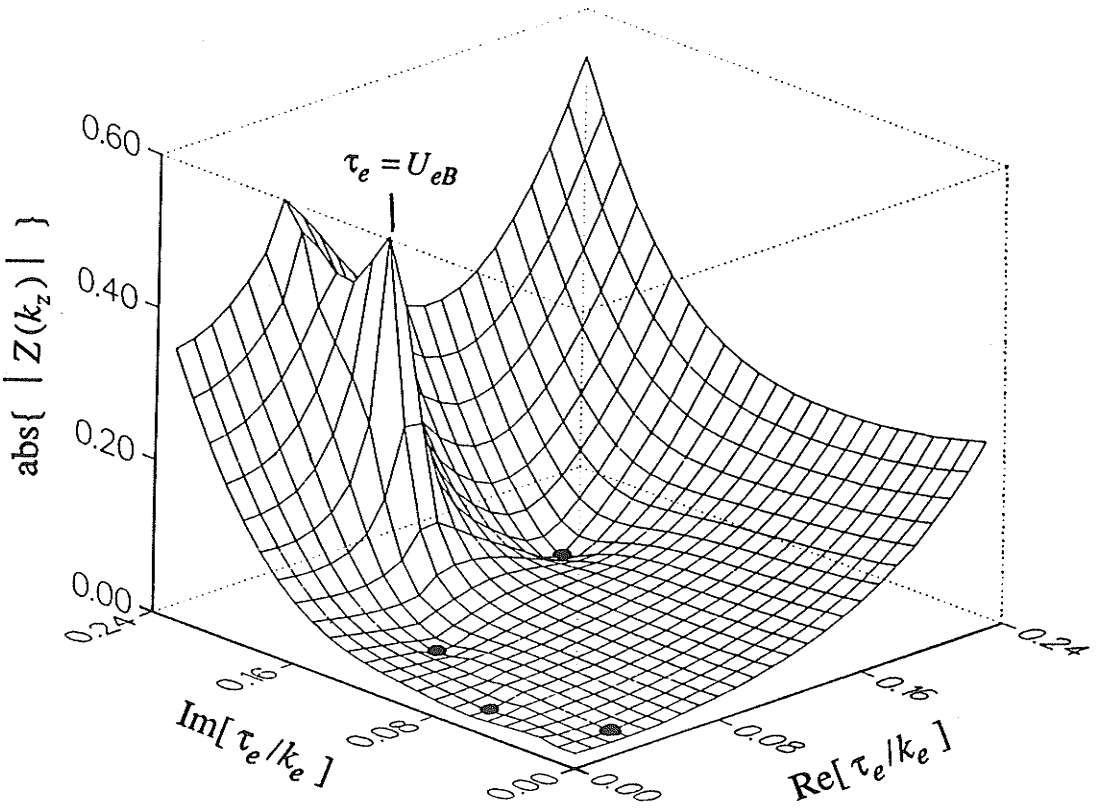

Figure 3.12: Evaluation of the mode equation $|[Z(k_z=\sqrt{\tau_e^2+k_e^2})]|$ over the complex τ_e/k_e plane for a two conductor system. Shown are the two transmission line and two fast-wave mode solutions.

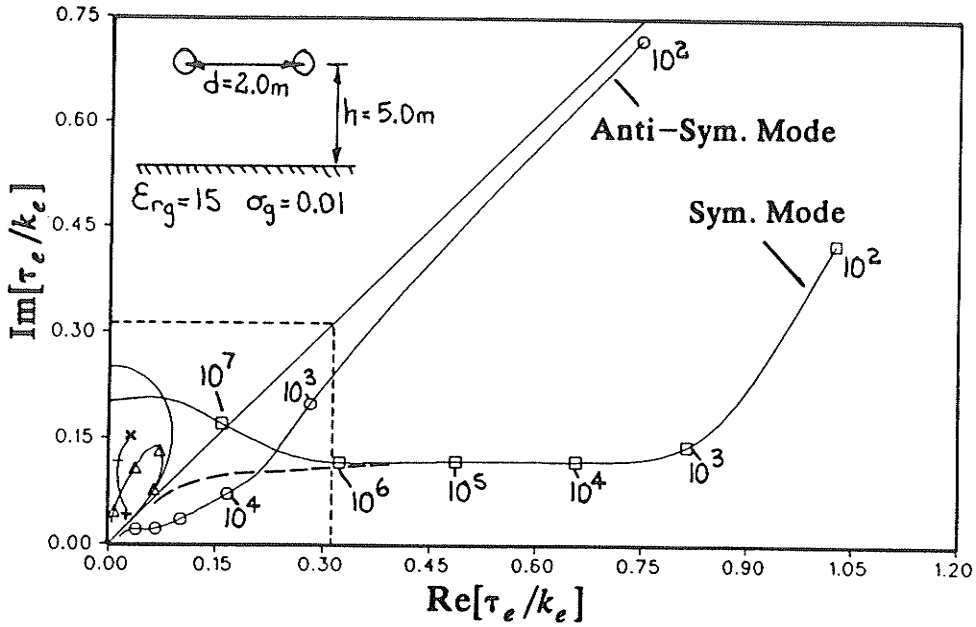

Figure 3.13a: Solutions of the mode equation τ_e^p/k_e as a function of frequency.

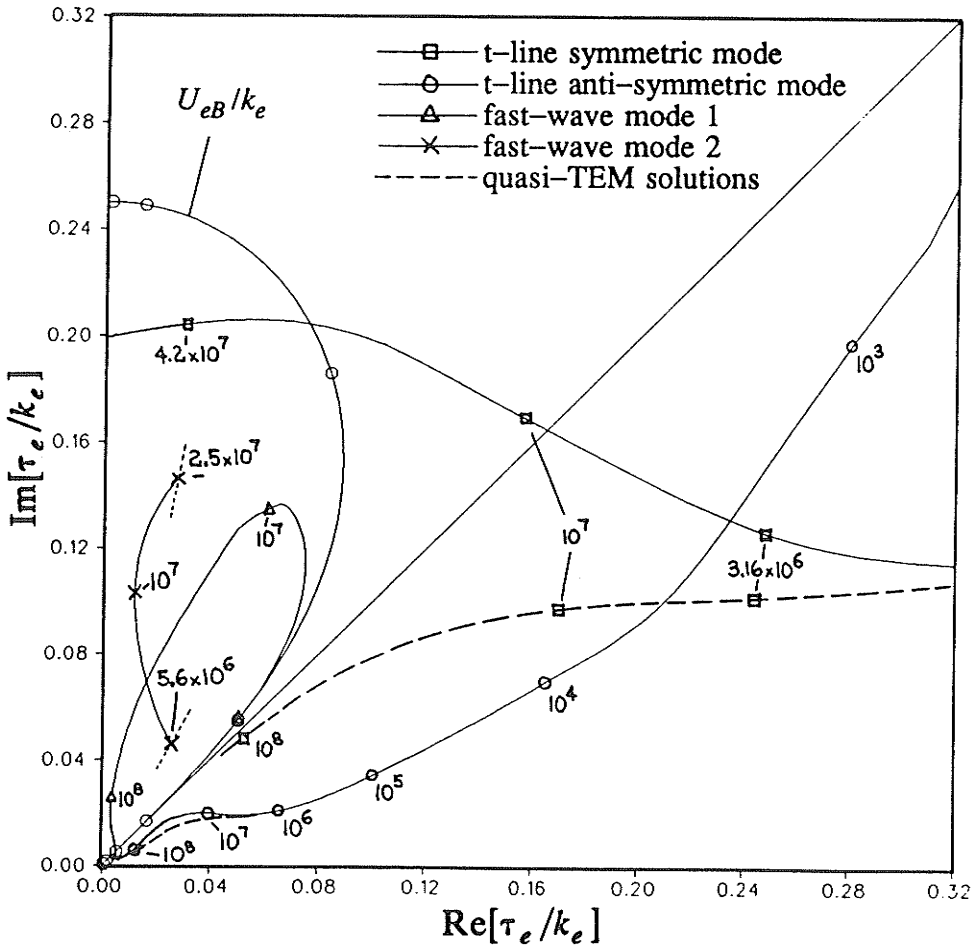

Figure 3.13b: Solutions of the mode equation τ_e^p/k_e as a function of frequency. Enlarged high frequency region of figure 3.13a.

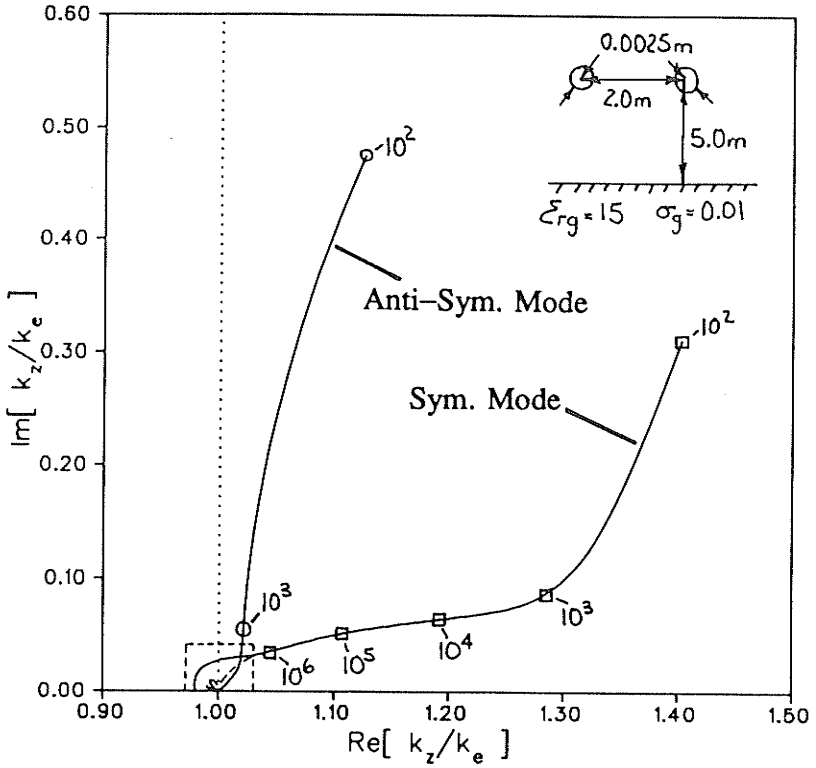

Figure 3.14a: Solutions of the mode equation k_z^p/k_e as a function of frequency.

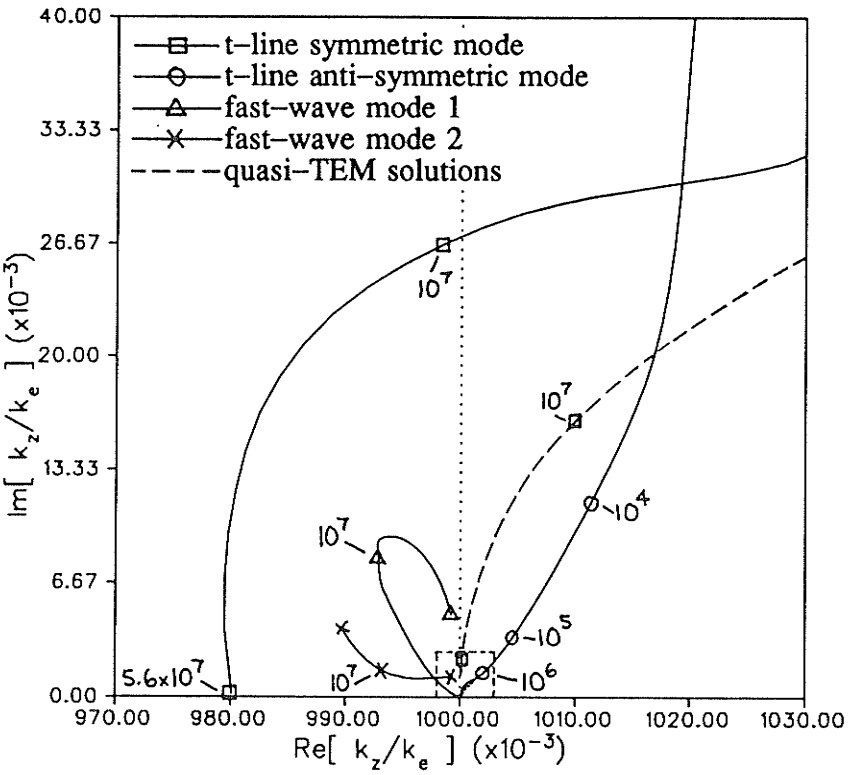

Figure 3.14b: High frequency region indicated in figure 3.14a.

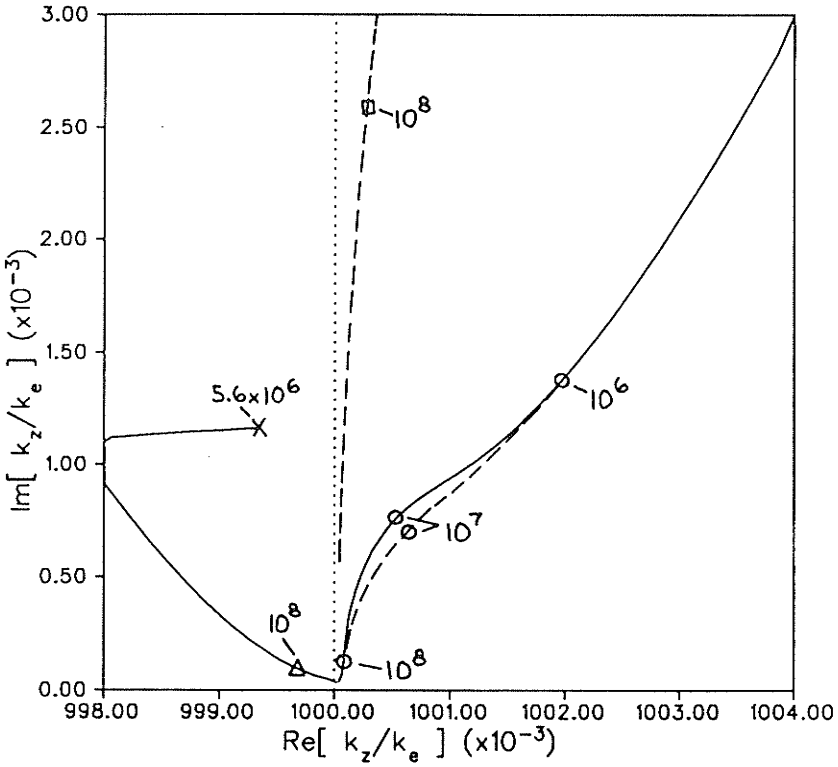

Figure 3.14c: Extremely high frequency region indicated in figures 3.14a,b.

3.4.2. Examination of Limiting Cases

In this section, the dominance of the pole and branch cut contributions in the determination of the induced currents on a thin-wire transmission line due to a finite source will be examined. As discussed in section 3.3, the contributions to the induced currents could be distinguished as a sum of the discrete modes excited by the source plus a set of branch cut contributions (3.38-3.41). These contributions were separated by deforming the path of integration in the inverse transformation (3.22) from the real axis to encompass the poles and branch cuts. In one extreme, when the source is electrically near the transmission line, the discrete modes contributions are expected to dominate. The formulation of the currents in terms of only the discrete modes was the topic of sections 3.3.1-3.3.3, with their properties characterized in the last section. In the other extreme, when the source is electrically far from the transmission line, or when the observation point is *very* far from the source, the branch cut contributions to the currents is expected to dominate. Further, in the far field, an asymptotic evaluation at the saddle point along the radiation branch cut Γ_{RAD}, for the upper half-space should provide adequate results (plane wave incidence is assumed). This assumption was examined in section 3.3.4, where results were obtained for specific sources through the method of steepest descent. The use of only the saddle point evaluation,

neglects the contributions from the poles as well as the two other branch cuts Γ_{RAD^s}, Γ_{SUR}. As pointed out in section 3.3.4, however, the surface wave branch cut Γ_{SUR} may become important at grazing angles of incidence with respect to the interface.

The case of a single conductor transmission line, excited by a vertical electric dipole source (VED) will be used to examine these limiting cases. The exact solution to the induced currents due to a VED is obtained by using the complete spectral transformation (3.22), where the elements of the impedance matrix $[Z(k_z)]$ are given in (3.18), and the axial components of the imposed electric field $[E_z^S(k_z)]$ due to the VED are given from (3.26). The resulting currents due to the discrete mode contributions are determined using (3.39), where the values of the propagation constants k_z^p are found from the solution of the mode equation (3.46). It is important to note that the discrete mode results are not the same as the transmission line approximation formulation (3.45). Finally, the saddle point contribution to the induced currents is formulated using (3.68-3.70). For the cases studied in this section, the transmission line dimensions will be chosen for the quasi-TEM region ($h/\lambda_e \ll 1$), and only the distance from the VED source to the transmission line will be varied to extremes.

Referring to figure 3.6, a single copper conductor of radius $a=1.0cm$ situated at a height $h=10.0m$ $(x=0,y=h)$ will be considered. A frequency of $100KHz$ $(\lambda_e=3km)$ is chosen along with an earth characterized by a relative permittivity $\varepsilon_{rg}=5$ and a conductivity $\sigma_g=0.01$. The first case will examine the validity of the steepest descent approximation (modeling the incident field as an incident plane wave). The exciting VED will be located directly over the transmission line $(x_s=0m,z_s=0m)$, at three different heights above the interface; $y_s=3km,9km,15km$, these corresponding to $(y_s=1\lambda_e,3\lambda_e,5\lambda_e)$. Figure 3.15 gives the magnitude of the induced current $|I(z)|$ as calculated by numerically integrating the exact expression (solid curves), and using the saddle point evaluation (dashed curves). Since for these cases $\phi=90^o$ ($\Psi=0^o$), the angle of incidence $\gamma=\theta$ indicates the position along the conductor axis $|z-z_s|=y_s\cot\gamma$; ie. for $y_s=1\lambda_e$ and $\gamma=30^o$ then $|z-z_s|=1.732\lambda_e$. By examining figure 3.15, the saddle point contribution is accurate when the dipole is electrically far from the interface and not in the grazing angle region. These observations correspond to the condition $|\tau_e r_s| = |-jk_e\sqrt{1-\cos^2\gamma}\, r_s| \gg 1$ (or $2\pi\sin\theta r_s/\lambda_e \gg 1$ when $\phi=90^o$) imposed when (3.22) was evaluated using its asymptotic expressions.

For the results of figure 3.15, the VED was positioned so that the incident angle $\phi=90^o$ in all cases. As discussed in section 3.3.4, the contribution from the surface wave branch cut Γ_{SUR} becomes important for grazing angles of incidence with respect to the interface $\theta\to 0^o$ (when $\gamma\to 0^o$ or $\phi\to 0^o$ since $\sin\theta = \sin\gamma\sin\phi$). Thus, only when $\gamma\to 0^o$ in figure 3.15 could the effect of the branch cut influence the induced currents. Note the contribution from the branch cut Γ_{RAD^s}, in the form of a lateral wave, is negligible since the conductivity of the interface is fairly high at the chosen operating frequency (the associated branch point $n=30.03+j29.94$). To examine the influence of

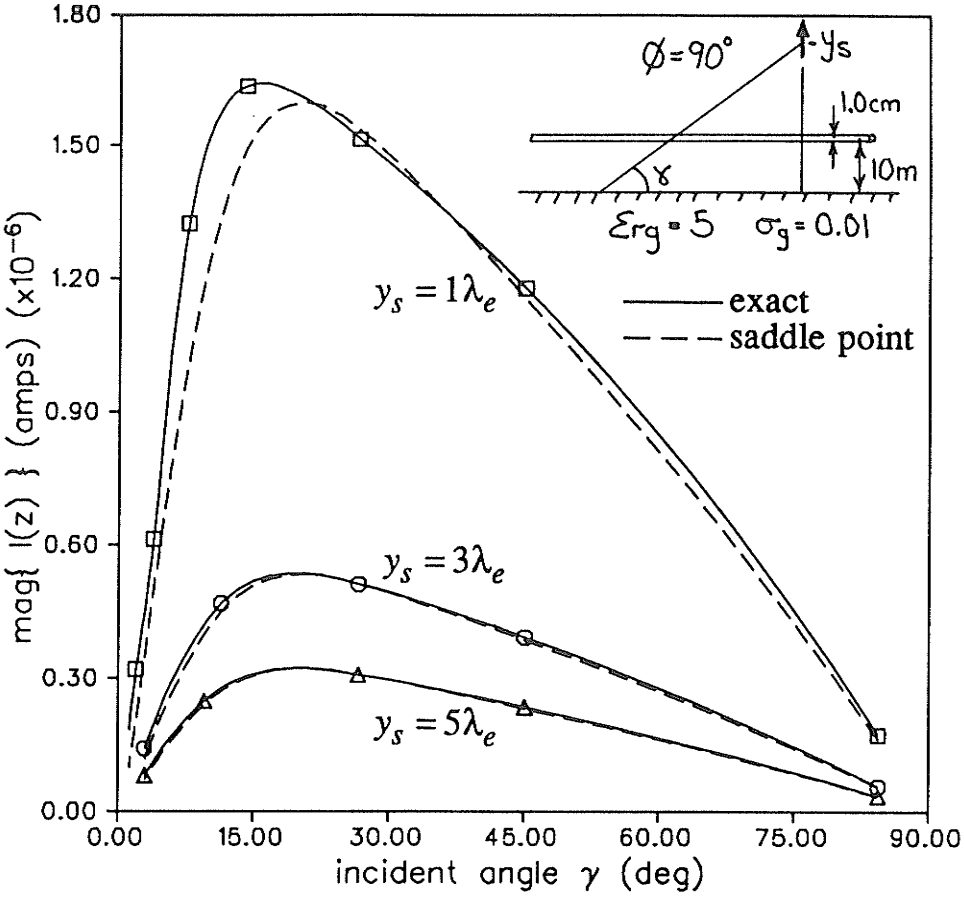

Figure 3.15: Comparison of the exact and saddle point contribution to the current induced on a conductor as a function of incident angle and VED height.

the surface wave branch cut, the transverse distance r_s from the transmission line to the VED will be fixed $r_s=3km=1\lambda_e$ and the angle ϕ will be varied; $\phi=5^o$, 30^o, 90^o, these corresponding to dipole positions $(x_s=2988m, y_s=261m)$, $(x_s=2598m, y_s=1500m)$, and $(x_s=0.0m, y_s=3000m)$, respectively. The results for the induced current at various observation points along the conductor axis is shown in figure 3.16, where $\gamma = \sin^{-1}(r_s / \mid z-z_s \mid)$. The results show that even though the condition $\mid \tau_e r_s \mid > 1$ is met for all angles ϕ, there is a large error in the induced current for grazing angles with respect to the interface as expected due to the effect of the surface wave branch cut.

Finally, the dominance of the discrete mode and saddle point (plane wave incidence) contributions to the current in the two extreme cases will be examined. The results of varying the VED distance from the transmission line is examined in figure 3.17. For this case the dipole will be located directly above the transmission line at a

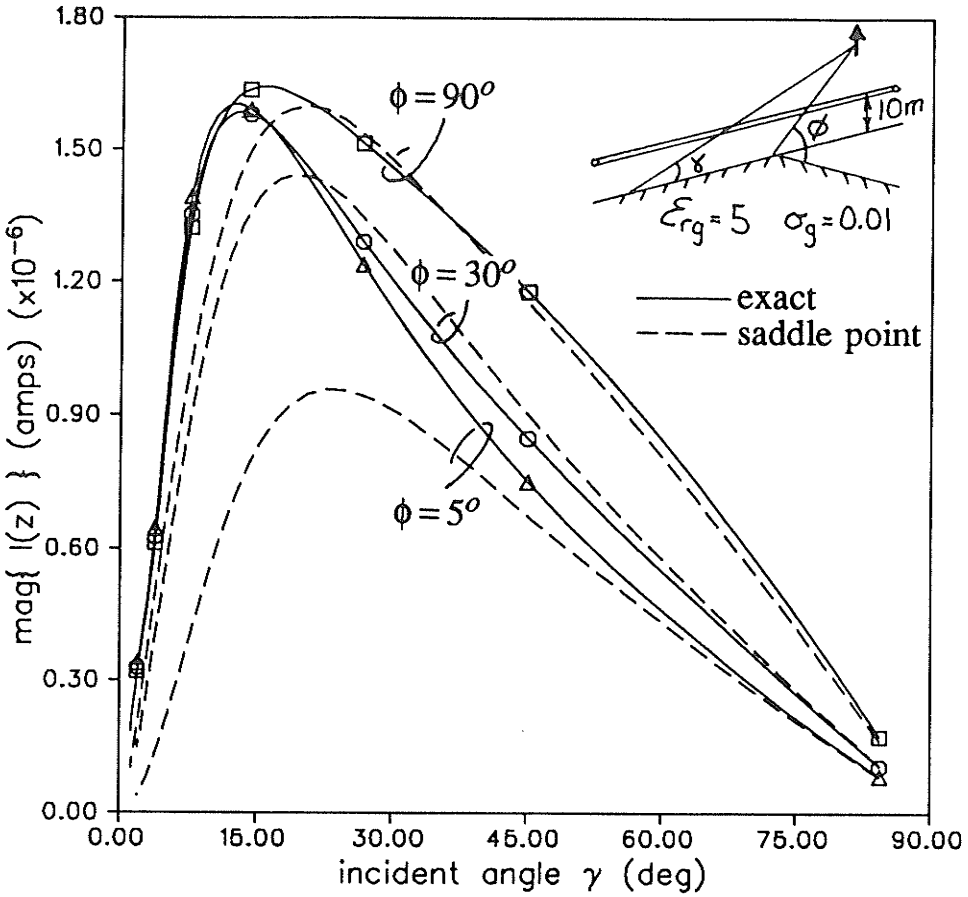

Figure 3.16: Comparison of the exact and saddle point contribution to the current induced on a conductor as a function of incident angle and grazing angle with respect to the interface.

height y_s (x_s=0,z_s=0), with the observation point along the conductor axis fixed at $|z-z_s|=3km=1\lambda_e$. As discussed in the results of section 3.4.1, there are two discrete modes of propagation for the single conductor structure. Since the structure dimensions are much less than the free space wavelength at the frequency considered, $h/\lambda_e=1/300\ll 1$, the dominant mode will be the transmission line mode (defined as k_z^{TL} in the last section). The normalized propagation constant for the structure has been calculated as $k_z^{TL}/k_e=1.0440+j0.0266$ for this case (the corresponding quasi-TEM result is $k_z^{TEM}/k_e=1.0440+j0.0263$). At these frequencies, the contribution from the other discrete mode (defined as k_z^{FW}), which is found near the surface wave pole $\lambda_B/k_e=n/\sqrt{n^2+1}=1.0+j2.8\times10^{-4}$, is negligible and will not be examined. Figure 3.17 shows that when the VED is electrically far from the transmission line ($y_s>\lambda_e$), the main contribution to the current is due to the branch cut and can be accurately modeled by the plane wave incidence model. When the VED is electrically near the

transmission line ($y_s < \lambda_e/20$), the discrete mode contribution to the current dominates. Note that the dominance of either of the limiting approximations will depend also on the observation distance $|z-z_s|$, and the accuracy of the plane wave incidence model will depend on the angle θ as discussed in the last paragraph. An examination of the contributions to the current (as well as the input impedance) due to a delta function voltage source has also been examined by Chang [Chang3].

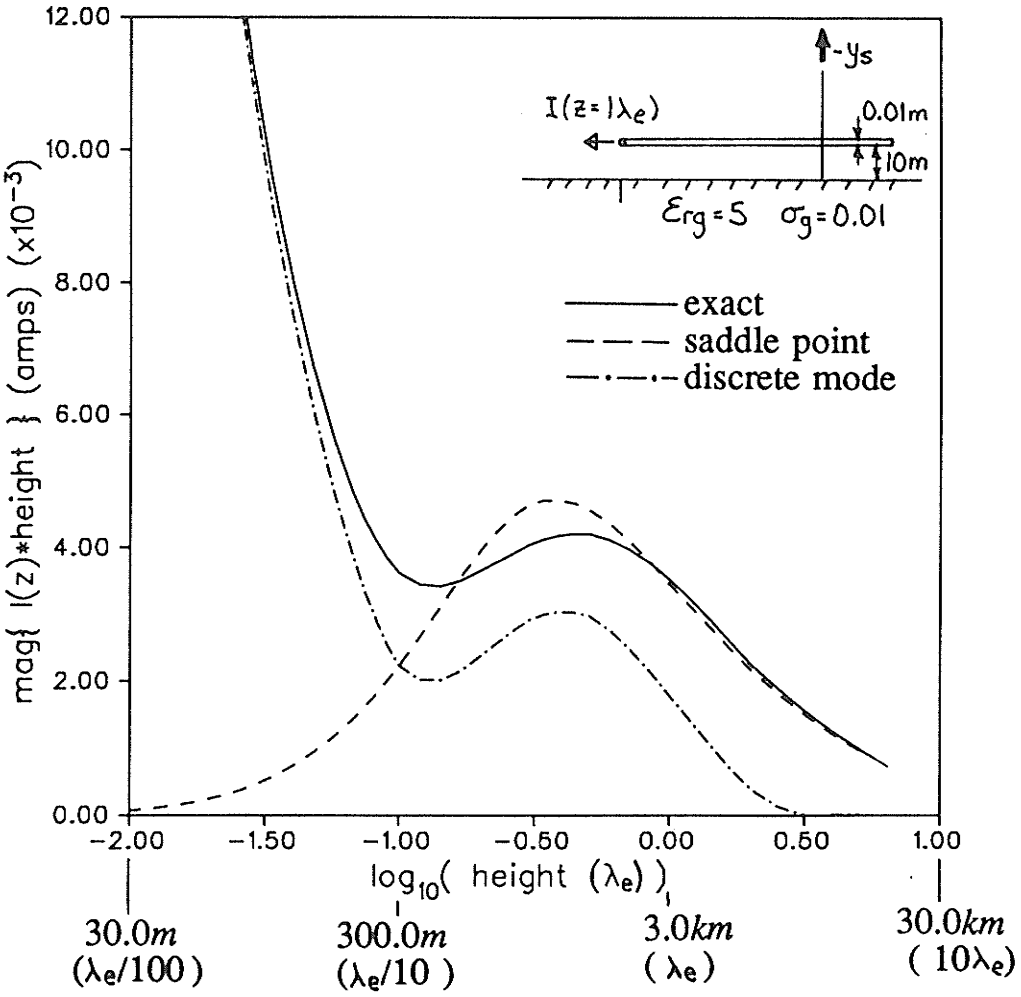

Figure 3.17: Comparison of the exact, saddle point and discrete mode contributions to the current induced on a conductor as a function of the VED height.

3.4.3. Discussion

In general there are more modes than conductors supported by an N-conductor thin-wire system ($P \geq N$). N of the modes are of the traditional quasi-TEM type (these have been denoted as transmission line modes). The remaining $P-N$ modes occur

due to solutions of the mode equation in the region of the surface wave pole singularity (these have been denoted as fast-wave modes). Not all of the additional fast-wave modes necessarily fall on the proper Riemann sheet, and at extremely low or high frequencies, they do not make a large contribution to the structure currents or radiated fields. By examining the results presented in section 3.4 and in [Bridges3], the quasi-TEM approximation was shown to be valid under the conditions that all structure dimensions are small compared to the free space wavelength ($|\overline{\rho}/\lambda_e| < 1/10$) and that the refractive index of the interface is large ($|n| > 10$). As well, an improved small argument approximation for evaluating the mode equation was presented in [Bridges3], and was shown to relax the restriction on $|n|$, thus substantially increasing the validity of the results.

The use of either the discrete mode contributions in the near field (transmission line approximation), or the saddle point contribution in the far field (geometrical optics approximation), was examined for determining the induced currents due to a vertical electric dipole source. The currents induced on the structure were found to be dominated by the discrete mode contributions under the condition that the transverse distance from the source to the transmission line is much less than the free space wavelength ($|\overline{r}_s/\lambda_e| < 1/20$). In order for the saddle point evaluation to yield accurate results, it was required that the transverse distance from the source to the transmission line is much greater than the *transverse component* of the free space propagation constant ($|\overline{r}_s\sqrt{1-\cos^2\gamma}/\lambda_e| > 3$). It must be noted that near grazing angles of incidence with respect to the interface $\theta \rightarrow 0^o$, contributions from the TM surface wave and possibly from leaky wave poles may also become important. In the numerical cases examined, the dimensions of the transmission line structure were always much less than the free space wavelength, which led to two limiting approximations for the determination of the induced currents. At extremely high frequencies, when the dimensions of the transmission line are greater than the free space wavelength, the steepest descent method can also be applied to the calculation of the transmission line parameters. The range of validity of the steepest descent approximation is especially important in electromagnetic pulse studies, where the source is almost always modeled as an incident plane wave. To this extent, an analysis of the transient plane wave coupling to multiple conductor structures has been examined and is available in the literature [Bridges4, Bridges6].

Chapter 4
Characteristic Impedance of Guided Wave Structures

An exact solution can be obtained for only a small fraction of the many problems encountered in electromagnetic modeling, and usually approximate techniques must be utilized to enable the theories to be useful for practical applications. One method of simplifying problems involving guiding wave structures is the transmission line approach, where only the discrete modes supported by the structure are considered. Using this approach, problems are treated as simple transmission lines with properties that have an exponential axial dependence. This enables the structure under consideration to be modeled as a network component and then used in complex systems with other guided wave structures or even lumped element devices. To use the transmission line approach, the accurate characterization of each of the discrete mode properties, represented in terms of a propagation constant and a characteristic impedance, is required. The determination of the propagation constants is a straightforward task since there is a direct physical relationship to the axial dependence of the electromagnetic quantities. The determination of the characteristic impedances on the other hand, is not straight forward, since there is no direct relationship between the electromagnetic quantities (these being solutions of Maxwell's equations) and the circuit quantities modeling the structure (modal voltage, modal current, and characteristic impedance).

In keeping with the traditional work of Schelkunoff [Schelkunoff2, Schelkunoff3, Marcuvitz] for the description of waveguides, the present methods of specifying the characteristic impedance of guided wave structures are categorized as either a voltage-current, power-voltage, or power-current definition. The modal circuit quantities, voltage and current, can be related in some manner to the strengths of the transverse electric and magnetic fields, respectively, in terms of specified path integrals. These integrals, however, will only be path independent in the TEM case, and only for this special situation will there then be a unique definition of the circuit quantities [Getsinger]. In the TEM limit there is a direct relationship to the electromagnetic quantities and all three of the above definitions of characteristic impedance will be equivalent. As there is no direct relationship to the electromagnetic quantities for general non-TEM structures, the three definitions will not be equivalent and the choice of which is most appropriate for a given structure geometry has been a topic of much debate.

When the transmission line approach is used to solve *closed* waveguide problems [Kerns1, Kerns2, Schwinger], the set of discrete modes supported by the structure (infinite in the case of closed structures) forms a complete spectral basis for the representation of the fields. Instead of retaining the modal field quantities for solving problems, each of the discrete modes is characterized by a propagation constant and a characteristic impedance. Then using these circuit quantities, a network solution can be obtained which is exact to the extent that all modes of the infinite set are considered. For closed structures, the circuit quantities will be scalable with respect to the field quantities, and thus any chosen definition for the characteristic impedance will suffice as long as it remains consistent throughout the analysis. Unlike *closed* structures, the set of discrete modes supported by *open* structures forms only a part of the spectral basis for the expansion of the field quantities. A complete basis also requires the contributions from continuous spectral components, as discussed in section 2.3. For the modeling of many practical problems, however, an adequate approximation to the behaviour of the structure can be obtained in terms of the discrete modal quantities alone, thus still allowing the use of the transmission line approach for a solution. Unlike the closed waveguide case however, the definition used to determine the characteristic impedance will no longer be arbitrary, but must be chosen to accurately represent the circuit requirements of the transmission line model. For the coupling of open guided wave structures to TEM components (lumped element devices), this means the use of a definition which best matches the TEM circuit behaviour of the structure. With the recent advances in high speed digital devices and microwave circuit applications, there has been much controversy over the choice of an accurate definition for the determination of the characteristic impedance [Jansen3, Jansen4, Getsinger]. The various definitions currently under use and their comparisons have been reviewed in detail by Brews and Fache [Brews1, Brews2, Fache2]. For microstrip structures all three definitions have been defended, the power-current definition usually being adopted as the most appropriate [Jansen2, Jansen4, Fukuoka, Tripathi2]. The determination of the power in these cases, is calculated by integrating the axially directed power density over the infinite transverse dimensions of the structure, which can become a complicated task for complex geometries. Further, the axially directed power will yield the total propagated power for the discrete mode only in the *lossless* case.

In this chapter, an alternative approach to determining the characteristic impedances of guided wave structures is presented (including lossy open structures). Like the propagation constants, the characteristic impedances will be extracted directly from the integral equation formulation of the problem under consideration. The special case of a single thin-wire transmission line located over a lossy earth will be used as an example. The characteristic impedances for this case will be determined using the proposed definition and then compared to the results determined using the definitions currently available in the literature.

4.1. DEFINITION OF CHARACTERISTIC IMPEDANCE

The concept of characteristic impedance is a modal property of the guiding wave structure. For each of the possible discrete modes that the structure supports, there will be a distinct transverse field configuration and a corresponding current distribution on the surface defining the structure. In order to define a characteristic impedance for the mode, these electromagnetic quantities must be related in some manner to the *modal* circuit quantities. In the most general case, the concept of a *modal current* can be defined simply as a quantity which is proportional to the strength of the transverse magnetic field. Similarly, the concept of a *modal voltage* can be defined as a quantity which is proportional to the strength of the transverse electric field. Following these definitions, the characteristic impedance then relates the strengths of the transverse electric and magnetic fields for a particular discrete mode. However, since the relationship between the transverse electric field and a *voltage* and the transverse magnetic field and a *current* are dependent on some proportionality constants, this leaves the characteristic impedance of the structure to be arbitrarily assigned. A line integral is usually used to evaluate the proportionality constants, with the path of integration for voltage or current chosen to best suit the specific geometry being studied (a voltage can best be defined for a gap and a current can best be defined for a thin conductor). Only in the quasi-TEM limit, will there be an exact meaning to these definitions. This chapter presents a new definition of characteristic impedance, which relates the equivalent currents on the surface of the guiding wave structure to the modal contribution of the fields exciting the structure. The definition does not depend on a choice of line integral paths, but follows directly from the integral equation formulation of the problem. As well, the definition collapses to the TEM result in the quasi-static limit, as will be shown by some examples later in the chapter.

As discussed in section 2.3, for general unbounded region problems, the discrete modes are only a part of the complete spectral content of the fields. The use of the discrete modes alone to represent the structure properties, however, allows a much simplified transmission line approach to the solution of many problems [Tripathi1, Tripathi2, Farr, Djordjevic1, Djordjevic2, Legro]. In order to use the transmission line approach, the propagation constants and characteristic impedances of the discrete modes are required (these are needed to couple the transmission line into a network of TEM or lumped elements). As formulated in section 2.2, and with reference to figure 2.1, the current induced on a guiding wave structure due to some exciting source is given from the solution of the spectral domain integral equation (2.15)

$$\hat{h}(\bar{\rho}) \times \tilde{L}^{-1}\{\tilde{\bar{g}}(\bar{\rho},k_z)\} = \hat{h}(\bar{\rho}) \times \tilde{\bar{f}}^{inc}(\bar{\rho},k_z) \quad ; \bar{\rho} \in C \quad , -\infty < k_z < \infty \tag{4.1}$$

$$\tilde{L}^{-1}\{\tilde{\bar{g}}(\bar{\rho},k_z)\} = \int_C \tilde{\bar{\bar{G}}}(\bar{\rho},\bar{\rho}',k_z)\tilde{\bar{g}}(\bar{\rho}',k_z)\,d\bar{\rho}' = \tilde{\bar{f}}^{scat}(\bar{\rho},k_z) \tag{4.2}$$

where C is the generating contour defining the structure, and $\hat{h}(\bar{\rho})$ is the unit normal

vector to the surface. $\overline{\overline{f}}^{inc}(\overline{\rho})$ is the field due to the source and $\overline{\overline{f}}^{scat}(\overline{\rho})$ is the field scattered from the structure due to the induced currents. As defined in chapter 2, the Green's function $\overline{\overline{G}}(\overline{\rho},\overline{\rho}',k_z)$ is formulated for the specific geometry under consideration, with a layered external region specifically addressed in section 2.5. As outlined in section 2.3, the discrete modes supported by the guided wave structure can be determined from (4.1) by considering only the homogeneous solutions of the integral equation as

$$\hat{n}(\overline{\rho}) \times \tilde{L}^{-1}\{\overline{\overline{g}}_p(\overline{\rho},k_z^p)\} = 0 \quad ; \overline{\rho} \in C \quad \rightarrow k_z^p \quad ; p=1,2,...,P \tag{4.3}$$

$$\overline{\overline{f}}_p^{scat}(\overline{\rho},k_z^p) = \tilde{L}^{-1}\{\overline{\overline{g}}_p(\overline{\rho},k_z^p)\}$$

where k_z^p are the resulting eigenvalues (propagation constants) and $\overline{\overline{g}}_p(\overline{\rho})\,;\overline{\rho} \in C$ and $\overline{\overline{f}}_p^{scat}(\overline{\rho})$ are the modal currents and corresponding modal fields for the pth mode supported by the structure, respectively. All modal quantities have an axial dependence of the form $\exp\{\pm jk_z^p z\}$. The excitation of a particular mode by a given source depends on the extent to which the modal and exciting fields are matched, which can be determined as $<\overline{\overline{f}}_p^{scat}(\overline{\rho},k_z^p), \overline{\overline{f}}^{inc}(\overline{\rho},k_z=k_z^p)>$, where $<,>$ is an appropriate inner product for the geometry considered. If the modal field $\overline{\overline{f}}_p^{scat}$ due to the induced current $\overline{\overline{g}}_p$ is normalized by dividing by the *modal current* I_p, and the incident field is made proportional to a *modal voltage* V_p, then a characteristic impedance can be realized as

$$< V_p \overline{\overline{f}}^{inc}(\overline{\rho},k_z^p) \, , \, \tilde{L}^{-1}\left\{ \overline{\overline{g}}_p(\overline{\rho},k_z^p)/I_p \right\} > = \mathbf{N} = 1 \quad \rightarrow Z_{Cp} = \frac{V_p}{I_p} \tag{4.4}$$

where $\mathbf{N}$ is some normalization constant, chosen here to be unity. This definition is still arbitrary since the reference points for which $\overline{\overline{f}}^{inc}$ and $\overline{\overline{g}}_p$ are normalized remains to be chosen. To rectify this problem, a definition for the characteristic impedance will be extracted directly from the complete spectral domain integral equation (4.1).

The determination of the current induced on a guided wave structure due to some exciting source can be determined from the integral equation (4.1). The solution of this integral equation for arbitrary geometries usually requires a numerical technique. As developed in section 2.2, a moment method solution can be obtained by expanding the current in terms of an appropriate basis to represent the unknown currents $\overline{\overline{g}}(\overline{\rho},k_z)$ as

$$\overline{\overline{g}}(\overline{\rho},k_z) = \sum_{n=1}^{N} x_n(\overline{\rho})\overline{I}_n(k_z) = [x(\overline{\rho})]^t[\overline{I}(k_z)] \tag{4.5}$$

where $x_n(\overline{\rho})$ is one of a set of basis functions and $\overline{I}_n$ is a scalar constant. The determination of the currents $\overline{\overline{g}}(\overline{\rho},k_z)$ induced on the structure due to the exciting source is obtained by applying the moment method to the complete integral equation (4.1). Once the currents are determined in the spectral domain, the inverse Fourier transform

(2.12) can be used to determine the resulting currents in their spacial domain form $\bar{g}(\bar{\rho},z)=\Gamma_z^{-1}\{\tilde{\bar{g}}(\bar{\rho},k_z)\}$. When considering the discrete mode contributions to the current, only the residue contributions to the complete solution are evaluated. The excitation of the pth modal current by the source is thus determined using (2.33) as

$$\begin{aligned}\bar{g}_p(\bar{\rho},z) &= [x(\bar{\rho})]^t\, 2\pi j \operatorname*{Res}_{k_z=k_z^p}\left\{[\bar{I}(k_z)]\right\} \\ &= +j\lim_{k_z\to k_z^p}\left\{(k_z-k_z^p)[x(\bar{\rho})]^t[\bar{\bar{Z}}(k_z)]^{-1}[\bar{F}^{inc}(k_z)]e^{+jk_z|z|}\right\} \qquad (4.6)\end{aligned}$$

$$\begin{aligned}\bar{\bar{Z}}_{mn}(k_z) &= <w_m(\bar{\rho}),\hat{h}(\bar{\rho})\times\tilde{L}^{-1}\{x_n(\bar{\rho})\}> \\ &= <w_m(\bar{\rho}),\hat{h}(\bar{\rho})\times\int_C \tilde{\bar{\bar{G}}}(\bar{\rho},\bar{\rho}',k_z)x_n(\bar{\rho}')\,d\bar{\rho}'> \qquad (4.7)\\ \bar{F}_m^{inc}(k_z) &= <w_m(\bar{\rho}),\hat{h}(\bar{\rho})\times\tilde{\bar{f}}^{inc}(\bar{\rho},k_z)>\end{aligned}$$

where $<,>$ is an appropriate inner product and $w_n(\bar{\rho})$ is one of a set of chosen testing functions as described in section 2.2. $\tilde{\bar{f}}^{inc}$ is the imposed field at the structure surface due to the exciting source. To obtain the discrete modes k_z^p supported by the structure, the moment method can be applied to the homogeneous form of the integral equation (4.3). The discrete modes are then the solutions of the set of resulting linear equations

$$\left.\begin{aligned}&\left|[\bar{\bar{Z}}(k_z)]\right| = 0 \;\rightarrow\; k_z^p \\ &[\bar{\bar{Z}}(k_z^p)][\bar{v}^p] = 0\end{aligned}\right\}\quad ;\, p=1,2,\ldots,P \qquad (4.8)$$

The solutions k_z^p are the propagation constants of the pth mode, with the eigenvectors $\bar{v}^p$, corresponding to k_z^p, giving the current distribution on the guiding wave structure. The surface current $\bar{g}_p$ can now be written in terms of a *modal* quantities as

$$\bar{g}_p(\bar{\rho},z) = [x(\bar{\rho})]^t[\bar{v}^p]\bar{i}_p \qquad (4.9)$$

$$\bar{i}_p = \frac{1}{2\bar{\bar{Z}}_{Cp}}\bar{f}_p \qquad (4.10)$$

$$\bar{f}_p = [\bar{q}^p]^t[\bar{F}^{inc}(k_z^p)] \qquad (4.11)$$

where $\bar{i}_p$ is the strength of the pth *modal current* and $\bar{f}_p$ is the strength of the exciting field referenced at the conductor surface. $\bar{f}_p$ can be thought of as the *modal voltage*. Similar to $\bar{v}^p$ giving the current distribution, $\bar{q}^p$ gives the field distribution at the structure surface for the pth mode. Thus, in (4.11), the *modal voltage* $\bar{f}_p$ has been defined as the strength with which the incident field matches the modal field at the structure surface. A characteristic impedance can now be defined which is a

function of only the structure geometry as

$$\overline{\overline{Z}}_{Cp} = -\frac{j}{2}\frac{1}{\overline{N}_v^p\,\overline{N}_q^p}\frac{\partial}{\partial k_z}\left\{ |\,\overline{\overline{Z}}(k_z)\,| \right\}_{k_z=k_z^p} \tag{4.12}$$

where $\overline{\overline{Z}}_{Cp}$ is the characteristic impedance of the pth mode for the guiding wave structure. This definition is valid for all general guided wave structures, both open and closed. The transform vectors $\overline{v}^p$, $\overline{q}^p$ and the normalization constants $\overline{N}_v^p$, $\overline{N}_q^p$ are given from the impedance matrix $\overline{\overline{Z}}(k_z)$ as

$$\begin{aligned}
\overline{v}_j^p &= \mathrm{cof}_{1j}\{\overline{\overline{Z}}(k_z^p)\}/\overline{N}_v^p \quad ;\ j=1,2,...,N \\
\overline{q}_i^p &= \frac{\mathrm{cof}_{i1}\{\overline{\overline{Z}}(k_z^p)\}}{\mathrm{cof}_{11}\{\overline{\overline{Z}}(k_z^p)\}}/\overline{N}_q^p \quad ;\ i=1,2,...,N \\
\overline{N}_v^p &= \left[\sum_{i=1}^{N}\overline{v}_i^p\right]^{1/2}, \qquad \overline{N}_q^p = \left[\sum_{i=1}^{N}\overline{q}_i^p\right]^{1/2}
\end{aligned} \tag{4.13}$$

where the function $\mathrm{cof}_{ij}\{Z\}$ gives the cofactor of the ijth element of the matrix Z. Note that if $\overline{\overline{Z}}(k_z^p)$ is symmetric, then $[\overline{q}^p]=[\overline{v}^p]$ and accordingly $\overline{N}_q^p=\overline{N}_v^p$. As developed further in chapter 2 (2.35-3.42), a matrix equation solution can be developed to solve for the currents due to the complete set of discrete modes.

4.2. CHARACTERISTIC IMPEDANCE OF A SINGLE THIN-WIRE OVER A LOSSY INTERFACE

The excitation of thin-wire structures located over a lossy interface was discussed in detail in chapter 3. The geometry considered, as was shown in figure 3.2, consisted of a system of N thin-wire circular conductors located above a lossy half-space. The formulation utilized the thin-wire approximation, where only the axially directed electric current $\overline{\overline{g}}(\overline{\rho})=J_z(\overline{\rho})\hat{z}$ was assumed to be significant and thus continuity of only the $\hat{z}$ component of the electric field $\overline{\overline{f}}(\overline{\rho})=E_z(\overline{\rho})\hat{z}$; $\overline{\rho}\in C$ on the structure surface needed to be enforced. The integral equation (4.1) then required only the Green's function component $G_{zz}(\overline{\rho},\overline{\rho}',k_z)$. In chapter 3, the elements of the impedance matrix $[Z(k_z)]$ for a system of thin-wire conductors over a single lossy interface were formulated (3.18-3.20). As well, the modal representation of the currents and fields were also developed (3.46-3.52). These results will be used to evaluate the characteristic impedance of a single thin-wire transmission line.

In this section, the characteristic impedance of a single thin-wire conductor system above a lossy half-space will be examined in detail, as shown in figure 4.1. The conductor is located at a height h $(x=0,y=h)$ above the interface and has a radius a. The region $y>0$ is considered to be free space, characterized by a permittivity ε_e and a permeability μ_e. The region $y<0$ is designated as the lossy earth, characterized by a

permittivity ε_g, a permeability μ_g, and a conductivity σ_g. The electrical properties of the conductor are characterized by a permittivity ε_w, a permeability μ_w, and a conductivity σ_w. The characteristic impedance of the system will be determined by examining the excitation of the conductor by a delta function voltage source $V^S\delta(z-z_s)$, located at $z=z_s$ along the conductor axis. The case of a delta function source is specifically chosen, since for this excitation, an exact evaluation of the modal voltage and current can be made, and thus a precise definition for the characteristic impedance can be found.

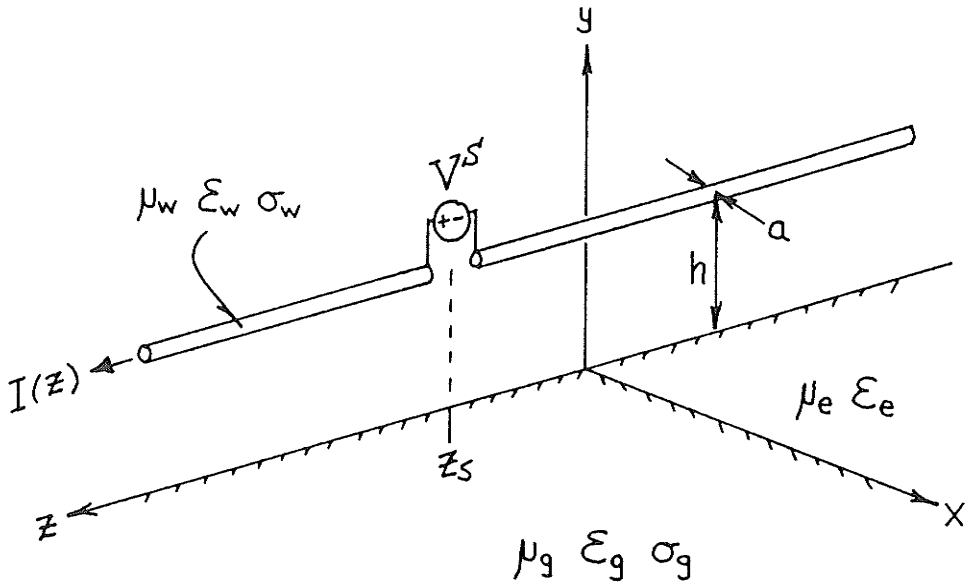

Figure 4.1: Single thin-wire conductor located over a lossy half-space.

Using the theory developed in chapter 3 for thin-wire structures, the induced current on the single conductor transmission line due to a delta function source can be determined through an integral transform as

$$I(z) = \frac{1}{2\pi}\int_{-\infty}^{\infty} Z(k_z)^{-1} < E_z^S(k_z) > e^{+jk_z z}\, dk_z \tag{4.14}$$

$$< E_z^S(k_z) > = V^S e^{-jk_z z_s} \tag{4.15}$$

$$Z(k_z) = Z^w(k_z) - Z^e(k_z) \tag{4.16}$$

where $I(z)$ is the induced current on the conductor. The impedance matrix (4.16) consists of two terms, an external impedance term $Z^e(k_z)$ representing the mutual coupling between the conductors, and a self impedance term $Z^w(k_z)$ representing the conductors surface impedance. The derivation of the impedance matrix elements for the single conductor system, is accomplished by determining the fields external and internal to the conductor, which carries a current of the form $I(k_z)e^{+jk_z z}$. As determined in

section 3.2.1, the fields can be deduced by solving the two-dimensional wave equation in each of the material regions such that

$$Z^e(k_z) = \left[\frac{-j\omega\mu_e}{2\pi k_e^2}\right]\frac{1}{(\tau_e a)K_1(\tau_e a)}\Big[\tau_e^2 K_0(\tau_e a) - I_0(\tau_e a)[\tau_e^2 K_0(\tau_e 2h) + k_e^2 \mathbf{J}(\tau_e, 2h\hat{y}) - k_z^2 \mathbf{G}(\tau_e, 2h\hat{y})]\Big] \tag{4.17}$$

$$\mathbf{J}(\tau_e, \bar{\rho}^*) = \int_{-\infty}^{\infty} \frac{1}{U_e + U_g} e^{-U_e(y+h)+jk_x x}\, dk_x \tag{4.18a}$$

$$\mathbf{G}(\tau_e, \bar{\rho}^*) = \int_{-\infty}^{\infty} \frac{1}{n^2 U_e + U_g} e^{-U_e(y+h)+jk_x x}\, dk_x \tag{4.18b}$$

$$U_e = \sqrt{k_x^2+\tau_e^2} \quad , \quad U_g = \sqrt{k_x^2+\tau_g^2}$$

where $|\bar{\rho}^*| = \sqrt{x^2+(y+h)^2}$. Here $k_e = \sqrt{\omega^2\mu_e\varepsilon_e}$ is the propagation constant in the air medium, $k_g = \sqrt{\omega^2\mu_g\varepsilon_g + j\omega\mu_g\sigma_g}$ is the propagation constant in the ground medium. $\tau_e = \sqrt{k_z^2-k_e^2}$ and $\tau_g = \sqrt{k_z^2-k_g^2}$ are the transverse propagation constants in the air and earth media, respectively. The real parts of the irrationals $\mathrm{Re}[U_e, U_g] \geq 0$ and $\mathrm{Re}[\tau_e, \tau_g] \geq 0$ have been chosen to retain a positive value. $I_0(z)$, $K_0(z)$, $K_1(z)$ are modified Bessel functions of complex argument and $n = k_g/k_e$ is the refractive index of the air-earth interface. For thin solid conductors the internal impedance matrix was defined in section 3.2.1 as

$$Z^w(k_z) = \left[\frac{+j\omega\mu_w}{2\pi k_w^2}\right]\frac{\tau_w^2 I_0(\tau_w a)}{(\tau_w a)I_1(\tau_w a)} \tag{4.19}$$

where $\tau_w = \sqrt{k_z^2-k_w^2}$ and $k_w = \sqrt{\omega^2\mu_w\varepsilon_w + j\omega\mu_w\sigma_w}$. $I_0(z)$, $I_1(z)$ are the modified Bessel functions.

Using the inverse transform (4.14) determines the complete spectral contribution to the current. The discrete mode contributions to the current are given from the residue contributions only as

$$\mathrm{I}(z) = \sum_{p=1}^{P} I_p(z) = +j\sum_{p=1}^{P} \lim_{k_z \to k_z^p} \left\{(k_z - k_z^p)Z(k_z)^{-1}\right\} V^S e^{+jk_z^p |z-z_s|} \tag{4.20}$$

where the propagation constants k_z^p are determined from the solution of the mode equation (the single thin-wire case of (3.46)) as

$$\left.\begin{aligned} |Z(k_z)| &= 0 \\ Z(k_z^p)V^p &= 0 \end{aligned}\right\} \quad ; p = 1,2,\ldots,P \tag{4.21}$$

A detailed discussion of the possible solutions of the discrete modes was given in chapter 3. Note that there can be more than one solution for a single conductor ($P \geq N$ for the general N conductor system). In terms of modal quantities, the induced current is then determined from the single thin-wire case of (3.48) as

$$\mathrm{I}(z) = \sum_{p=1}^{P} \mathrm{v}^p \mathrm{i}_p(z) = [T][2Z_C]^{-1}[D(z, z_s)][T]^t V^S \tag{4.22}$$

$$D_{ij}(z, z_s) = \begin{cases} e^{+jk_z^p |z-z_s|} & , i=j=p \\ 0 & , i \neq j \end{cases}$$

$$[T] = \left[1, 1, \cdots, 1 \right]_{1\times P}$$

Since for a single thin-wire system the normalized eigenvector is unity $\mathrm{v}^p = 1$ for all modes, the modal current will be equivalent to the conductor current $\mathrm{i}_p = I_p$. Similarly, the modal fields will be equal to the conductor fields. $[Z_C]_{P\times P}$ is a diagonal matrix with diagonal elements representing the characteristic impedance Z_{Cp} of the pth mode. Considering only the pth modal current at the source location $z=z_s$, the characteristic impedance can be formulated as

$$\mathrm{i}_p(z=z_s) = \frac{1}{2Z_{Cp}} V^S \tag{4.23}$$

$$Z_{Cp} = -\frac{j}{2}\frac{\partial}{\partial k_z}\left\{ |Z(k_z)| \right\}_{k_z=k_z^p} \tag{4.24}$$

This definition of characteristic impedance can be physically rationalized by considering the equivalent circuit of figure 4.2. For the single conductor, a zero voltage reference can be specified at the center of the delta function source, with this chosen reference being independent of any integration path. Thus, the modal current that the source excites, defines the characteristic impedance of the structure for that particular mode. This definition can then be extended to multiple conductor systems as done in 3.3.1, or even to general guided wave structures as used in 2.3 or 4.1.

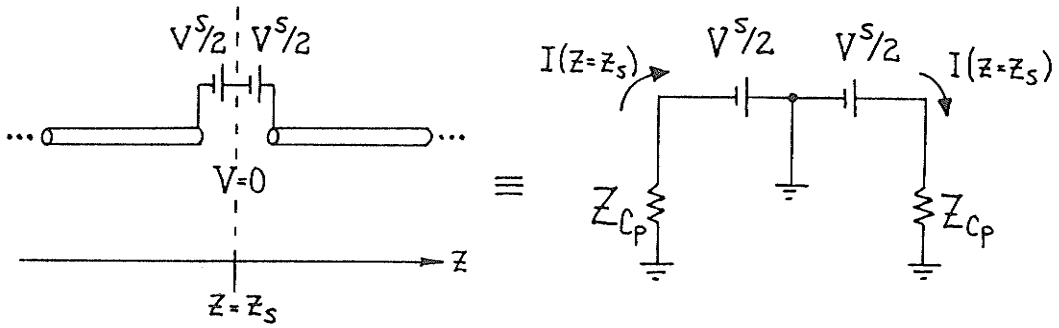

Figure 4.2: Equivalent circuit model for the delta function source excited transmission line.

For the single conductor case, an analytical expression can be derived for the characteristic impedance (this can also be done for the multiple conductor case but the result becomes complicated and a numerical evaluation is more appropriate). Evaluating the expression (4.24) yields

$$Z_{Cp} = Z_{Cp}^{w} + (-jk_z^p)Y^{sh}(k_z^p)^{-1} + \varepsilon_{NS}(k_z^p) \tag{4.25}$$

$$Z_{Cp}^{w} = -\frac{j}{2}\frac{\partial}{\partial k_z}Z^{w}(k_z^p) = \frac{Z_w}{2\pi}\frac{k_z^p}{k_w}\left[\frac{I_0(\tau_w a)}{(\tau_w a)I_1(\tau_w a)} + \frac{1}{2}\left[1 - \frac{I_0^2(\tau_w a)}{I_1^2(\tau_w a)}\right]\right] \tag{4.26}$$

$$Y^{sh}(k_z^p)^{-1} = \left[\frac{+jZ_0}{2\pi k_e}\frac{1}{(\tau_e a)K_1(\tau_e a)}\right]\left[K_0(\tau_e a) - I_0(\tau_e a)[K_0(\tau_e 2h) - \mathbf{G}(\tau_e, 2h\hat{y})]\right] \tag{4.27}$$

$$\begin{aligned}\varepsilon_{NS}(k_z^p) = -\left[\frac{Z_0}{2\pi}\frac{k_z^p}{k_e}\frac{1}{(\tau_e a)K_1(\tau_e a)}\right]\frac{1}{2}\Bigg\{&[(\tau_e a)K_1(\tau_e a) - I_0(\tau_e a)(\tau_e 2h)K_1(\tau_e 2h)] \\ &- I_0(\tau_e a)\int_{-\infty}^{\infty}\left[\frac{k_e^2}{U_e + U_g}(U_g 2h + 1) - \frac{(k_z^p)^2}{n^2U_e + U_g}\left(U_g 2h + \frac{n^2U_g + U_e}{n^2U_e + U_g}\right)\right]\frac{e^{-U_e 2h}}{U_e U_g}dk_x \\ &+ \left[\frac{a}{\tau_e}\right]I_1(\tau_e a)\left[\tau_e^2 K_0(\tau_e 2h) + k_e^2\mathbf{J}(\tau_e, 2h\hat{y}) - k_z^{p\,2}\mathbf{G}(\tau_e, 2h\hat{y})\right]\Bigg\}\end{aligned} \tag{4.28}$$

where Z_0 and Z_w are the intrinsic impedances of the upper half-space and the conductor media, respectively. The characteristic impedance Z_{Cp} has been realized in the form of three contributing terms. The term Z_{Cp}^{w} gives the contribution due to the imperfectly conducting wire (this due to the self impedance term $Z^{w}(k_z)$ given by (4.19)). This term is usually negligible for good conductors. The remaining two terms in (4.25) are due to the mutual impedance term $Z^{e}(k_z)$ given by (4.17), which involves the modified Bessel functions K_0 and the infinite integrals **J** and **G**. Noting that in the quasi-TEM limit, the terms K_0, **J**, **G** vary slowly as a function of k_z, the second term in (4.25) gives the contribution to the impedance with K_0, **J**, **G** assumed stationary when evaluated at the point $k_z = k_z^p$. This term will usually be the dominant contribution to the characteristic impedance and is related to the equivalent circuit representation of the transmission system as will be shown in the next section. The remaining term ε_{NS} gives the contribution due to the non-stationary nature of K_0, **J**, **G** about the wavenumber $k_z = k_z^p$. This term becomes important in the non-quasi-TEM evaluation region. Note that the last term in ε_{NS} is negligible for very thin conductors since $I_1(\tau_e a) \to 0$ for $\tau_e a \to 0$. Thus, under the limit $\tau_e a \to 0$, (4.28) can be simplified as

$$\varepsilon_{NS}(k_z^p) = \frac{Z_0}{2\pi}\frac{k_z^p}{k_e}\frac{-1}{2}\left\{[\,1-(\tau_e 2h)K_1(\tau_e 2h)] - \int_{-\infty}^{\infty}\left[\frac{k_e^2}{U_e+U_g}(U_g 2h+1)\right.\right.$$

$$\left.\left. - \frac{k_z^{p\,2}}{n^2U_e+U_g}\left(U_g 2h+\frac{n^2U_g+U_e}{n^2U_e+U_g}\right)\right]\frac{e^{-U_e 2h}}{U_e U_g}dk_x\right\} \tag{4.29}$$

The formulations presented in this section defining the propagation constants (4.21) and the characteristic impedances (4.24) of the discrete modes come directly from the integral equation solution and are dependent on only the geometry of the structure.

4.3. CIRCUIT EQUIVALENT METHOD

As previously discussed, the propagation constants and characteristic impedances of each of the discrete modes are required in order to use the transmission line approach. In this section, the derivation of these properties from the equivalent circuit representation of the single conductor transmission line will be discussed, and compared to the new method that was presented in the last section. As discussed in section 3.3.3, the impedance matrix (4.16) can be formulated in terms of the transmission line equivalent circuit parameters as

$$Z(k_z) = Z^{ser}(k_z) + k_z^2 Y^{sh}(k_z)^{-1} \tag{4.30}$$

$$(Y^{sh}(k_z))^{-1} = \frac{1}{-j\omega\varepsilon_e 2\pi}\frac{1}{(\tau_e a)K_1(\tau_e a)} \cdot\left[K_0(\tau_e a) - I_0(\tau_e a)[K_0(\tau_e 2h) - \mathbf{G}(\tau_e, 2h\hat{y})]\right] \tag{4.31}$$

$$Z^{ser}(k_z) = Z^w(k_z) - \frac{j\omega\mu_e}{2\pi}\frac{1}{(\tau_e a)K_1(\tau_e a)} \cdot\left[K_0(\tau_e a) - I_0(\tau_e a)[K_0(\tau_e 2h) - \mathbf{J}(\tau_e, 2h\hat{y})]\right] \tag{4.32}$$

where Z^{ser} is the series impedance and Y^{sh} is the shunt admittance equivalent circuit parameters for the structure. The solutions of the mode equation k_z^p and the characteristic impedances Z_{Cp} can then be formulated using (4.21) and (4.24) in terms of the structure equivalent circuit parameters as

$$|\,Z(k_z^p)\,| = 0 \;\rightarrow\; k_z^p = \sqrt{-Z^{ser}(k_z^p)Y^{sh}(k_z^p)} \tag{4.33}$$

$$Z_{Cp} = -\frac{j}{2}\frac{\partial}{\partial k_z}\left\{Z^{ser}(k_z) + k_z^2 Y^{sh}(k_z)^{-1}\right\}_{k_z=k_z^p}$$

$$= \sqrt{-Z^{ser}(k_z^p)Y^{sh}(k_z^p)^{-1}} - \frac{j}{2}\frac{\partial}{\partial k_z}\left\{Z^{ser}(k_z) + (k_z^p)^2 Y^{sh}(k_z)^{-1}\right\}_{k_z=k_z^p} \quad (4.34)$$

The first term in (4.34) is the same as the stationary part of (4.25), with the remaining term in (4.34) being equivalent to $Z_{Cp}^{w} + \varepsilon_{NS}$ in (4.25). The lossless cases of (4.33) and (4.34) can be shown to be equivalent to the results of Hashimoto [Hashimoto], who derived a rigorous full-wave solution for the characteristic impedance of microstrip structures based on a circuit equivalent approach.

If the characteristic impedance is obtained directly from the two-dimensional transmission line equations, only the stationary part of (4.34) will result as

$$-\frac{\partial}{\partial z}I_p = Y^{sh}(k_z^p)V_p \quad \rightarrow \quad Z_{Cp} = \frac{V_p}{I_p} = (-jk_z^p)Y^{sh}(k_z^p)^{-1} \quad (4.35)$$

where I_p is the modal current and V_p is the modal voltage. The evaluation of k_z^p using (4.33) gives the same result as the mode equation (4.21) for all conditions. However, the definition of Z_{Cp} using (4.35) is not equivalent to the definition (4.24) under all conditions, and is only valid if $Z^{ser}(k_z^p)$ and $Y^{sh}(k_z^p)$ (and thus K_0, **J**, **G**) are assumed stationary about $k_z=k_z^p$. The transmission line representation for V_p, I_p in (4.35) is thus only accurate in the quasi-TEM region. Further, it is useful to note that in using the quasi-TEM approximation, the equivalent circuit parameters (4.31,4.32) are evaluated under the condition $k_z=k_e$ ($\tau_e=0$), and thus are functions of only the transmission line geometry.

The two-dimensional circuit approach is often used in the analysis of microstrip structures [Kobayashi1, Bhartia, Whitaker], where the propagation constants k_z^p are determined accurately by solving an integral equation similar to the form (4.21). These propagation constants are usually presented in terms of an effective dielectric constant $k_z^p = k_e\sqrt{\varepsilon_{eff}^p}$. In many studies, the characteristic impedance Z_{Cp} is then determined using ε_{eff}^p and a geometry dependent factor $Z_{Cp} = \mathrm{F(geometry)}Z_0/\sqrt{\varepsilon_{eff}^p}$. This is equivalent to the circuit based form (4.35), except that F is not only considered stationary about $k_z=k_z^p$, but is also assumed independent of k_z^p. This assumption that F and thus Y^{sh} is dependent only on geometry is only valid in the TEM case. Alternative approaches to determining the characteristic impedance use path integrals to define a voltage or through a power definition, as will be discussed in the next sections.

4.4. LINE INTEGRAL METHOD

Another alternate method for obtaining the characteristic impedance that is often used in many applications, is based on a voltage-current definition $Z=V/I$. When considering thin-wire structures, a modal current can be precisely specified as the total

axial current flowing in the conductor. However, in order to specify a modal voltage, a zero voltage reference point must be chosen as well as a path of integration (transverse to the transmission line) such that

$$Z_{Cp} = \frac{V_p}{I_p} = -\frac{1}{I_p}\int_L \bar{E}(\bar{\rho},k_z^p)\cdot d\bar{l} \tag{4.36}$$

where the chosen path L is from the zero reference voltage point (usually specified as $|\bar{\rho}| = \infty$) to the center of the conductor $\bar{\rho}=(0,h)$, as shown in figure 4.3. The field $\bar{E}(\bar{\rho},k_z^p)$ is the modal field resulting from the pth modal current I_p. In general, for the non-TEM case, the evaluation of the modal voltage will be dependent on the chosen path of integration L. In the low frequency limit, when the earth behaves as a good conductor and the distance from the earth to the conductor is much less than the free space wavelength, the $y=0$ interface can be considered as the zero reference and almost any direct path from the earth to the conductor will be adequate. When the earth becomes lossy, the voltage at the interface can *not* be assumed as the zero reference (the voltage at points along the interface will no longer be constant as well). Extending the integration path to a point below the interface has been one attempt at rectifying this problem [Wedepohl, Efthymiadis].

The line integral method has also been used to evaluate the characteristic impedance of microstrip structures [Das, Zhang]. For this case the metallic ground plane of the microstrip is chosen as the zero reference and since the distance to the strip conductor is usually less than the wavelength in the supporting dielectric, the quasi-TEM assumption is usually valid. An extension to the line integral approach is to evaluate the voltage as an average over many possible paths from the zero reference ground plane to the strip conductor. As an example, the average value of the electric field under the entire strip can be used in (4.36) in the microstrip case. As in the conductor above lossy earth situation, however, the line integral method breaks down for the general non-TEM case.

Concentrating on the single thin-wire system above a lossy interface, as shown in figure 4.3, the characteristic impedance will be evaluated by chosing a path of integration along the y-axis as

$$Z_{Cp} = -\frac{1}{I_p}\int_L E_y(\bar{\rho},k_z^p)dy \tag{4.37}$$

$$E_y(\bar{\rho},k_z^p) = [\nabla\nabla\cdot\bar{\Pi} + k^2\bar{\Pi}]\cdot\hat{y} = -\frac{\partial}{\partial y}(-\nabla\cdot\bar{\Pi}) + k^2\Pi_y$$

$$= -\nabla_y\Phi(\bar{\rho}) + j\omega A_y(\bar{\rho}) \tag{4.38}$$

where $\bar{\Pi}$ is the appropriate Hertz potential vector. Since the path of integration is along the y-axis, only the E_y field component is required in (4.36), which is determined from the potential vectors $\bar{\Pi}^e$, $\bar{\Pi}^g$, or $\bar{\Pi}^w$, the choice being dependent on the medium in which E_y is evaluated (air, earth or conductor, respectively). The

appropriate potential functions for each air or earth medium were derived in appendix A or as described in chapter 3 for thin-wire structures over a single interface. For discussion purposes, the field in (4.38) has been written in terms of the scalar potential Φ and the vector potential component $\mathbf{A}_y$. Two possible paths of integration L will be examined. They are determined by chosing the zero reference point at either $\overline{\rho}=(0,+\infty)$ or $\overline{\rho}=(0,-\infty)$ such that L is defined as

$$L:\begin{cases} L1:\ \overline{\rho}=(0,+\infty) \rightarrow \overline{\rho}=(0,h) \\ L2:\ \overline{\rho}=(0,-\infty) \rightarrow \overline{\rho}=(0,h) \end{cases} \tag{4.39}$$

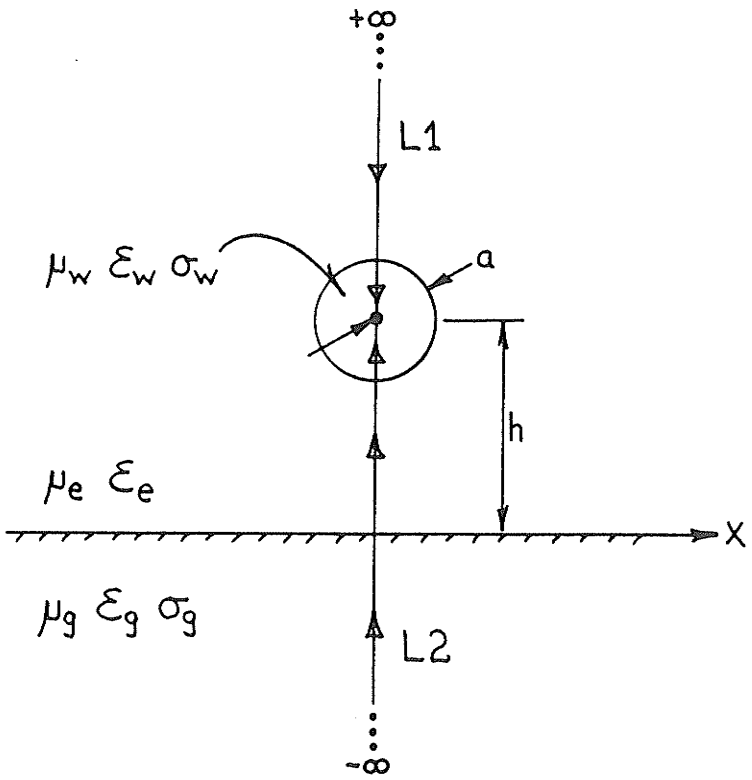

Figure 4.3: Line integral paths in the evaluation of the conductor voltage.

Using (4.37), the characteristic impedance can be evaluated by integrating along each of the chosen paths to yield

$$Z_{Cp} = \frac{<\Phi^e(\overline{\rho}=(0,h))>}{I_p} + \frac{\Phi^w(|\overline{\rho}|=0)-\Phi^w(|\overline{\rho}|=a)}{I_p} - \frac{j\omega}{I_p}\int_L \mathbf{A}_y(\overline{\rho})dy$$
$$+\begin{cases} -\dfrac{\Phi^e(\overline{\rho}=(0,+\infty))}{I_p} & ;\ \text{path } L1 \\ -\dfrac{\Phi^e(\overline{\rho}=(0,0)) + \Phi^g(\overline{\rho}=(0,0)) - \Phi^g(\overline{\rho}=(0,-\infty))}{I_p} & ;\ \text{path } L2 \end{cases} \tag{4.40}$$

where Φ^e and Φ^g are the scalar potentials in the air and ground media, respectively.

Φ^w is the scalar potential internal to the conductor, which can be neglected for good conductors. The term $<\Phi^e(\bar{\rho}=(0,h))>$ is the average value of the scalar potential Φ^e around the circumference of the conductor, which can be determined form the potential functions derived in appendix A (A.76,A.77) as

$$\Phi^e(\bar{\rho},k_z^p) = (-jk_z^p)\frac{+j\omega\mu_e}{2\pi k_e^2}\frac{I_p}{(\tau_e a)K_1(\tau_e a)}\left[K_0(\tau_e \mid \bar{\rho}_D \mid) - K_0(\tau_e \mid \bar{\rho}_D^* \mid) + \mathbf{G}(\tau_e,\bar{\rho}_D^*)\right]$$

$$\mid \bar{\rho}_D \mid = \sqrt{x^2+(y-h)^2} \quad , \quad \mid \bar{\rho}_D^* \mid = \sqrt{x^2+(y+h)^2} \tag{4.41}$$

$$\frac{<\Phi^e(\bar{\rho}=(0,h),k_z^p)>}{I_p} = (-jk_z^p)Y^{sh}(k_z^p)^{-1} \tag{4.42}$$

where $Y^{sh}(k_z^p)$ was defined in (4.31) as the shunt admittance of the transmission line equivalent circuit. The remaining terms in (4.40) can be evaluated to give the final result

$$Z_{Cp} = \begin{cases} (-jk_z^p)Y^{sh}(k_z^p)^{-1} + Z_{Cp}^w + <\mathbf{I}_e(y=h)> & ;\ \text{Path } L1 \\ (-jk_z^p)Y^{sh}(k_z^p)^{-1} + Z_{Cp}^w + <\mathbf{I}_e(y=h)> & \\ \qquad - \dfrac{\Phi^e(\bar{\rho}=(0,0))}{I_p} - \mathbf{I}_e(y=0) + \mathbf{I}_g(y=0) & ;\ \text{Path } L2 \end{cases} \tag{4.43}$$

$$\frac{\Phi^e(\bar{\rho}=(0,0))}{I_p} = (-jk_z^p)\left[\frac{jZ_0}{2\pi k_e}\right]\frac{1}{(\tau_e a)K_1(\tau_e a)}\mathbf{G}(\tau_e,\bar{\rho}_D^*) \tag{4.44}$$

$$\begin{aligned}\mathbf{I}_e(y) &= -\frac{j\omega}{I_p}\int_{\infty}^{y}\mathbf{A}_y^e(\bar{\rho})dy \\ &= -\frac{Z_0}{2\pi}k_z^p k_e\int_{-\infty}^{\infty}\left[\frac{1}{U_e+U_g} - \frac{1}{n^2U_e+U_g}\right]\frac{1}{U_e^2}e^{-U_e(y+h)}dk_x\end{aligned} \tag{4.45}$$

$$\begin{aligned}\mathbf{I}_g(y) &= -\frac{1}{I_p}\int_{-\infty}^{y}E_y^g(\bar{\rho})dy = \frac{\Phi^g(\bar{\rho}=(0,y))}{I_p} - \frac{j\omega}{I_p}\int_{-\infty}^{y}\mathbf{A}_y^g(\bar{\rho})dy \\ &= \frac{Z_0}{2\pi}\frac{k_z^p}{k_e}\int_{-\infty}^{\infty}\left[\frac{1}{n^2U_e+U_g}\frac{U_e}{U_g}\right]e^{-U_e h+U_g y}dk_x\end{aligned} \tag{4.46}$$

The first term in (4.43) can be identified as the same result obtained in the circuit equivalent method (4.35). This term is the dominant term in the quasi-TEM limit.

4.5. POWER-CURRENT METHOD

In the previous section, a voltage-current definition was used to define the characteristic impedance. This approach is inaccurate in the general non-TEM case since the definition of a modal voltage relies on a line integration which depends on the path of integration chosen. For many applications, a power-current definition of characteristic impedance $Z=P/(I\,I^*)$ is more suitable. This definition is the one usually employed in advanced microstrip or MMIC structure analysis [Jansen1, Jansen2, Jansen5, Itoh, Fukuoka, Tripathi2]. The method is most appropriate when the concept of a modal current can be precisely defined, this being when the conductor dimensions are much less than a wavelength (this is appropriate for the thin-wire transmission line case). Once a modal current I_p is specified, the axially directed power P_p for that mode can be determined so that the characteristic impedance, for the pth mode, will be

$$Z_{Cp} = \frac{P_p}{|I_p|^2} = \frac{1}{|I_p|^2}\int_{-\infty}^{\infty}\int [\overline{E}(\overline{\rho})\times\overline{H}^*(\overline{\rho})]\cdot\hat{z}\,d\overline{\rho}\Bigg]_{k_z=k_z^p}$$

$$= \sum_{i=1}^{M}\frac{P_p^i}{|I_p|^2} = \frac{1}{|I_p|^2}\sum_{i=1}^{M}\int_{A_i}\int [\overline{E}^i(\overline{\rho})\times\overline{H}^{i*}(\overline{\rho})]\cdot\hat{z}\,d\overline{\rho}\Bigg]_{k_z=k_z^p} \qquad (4.47)$$

where the axial power has been calculated as a sum of the powers in each of the M separate material regions. A_i denotes the cross sectional area of the ith region, $\overline{E}^i$ and $\overline{H}^i$ are the fields in this region, and * denotes complex conjugate. For the case of a thin-wire conductor over a lossy half-space as shown in figure 4.4, there are three material regions; the air ($i=e$), the lossy ground ($i=g$), and region internal to the conductor ($i=w$).

Evaluation of the power integrals for all the three regions directly in the form (4.47) becomes complicated for the region $i=e$, since the area A_e is defined by both cylindrical and cartesian coordinate boundaries. To simplify this, the power integral P_p^e over the surface A_e will be calculated in two parts, as shown in figure 4.4b), as

$$P_p^e = \int_0^{\infty}\int_{-\infty}^{\infty}[\overline{E}^e(\overline{\rho})\times\overline{H}^{e*}(\overline{\rho})]\cdot\hat{z}\,dxdy - \int_0^{2\pi}\int_0^{a}[\overline{E}^e(\overline{\rho})\times\overline{H}^{e*}(\overline{\rho})]\cdot\hat{z}\,\rho d\rho d\phi\Bigg]_{k_z=k_z^p}$$

$$= P_p^{e1} - P_p^{e2} \qquad (4.48)$$

where the first integral is over the entire upper half-space $y>0$, and the second integral subtracts the contribution in the region occupied by the conductor. Note that this procedure causes both integrands in (4.48) to be divergent. However, the singular portions of each are equal and can be extracted as will be shown later in this section. This problem of different boundary geometry types does not occur for microstrip structures, where an infinitely thin strip with a specified current distribution is usually chosen to model the conductor.

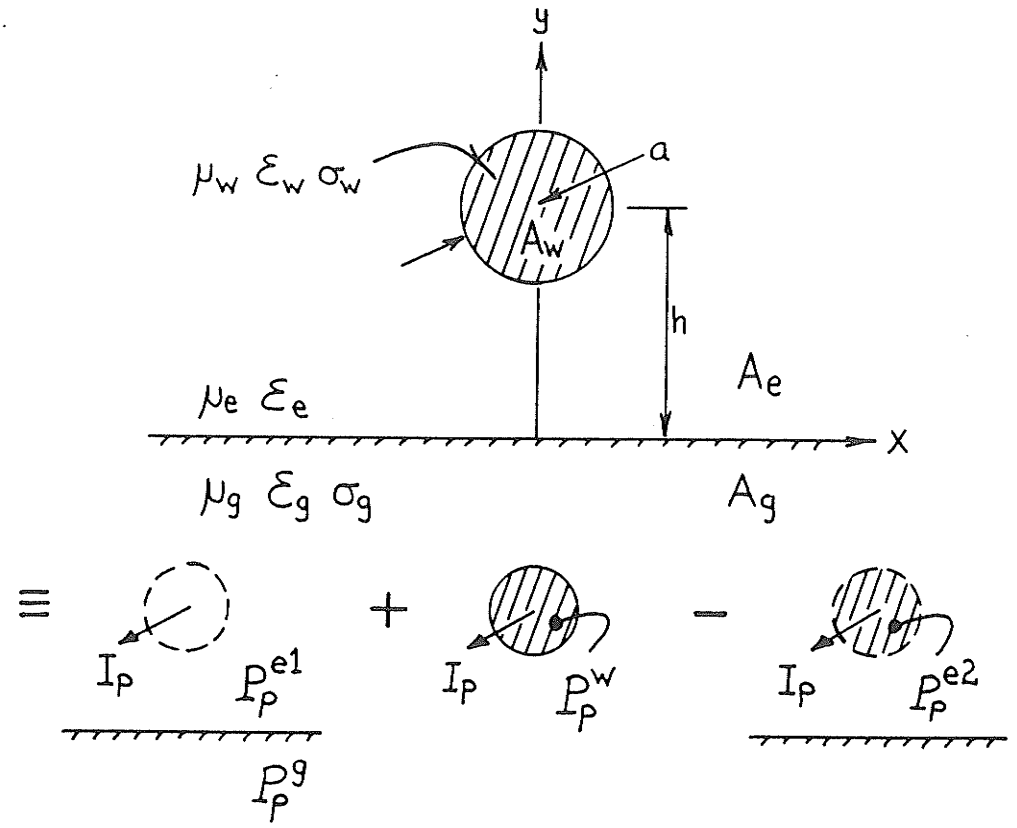

Figure 4.4: Transverse regions of the transmission line for power integration.

Using the simplification (4.48), the contributions to the characteristic impedance due integral over the upper half-space P_p^{e1} ($y>0$), and due the integral over the lower half-space P_p^g ($y<0$) can be evaluated in the form

$$\frac{P_p^i}{|I_p|^2} = \frac{1}{|I_p|^2}\int_{Y_i}\int_{-\infty}^{\infty}[E_x^i H_y^{i*} - E_y^i H_x^{i*}]dxdy\Bigg]_{k_z=k_z^p} \quad ; i = e1, g \qquad (4.49)$$

where $\{Y_{e1}: 0\rightarrow\infty\}$ and $\{Y_g: -\infty\rightarrow 0\}$. This general form can be used to solve a geometry involving any number of planar regions, simply by specifying the paths Y_i for each region. Thus, analysis of a microstrip structure for example can be formulated using the form of (4.49) by properly specifying the layers. The required field components in (4.49) for the special case of a line current above a lossy earth can be found from the derivations in appendix A.

The calculation of the axially directed power in each region ($e1, g$), involves the evaluation of double infinite integrals. Noting that the fields in each region can be described in terms of infinite integrals, a much simpler form for (4.49) can be

determined by substituting for the fields with their spectral domain transforms (an equivalent form has been used for microstrip [Hashimoto]) as

$$\int_{Y_i}\int_{-\infty}^{\infty} E^i H^{i*}\,dxdy = \int_{Y_i}\int_{-\infty}^{\infty} \frac{1}{2\pi}\int_{-\infty}^{\infty} e^i(u)e^{+jux}\,du\;\frac{1}{2\pi}\int_{-\infty}^{\infty} h^{i*}(-v)e^{+jvx}\,dv\;dxdy$$

$$= \int_{Y_i}\frac{1}{4\pi^2}\int_{-\infty}^{\infty} e^i(u)\int_{-\infty}^{\infty} h^{i*}(v)2\pi\delta(u-v)\,dvdu\;dy$$

$$= \frac{1}{2\pi}\int_{-\infty}^{\infty}\int_{Y_i} e^i(u)\,h^{i*}(u)\,dydu \tag{4.50}$$

Using the above substitution, the power integrals in (4.49) can then be evaluated as

$$\frac{P_p^i}{|I_p|^2} = \frac{1}{|I_p|^2}\int_{-\infty}^{\infty}\frac{1}{2\pi}\int_{Y_i}[e_x^i(k_x)h_y^{i*}(k_x) - e_y^i(k_x)h_x^{i*}(k_x)]\,dy\,dk_x\Bigg]_{k_z=k_z^p} \tag{4.51}$$

In this from, the integration with respect to y can then be evaluated analytically, reducing the double infinite integral to a single integration. As well, the expressions for the transformed fields $\overline{e}(k_x)$ and $\overline{h}^*(k_x)$ will be of a simple algebraic from. Finally, the evaluation of the power integrals for the upper half-space P_p^{e1} and the lower half-space P_p^g can now be deduced from the axially directed power of a conducting strip over a lossy half-space as derived in appendix C. Thus, considering a delta function line source, carrying a current I_p, the desired integrals (4.51) can be determined from (C.9,C.12) with the strip current distribution $j_z^p(k_x)$ replaced by

$$j_z^p(k_x) = I_p\frac{1}{(\tau_e a)K_1(\tau_e a)} \tag{4.52}$$

The factor $(\tau_e a)K_1(\tau_e a)$ has been included to account for the finite size of the thin-wire circular conductor.

The remaining power integrals P_p^w and P_p^{e2} represent the axial power internal to the conductor medium in (4.47), and the portion of the power in the medium e occupied by the conductor in (4.48), respectively. The first can be determined using (4.48) and the fields internal to the circular conductor [Stratton] as

$$P_p^w = \int_0^{2\pi}\int_0^a [\overline{E}^w(\overline{\rho})\times\overline{H}^{w*}(\overline{\rho})]\cdot\hat{z}\,\rho d\rho\,d\phi\Bigg]_{k_z=k_z^p}$$

$$= \int_0^{2\pi}\int_0^a E_\rho^w(\overline{\rho})H_\phi^{w*}(\overline{\rho})\rho d\rho\,d\phi\Bigg]_{k_z=k_z^p} \tag{4.53}$$

$$E_\rho^w(\bar{\rho}) = I_p \frac{\omega\mu_w k_z^p}{2\pi k_w^2} \frac{I_1(\tau_w \rho)}{a\, I_1(\tau_w a)} = I_p \frac{Z_w}{2\pi a} \frac{k_z^p}{k_w} \frac{I_1(\tau_w \rho)}{I_1(\tau_w a)} \tag{4.54}$$

$$H_\phi^w(\bar{\rho}) = I_p \frac{1}{2\pi a} \frac{I_1(\tau_w \rho)}{I_1(\tau_w a)} \tag{4.55}$$

where Z_w is the intrinsic impedance of the conductor. The power integral P_p^{e2}, giving the contribution of the fields in the region e occupied by the conductor, can be evaluated by decomposing the fields into a primary component (the conductor is in a homogeneous medium) plus a secondary component due to the reflected fields off the interface as

$$\begin{aligned} P_p^{e2} &= \int_0^{2\pi}\int_0^a [\,(\bar{E}^{eP}(\bar{\rho})+\bar{E}^{eS}(\bar{\rho}))\times(\bar{H}^{eP}(\bar{\rho})+\bar{H}^{eS}(\bar{\rho}))^*\,]\cdot\hat{z}\,\rho d\rho\, d\phi \Big]_{k_z=k_z^p} \\ &\approx \int_0^{2\pi}\int_0^a [\bar{E}^{eP}(\bar{\rho})\times\bar{H}^{eP*}(\bar{\rho})]\cdot\hat{z}\,\rho d\rho\, d\phi \Big]_{k_z=k_z^p} \end{aligned} \tag{4.56}$$

Since the secondary fields behave as a constant value over the small area of the thin-wire conductor, their cross product with the primary fields will be negligible and have appropriately been ignored in (4.56). The remaining integration of the primary fields results in a divergent integrand, behaving as $1/\rho$ for $\rho\to 0$, which can be evaluated in two parts as

$$\begin{aligned} P_p^{e2} \approx \frac{Z_0}{2\pi} \frac{|I_p|^2}{|(\tau_e a)K_1(\tau_e a)|^2} \int_{-\infty}^{\infty} \left[\frac{k_z^p}{k_e}\frac{2}{U_e+U_e^*}\right]\left[\frac{k_x^2}{4U_eU_e^*}+\frac{1}{4}\right] dk_x \\ - \int_0^{2\pi}\int_a^{\infty} E_\rho^{eP}(\bar{\rho})H_\phi^{eP*}(\bar{\rho})\,\rho d\rho\, d\phi \Big]_{k_z=k_z^p} \end{aligned} \tag{4.57}$$

$$E_\rho^{eP}(\bar{\rho}) = I_p \frac{Z_0}{2\pi}\frac{k_z^p}{k_e}\frac{K_1(\tau_e\rho)}{aK_1(\tau_e a)} \tag{4.58}$$

$$H_\phi^{eP}(\bar{\rho}) = I_p \frac{Z_0}{2\pi}\frac{k_z^p}{k_e}\frac{K_1(\tau_e\rho)}{aK_1(\tau_e a)} \tag{4.59}$$

The second integral in (4.57) is convergent an can be evaluated numerically. The first integral on the other hand, is divergent, but is also identical to the divergent part of (4.51) in the expression for P_p^{e1}. Thus, since $P_p^e = P_p^{e1} - P_p^{e2}$, these divergent terms cancel in the final result.

4.6. CHARACTERISTIC IMPEDANCE RESULTS FOR THIN-WIRE STRUCTURES

In this section, the characteristic impedances of thin-wire structures located above a lossy interface are calculated. Results obtained using the new definition proposed in section 4.2 will be compared to those determined using the equivalent circuit method (section 4.3), the voltage-current method (section 4.4), and the power-current definition (section 4.5). A discussion of the discrete modes of propagation k_z^p supported by thin-wire structures was presented in detail in chapter 3. For single conductor systems, there are normally two discrete mode solutions. One of the modes is found near the quasi-TEM solution for the structure (this mode was denoted as the transmission line mode k_z^{TL} in section 3.4.1). The other discrete mode is located near the branch point k_{zB} in the complex k_z plane which represents the TM surface wave supported by the half-space geometry (this mode was denoted as the fast wave solution k_z^{FW} in section 3.4.1). Figure 3.11 demonstrated that there was two types of behaviour of the mode solutions in the complex k_z plane as a function of frequency, depending on the half-space electrical properties and the height of the conductor above the interface. In order to examine both types of behaviour, two structure geometries will be studied in this section. As well, a comparison of the modal characteristic impedance with the exact input impedance, as calculated using the complete spectral domain transform, will be made.

Two different single conductor systems located above a lossy earth will be examined. In both systems, the conductor radius is $a=0.0025m$ and the earth electrical properties are specified as $\mu_{rg}=1.0$, $\varepsilon_{rg}=15$, and $\sigma_g=0.01$. The normalized propagation constants k_z^{TL}/k_e, k_z^{FW}/k_e as a function of frequency for two different conductor heights is shown in figure 4.5. In one case the conductor height is chosen as $h=1.0m$, so that the fast wave solution is always near the surface wave branch point and the transmission line solution remains the dominant contribution to the current throughout the entire frequency spectrum. In the second case the conductor height is chosen as $h=5.0m$, so that the roles of the two mode solutions interchange as the operating frequency is increased (the k_z^{TL} mode becomes the k_z^{FW} mode and visa versa). The real and imaginary parts of the characteristic impedances Z_{Cp}, $p=TL,FW$ for the two cases are given in figure 4.6, as calculated using the proposed definition (4.24). Examining the $h=1.0m$ case, the magnitude of the characteristic impedance of the fast wave mode Z_{CFW} is extremely large except for a small portion of the frequency spectrum near $30MHz$, this being where k_z^{TL} and k_z^{FW} are in close proximity to each other. Examining the $h=5.0m$ case shows that, as with the propagation constants, the roles of the characteristic impedances of the two modes interchange for large conductor heights as the frequency is increased. Since the characteristic impedance of the fast-wave mode is extremely large except at a small portion of the frequency spectrum, it is expected that energy will not be efficiently coupled to this mode in most situations.

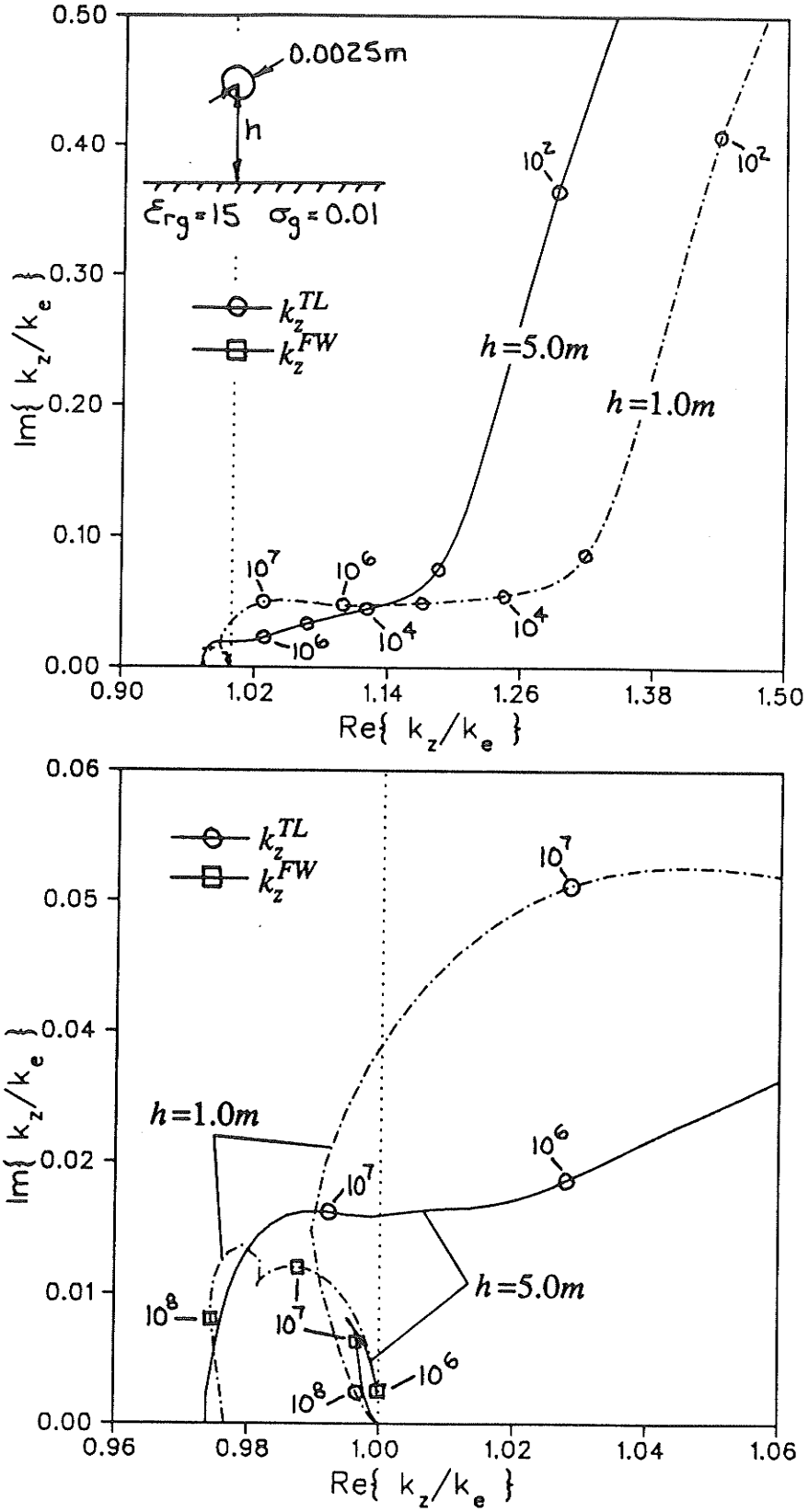

Figure 4.5: Discrete mode solutions k_z^{TL}/k_e and k_z^{FW}/k_e for two conductor heights.

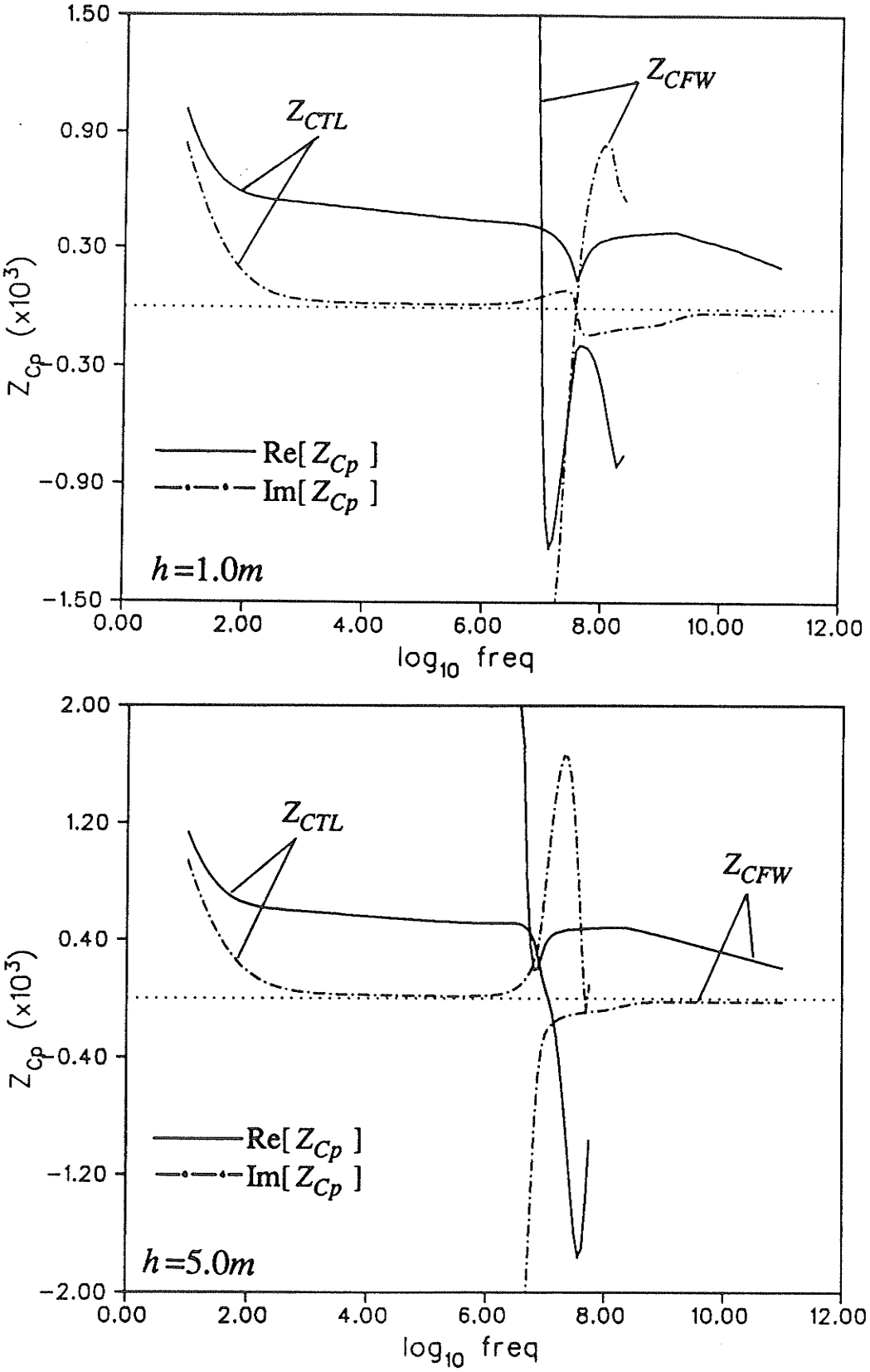

Figure 4.6: Characteristic impedances of the *TL* and *FW* modes as a function of frequency calculated using the proposed definition for h=1.0m, 5.0m.

Figures 4.7 and 4.8 compare the results of the new definition for the characteristic impedance (4.25) to four other commonly used definitions. These specifically are; the circuit equivalent method (4.35), where the transmission line circuit parameters $Z^{ser}(k_z^p)$ and $Y^{sh}(k_z^p)$ are assumed to be stationary about the root $k_z = k_z^p$; the voltage-current method (4.43), where two different line integral paths are used to define the voltage; and the power-current method (4.47), where an integration of the axially directed power density over the structure cross-section is used to obtain the power propagated by the mode. For both cases, as the frequency becomes very small, all methods converge to the circuit equivalent result. For extremely large frequencies, the structure behaves as an infinite conductor located in free space. For this situation, the circuit equivalent and voltage-current methods converge to the same result, with the power-current and the proposed definition becoming the same except for a small constant difference in the imaginary parts of the characteristic impedances. The voltage-current definition results, calculated using the path $L1$, began to deviate from the results of all the other definitions at a much lower frequency. This is due to the fields at large heights above the conductor giving a major contribution to the line integral, thus being more affected by the TEM assumption. The results calculated using the path $L2$ did not show this behaviour since the major contribution to the line integral is from the small region between the earth and the conductor. Examining figures 4.6 and 4.7 for the $h=1.0m$ case, shows that near a frequency of $3\times10^7 Hz$ the characteristic impedance Z_{CTL} becomes very small. At this point the excitation efficiency of the TL mode is very good. This result may have applications in surface wave antenna design.

To complete the results, the characteristic impedance Z_{CTL} of the dominant discrete mode will be compared to the input impedance Z_{in} seen by a delta function voltage source V^S located at some point along the infinite transmission line. If the discrete modal contribution dominates the current, then the two impedances should be equivalent $Z_{in} \approx 2Z_{CTL}$, as discussed in section 3.3.2. The input impedance Z_{in} is calculated by determining the complete spectral domain contribution to the current at the source location, as given by the transform (3.29) in chapter 3. The real and imaginary parts of the input impedances as a function of frequency for the two cases considered in this section are given in figures 4.9 and 4.10. The results show that the discrete mode assumption is valid as long as the height of the conductor is less than the free space wavelength. For heights comparable to the free space wavelength, the branch cut contributions to the current present in the complete spectral domain transform become important.

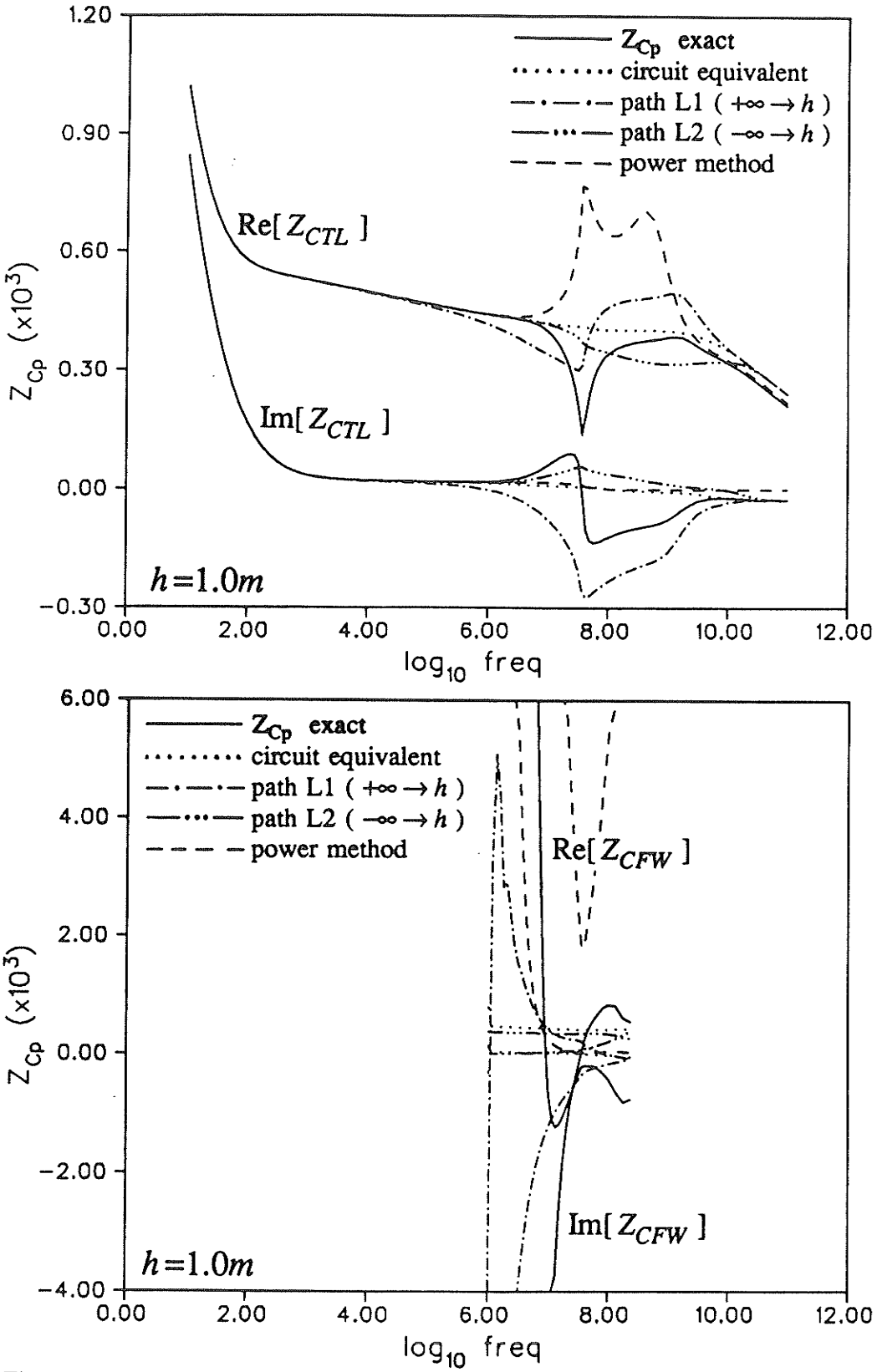

Figure 4.7: Comparison of the various definitions for characteristic impedance as a function of frequency for h=1.0m.

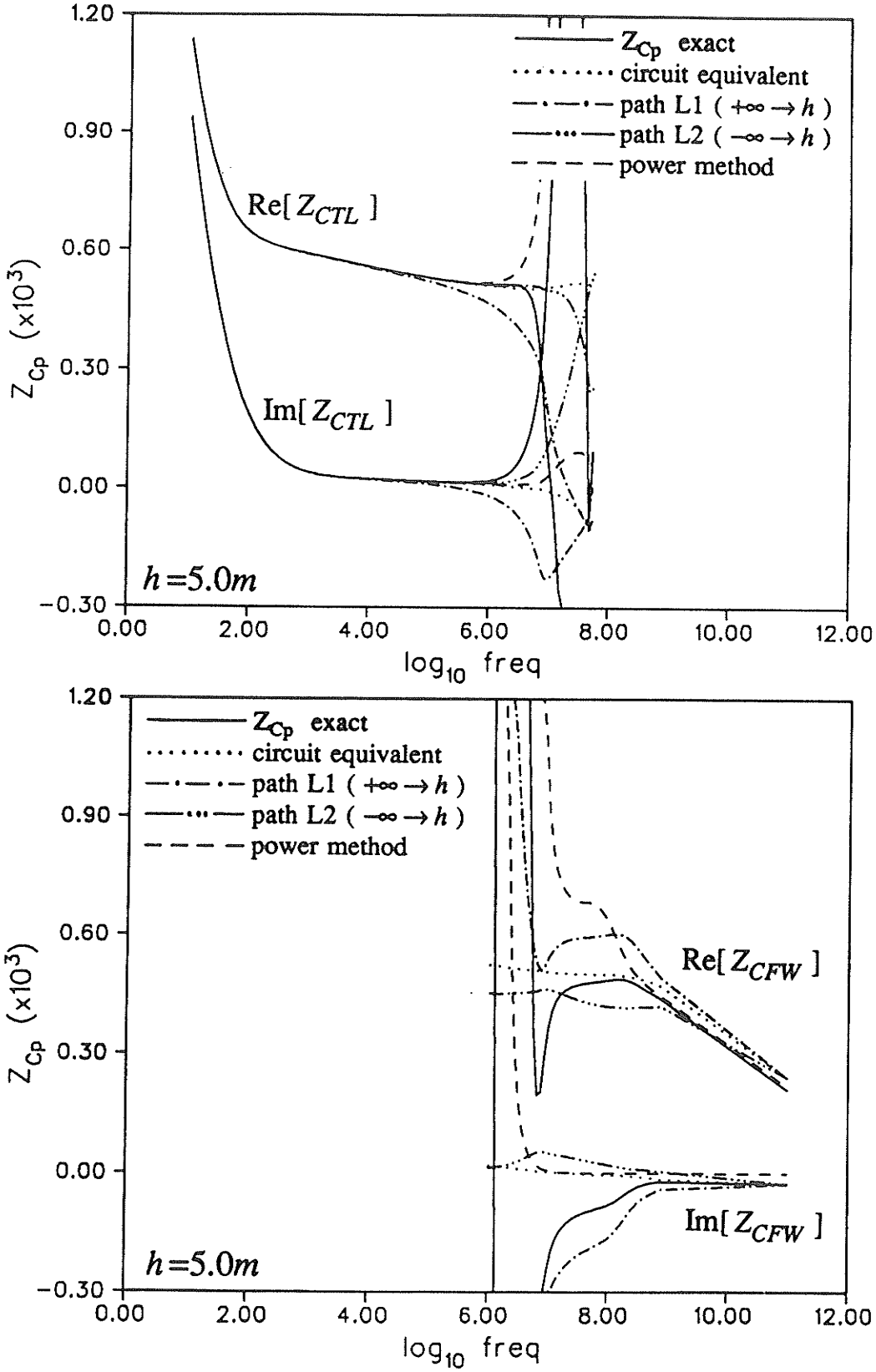

Figure 4.8: Comparison of the various definitions for characteristic impedance as a function of frequency for h=5.0m.

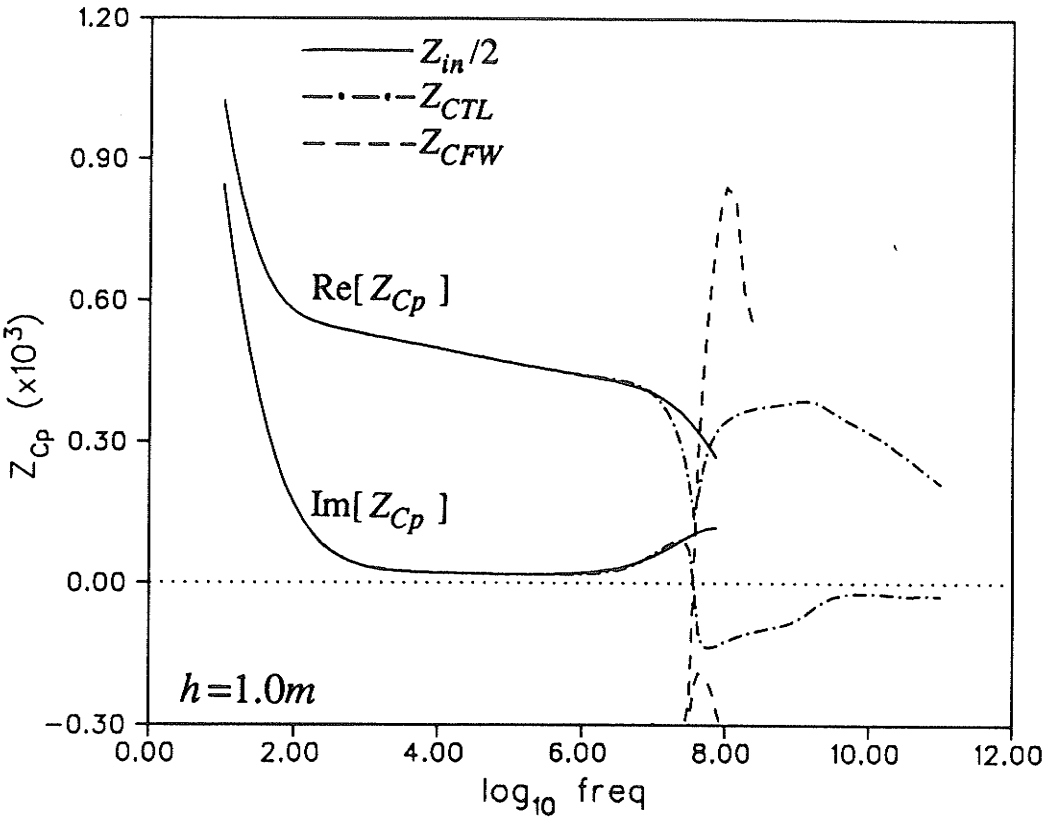

Figure 4.9: Comparison of the input impedance as calculated using the exact spectral-domain solution and the discrete mode contribution for h=1.0m.

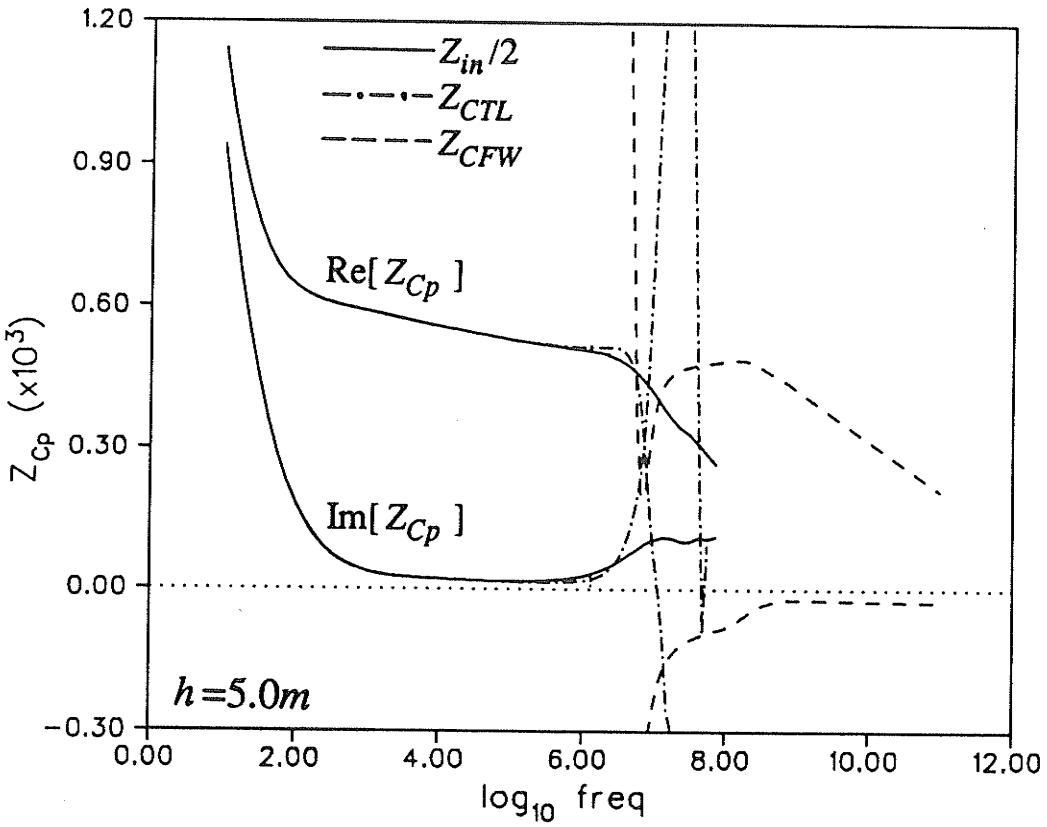

Figure 4.10: Comparison of the input impedance as calculated using the exact spectral-domain solution and the discrete mode contribution for h=5.0m.

Chapter 5
Wave Propagation Along a Conductor Near Or At a Lossy Interface

The study of wave propagation along conductors located near or at a lossy planar interface is of interest in low frequency radio transmission, geoelectromagnetics for remote sensing applications, as well as in the power engineering field for transmission line analysis. It is important to determine the effect of the interface on the propagation and radiation characteristics of the geometry, especially if it is highly lossy as in the case of the earth. In the past, and as extensively examined in chapter 3, almost all theories have treated the problem assuming a thin-wire approximation to model the conductor [Carson, Sunde, Wait5, Kuester2]. This means only axially directed currents having a uniform azimuthal distribution are assumed to propagate. Even the solution to this simplified model has proven difficult; beginning with Carson in 1926 [Carson] who took an approximate circuit approach, to Wait [Wait5] who presented an exact solution in integral form. All this work, based on the thin-wire approximation, has been successfully applied to many practical problems. However, if the conductor is not thin or is located near the interface, the azimuthal current distribution will not be uniform and azimuthal current components will also be present.

For a conductor located well above the lossy interface, the propagation constant of the guided waves along the structure will be close to the wavenumber of the upper medium (free space in the case of transmission lines above an earth). For a conductor buried deep in the lossy medium, the propagation constant will be close to that of the medium in which it is embedded. However, the evaluation of the propagation constant for the structure becomes difficult when the conductor is located near or at the media interface. For the case of an infinitely thin conductor located at the interface between two media, Coleman [Coleman] showed that the propagation constant will be equal to the mean-square average of the wavenumbers of the two media. Wait and Spies [Wait4] determined the resulting fields for an axially uniform line current on an infinitely thin conductor located at the interface. Wait [Wait5] then presented exact expressions in integral form for the current on a single circular conductor located above a lossy interface, under the assumption of the thin-wire approximation. Chang and Wait [Chang1] determined the propagation constants for both above ground and buried conductors near a lossy interface at ELF frequencies. At these low frequencies, it is assumed that the height of the conductor is much less than the skin depth of the

earth and closed form expressions for approximating the infinite integrals representing both conduction and displacement current effects were derived. They also used the assumption of a uniform axially directed current distribution around the conductor in deriving the propagation constant for the limiting case of a vanishing height when the conductor radius to height ratio was fixed. Olsen and Pankaskie [Olsen7] give results of the propagation constant calculated for a finite radius conductor with a uniform current distribution located at the interface between two media. The results are compared to those calculated using Carson's quasi-TEM approximation [Carson], which are shown to be invalid in this case. Pogorzelski and Chang [Pogorzelski] formulated the problem of a circular conductor located near a lossy planar interface by taking into account a non-uniform azimuthal current distribution. The formulation examined the effect of only the zero and first order azimuthal and axial Fourier current components on the propagation constant. In a series of papers by Butler et al. [Butler1, Butler2, Butler3, Xu], a scattering approach was taken to determine the current induced on a perfectly conducting cylinder located near the interface between two media by a known excitation. These studies are made for various conductor shapes; circular, square, strips, etc. The formulation in these papers and others [Newman1], however, is a two-dimensional one considering either a TE or TM axially invariant excitation. Further, their work was oriented towards scattering from conductors laying on or near a dielectric interface (the media considered had small losses), whereas this work is concerned mainly with a highly lossy interface, with the effect on the current distribution being much more pronounced in the latter case.

In this chapter, the propagation constants and associated current distributions for the discrete characteristic modes supported by cylindrical conductors located near or at a lossy planar interface are determined. An axially directed current is still assumed, but an arbitrary azimuthal distribution is taken into account in the formulation. Although the formulation is general for any size, numerical results for cases where the dimensions of the conductor are much less than the free space wavelength will be considered here. Some of the important questions that are examined are:

1. Is the use of the thin-wire approximation valid for small conductor heights and if not, what must the height to radius ratio be for it to be acceptable?
2. How does a non-uniform current distribution effect the propagation constant and radiated fields for the structure?
3. Can the quasi-TEM approximation (Carson's circuit based formulas) be used to determine the fields of a conductor near the earth or are more exact expressions for the conduction and displacement currents required?
4. A dramatic change in the propagation constant occurs "*just*" as the conductor comes in contact with the interface ($h \rightarrow 0$) if the lower medium is highly conducting (as in the case of a typical earth at frequencies below 1MHz). Before contacting the interface, the propagation constant is near the free space value, and

once it is buried, it is near that of the lower medium. Is the propagation constant equal to the average value of these two limits when at the interface (h=0) and what is the current distribution on the conductor for this case?

5.1. INTEGRAL EQUATION FORMULATION AND NUMERICAL SOLUTION

The problem considered consists of a single arbitrary shaped cylindrical conductor located above and parallel to a lossy homogeneous interface as shown in figure 5.1. The region $y>0$ is considered to be free space, characterized by a permittivity ε_e and a permeability μ_e. The region $y<0$ is designated as the lossy earth, characterized by a permittivity ε_g, a permeability μ_g, and a conductivity σ_g. The conductor is defined by the surface S, which is invariant in the z-dimension and defined by the generating curve $C \in \rho(x,y)$. It is required to determine the characteristic propagating modes and associated current distributions $\overline{J}(\overline{r})$; $\overline{r} \in S$ on the surface of the conductor for a given geometry.

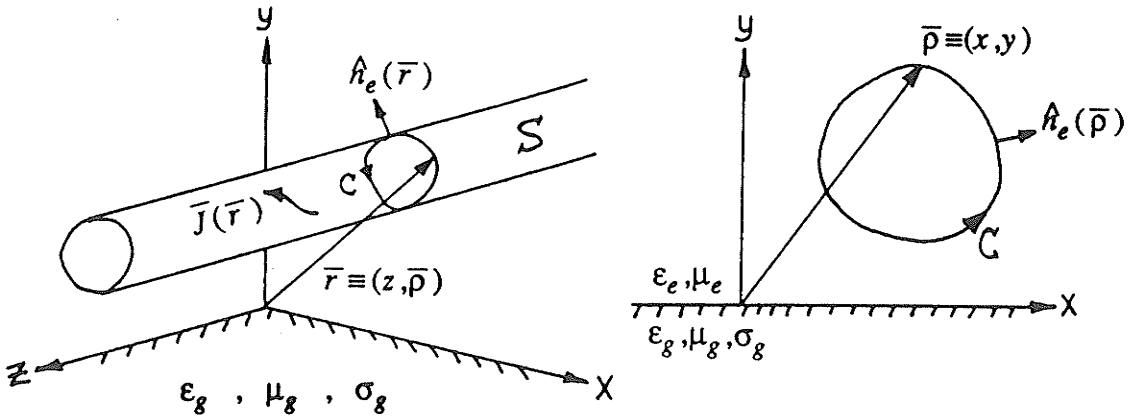

Figure 5.1: Conductor over lossy interface geometry.

The solution of the problem is facilitated by solving the wave equation in each media region (the conductor and upper and lower half-spaces) and satisfying the boundary conditions at their interfaces. As developed in chapter 2, this results in an integral equation (2.10), whose solution yields the unknown current distribution on the surface S. For a perfect electric conductor located in the upper half-space, only the total electric field tangential to the conductor surface is required to be zero, and thus, only the Green's function components $\overline{\overline{G}}_e = \overline{\overline{G}}_e^{ee(ee)}$ in the integral equation are required. An integral equation for the solution of the problem considered in figure 5.1 can then be formulated as

$$\hat{h}_e(\overline{r}) \times \left[\iint_S \overline{\overline{G}}_e(\overline{r},\overline{r}')\overline{J}(\overline{r}')d\overline{r}' + \overline{E}_e^{inc}(\overline{r}) \right] = 0 \quad ; \overline{r} \in S \tag{5.1}$$

where $\hat{n}_e(\bar{r})$ is the unit vector normal to the surface S at $\bar{r}$. This is simply an electric field integral equation which must be satisfied over the infinite length of the conductor. $\overline{\overline{G}}_e(\bar{r},\bar{r}')$ is the Green's function giving the electric field due to a delta function line source, which is formulated to take into account the effect of the lossy planar interface, and can be deduced from appendix A. $\bar{E}_e^{inc}(\bar{r})$ is the field incident on the conductor due to some external source and $\bar{J}(\bar{r})$ is the current induced on the surface of the structure. The formulation as presented in (5.1) is the general case, where the current induced by any desired source can be determined by properly specifying the incident electric field. The allowance for a non-perfect conducting cylinder can also easily be incorporated into (5.1) using the impedance boundary condition at the surface or the complete integral equation form (2.10) developed in chapter 2. As in section 2.2, when the physical geometry of the conductor-half-space problem is invariant with respect to the z-dimension, a solution to the integral equation can be obtained in the spectral domain by utilizing the spacial Fourier transform pair

$$f(k_z) = \int_{-\infty}^{\infty} \mathrm{f}(z) e^{-jk_z z}\, dz \quad , \quad \mathrm{f}(z) = \frac{1}{2\pi}\int_{-\infty}^{\infty} f(k_z) e^{+jk_z z}\, dk_z \tag{5.2}$$

The integral equation (5.1) can then be solved as a two-dimensional problem as

$$\hat{n}_e(\bar{\rho}) \times \left[\int_C \overline{\overline{G}}_e(\bar{\rho},\bar{\rho}';k_z)\bar{J}(\bar{\rho}';k_z)d\bar{\rho}' + \bar{E}_e^{inc}(\bar{\rho},k_z)\right] = 0 \quad ; \bar{\rho}\in C \ , -\infty < k_z < \infty \tag{5.3}$$

where all fields and currents are now assumed to have an axial dependence of the form $e^{+jk_z z - j\omega t}$. The path of integration in the integral equation (5.3) is now over the generating curve C. In the cases studied in this chapter only an axially directed current component will be assumed to propagate on the conductor, $\bar{J}(\bar{\rho},k_z)=J_z(\bar{\rho},k_z)\hat{z}$. Thus, continuity of only the tangential $\hat{z}$ components of the electric field on the conductor surface is required and only the component $G_{ezz}(\bar{\rho},\bar{\rho}';k_z)$ is used. The resulting integral equation is valid for an arbitrary source excitation, and can be solved using a moment method approach as derived in chapter 2. However, interest is in the homogeneous solutions of (5.3) for determining the characteristic modes that can propagate on the structure and in the resulting current distributions for these modes. Taking $\bar{E}_e^{inc}(\bar{\rho},k_z)=0$ in the homogeneous case, these results are then determined by solving the scalar integral equation

$$\int_C G_{ezz}(\bar{\rho},\bar{\rho}';k_z)J_z(\bar{\rho}';k_z)d\bar{\rho}' = 0 \quad ; \bar{\rho}\in C \tag{5.4}$$

Here the eigenvalues $k_z = k_z^p \ ; p=1,2,...,P$ satisfying (5.4) are the characteristic propagation constants for the structure, which are in general complex. Solutions of this mode equation define currents and fields which have an axial dependence of the form $\exp\{\pm jk_z^p z - j\omega t\}$. The current distribution on the conductor for each mode is given

from the eigenvectors of (5.4) as

$$J_z(\bar{\rho},z) = J_z^p(\bar{\rho})e^{\pm jk_z^p z - j\omega t} \quad ; p=1,2,...,P \tag{5.5}$$

The solution of the mode equation (5.4) will be determined numerically using the method of moments following the procedure discussed in chapter 2 (2.16-2.22) and as shown in figure 5.2. In this section, the unknown current distribution around the contour C will be expanded using a pulse function basis $\Pi_n(\bar{\rho})$ as

$$J_z^p(\bar{\rho}) = \sum_{n=1}^{N} I_n^p \Pi_n(\bar{\rho}) \quad , \quad \Pi_n(\bar{\rho}) = \begin{cases} 1/\Delta c_n & , \bar{\rho} \in \Delta c_n \\ 0 & , \text{otherwise} \end{cases} \tag{5.6}$$

where the contour C has been approximated by N discrete line segments Δc_n with the value of the total current on each segment given by the constant I_n^p. Note that the expansion of the current using this basis is approximate for finite N. Solution of the N constants I_n^p is facilitated by computing an appropriate inner product $<,>$ of (5.4) with some testing function basis. Choosing a delta function testing basis consisting of N matching points located at the centers of the segments Δc_n will yield the set of linear equations

$$<L\{J_z^p(\bar{\rho})\}, \delta(\bar{\rho}_m)> = \sum_{n=1}^{N} <L\{\Pi_n(\bar{\rho})\}, \delta(\bar{\rho}_m)> I_n^p = 0 \quad , \begin{cases} m=1,2,...,N \\ p=1,2,...,P \end{cases} \tag{5.8}$$

$$L\{f(\bar{\rho})\} = \int_C G_{ezz}(\bar{\rho},\bar{\rho}',k_z=k_z^p) f(\bar{\rho}') d\bar{\rho}'$$

$$<a(\bar{\rho}), b(\bar{\rho})> = \int_C a(\bar{\rho}') b(\bar{\rho}') d\bar{\rho}'$$

where $\bar{\rho}_m$ is the center of the segment Δc_m. The resulting set of linear equations (5.8)

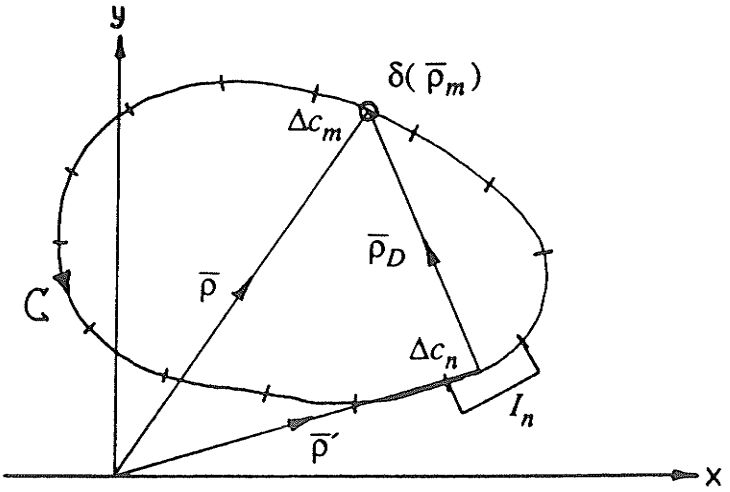

Figure 5.2: Pulse function expansion-delta function testing MOM solution.

can then be solved in matrix form as

$$[Z(k_z=k_z^p)][I^p] = 0 \quad ; p=1,2,...,P \tag{5.9}$$

$$\begin{aligned} Z_{mn}(k_z) &= -Z^e_{mn}(k_z) = -\langle L\{\Pi_n(\bar{\rho})\}, \delta(\bar{\rho}_m)\rangle \\ &= -\frac{1}{\Delta c_n}\int_{\Delta c_n} G_{ezz}(\bar{\rho}_m,\bar{\rho}',k_z)d\bar{\rho}' \end{aligned} \tag{5.10}$$

The possible solutions of these sets of linear equations yields P characteristic eigenvalues k_z^p representing the propagation constants, and their corresponding eigenvectors $[I^p]$ giving the current distribution.

The scalar Green's function $G_{ezz}(\bar{\rho},\bar{\rho}',k_z)$ which determines the $\hat{z}$ component of the electric field at the observation point $\bar{\rho}$ due to a delta function line source located at $\bar{\rho}'$ can be deduced in the same manner as the Green's functions formulated in appendix A. Assuming an axial dependence of the form $e^{+jk_z z}$, the fields of a delta function line source located at (x',y') can be deduced by solving the two-dimensional wave equation in each air and earth half-space, these being written in terms of potential vectors as

$$\begin{aligned} &[\nabla^2 - (k_z^2-k_e^2)]\,\bar{\Pi}^e = \frac{-j\omega\mu_e}{k_e^2}\delta(x-x')\delta(y-y')\hat{z} \qquad , y>0 \\ &[\nabla^2 - (k_z^2-k_g^2)]\,\bar{\Pi}^g = 0 \qquad , y<0 \end{aligned} \tag{5.11}$$

where $\bar{\Pi}^e$ and $\bar{\Pi}^g$ are the two-dimensional Hertz vector potentials in the air and earth regions, respectively. Here $k_e = \sqrt{\omega^2\mu_e\varepsilon_e}$ is the propagation constant in the air medium, and $k_g = \sqrt{\omega^2\mu_g\varepsilon_g + j\omega\mu_g\sigma_g}$ is the propagation constant in the ground medium. The associated fields in the upper half-space, and thus $G_{ezz}(\bar{\rho},\bar{\rho}',k_z)$, are determined from

$$\bar{E}_e = \nabla\nabla\cdot\bar{\Pi}^e + k_e^2\bar{\Pi}^e \quad , \quad \bar{H}_e = \frac{k_e^2}{j\omega\mu_e}\nabla\times\bar{\Pi}^e \quad , \quad G_{ezz}(\bar{\rho},\bar{\rho}',k_z) = \bar{E}_e(\bar{\rho})\cdot\hat{z} \tag{5.12}$$

A solution to (5.11) is obtained using the transform techniques (A.6-A.12) and then satisfying the boundary conditions at the air-earth interface. In the case of equal air and ground permeabilities ($\mu_g=\mu_e$), the Green's function is determined as

$$\begin{aligned} G_{ezz}(\bar{\rho},\bar{\rho}',k_z) = \frac{-j\omega\mu_e}{2\pi k_e^2}\Bigg\{ &\tau_e^2\left[K_0(\tau_e\,|\,\bar{\rho}_D\,|) - K_0(\tau_e\,|\,\bar{\rho}_D^*\,|)\right] \\ &- k_e^2\mathbf{J}(\tau_e,\bar{\rho}_D^*) + k_z^2\mathbf{G}(\tau_e,\bar{\rho}_D^*)\Bigg\} \end{aligned} \tag{5.13}$$

$$\bar{\rho}\equiv(x,y) \quad , \quad \bar{\rho}'\equiv(x',y') \quad , \quad \bar{\rho}_D\equiv(x-x',y-y') \quad , \quad \bar{\rho}_D^*\equiv(x-x',y+y')$$

$$\mathbf{J}(\tau_e,\overline{\rho}_D^*) = \int_{-\infty}^{\infty} \frac{1}{U_e+U_g} e^{+jk_x|x-x'|-U_e(y+y')}\, dk_x \tag{5.14a}$$

$$\mathbf{G}(\tau_e,\overline{\rho}_D^*) = \int_{-\infty}^{\infty} \frac{1}{n^2U_e+U_g} e^{+jk_x|x-x'|-U_e(y+y')}\, dk_x \tag{5.14b}$$

$$U_e = \sqrt{k_x^2+\tau_e^2} \quad , \quad U_g = \sqrt{k_x^2+\tau_g^2} \quad , \quad \mathrm{Re}[U_e,U_g] \geq 0$$

where $\tau_e = \sqrt{k_z^2-k_e^2}$ and $\tau_g = \sqrt{k_z^2-k_g^2}$ are the transverse propagation constants in the air and earth media, respectively. The real parts of the irrationals $\mathrm{Re}[U_e,U_g]\geq 0$ and $\mathrm{Re}[\tau_e,\tau_g]\geq 0$ have been chosen to retain a positive value on the correct Riemann sheet, these branch cuts being defined to ensure that the currents and fields decay at infinity. $K_0(z)$ is the modified Bessel function of complex argument and $n=k_g/k_e$ is the refractive index of the air-earth interface. In the derivation of (5.13), the term involving $K_0(\tau_e|\overline{\rho}_D|)$ is due to the primary field of the current source, and the term involving $K_0(\tau_e|\overline{\rho}_D^*|)$ is due to its image as if the earth were perfectly conducting. The remaining terms in integral form, (5.14) are the corrections due to the imperfectly conducting earth. Extension of the theory to account for a multiple layered earth model can be facilitated by modifying (5.14) [Wait9].

Using the Green's function $G_{ezz}(\overline{\rho},\overline{\rho}',k_z)$, the impedance matrix elements in (5.10) are given as [Bridges6]

$$Z_{mn}(k_z) = -Z_{mn}^e(k_z) = -\left[Z_{mn}^S(k_z) - Z_{mn}^M(k_z)\right] \tag{5.15}$$

$$Z_{mn}^S(k_z) = \begin{cases} \dfrac{-j\omega\mu_e}{2\pi k_e^2}\dfrac{1}{\Delta c_n}\displaystyle\int_{\Delta c_n} \tau_e^2 K_0(\tau_e|\overline{\rho}_D|)\, d\overline{\rho}' & ;\ m\neq n \\ \dfrac{-j\omega\mu_e}{2\pi k_e^2}\displaystyle\int_{-\infty}^{\infty} \dfrac{\tau_e^2}{2\sqrt{\lambda^2+\tau_e^2}}\dfrac{\sin(\lambda\Delta c_n/2)}{\lambda\Delta c_n/2}\, d\lambda & ;\ m=n \end{cases} \tag{5.16}$$

$$Z_{mn}^M(k_z) = \frac{-j\omega\mu_e}{2\pi k_e^2}\frac{1}{\Delta c_n}\int_{\Delta c_n}\left[\tau_e^2 K_0(\tau_e|\overline{\rho}_D^*|) + k_e^2\mathbf{J}(\tau_e,\overline{\rho}_D^*) - k_z^2\mathbf{G}(\tau_e,\overline{\rho}_D^*)\right] d\overline{\rho}' \tag{5.17}$$

$$\overline{\rho}_D \equiv (x_m-x',y_m-y') \quad , \quad \overline{\rho}_D^* \equiv (x_m-x',y_m+y')$$

The solutions of (5.9) giving the propagation constants k_z^p is a generalized eigenvalue problem facilitated by solving the determinant $|Z(k_z^p)|=0$, $p=1,2,...,P$. For each of the characteristic modes found, there corresponds an eigenvector $[I^p]$ for which the current distribution of each mode $J_z^p(\overline{\rho})$ can be determined using (5.5,5.6). In general, there will be $P\geq N$ distinct eigenvalues for each of which there corresponds an appropriate eigencurrent. The evaluation of the Fourier integrals $\mathbf{J}(\tau_e,\overline{\rho})$ and $\mathbf{G}(\tau_e,\overline{\rho})$ in (5.14) are difficult and usually numerical integration techniques must be

employed in the general case, with the analytical approximations and numerical evaluation methods for these integrals being discussed in appendix B.

5.2. THIN-WIRE AND QUASI-TEM APPROXIMATIONS

The solution of the set of linear equations (5.9) for the general case of an arbitrary shaped conductor involves the evaluation of a large number of infinite integrals. To simplify the problem, two common approximations which are often used in practice will be examined. The first is the thin-wire approximation, where the azimuthal current distribution around the conductor is assumed to be uniform. This approximation was derived and extensively discussed in chapter 3 for multiple conductor structures. The approximation is valid when the mean radius of the conductor is small compared to the wavelength in the medium in which it is embedded and if the distance from all other discontinuities (such as the air-earth interface or other conductors) is large compared to the conductor radius. It has been the basis of almost all the previous works in solving conductor-half-space problems. The thin-wire approximation for *circular* conductors can be derived directly from the integral equation solution (5.4) under the uniform current assumption

$$J_z(\overline{\rho},z) = J_z^p(\overline{\rho})e^{\pm jk_z^p - j\omega t} = \frac{I_o^p}{2\pi a}e^{\pm jk_z^p - j\omega t} \tag{5.18}$$

where a is the radius of the conductor and I_o^p is the total current flowing in the conductor for the pth mode. Replacing the current distribution with (5.18), the integral in (5.4) will yield the average value of the fields around the conductor circumference, which can be evaluated analytically (as done in chapter 3 (3.21) except a perfect conductor is assumed here) as

$$Z(k_z=k_z^p)I_o^p = 0 \qquad , p=1,2,...,P \tag{5.19}$$

$$\begin{aligned} Z(k_z) &= -\frac{1}{2\pi a}\int_C G_{ezz}(\overline{\rho},\overline{\rho}',k_z)d\overline{\rho}' \\ &= \frac{+j\omega\mu_e}{2\pi k_e^2} I_0(\tau_e a)\Big\{\tau_e^2 K_0(\tau_e a) \\ &\qquad - I_0(\tau_e a)\left[\tau_e^2 K_0(\tau_e 2h) + k_e^2 \mathbf{J}(\tau_e, 2h\hat{y}) - k_z^2 \mathbf{G}(\tau_e, 2h\hat{y})\right]\Big\} \end{aligned} \tag{5.20}$$

where h is the height of the conductor above the interface (to the conductor center). The modified Bessel function $I_0(z)$ takes into account the average value of the fields and enforces the boundary condition at the conductor-air interface. The functions $\mathbf{J}(\tau_e,\overline{\rho})$ and $\mathbf{G}(\tau_e,\overline{\rho})$ are the same Fourier integrals as defined in (5.14). Determining the eigenvalues of this single term linear equation (5.19) is much faster than solving the matrix equation (5.9).

As previously discussed, the propagation constant of an infinitely thin conductor located at the interface of the two media will be equal to the mean-square average value of their wavenumbers [Coleman]. This result can be derived from (5.20), in a similar manner as in [Chang1], by assuming the height to radius ratio to be constant ($h/a=const$) and considering the limiting case $h\rightarrow 0$, $a\rightarrow 0$. Under these conditions, the dominant terms in (5.20) can be identified to yield

$$Z(k_z) = \frac{+j\omega\mu_e}{2\pi k_e^2}\left[\tau_e^2 \ln\left(\frac{2h}{a}\right) + k_e^2 \ln\left(\tau_e 2h\right) - \frac{2k_z^2}{n^2+1}\ln\left(\tau_e 2h\right)\right] \tag{5.21}$$

$$I_0(\tau_e a) \xrightarrow[a\rightarrow 0]{} 1$$

$$K_0(\tau_e a) - K_0(\tau_e 2h) \xrightarrow[a,h\rightarrow 0]{} \ln\left(2h/a\right)$$

$$\mathbf{J}(\tau_e, 2h\hat{y}) \xrightarrow[a,h\rightarrow 0]{} -\ln(\tau_e 2h) \quad , \quad \mathbf{G}(\tau_e, 2h\hat{y}) \xrightarrow[a,h\rightarrow 0]{} \frac{-2}{n^2+1}\ln(\tau_e 2h)$$

Since the height to radius ratio is fixed, the solution of (5.19) with $Z(k_z)$ replaced by (5.21), gives the mean-square average result $k_z^p = k_z^{AVE} = \sqrt{(k_g^2+k_e^2)/2}$. The limiting approximations for $\mathbf{J}(\tau_e, \bar{\rho})$ and $\mathbf{G}(\tau_e, \bar{\rho})$ were discussed in appendix B.

A second method of simplifying the evaluation of the mode equation (5.9) is by employing the quasi-TEM approximation. As discussed in section 2.4.1 and 3.3.3, the quasi-TEM approximation assumes that the axial variation of the fields is equal to that of the upper medium ($k_z \approx k_e$) when solving the wave equation in each half-space (ie. setting $\tau_e = 0$ in (5.11)). In this manner, the fields in the upper half-space will be a solution of the two-dimensional Laplace equation. This low frequency approximation has been successfully applied to many engineering problems and is generally acceptable under the conditions that the dimensions of the transmission line should be much less than the wavelength in the upper medium ($a, h \ll \lambda_e$) as well as the refractive index of the air-earth interface should be large ($|n| \gg 1$) [King1, Bridges3]. However, even if these conditions hold the quasi-TEM approximation will not be valid as the conductor approaches the interface [Olsen7], a more detailed examination of this limitation being discussed latter in this chapter. Applying the quasi-TEM approximation by assuming $\tau_e = \sqrt{k_z^2 - k_e^2} \rightarrow 0$ in the wave equation (5.11), the Green's function and thus the impedance matrix elements (5.15-5.17) can be rederived in the simplified form

$$[Z(k_z)] = [Z^{ser}] + k_z^2 [Y^{sh}]^{-1} \tag{5.22}$$

$$Z_{mn}^{ser} \approx \frac{-j\omega\mu_e}{2\pi}\left[M_{mn} + \frac{1}{\Delta c_n}\int_{\Delta c_n} \mathbf{J}_c(\bar{\rho}_D^*)\, d\bar{\rho}'\right] \tag{5.23}$$

$$(Y^{sh})^{-1}_{mn} \approx \frac{1}{-j\,\omega\varepsilon_e 2\pi}\left[M_{mn} \right] \tag{5.24}$$

$$M_{mn} = \begin{cases} \dfrac{1}{\Delta c_n}\displaystyle\int_{\Delta c_n} \ln\left(|\,\bar{\rho}_D^{\,*}\,| \,/\, |\,\bar{\rho}_D\,| \right) d\bar{\rho}' & ,m\neq n \\ \left(1 - \ln\dfrac{\Delta c_n}{2} \right) + \dfrac{1}{\Delta c_n}\displaystyle\int_{\Delta c_n} \ln\left(|\,\bar{\rho}_D^{\,*}\,| \right) d\bar{\rho}' & ,m=n \end{cases} \tag{5.25}$$

$$\mathbf{G}(\tau_e=0,\bar{\rho}_D^{\,*}) \equiv 0 \quad , \quad \mathbf{J}(\tau_e=0,\bar{\rho}_D^{\,*}) \rightarrow \mathbf{J}_c(\bar{\rho}_D^{\,*})$$

$$\mathbf{J}_c(\bar{\rho}_D^{\,*}) = \frac{2}{n^2-1}\int_0^{\infty}\left[u - \sqrt{u^2-(n^2-1)} \right] e^{-uk_e(y_m+y')}\cos(uk_e\,|\,x_m-x'\,|\,)\,du \tag{5.26}$$

Here the series impedance Z^{ser}_{mn} and the shunt admittance Y^{sh}_{mn} terms are the equivalent per unit length circuit parameters for the structure. The solution to (5.9) can now be found as a standard eigenvalue problem. The logarithmic terms in (5.25) represent the primary field and its image under the conditions of a perfectly conducting earth. The integral term $\mathbf{J}_c(\bar{\rho}_D^{\,*})$ represents the conduction losses in the earth and the contribution of the integral $\mathbf{G}(\tau_e,\bar{\rho}_D^{\,*})$, representing displacement current losses in the earth, has been neglected completely. Expressions for evaluating the integral $\mathbf{J}_c(\bar{\rho}_D^{\,*})$ are discussed in appendix B.

5.3. SOME NUMERICAL RESULTS

In general, there will be many possible solutions to the mode equation (5.9), each representing a discrete guided mode $(k_z^p,\, J_z^p(\bar{\rho});p=0,1,2,...,P)$ on the transmission structure. The modes can be categorized as consisting of a zero-order common mode ($p=0$) plus a sum of higher-order differential modes ($p>0$). For the zero-order mode, the current distribution around the circumference of the conductor is primarily in phase, with the return current path through the lossy interface. On the other hand, the higher-order modes have a current distribution where both the forward and return current paths are along the conductor. Thus, the fields for the differential modes are confined mainly to the region around the conductor and the effect of the interface will not be as pronounced as for the common mode. The results presented in this section concentrate on the characterization of the zero-order mode propagation constant and current distribution since it is the dominant mode excited when the overall dimensions of the conductor are small compared to the free space wavelength, and is the mode most affected by the presence of the lossy interface.

The first geometry considered will be a circular conductor located over a lossy interface as shown in figure 5.3. The conductor has a fixed radius of $a=0.08m$ with the height h above the interface allowed to vary. The ground is characterized by the

electrical properties $\mu_{rg}=1.0$, $\varepsilon_{rg}=5.0$, $\sigma_g=0.01$ and an operating frequency of $100KHz$ is chosen. Under these conditions, the ground can be considered conducting ($n = 30.02+j29.94$). The parameter $\Delta = h-a$ in figure 5.3 indicates the distance from the interface to the bottom of the conductor. Figure 5.4 gives the normalized propagation constants k_z^p/k_e and the corresponding relative current distributions $J_z^p(\overline{\rho})$ for the first five modes ($p=0,1,2,3,4$) supported by the conductor for a height $h=0.24m$ ($\Delta/a=2.0$). The influence of the interface causes the current distribution to be more concentrated near $\phi=0^o$ (the bottom of the conductor) due to the proximity effect, the influence being greatest for the zero-order mode. Since the current will be symmetric about $\phi=0$, only the range $0\le\phi\le180$ is plotted, with $\phi=0$ the bottom and $\phi=180$ the top of the conductor as indicated in figure 5.3. Figure 5.5 gives the normalized zero-order mode propagation constant k_z^o/k_e for various conductor heights (using eqns. (5.9-5.17)). For heights $\Delta/a > 1$ the propagation constant is found near that of the upper half-space ($k_z^o/k_e \simeq 1$), and only when the conductor becomes very close to the interface $\Delta/a \ll 1$ does the deviation become significant. As the conductor comes in contact with the interface $\Delta/a \rightarrow 0$, the propagation constant converges to a value near the mean-square average k_z^{AVE}. Figure 5.6 gives the corresponding normalized current distribution $J_z^o(\phi)$ around the circumference of the conductor for various heights. The effect of the earth on the current distribution is much more pronounced than observed for the propagation constant. At a height of $\Delta/a = 1.5$ the deviation in the maximum current from a uniform distribution is 75%, whereas the error in k_z^o is only 2.4%. Even at the large height of $\Delta/a = 12.5$, the current deviation is still 18% and with only a 0.06% error in k_z^o. For heights $\Delta/a > 1$, the deviation in the current behaves as the first-order Fourier component $\cos\phi$, however, for smaller heights higher order terms are required for an accurate representation.

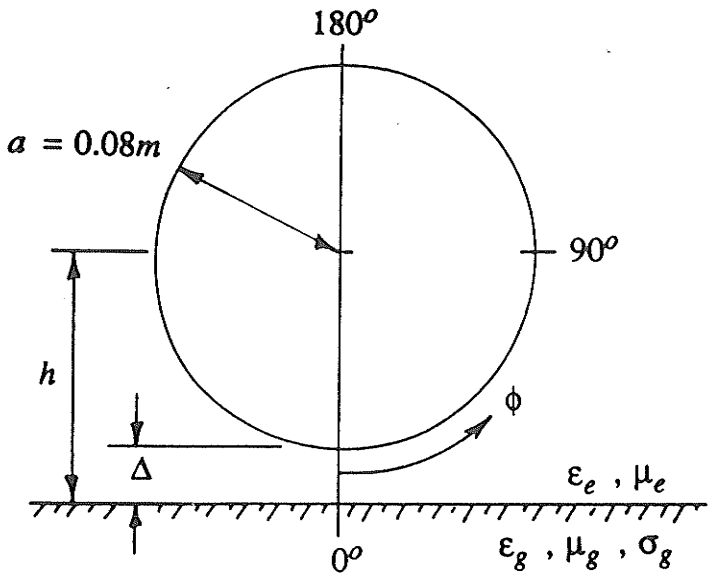

Figure 5.3: Circular conductor geometry.

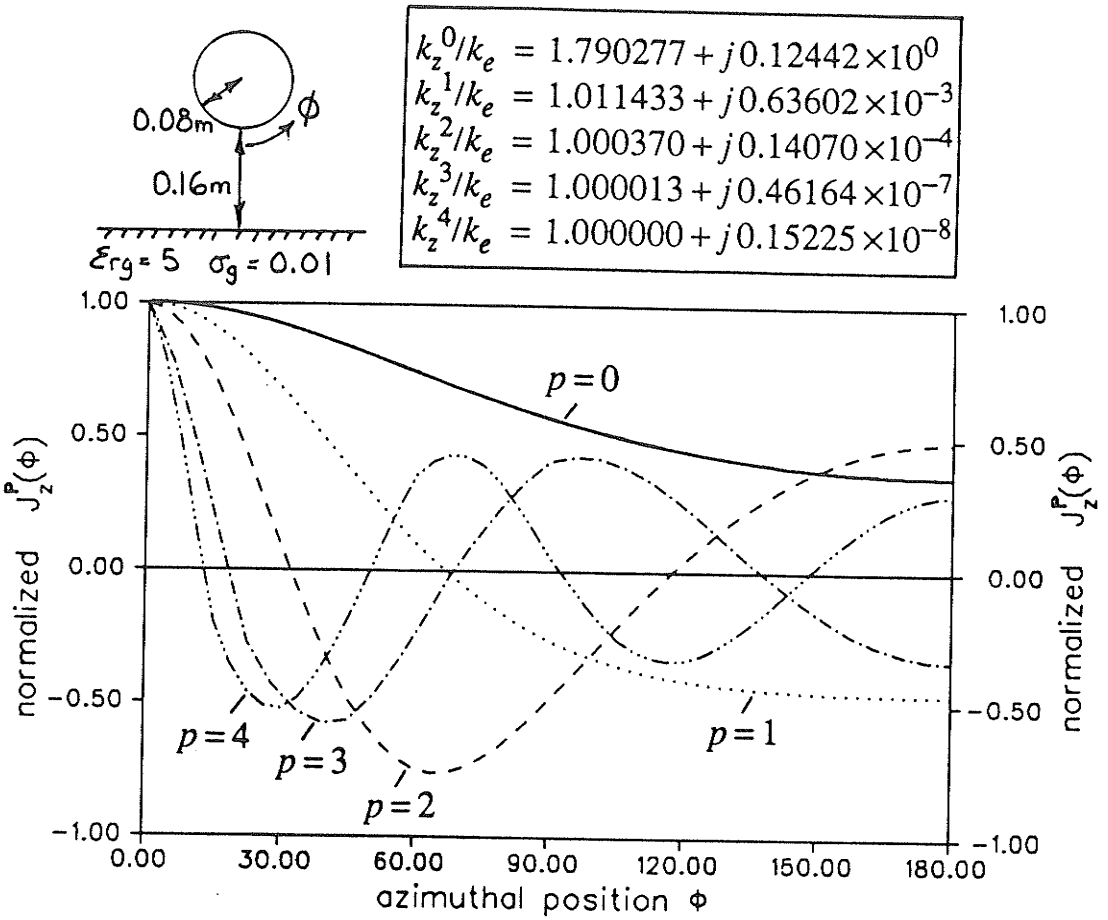

Figure 5.4: Propagation constants and current distributions for the first five modes supported by a circular conductor.

Figure 5.7 compares the zero order propagation constant k_z^o presented in figure 5.5 with the results calculated using the quasi-TEM approximation (eqns. (5.23-5.26)). For the case considered, the classical TEM conditions $|h,a| \ll \lambda_e = 3000m$ and $|n| = 42.4 \gg 1$ are all satisfied. The quasi-TEM approximation gives good results even when the conductor is very close to the interface $\Delta/a \geq 1/10$, however, beyond this point the approximation is unacceptable. The error is mainly due to the neglection of the displacement current term $\mathbf{G}(\tau_e, \bar{\rho}_D^*)$ contributing to the shunt admittance in (5.24). Figure 5.8 compares the propagation constant k_z^o presented in figure 5.5 with the results calculated using the thin-wire approximation (eqns. (5.18-5.20)) under the uniform current assumption. For the case shown, the thin-wire approximation is valid only if $\Delta/a > 1$. Note that as the conductor approaches the interface $\Delta \rightarrow 0$, the thin-wire result rapidly converges to the incorrect result determined by (5.20) with $h = \Delta + a \rightarrow a$. The dashed curve in figure 5.8 shows the variation of the propagation constant when the height to radius ratio is held constant $\Delta/a = 1.5$. The variation is

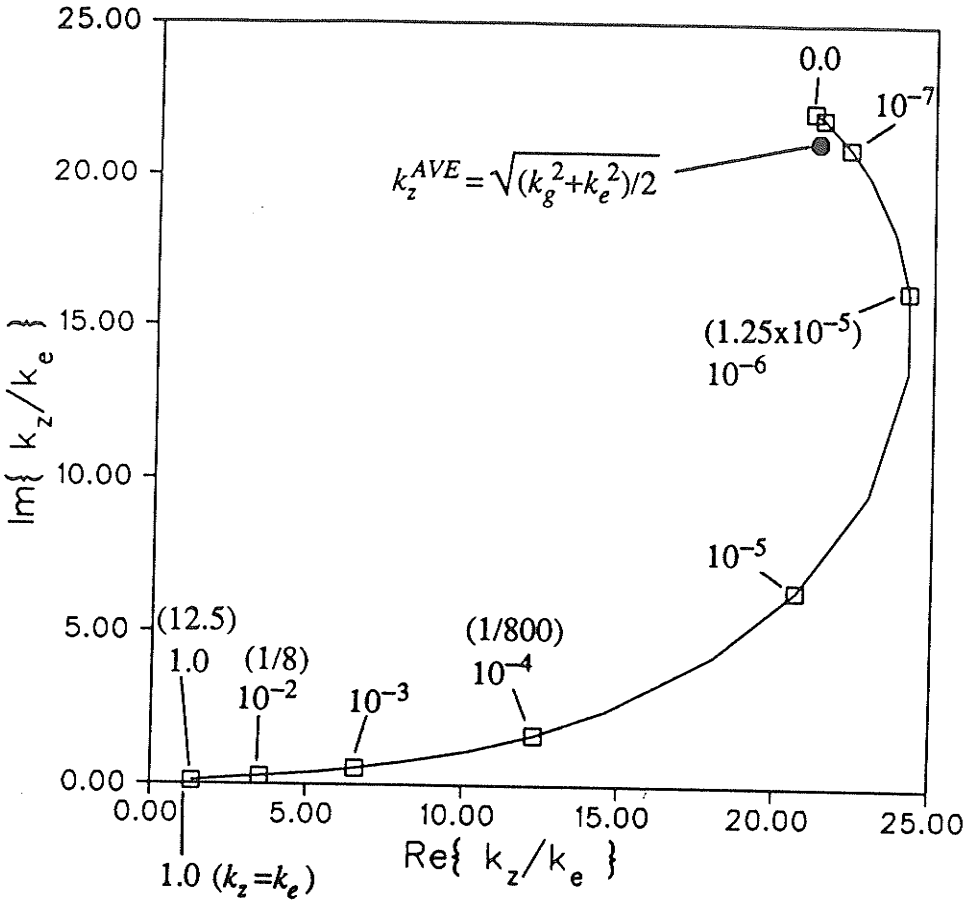

Figure 5.5: Zero-order mode propagation constant k_z^o/k_e for various conductor heights Δ.

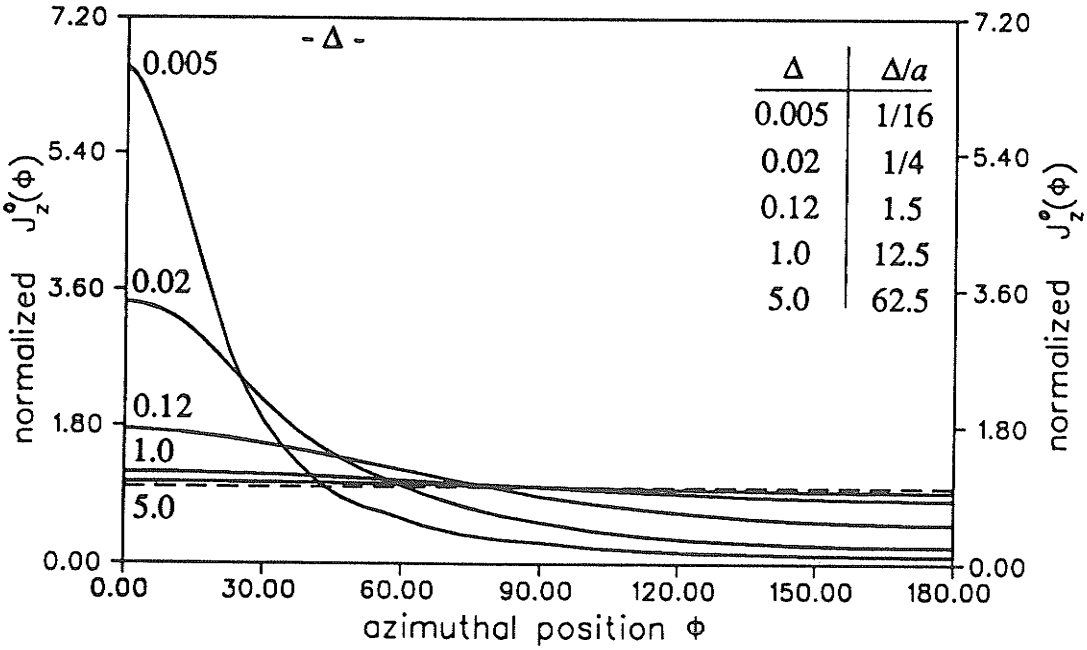

Figure 5.6: Azimuthal current distribution $J_z^o(\phi)$ for various conductor heights Δ.

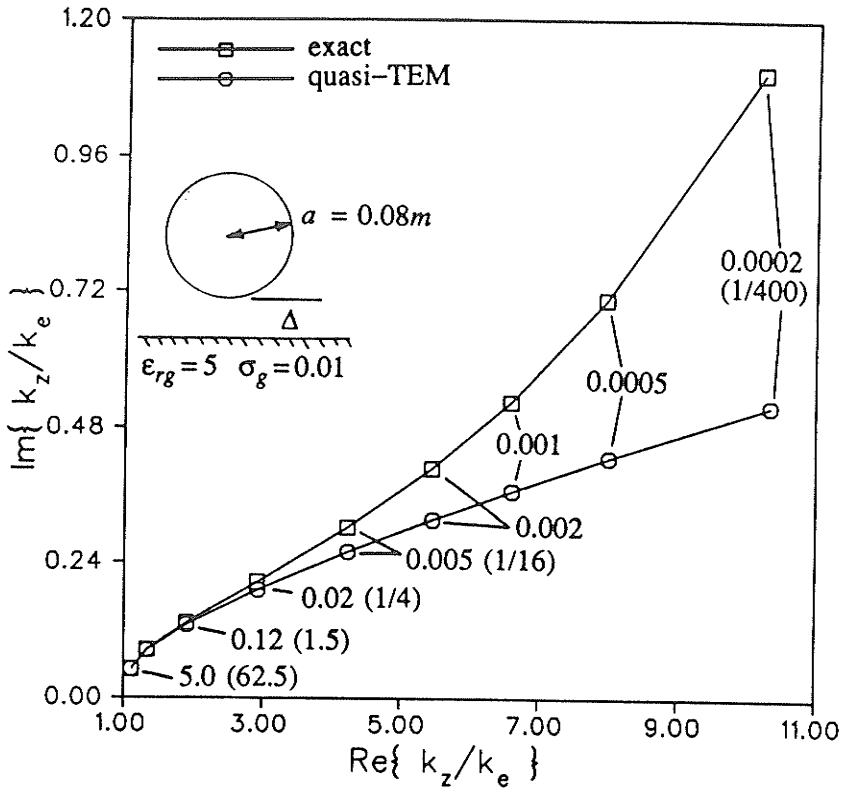

Figure 5.7: Comparison of the exact and quasi-TEM solutions for various conductor heights Δ.

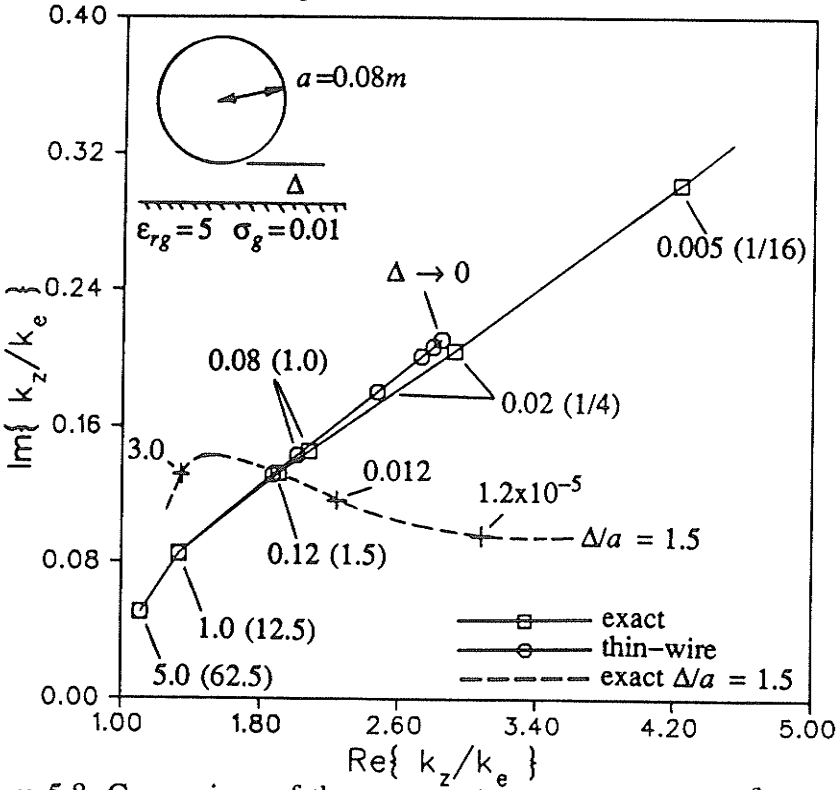

Figure 5.8: Comparison of the exact and thin-wire solutions for various conductor heights Δ.

very small for a wide range of conductor heights. This can be explained by examination of (5.23-5.25) where the dominant term M_{mn} (representing the static coupling) remains constant, with the conduction losses in (5.23) $\mathbf{J}_c$ causing a small perturbation. This result also indicates that the limiting process $h \to 0$, $a \to 0$ in (5.21), used to obtain the mean-square average value k_z^{AVE}, is achieved only when h and a are *extremely* small.

Figure 5.9 examines the effect of the conductor radius a in the limiting case when the conductor is lying on the interface $\Delta = 0$. A large range of radii are examined $0 < a \leq 10m$, and even though the convergence is extremely slow, the propagation constant converges to the mean-square average value $k_z^o \to k_z^{AVE}$ as the radius approaches the infinitesimal case $a \to 0$. Figure 5.9 indicates that once the conductor comes in contact with the interface, the effect of the radius is small and thus a good approximation for any geometry that touches the interface is the mean-square average value. The results from figure 5.5, for the specific radius $a = 0.08m$ as $\Delta \to 0$, is also included as the dashed curve.

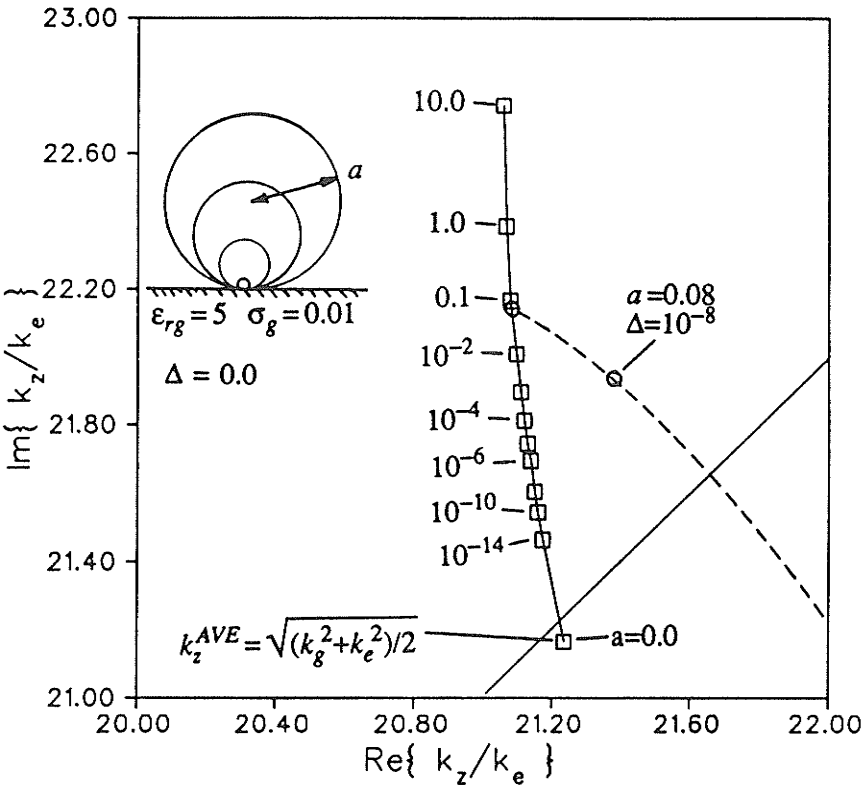

Figure 5.9: Zero-order mode propagation constant k_z^o/k_e for a conductor lying on the interface Δ=0 for various radii a. The dashed curve indicates the results for the varying height case of figure 5.5.

Figure 5.10 gives the zero-order mode fields for a circular conductor of radius $a=0.08m$ driven by a current of unit strength ($I_o^o=1$). The magnitude of the $\hat{z}$ component of the electric field along the interface $|E_{ez}(y=0)|$ is determined for various conductor heights. The fields are calculated using the Green's function (5.13). Results are given when an arbitrary current distribution is allowed (solid curves), as well as for the thin-wire approximation (dashed curves). It is observed that the thin-wire approximation is acceptable for calculating the fields even when $\Delta/a < 1$ as long as the observation point is not near the conductor (the exact value for the propagation constant must be used).

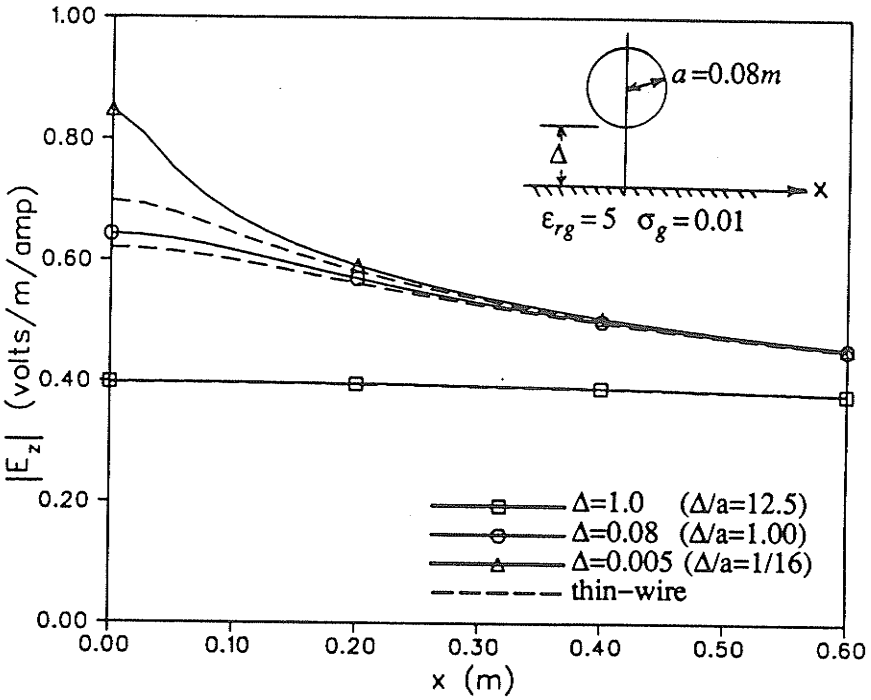

Figure 5.10: Electric field $|E_z(y=0)|$ at the interface for various conductor heights.

Lastly, Figures 5.11 and 5.12 examine the propagation constant and current distribution as a function of frequency for a conductor of radius $a=0.08m$ and height $\Delta=0.12m$ ($\Delta/a = 1.5$). The results determined using the thin-wire and quasi-TEM approximations are also given in figure 5.11. Over the portion of the frequency spectrum $f=10^6 \rightarrow 10^8 Hz$, the ground medium changes from behaving as a good conductor ($f=10^6$: $|n|=13.7 \approx \sqrt{\sigma_g/\omega\varepsilon_0}=12.8$) to behaving as a dielectric ($f=10^8$: $|n|=2.3 \approx \sqrt{\varepsilon_{rg}}=2.24$). Thus, even though the condition $|h,a| \ll \lambda_e$ holds, the quasi-TEM approximation is no longer valid past about $1MHz$ due to the condition $|n| \gg 1$ failing. The error in the thin-wire approximation remains relatively constant throughout the whole frequency range since $\Delta/a > 1$ is satisfied. Figure 5.12 shows there is not a large variation in the calculated current distribution as a function of frequency.

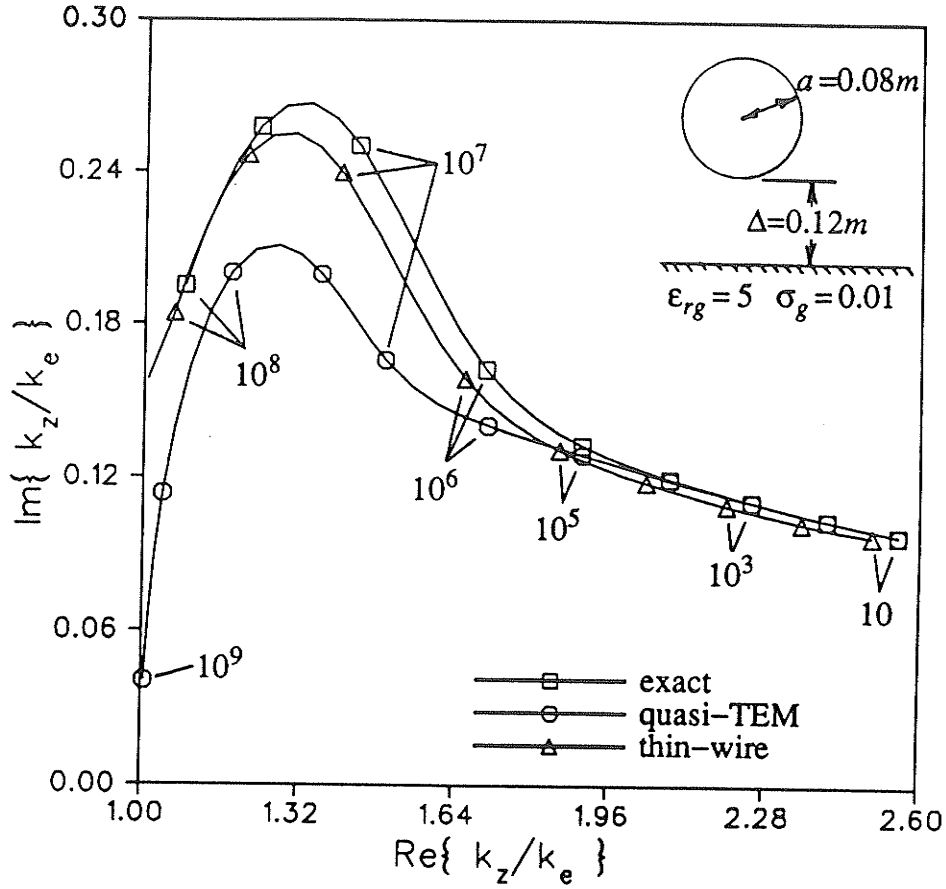

Figure 5.11: Propagation constant k_z^o/k_e as a function of frequency using the exact, quasi-TEM and thin-wire formulations.

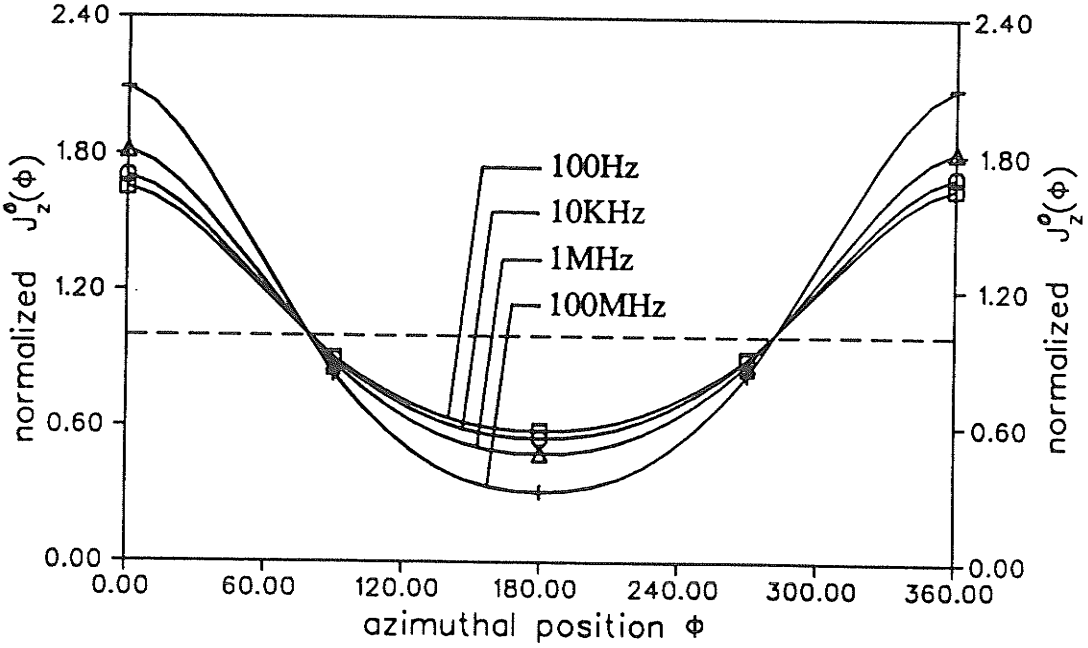

Figure 5.12: Azimuthal current distribution as a function of frequency.

5.4. FOURIER EXPANSION OF THE CURRENT DISTRIBUTION

In the previous sections, the unknown current distribution around the conductor was expanded in terms of a pulse function basis (5.6). In this section, a cylindrical Fourier expansion $\cos n\phi$ will be used as an alternative basis to represent the current distribution on circular conductors. The zero-order axial and first-order axial and azimuthal Fourier components were formulated by Pogorzelski [PogoF2] to investigate the effect of the interface on the propagation constant and current distribution of a circular wire above a lossy half-space. Note that the zero-order component $n=0$ is the thin-wire approximation derived in 5.2 and thoroughly examined in chapter 3. The choice of a Fourier basis is more appropriate than a pulse function basis for *circular* conductors since the primary fields will be orthogonal in the Fourier case. Thus, the only coupling between the expansion modes will be due to the presence of the interface (if the interface were not present, the interaction matrix (5.9) would be diagonal). As well, an analytical solution for the interaction matrix elements can be derived using addition theorems for cylindrical functions, whereas an integration was required for the pulse function basis (5.10). These advantages are lost however, when general (non-circular) conductor geometries are considered, and a pulse function or some other discrete basis is more suitable.

A solution to the mode equation (5.4) can be determined numerically by expanding the unknown current distribution for the pth mode, as shown in figure 5.13, using a Fourier basis defined as

$$J_z^p(\bar{\rho}) = \sum_{n=1}^{N} I_n^p \Psi_n(\bar{\rho}) \quad , \quad \Psi_n(\bar{\rho}) = \begin{cases} \dfrac{\cos n\phi}{2\pi a} & , |\,\bar{\rho}-\bar{\rho}_w\,| = a \\ 0 & , \text{otherwise} \end{cases} \tag{5.27}$$

where $\bar{\rho}_w = (0,h)$ is the location of the conductor center, a is its radius, and I_n^p is the total current for the nth Fourier component, for the pth mode. Note that the position vector $\bar{\rho}$ can be defined as a function $\bar{\rho}=(r,\phi)$. The procedure for solving for the unknown expansion coefficients is the same as that used in the previous section (5.8). In the solution used here, the testing basis is chosen to be the same as the expansion basis $w_m(\bar{\rho}) = \Psi_m(\bar{\rho})$ such that the resulting set of linear equations is formed as

$$[Z(k_z=k_z^p)][I^p] = 0 \quad ; p=1,2,\ldots,P \tag{5.28}$$

$$\begin{aligned} Z_{mn}(k_z) &= -Z_{mn}^e(k_z) = -<L\{\Psi_n(\bar{\rho})\}, \Psi_m(\bar{\rho})> \\ &= -\frac{1}{2\pi a}\int_C \cos m\phi \, \frac{1}{2\pi a}\int_C G_{ezzn}(\bar{\rho},\bar{\rho}',k_z)\cos n\phi' \, d\bar{\rho}' \, d\bar{\rho} \end{aligned} \tag{5.29}$$

where the contour C is the generating curve for the circular conductor and $G_{ezzn}(\bar{\rho},\bar{\rho}',k_z)$ is the Green's function for the nth-order two-dimensional electric multipole over a lossy half-space. As in the previous section, a perfectly conducting circular conductor will be assumed.

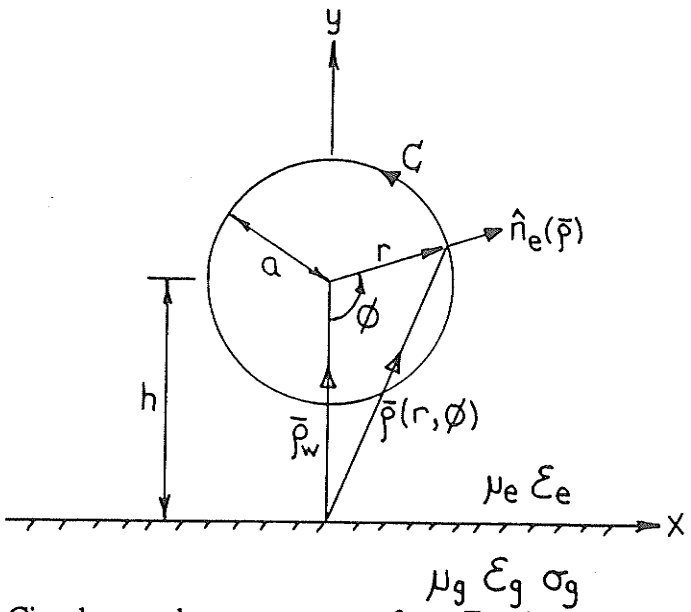

Figure 5.13: Circular conductor geometry for a Fourier expansion-Fourier testing MOM solution.

The Green's function for the nth-order electric multipole can be derived by determining the fields due to the delta function line source $I_n^p \cos n\phi$. Assuming an axial dependence of the form $e^{+jk_z z}$, the fields are deduced in the same manner as in section 5.1, by solving the two-dimensional wave equation in each of the air and earth half-spaces. These can be determined in terms of potential vectors for each of the nth-order multipoles as

$$\begin{aligned} [\nabla^2 - (k_z^2 - k_e^2)]\,\bar{\Pi}_n^e &= \frac{-j\omega\mu_e}{k_e^2} I_n^p \cos n\phi'\,\delta(\bar{\rho}-\bar{\rho}')\hat{z} \quad ; y>0 \\ [\nabla^2 - (k_z^2 - k_g^2)]\,\bar{\Pi}_n^g &= 0 \quad ; y<0 \end{aligned} \tag{5.30}$$

where $\bar{\Pi}_n^e$ and $\bar{\Pi}_n^g$ are the two-dimensional Hertz vector potentials in the air and earth regions, respectively. Here $k_e = \sqrt{\omega^2\mu_e\varepsilon_e}$ is the propagation constant in the air medium and $k_g = \sqrt{\omega^2\mu_g\varepsilon_g + j\omega\mu_g\sigma_g}$ is the propagation constant in the ground medium. $\bar{\rho}'$ is the location of the delta function line source. The associated fields, and thus the Green's functions required for the matrix elements (5.29), are determined from

$$\bar{E}_{en} = \nabla\nabla\cdot\bar{\Pi}_n^e + k_e^2\bar{\Pi}_n^e \;,\; \bar{H}_{en} = \frac{k_e^2}{j\omega\mu_e}\nabla\times\bar{\Pi}_n^e \;,\; G_{ezzn}(\bar{\rho},\bar{\rho}',k_z) = \bar{E}_{en}(\bar{\rho})\cdot\hat{z} \tag{5.31}$$

where the fields will have the same nth-order ϕ dependence as the potential functions. Only the $\cos n\phi$ electric multipoles are considered since they are even functions with respect to the interface ($x=x'$ plane). There will not be a perturbation in the azimuthal current distribution due to the $\sin n\phi$ multipoles since they are odd functions with respect to the interface.

In the rest of the derivation, only the n=0,1-order multipole potentials will be considered since they are easily derived. Noting that the solution to the homogeneous part of the upper half-space wave equation in (5.30) has the integral form

$$F_n(x,y,k_z) = F_n(r,\phi,k_z) = \int_{-\infty}^{\infty} f_n(k_x,k_z)e^{-\sqrt{k_x^2+k_z^2+k_e^2}\,|\,y-y'\,|\,+jk_x(x-x')}dk_x \qquad (5.32)$$

then it is seen that functions of the type $\partial F_n/\partial y$ will also be homogeneous solutions of (5.30). Specifying $r=\sqrt{(x-x')^2+(y-y')^2}$, $(y-y')/r=-\cos\phi$, the zero-order multipole potential can then be related to the first-order multipole potential as [PogoF2]

$$\overline{\Pi}_1^e = -\frac{I_1^p}{I_0^p}\frac{1}{\tau_e}\frac{\partial}{\partial y}\overline{\Pi}_0^e \qquad (5.33)$$

Since the zero- and first-order fields (5.31) will also be related in the same manner, the boundary conditions at the interface will be satisfied for $\overline{\Pi}_1^e$, $\overline{\Pi}_1^g$ if they are satisfied for $\overline{\Pi}_0^e$, $\overline{\Pi}_0^g$. The Green's function $G_{ezz0}(\overline{\rho},\overline{\rho}',k_z)$ for the zero-order multipole was derived in appendix A and also in section 5.2. Thus, the n=0,1 Green's functions are given from (5.31,5.33) as

$$G_{ezz0}(\overline{\rho},\overline{\rho}',k_z) = \frac{-j\omega\mu_e}{2\pi k_e^2}\Big[\tau_e^2[K_0(\tau_e\,|\,\overline{\rho}_D\,|\,) - K_0(\tau_e\,|\,\overline{\rho}_D^*\,|\,)] - k_e^2\mathbf{J}(\tau_e,\overline{\rho}_D^*) + k_z^2\mathbf{G}(\tau_e,\overline{\rho}_D^*)\Big] \qquad (5.34)$$

$$G_{ezz1}(\overline{\rho},\overline{\rho}',k_z) = \frac{-j\omega\mu_e}{2\pi k_e^2}\frac{-1}{\tau_e}\frac{\partial}{\partial y}\Big[\tau_e^2[K_0(\tau_e\,|\,\overline{\rho}_D\,|\,) - K_0(\tau_e\,|\,\overline{\rho}_D^*\,|\,)] - k_e^2\mathbf{J}(\tau_e,\overline{\rho}_D^*) + k_z^2\mathbf{G}(\tau_e,\overline{\rho}_D^*)\Big] \qquad (5.35)$$

$$|\,\overline{\rho}_D\,| = \sqrt{(x-x')^2+(y-y')^2}\quad,\quad |\,\overline{\rho}_D^*\,| = \sqrt{(x-x')^2+(y+y')^2}$$

with $\mathbf{J}(\tau_e,\overline{\rho})$ and $\mathbf{G}(\tau_e,\overline{\rho})$ being defined in (5.14).

The first integration over C in (5.29) determines the average value of the nth-order Green's functions and can be solved using the addition theorem for cylindrical functions [AbroC19] as

$$\begin{aligned}\frac{1}{2\pi a}\int_C G_{ezzn}(\overline{\rho},\overline{\rho}',k_z)\cos n\phi'\,d\overline{\rho}' &= G_{ezzn}(\overline{\rho},\overline{\rho}_w,k_z)\frac{1}{2\pi a}\int_C\Big[I_0(\tau_e a)+2\sum_{k=1}^{\infty}I_k(\tau_e a)\cos k\phi'\Big]\cos n\phi'\,d\overline{\rho}' \\ &= G_{ezzn}(\overline{\rho},\overline{\rho}_w,k_z)I_n(\tau_e a) \qquad (5.36)\end{aligned}$$

where $I_n(z)$ is the modified Bessel function of order n. The remaining integration in

(5.29) can be evaluated in two parts, one for the primary components $F_n(\bar{\rho}_D)$, and one for the secondary reflected components $F_n(\bar{\rho}_D^*)$, as shown in figure 5.14. The primary components are easily evaluated since they have a simple $\cos n\phi$ variation such that

$$\frac{1}{2\pi a}\int_C K_n(\tau_e \mid \bar{\rho}_D \mid)\cos n\phi \cos m\phi \; d\bar{\rho} \;=\; \begin{cases} K_0(\tau_e a) & , m=n=0 \\ \frac{1}{2}K_1(\tau_e a) & , m=n=1 \\ 0 & , m\neq n \end{cases} \tag{5.37}$$

where the primary fields have been represented in their modified Bessel function form. The integration of the secondary components, can be evaluated in their integral form as

$$\begin{aligned} &\frac{1}{2\pi a}\int_C F_n(\bar{\rho}_D^*)\cos m\phi \, d\bar{\rho} \\ &= \frac{1}{2\pi a}\int_C \int_{-\infty}^{\infty} f_n(k_x) e^{-U_e(h+y)+jk_x x}\, dk_x \cos m\phi \; d\bar{\rho} \\ &= \int_{-\infty}^{\infty} f_n(k_x) e^{-U_e 2h} \; \frac{1}{2\pi a}\int_0^{2\pi} e^{+U_e a\cos\phi + jk_x a\sin\phi}\cos m\phi \; a\, d\phi \; dk_x \end{aligned} \tag{5.38}$$

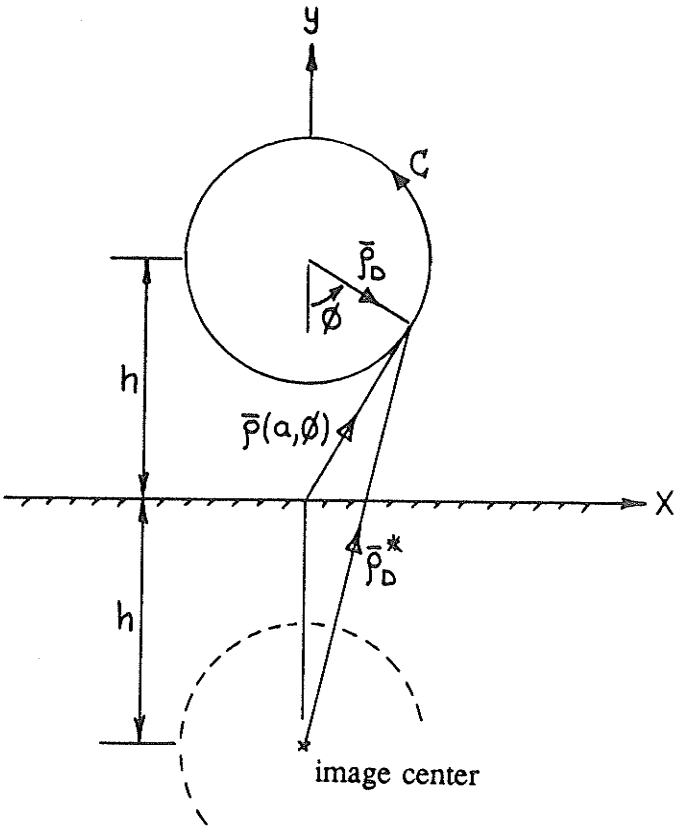

Figure 5.14: Integration coordinates for inner-product calculation.

Using the transform $k_x = -j\tau_e \sin\phi_0$, $U_e = \tau_e \cos\phi_0$ and again the addition theorem for cylindrical functions

$$\frac{1}{2\pi a}\int_C F_n(\bar{\rho}_D^*)\cos m\phi \, d\bar{\rho}$$

$$= \int_{-\infty}^{\infty} f_n(k_x) e^{-U_e 2h} \frac{1}{2\pi a}\int_0^{2\pi} e^{+\tau_e a\cos(\phi-\phi_0)}\cos m\phi \, a\,d\phi \, dk_x$$

$$= \int_{-\infty}^{\infty} f_n(k_x) e^{-U_e 2h} \frac{1}{2\pi a}\int_0^{2\pi} [I_0(\tau_e a) + 2\sum_{k=1}^{\infty} I_k(\tau_e a)\cos k(\phi-\phi_0)]\cos m\phi \, a\,d\phi \, dk_x$$

$$= \begin{cases} I_0(\tau_e a) F_n(2h\hat{y}) & , m = 0 \\ \int_{-\infty}^{\infty} f_n(k_x) e^{-U_e 2h} \frac{U_e}{\tau_e} I_1(\tau_e a)\,dk_x = I_1(\tau_e a)\frac{-1}{\tau_e}\frac{\partial}{\partial y} F_n(2h\hat{y}) & , m = 1 \end{cases} \quad (5.39)$$

where $\cos(\phi-\phi_0) = U_e/\tau_e \cos\phi$ since the $\sin\phi$ term is orthogonal. Thus, the interaction matrix elements of (5.29) can be deduced for the n=0,1 Fourier components as

$$[Z(k_z)][I^p] = -\begin{bmatrix} Z_{00}^e(k_z) & Z_{01}^e(k_z) \\ Z_{10}^e(k_z) & Z_{11}^e(k_z) \end{bmatrix}\begin{bmatrix} I_0^p \\ I_1^p \end{bmatrix} = 0 \quad (5.40)$$

$$Z_{00}^e(k_z) = \frac{-j\omega\mu_e}{2\pi k_e^2} I_0(\tau_e a)\left[\tau_e^2 K_0(\tau_e a) - I_0(\tau_e a)\mathrm{B}(\tau_e, 2h\hat{y})\right]$$

$$Z_{01}^e(k_z) = \frac{-j\omega\mu_e}{2\pi k_e^2} I_1(\tau_e a)\left[I_0(\tau_e a)\frac{1}{\tau_e}\frac{\partial}{\partial y}\mathrm{B}(\tau_e, 2h\hat{y})\right]$$

$$Z_{10}^e(k_z) = \frac{-j\omega\mu_e}{2\pi k_e^2} I_0(\tau_e a)\left[I_1(\tau_e a)\frac{1}{\tau_e}\frac{\partial}{\partial y}\mathrm{B}(\tau_e, 2h\hat{y})\right] \quad (5.41)$$

$$Z_{11}^e(k_z) = \frac{-j\omega\mu_e}{2\pi k_e^2} I_1(\tau_e a)\left[\frac{-\tau_e}{2}\frac{\partial}{\partial y}K_0(\tau_e a) - I_1(\tau_e a)\frac{1}{\tau_e^2}\frac{\partial^2}{\partial y^2}\mathrm{B}(\tau_e, 2h\hat{y})\right]$$

$$\mathbf{B}(\tau_e, \bar{\rho}^*) = \tau_e^2 K_0(\tau_e \mid \bar{\rho}^* \mid) + \mathbf{J}(\tau_e, \bar{\rho}^*) - \mathbf{G}(\tau_e, \bar{\rho}^*)$$

where the following relations can be used to simplify (5.41)

$$\frac{\partial}{\partial y}K_0(\tau_e \mid \bar{\rho}^* = 2h\hat{y} \mid) = -\tau_e K_1(\tau_e 2h)$$

$$\frac{\partial^2}{\partial y^2}K_0(\tau_e \mid \bar{\rho}^* = 2h\hat{y} \mid) = \frac{\tau_e}{2h}K_1(\tau_e 2h) + \tau_e^2 K_0(\tau_e 2h) \quad (5.42)$$

The solutions of the mode equation $|Z(k_z^p)| = 0$ yield the propagation constants k_z^p ; $p = 0,1,2,...P$. The current distribution for each mode can be determined from the

eigenvectors of (5.40) and using (5.27) as

$$\frac{I_1^p}{I_0^p} = -\frac{Z_{00}^e(k_z^p)}{Z_{01}^e(k_z^p)} = -\frac{Z_{10}^e(k_z^p)}{Z_{11}^e(k_z^p)} \tag{5.43}$$

$$J_z^p(\overline{\rho}) = J_z^p(r=a,\phi) = \frac{I_0^p}{2\pi a} + \frac{I_1^p}{2\pi a}\cos\phi \tag{5.44}$$

where the total axial current flowing in the conductor is given by the I_0^p component. The first term of the Fourier expansion is simply the thin-wire approximation derived in section 5.2.

In the previous section, a study of the normalized common-mode propagation constant k_z^o/k_e was made for a circular conductor above a lossy interface. Figure 5.9 compared the exact results to those obtained using the thin-wire approximation. For this case, the conductor had a fixed radius of $a=0.08m$ with the height h above the interface varied ($\Delta = h-a$) as referred to figure 5.3. The ground was characterized by $\mu_{rg}=1.0$, $\varepsilon_{rg}=5.0$, $\sigma_g=0.01$ and an operating frequency of $100KHz$ was chosen. Again

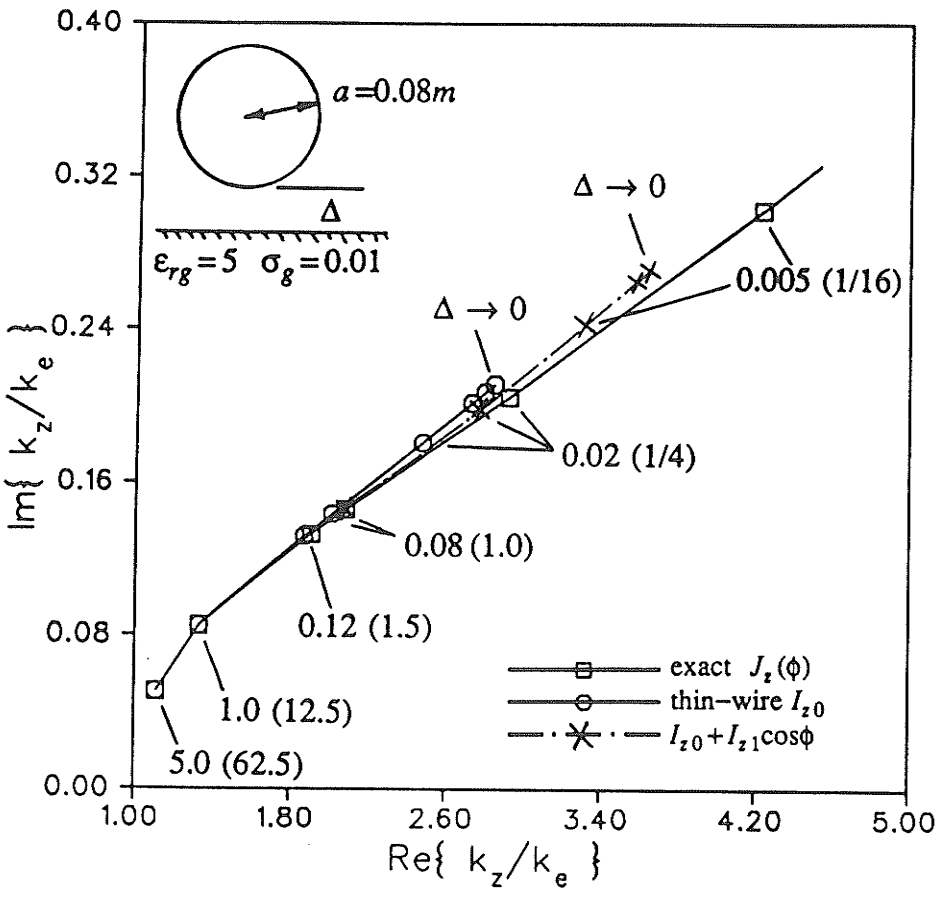

Figure 5.15: Comparison of k_z^o/k_e using the exact, thin-wire and first-order Fourier formulations for various conductor heights Δ.

using this case, figure 5.15 compares these results with the propagation constant k_z^o/k_e obtained when the zero- and first-order Fourier components are used $I_0^o + I_1^o \cos\phi$ (eqns. (5.40-5.44)). The use of the additional Fourier component increases the range of validity of the thin-wire result to approximately $\Delta/a > 1/4$. Figure 5.16 gives a comparison of the corresponding normalized current distribution $J_z^o(\phi)$ around the circumference of the conductor. For heights $\Delta/a > 1$, the deviation in the current behaves as $\cos\phi$, however, for smaller heights higher order Fourier terms are required for an accurate representation.

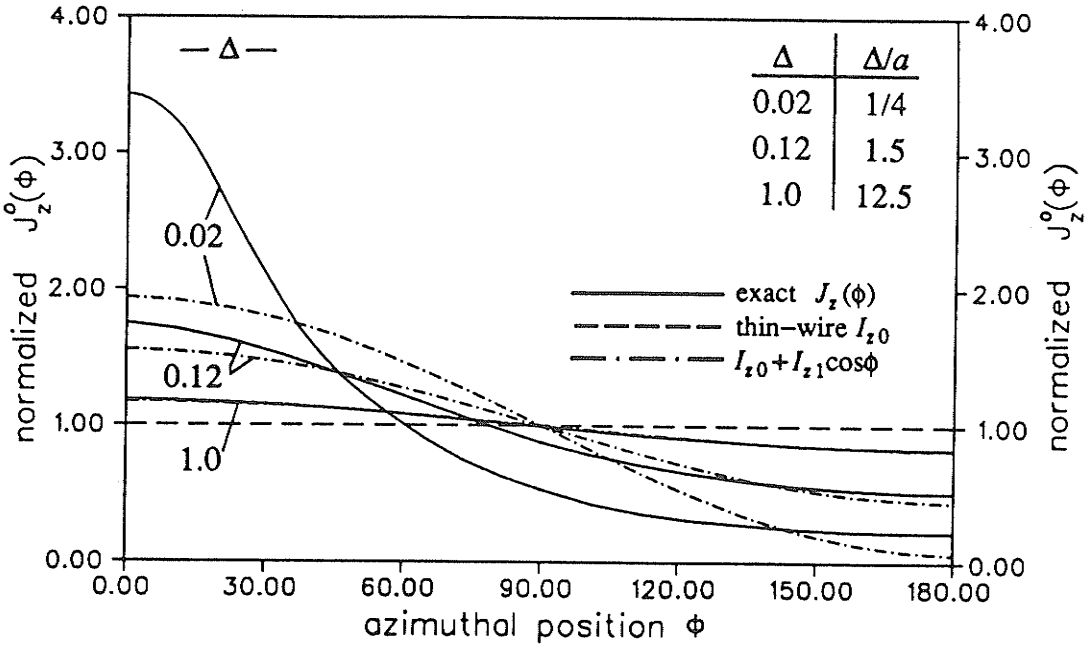

Figure 5.16: Comparison of $J_z^o(\phi)$ using the exact, thin-wire and first-order Fourier formulations for various conductor heights Δ.

5.5. DISCUSSION

In this chapter, the discrete modal properties, propagation constant and current distribution, supported by arbitrary shaped conductors located near or at a lossy interface were studied. The formulation presented allowed for a non-uniform azimuthal, but axially directed, current distribution. Although the formulation is applicable to any sized conductor and to arbitrary earth electrical properties, numerical results were determined for cases where the overall dimensions of the conductor were smaller than the free space wavelength and when the earth behaved as a good conductor. As well, most of the results presented concentrated on the characterization of the zero-order mode propagation constant k_z^o since this mode is the one most effected by the presence of the interface. The results indicated that the effect of the lossy earth was *much*

more pronounced on the current distribution than on the propagation constant (a 20% deviation in the current distribution was observed for $\Delta/a=12.5$, a similar error in k_z^o occurring only when $\Delta/a<1$). The thin-wire approximation was found to be valid only under the condition $\Delta/a>1$, and the inclusion of the first-order as well as zero-order Fourier components only improves the validity to $\Delta/a>1/4$. In general, the Fourier expansion basis requires many terms to adequately represent the current distribution when the conductor is near the interface, a pulse function or other discrete sectional basis being more appropriate. The quasi-TEM approximation was found to be adequate for even small heights. A significant error in the quasi-TEM results occur only when the conductor becomes *very* close to the interface $\Delta/a<1/10$ (as long as the TEM conditions that all dimensions are much less than the free space wavelength and the earth behaves as a conductor still apply). A good approximation to the propagation constant when the conductor is *in contact* with the interface is the mean-square average value $k_z^o \simeq k_z^{AVE}$. The conductor radius has little effect in this situation, and was shown to approach the average value k_z^{AVE} in the limit of a diminishing radius $a \rightarrow 0$ (even though the convergence to this limit is *extremely* slow). The resulting fields for the zero-order mode are accurately predicted by the thin-wire approximation for all conductor heights as long as the observation point is not near the conductor $|\bar{\rho}| > 2a$. This observation is only valid if the correct value for the propagation constant k_z^o is used, as calculated by the complete expansion basis for the current distribution. Even though the exact calculation of the propagation constant may be time consuming, the use of the thin-wire approximation for calculating the fields external to the region of the conductor is very efficient.

Even though the presented moment method solution, using a pulse function basis, can be used to model arbitrary shaped conductors, the previous sections considered only circular structures. The circular configuration was used since it has previously been the most extensively studied geometry, and can be applied to many practical applications. As well, an analytical solution to the thin-wire assumption (and first-order Fourier mode) can be obtained for the circular geometry. To briefly examine situations when the conductor is *not* of a circular configuration, the case of a perfectly conducting rectangular strip located over the lossy half-space will be considered. Strips of various width to height ratios (w/h) will be examined, but all geometries will maintain the same total circumference ($2h+2w=0.32m$) and the same distance from the interface to the bottom of the strip ($\Delta = 0.08m$). As in previous cases studied, the earth will be characterized by the electrical properties $\mu_{rg}=1.0$, $\varepsilon_{rg}=5.0$, $\sigma_g=0.01$, and an operating frequency of $100KHz$ is chosen. Figure 5.17 gives the normalized zero-order mode propagation constants k_z^o and figure 5.18 gives the corresponding normalized current distributions $J_z^o(\bar{\rho})$ for four width to height ratios $w/h=1,3,7,15$ ($[w,h]=[0.08,0.08],[0.12,0.04],[0.14,0.02],[0.15,0.01]$). Figure 5.17 indicates that the shape of the conductor has only a small effect on the propagation constant as long as the distance between the bottom of the conductor and the interface remains

constant. This is reasonable since the conductor size is much less than the free space wavelength. Also as expected, due to the skin effect, the current distribution is maximum near the corners of the strip. As observed for circular conductors, the presence of the interface causes the current to be concentrated near the bottom of the strip.

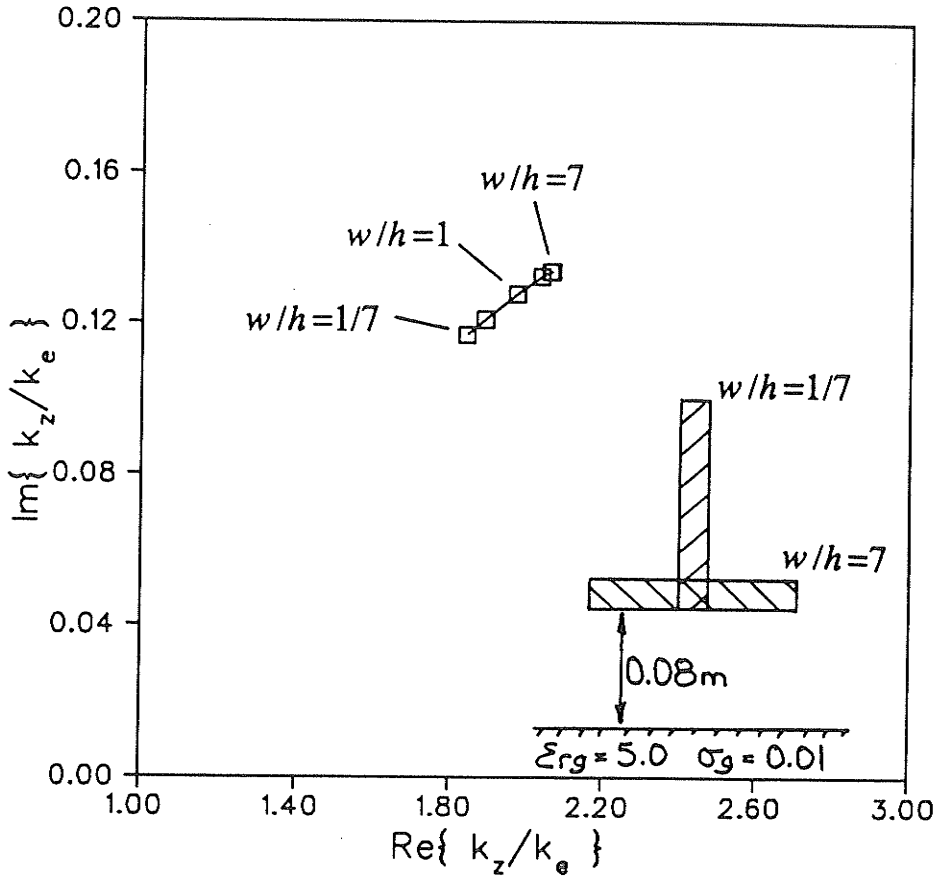

Figure 5.17: Zero-order mode propagation constant k_z^o/k_e for a strip with various width/height ratios.

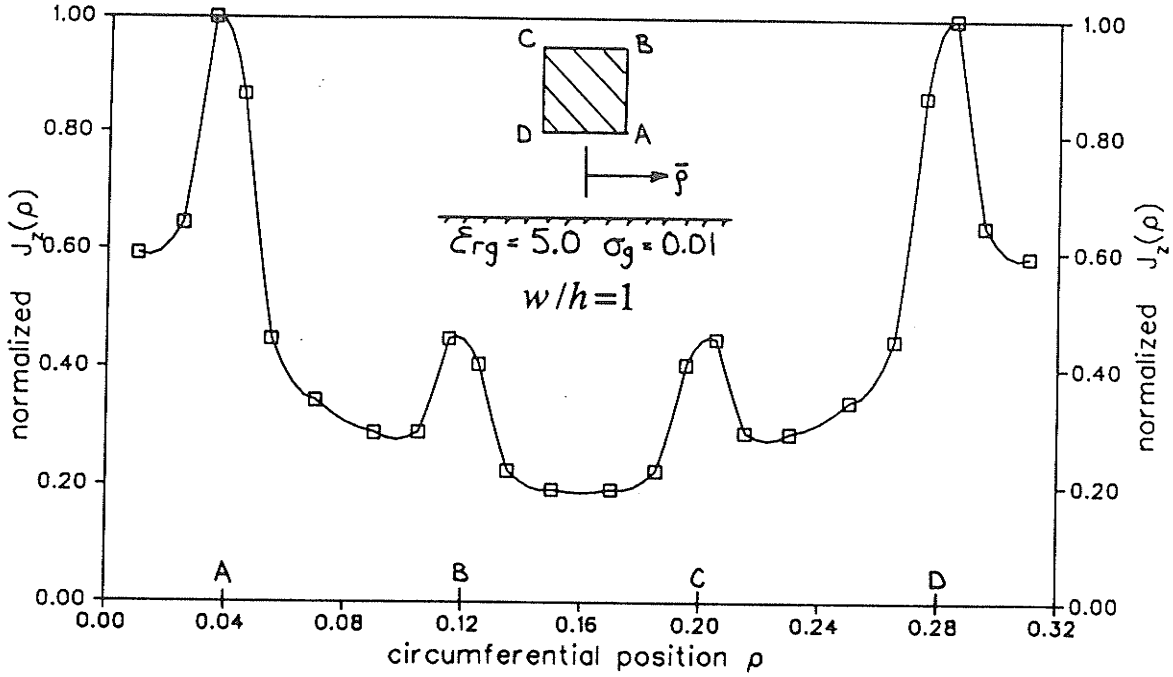

Figure 5.18a: Current distribution J_z^o on a strip with w/h=1.

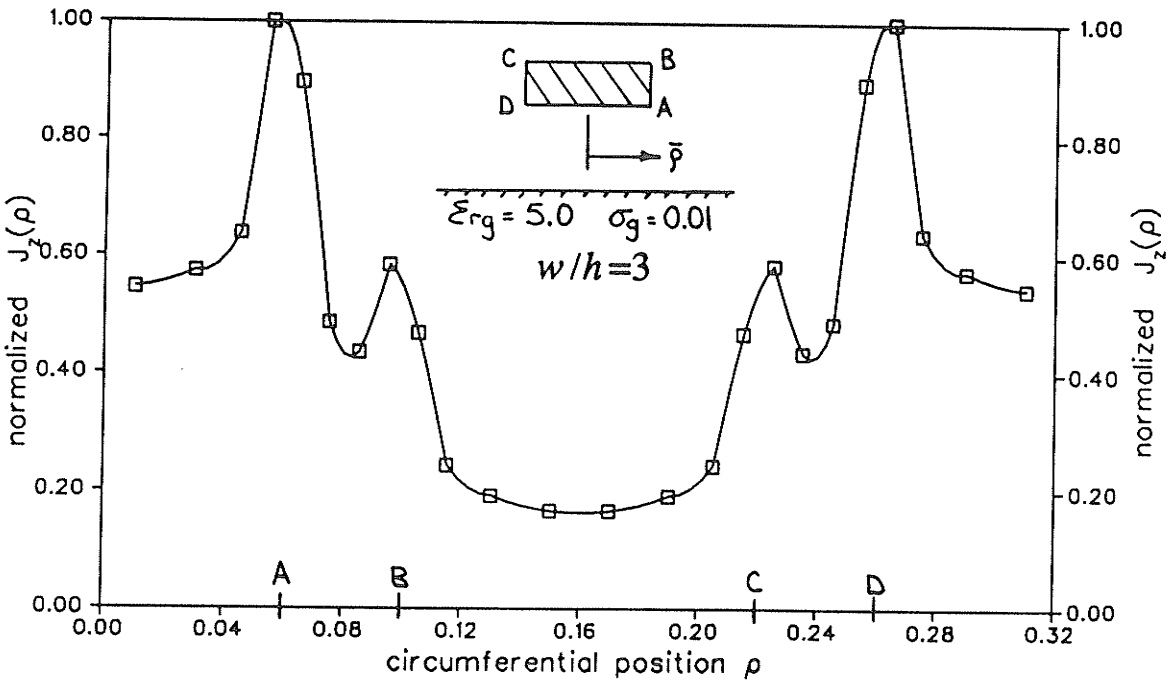

Figure 5.18b: Current distribution J_z^o on a strip with w/h=3.

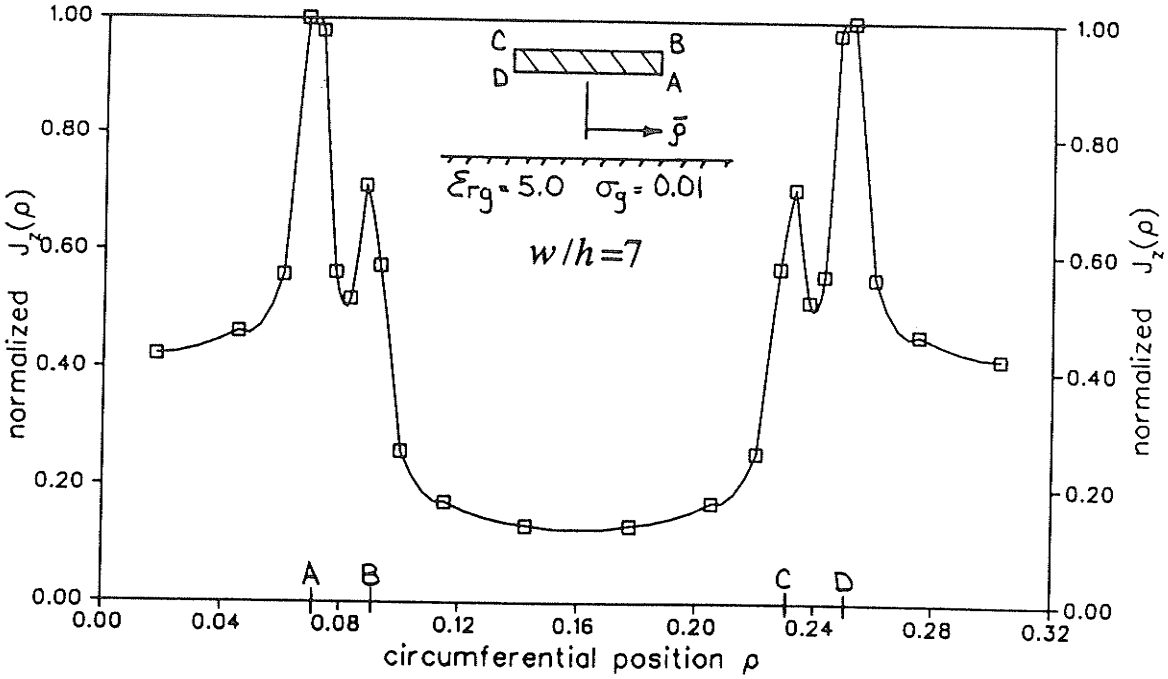

Figure 5.18c: Current distribution J_z^o on a strip with w/h=7.

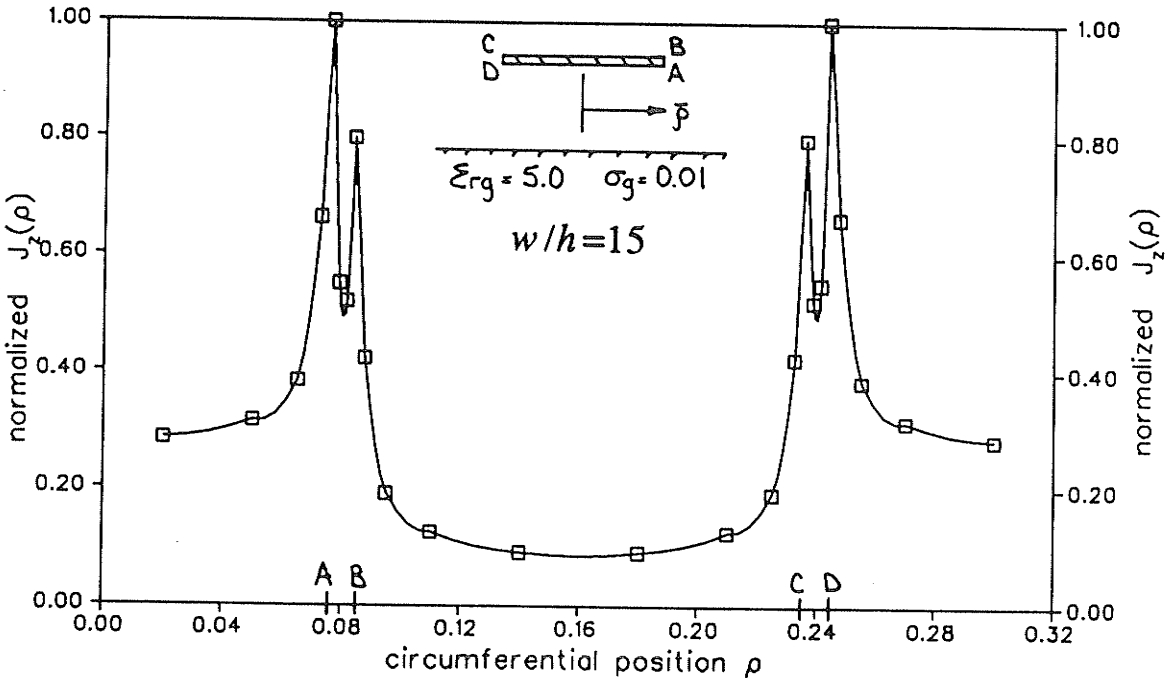

Figure 5.18d: Current distribution J_z^o on a strip with w/h=15.

Chapter 6
Conclusions and Suggestions for Further Study

In this thesis a general framework for the analysis of guided wave structures has been presented. A theory was developed for both open and closed cylindrical structures through a hybrid Green's function-integral equation approach, which was subsequently solved using a spectral domain technique in the infinite axial dimension and a moment method in the bounded transverse dimension. Specific attention was paid to the use of only the discrete mode contributions as an approximation to the complete field solution. In order to characterize the properties of the discrete modes, a method of solving for the propagation constants and a new definition for the characteristic impedances of a general cylindrical structure were presented. The formulation of the case when the guided wave structure is embedded in a stratified supporting medium was then considered, and the wave properties characteristic to this geometry were examined. It was shown that the cylindrical/planar geometry supported a continuous spectrum of radiation modes propagating into the uppermost and lowermost half-spaces, a continuous spectrum of surface waves trapped by the layered media, and a set of discrete modes which were guided by the cylindrical structure.

Examples of various special cases which could be modeled using the cylindrical/planar geometry were examined in chapters three, four and five of the thesis. The thin-wire approximation was used to examine the excitation of and wave propagation along multiple conductor transmission lines located over a lossy earth. Numerical results were presented for the discrete mode propagation constants and for the currents excited by external dipole and delta function voltage sources. It was shown that an N-conductor system can support more than N discrete modes, these being in addition to the traditional quasi-TEM type modes. The additional guided modes were identified as fast-wave modes with attenuation constants that are usually less than the quasi-TEM type modes. The numerical results demonstrated that the quasi-TEM approximation is valid under the conditions that all structural dimensions are much less than the free space wavelength ($<\lambda_e/10$), and that the refractive index at the interface is large ($|n|>10$). The validity of using the transmission line approximation in the near field and the saddle point contribution on the far field was examined by considering the induced currents due to a vertical electric dipole source located in the upper half-space. As expected, the discrete mode contributions dominated the

currents when the transverse distance from the source to the transmission line was much less than the free space wavelength ($<\lambda_e/20$), and the saddle point contribution dominated when the transverse distance was greater than the transverse component of the propagation constant ($>3\lambda_{\rho e}$). The formulation of the multiple conductor geometry and the validity of the various approximation techniques is important for application in many electromagnetic coupling and interference problems.

For a transmission line analysis of guided wave structures, methods for characterizing the discrete mode properties, propagation constants and characteristic impedances, must be defined. The solution of the propagation constants is straight forward as there is a direct physical relationship with the electromagnetic quantities. The definition of the characteristic impedances, however, is arbitrary since there is no direct relationship between the electromagnetic quantities and the circuit quantities modeling the structure except in the TEM limit. In light of this, an alternative definition for the characteristic impedance of guided wave structures was proposed in chapter four. The definition followed directly from the hybrid Green's function-integral equation solution of the structure and collapsed to the TEM result in the quasi-static limit. As an example to study the proposed definition, the case of a thin-wire conductor located over a lossy half-space was addressed.

In the past almost all theories have treated the problem of a conductor over a lossy earth assuming a thin-wire approximation to model the conductor. In chapter five, the discrete modal properties, propagation constants and current distributions, supported by arbitrary shaped conductors located near or at a lossy interface were studied. An exact formulation of the problem, which is valid even when the conductor is in contact with the interface, was presented. Results for the case of a circular conductor located over an earth having typical electrical properties were given and a comparison was made to the various other approximation methods which have been utilized throughout the literature. The results indicated that the thin-wire approximation is valid only when the distance from the interface to the conductor is greater than the dimensions of the conductor. As long as the traditional TEM conditions that all dimensions are much less than the free space wavelength and the earth behaves as a good conductor hold, the quasi-TEM approximation can be used for small heights, with a significant error occurring only when the conductor becomes *very* close to the interface. The use of a Fourier expansion basis was shown to require many terms to adequately represent the current distribution when the conductor is near the interface, a pulse function or other discrete sectional basis being more appropriate. The use of the thin-wire approximation for calculating the fields external to the region of the conductor was shown to be very efficient as long as the observation point is not near the conductor. Lastly, under most conditions a good approximation to the propagation constant when the conductor is *in contact* with the interface is the mean-square average value $k_z^o \simeq k_z^{AVE}$.

The derivation of the Green's functions for sources which are embedded in a stratified media geometry was presented in appendix A, with the case of a single homogeneous half-space being emphasised. Appendix B presented various techniques for the evaluation of these Green's functions, commonly known as Sommerfeld integrals, these including some new closed form expressions for the lossy half-space case. A technique for the numerical integration of certain Sommerfeld type integrals was also presented, the proposed method having the advantage that it is capable of integrating these integrals in the far field region.

6.1. SUGGESTIONS FOR FURTHER STUDY

Even though the numerical results presented in the thesis concentrated almost solely on structures over a lossy half-space, the formulations presented in chapter two attempted to encompass the problem of guided wave structures in general. Thus, there remains many opportunities to apply these formulations to more complex geometries. As well, the studies involving structures over a lossy half-space have shown some interesting properties which may be exploited with further effort. They also have lead to many additional problems which should be investigated.

1. The study of thin-wire structures over a lossy half-space showed that it was possible to find discrete propagating modes which had attenuations much less than the traditional quasi-TEM type modes. It has been suggested that the utilization of these modes for leaky wave antennas or low loss transmission lines may be promising [Olsen2]. As discussed in chapter four, however, the excitation efficiency of these additional modes is extremely low for typical sources (the characteristic/input impedances are very large). An examination of possible sources which can adequately excite these modes may be fruitful.
2. In chapter three, the discrete mode and saddle point contributions to the current induced on a transmission line due to a dipole source were determined. In the far field, it was shown that the surface wave contributions to the currents were not negligible near grazing angles of incidence with respect to the interface. The surface wave component can be extracted by considering the pole/branch cut contributions in the steepest descent evaluation as discussed in section 3.3.4. The inclusion of this extra term is important in radio transmission and interference problems, where both the source and the transmission line are usually located near the surface of the earth.
3. In the results presented in chapter four, it was shown that the characteristic impedance of one of the discrete modes was very small over a certain band of frequencies, for a given transmission line geometry. Coupling devices may be

designed to take advantage of this, since the excitation efficiency of the mode in this frequency band is very high.

4. Chapter four proposed an alternative definition for the characteristic impedances of the discrete modes supported by a guided wave structure. The special case of a thin-wire transmission line located over a lossy earth was considered as an example. Since much of the present controversy is in the proper definition of the characteristic impedance of microstrip structures, numerical results should be extended to examine this problem.

5. The study of arbitrary shaped conductors which could be located near or at an interface between two media in chapter five, considered only axially directed electric currents $J_z(\overline{\rho})$ on the structure. This assumption will only be valid for structures that are much smaller than the wavelength of the medium in which they are embedded. If large structures or excitation by TE sources are to be considered, the inclusion of a transverse current component $J_\rho(\overline{\rho})$ must also be incorporated. This additional complexity was addressed in the general formulation presented in chapter two. Both axial and transverse current components have been previously considered in the analysis of microstrip problems [Itoh, Fache].

6. The results of chapter five only considered the case of a conductor which could be located near or at the interface of two media, but must totally reside in only one of them. This work should be extended to examine the case of partially buried conductor geometries, which can be deduced from the formulation presented in chapter two. The results may be useful in the modeling of MMIC and optical waveguide structures.

7. Appendix B presented a numerical technique for the integration of some of the Sommerfeld type integrals occurring in layered media problems. Simpon's method with an exponential weighting function was used to evaluate the resulting kernel. The use of a more advanced integration method, such as a Gaussian quadrature technique again with an exponential weighting, would greatly improve the performance of the numerical evaluation.

References

1. **[Aboul-Atta]** O. Aboul-Atta, L. Shafai and M.Z. Tarnawecky, "On the Theory of Infinite Line Above Ground," Technical Rep. TR81-7, Dept. of Elect. Eng., Univ. of Manitoba, 1981.
2. **[Abramowitz]** M. Abramowitz and I. Stegun, *Handbook of Mathematical Functions*, National Bureau of Standards, 1964.
3. **[Agrest]** M.M. Agrest and M.S. Maksimov, *Theory of Incomplete Cylindrical Functions and Their Applications*, Springer, New York, pp. 21-75, 1971.
4. **[Alexopoulos1]** N.G. Alexopoulos and I.E. Rana, "Mutual Impedance Computation Between Printed Dipoles," IEEE Trans. Antennas Prop., vol. AP-29, pp. 106-111, 1981.
5. **[Alexopoulos2]** N.G. Alexopoulos, "Integrated-Circuit Structures on Anisotropic Substrates," (review paper) IEEE Trans. Microwave Theory Tech., vol. MTT-33, pp. 847-881, 1985.
6. **[Bagby]** J.S. Bagby and N.P. Nyquist, "Dyadic Green's Functions for Integrated Electronic and Optical Circuits," IEEE Trans. Microwave Theory Tech., vol. MTT-35, pp. 206-210, 1987.
7. **[Bahl]** I.J. Bahl and R. Garg, "Simple and Accurate Formulas for Microstrip with Finite Strip Thickness," Proc. of IEEE, vol. 65, pp. 1611-1612, 1977.
8. **[Bannister1]** P.R. Bannister, "Electric and Magnetic Fields Near a Long Horizontal Line Source Above the Ground," Radio Science, vol. 3, pp. 203-204, 1968.
9. **[Bannister2]** P.R. Bannister, "On the Impedance of a Finite-Length Horizontal Wire Located Near the Earth's Surface," IEEE Trans. Antennas Prop., vol. AP-24, pp. 244-245, 1976.
10. **[Bannister3]** P.R. Bannister, "Extension of Quasi-Static Range Finitely Conducting Earth-Image Theory Techniques to Other Ranges," IEEE Trans. Antennas Prop., vol. AP-26, pp. 507-508, 1978.
11. **[Bannister4]** P.R. Bannister, "Summary of Image Theory Expressions for the Quasi-Static Fields of Antennas at or Above the Earth's Surface," Proc. of IEEE, vol. 67, pp. 1001-1008, 1979.
12. **[Banos]** A. Banos, *Dipole Radiation in the Presence of a Conducting Half Space*, Pergamon Press, New York, 1966.

13. **[Bhartia]** P. Bhartia and P. Pramanick, "A New Microstrip Dispersion Model," IEEE Trans. Microwave Theory Tech., vol. MTT-32, pp. 1379-1384, 1984.

14. **[Brews1]** J.R. Brews, 'Transmission Line Models for Lossy Waveguide Interconnections in VLSI," IEEE Trans. Electron Devices, vol. ED-33, pp. 1356-1365, 1986.

15. **[Brews2]** J.R. Brews, "Characteristic Impedance of Microstrip Lines," IEEE Trans. Microwave Theory Tech., vol. MTT-35, pp. 30-34, 1987.

16. **[Bridges1]** G.E. Bridges and O. Aboul-Atta, "Accuracy of the Electromagnetic Transient in Overhead Transmission Lines," Electronics Letters, vol. 20, pp. 5-7, 1984.

17. **[Bridges2]** G. Bridges and O. Aboul-Atta, "Electromagnetic Wave Propagation Along Multiple Conductor Structures Above a Lossy Earth," Proc. ANTEM'86 Symp. on Antenna Tech. and Applied Electromagnetics, Winnipeg, Canada, Aug., 1986.

18. **[Bridges3]** G. Bridges, O. Aboul-Atta, L. Shafai, "Solution of Discrete Modes for Wave Propagation Along Multiple Conductor Structures Above a Dissipative Earth," Canadian Jour. of Physics, vol. 66, pp. 428-438, 1988.

19. **[Bridges4]** G.E. Bridges and L. Shafai, "Transient Plane Wave Coupling to Transmission Lines Above a Lossy Earth," Proc. IEEE-AP/URSI Intl. Symp., Syracuse, NY, pp. 676-679, 1988.

20. **[Bridges5]** G.E. Bridges and L. Shafai, "Wave Propagation and Current Distribution for a Conductor Impinging on a Lossy Interface," Proc. ANTEM'88 Symp. on Antenna Tech. and Applied Electromagnetics, Winnipeg, Canada, Aug., 1988.

21. **[Bridges6]** G.E. Bridges and L. Shafai, "Plane Wave Coupling to Multiple Conductor Transmission Lines Above a Lossy Earth," IEEE Trans. Electromagnetic Compatibility, vol. EMC-31, pp. 21-33, 1989.

22. **[Bridges7]** G.E. Bridges and L. Shafai, "Wave Propagation Along a Conductor Near or At a Lossy Interface," IEEE Trans. Antennas Prop., (submitted for review).

23. **[Burke]** G.J. Burke, Miller, Brittingham, Lager, Lytle, Okada, "Computer Modeling of Antennas Near the Ground," Electromagnetics, vol. 1, pp. 29-49, 1981.

24. **[Butler1]** C.M. Butler, "Current Induced on a Conducting Strip Which Resides on the Planar Interface Between Two Semi-Infinite Half-Spaces," IEEE Trans. Antennas Prop., vol. AP-32, pp. 226-231, 1984.

25. **[Butler2]** C.M. Butler, X. Xu, A.W. Glisson, "Current Induced on a Conducting Cylinder Located Near the Planar Interface Between Two Semi-Infinite Half-Spaces," IEEE Trans. Antennas Prop., vol. AP-33, pp. 616-624, 1985.

26. **[Butler3]** C.M. Butler, "General Solutions of the Narrow Strip (and Slot) Integral Equations," IEEE Trans. Antennas Prop., vol. AP-33, pp. 1085-1090, 1985.

27. **[Chang1]** D.C. Chang and J.R. Wait, "Extremely Low Frequency (ELF) Propagation Along a Horizontal Wire Located Above or Buried in the Earth," IEEE Trans. Communications, vol. COM-22, pp. 421-427, 1974.

28. **[Chang2]** D.C. Chang and R.J. Fisher, "A Unified Theory on Radiation of a Vertical Electric Dipole Above a Dissipative Earth," Radio Science, vol. 9, pp. 1129-1138, 1974.

29. **[Chang3]** D.C. Chang and R.G. Olsen, "Excitation of an Infinite Antenna Above a Dissipative Earth," Radio Science, vol. 10, pp. 823-831, 1975.

30. **[Carpentier1]** M.P. Carpentier and A.F. dos Santos, "New Representation for the Current in a Horizontal Wire Above Ground," Electronics Letters, vol. 15, pp. 554-557, 1979.

31. **[Carpentier2]** M.P. Carpentier and A.F. dos Santos, "Validity of the Quasi-TEM Approximation for the Modes Supported by a Horizontal Wire Above Ground," Electronics Letters, vol. 16, pp. 85-86, 1980.

32. **[Carpentier3]** M.P. Carpentier and A.F. dos Santos, "Nonspectral Representation for the Field of a Horizontal Wire Above Ground," Radio Science, vol. 19, pp. 812-828, 1984.

33. **[Carson]** J.R. Carson, "Wave Propagation in Overhead Wires with Ground Return," Bell System Technical Journal, vol. 5, pp. 539-554, 1926.

34. **[Chen]** K.C. Chen, "Time Harmonic Solutions for a Long Horizontal Wire Over the Ground with Grazing Incidence," IEEE-AP, vol. AP-33, pp. 233-243, 1985.

35. **[Chiba]** J. Chiba, "Studies in Overhead Wire-Goubau Line Above Ground," IEEE Trans. Microwave Theory Tech., vol. MTT-25, pp. 83-93, 1977.

36. **[Clemmow]** P.C. Clemmow, *The Plane Wave Spectrum Representation of Electromagnetic Fields*, Pergamon Press, New York, 1966.

37. **[Collin]** R.E. Collin, *Field Theory of Guided Waves*, McGraw-Hill, New York, 1960.

38. **[Coleman]** B.L. Coleman, "Propagation of Electromagnetic Disturbances Along a Thin Wire in a Horizontally Stratified Medium," Phil. Mag., vol. 41, pp. 276-288, 1950.

39. **[Courbet]** G. Courbet, P. Degauque, B. Demoulin, R. Gabillard, "Contribution of the Discrete Modes to the Current Propagating Along a Wire Parallel to a Moderate Conducting Earth," Electronics Letters, vol. 15, pp. 174-175, 1979.

40. **[Das]** N.K. Das and D.M. Pozar, "Generalized Spectral-Domain Green's Function for Multilayer Dielectric Substrates with Application to Multilayer Transmission Lines," IEEE Trans. Microwave Theory Tech., vol. MTT-35, pp. 326-335, 1987.

41. **[Degauque1]** P. Degauque, G. Courbet, M. Heddebaut, "Propagation Along a Line Parallel to the Ground Surface: Comparison Between the Exact Solution and the Quasi-TEM Approximation," IEEE Trans. Electromagnetic Compatibility, vol. EMC-25, pp. 422-427, 1983.

42. **[Degauque2]** P. Degauque and A. Zeddam, "Remarks on the Transmission-Line Approach to Determining the Current Induced on Above-Ground Cables," IEEE Trans. Electromagnetic Compatibility, vol. EMC-30, pp. 77-80, 1988.

43. **[Deri]** A. Deri, G. Tevan, A. Symelyn, A. Castanheira, "The Complex Ground Return Plane, A Simplified Model for Homogeneous and Multi-Layer Earth Return," IEEE Trans. Power Apparatus and Systems, vol. PAS-100, pp. 3686-3693, 1981.

44. **[Djordjevic1]** A.R. Djordjevic and T.K. Sarkar, "Analysis of Time Response of Lossy Multiconductor Transmission Line Networks," IEEE Trans. Microwave Theory Tech., vol. MTT-35, pp. 898-908, 1987.

45. **[Djordjevic2]** A.R. Djordjevic, T.K Sarkar, R.F. Harrington, "Time-Domain Response of Multiconductor Transmission Lines," Proc. of IEEE, vol. 75, pp. 743-764, 1987.

46. **[Dommel]** H.W. Dommel, R.E. Judkins and D.E. Nordell, "Discussion of 'Electromagnetic Effects of Overhead Transmission Lines Practical Problems, Safeguards, and Methods of Calculation'," IEEE Trans. Power Apparatus and Systems, vol. PAS-93, pp. 892-904, 1974.

47. **[dosSantos]** A.F. dos Santos, "Electromagnetic-Wave Propagation Along a Horizontal Wire Above Ground," Proc. IEE (London), vol. 119, pp. 1103-1109, Aug., 1972.

48. **[Efthymiadis]** A.E. Efthymiadis and L.M. Wedepohl, "Propagation Characteristics of Infinitely-Long Single-Conductor Lines by the Complete Field Solution Method," Proc. of IEE, vol. 125, pp. 511-517, 1978.

49. **[Erdelyi]** A. Erdelyi ed., *Tables of Integral Transforms; Bateman Manuscript Project*, McGraw-Hill, New York, 1954.

50. **[EPRI]** Electric Power Research Institute, *Transmission Line Reference Book, 345kV and Above*, EPRI: Palo Alto, CA 94304, 1975.

51. **[Fache1]** N. Fache and D. De Zutter, "Rigorous Full-Wave Space-Domain Solution for Dispersive Microstrip Lines," IEEE Trans. Microwave Theory Tech., vol. MTT-36, pp. 731-737, 1988.

52. **[Fache2]** N. Fache and D. De Zutter, "Circuit Parameters for Single and Coupled Microstrip Lines by a Rigorous Full-Wave Space-Domain Analysis," IEEE Trans. Microwave Theory Tech., vol. MTT-37, pp. 421-425, 1989.

53. **[Farr]** E.G. Farr, C.H. Chan, R. Mittra, "A Frequency-Dependent Coupled-Mode Analysis of Multiconductor Microstrip Lines with Application to VLSI Interconnection Problems," IEEE Trans. Microwave Theory Tech., vol. MTT-34, pp. 307-310, 1986.

54. **[Felsen]** L.B. Felsen and N. Marcuvitz, *Radiation and Scattering of Waves*, Prentice-Hall, New York, 1973.

55. **[Fontaine]** J.M. Fontaine, A. Umbert, B. Djebari, J. Hamelin, "Ground Effects in the Response of a Single-Wire Transmission Line Illuminated by an E.M.P.," Electromagnetics, vol. 2, pp. 43-54, 1982.

56. **[Fukuoka]** Y. Fukuoka, Q. Zhang, D.P. Neikirk, T. Itoh, "Analysis of Multilayer Interconnection Lines for a High-Speed Digital Integrated Circuit," IEEE Trans. Microwave Theory Tech., vol. MTT-33, pp. 527-532, 1985.

57. **[Gardiol]** F.E. Gardiol, "Tips for Evaluating Sommerfeld Integrals," IEEE Antennas Propagation Newsletter, pp. 24-25, Oct., 1986.

58. **[Getsinger]** W.J. Getsinger, "Measurement and Modeling of the Characteristic Impedance of Microstrip," IEEE Trans. Microwave Theory Tech., vol. MTT-31, pp. 624-632, 1983.

59. **[Grinberg]** G.A. Grinberg and B.E. Bonshtedt, "Foundations of an Exact Theory of Transmission Line Fields," Zhurnal Tekhnicheskoi Fiziki, vol. 24, pp. 67-95, 1954; translated by E.F. Kuester, Sci. Rep. No. 27, Electromagnetics Laboratory, Dept. of Elect. Eng., Univ. of Colorado, 1977.

60. **[Hashimoto]** M. Hashimoto, "A Rigorous Solution for Dispersive Microstrip," IEEE Trans. Microwave Theory Tech., vol. MTT-33, pp. 1131-1137, 1985.

61. **[Harrington1]** R.F. Harrington, *Time-Harmonic Electromagnetic Fields*, McGraw-Hill, New York, 1961.

62. **[Harrington2]** R.F. Harrington, *Field Computation by Moment Methods*, Macmillan, New York, 1968.

63. **[Harrington3]** R.F. Harrington, D.R. Wilton, C.M. Butler, R. Mittra, C.L. Bennett, *Lectures on Computational Methods in Electromagnetics*, SCEEE Press, St. Cloud, FL, 1981.

64. **[Harrington4]** R.F Harrington and C. Wei, "Losses on Multiconductor Transmission Lines in Multilayered Dielectric Media," IEEE Trans. Microwave Theory Tech., vol. MTT-32, pp. 705-710, 1984.

65. **[Hessel]** A. Hessel, "General Characteristics of Traveling-Wave Antennas," Ch. 19 in R.E. Collin and F.J. Zucker eds., *Antenna Theory*, McGraw-Hill, New York, 1969.

66. **[Hill]** D. A. Hill and J.R. Wait, "Coupling Between a Dipole Antenna and an Infinite Cable Over an Ideal Ground Plane," Radio Science, vol. 12, pp. 231-238, 1977.

67. **[Itoh]** T. Itoh, "Spectral Domain Immitance Approach for Dispersion Characteristics of Generalized Printed Transmission Lines," IEEE Trans. Microwave Theory Tech., vol. MTT-28, pp. 733-736, 1980.

68. **[Jackson1]** R.W. Jackson and D.M. Pozar, "Full-Wave Analysis of Microstrip Open-End and Gap Discontinuities," IEEE Trans. Microwave Theory Tech., vol. MTT-33, pp. 1036-1042, 1985.

69. **[Jackson2]** D.R. Jackson and N.G. Alexopoulos, "Analysis of Planar Strip Geometries in a Substrate-Superstrate Configuration," IEEE Trans. Antennas Prop., vol. AP-34, pp. 1430-1438, 1986.

70. **[Jackson3]** D.R. Jackson and N.G. Alexopoulos, "An Asymptotic Extraction Technique for Evaluating Sommerfeld-Type Integrals," IEEE Trans. Antennas Prop., vol. AP-34, pp. 1467-1470, 1986.

71. **[Jansen1]** R.H. Jansen, "High-Speed Computation of Single and Coupled Microstrip Parameters Including Dispersion, High-Order Modes, Loss and Finite Strip Thickness," IEEE Trans. Microwave Theory Tech., vol. MTT-26, pp. 75-82, 1978.

72. **[Jansen2]** R.H. Jansen, "Unified User-Oriented Computation of Shielded, Covered and Open Planar Microwave and Millimeter-Wave Transmission-Line Characteristics," IEE Jour. Microwaves, Optics and Acoustics, vol. 3, pp. 14-22, 1979.

73. **[Jansen3]** R.H. Jansen and N.H. Koster, "New Aspects Concerning the Definition of Microstrip Characteristic Impedance as a Function of Frequency," Proc. IEEE-MTT Intl. Symp., Dallas, TX, pp. 305-307, 1982.

74. **[Jansen4]** R.H. Jansen and M. Kirschning, "Arguments and an Accurate Model for the Power-Current Formulation of Microstrip Characteristic Impedance," Arch. Elek. Uberstrangungstech., vol. 37, pp. 108-112, 1983.

75. **[Jansen5]** R.H. Jansen, "The Spectral-Domain Approach for Microwave Integrated Circuits," (review paper) IEEE Trans. Microwave Theory Tech., vol. MTT-33, pp. 1043-1056, 1985.

76. **[Kaidanov]** F.G. Kaidanov, M.V. Kostenko, L.S. Perel'man, "Precise Determination of Transmission-Line Constants and Analysis of the Telegraph Equations, For Example for a Two-Conductor Transmission Line," Elec. Technol. USSR, vol. 2, pp. 179-198, 1965.

77. **[Kami]** Y. Kami and R. Sato, "Circuit-Concept Approach to Externally Excited Transmission Lines," IEEE Trans. Electromagnetic Compatibility, vol. EMC-27, pp. 177-183, 1985.

78. **[Kerns1]** D.M. Kerns, "Definitions of v, i, Z, Y, a, b, Γ, and S," Proc. of IEEE, vol. 55, pp. 892-900, 1967.

79. **[Kerns2]** D.M. Kerns and R.W. Beatty, *Basic Theory of Waveguide Junctions and Introductory Microwave Network Analysis*, Pergamon Press, New York, 1967.

80. **[Kikuchi]** H. Kikuchi, "Wave Propagation Along an Infinite Wire Above Ground at High Frequencies," Electrotech. Jour. of Japan, vol. 2, pp. 73-78, 1956.

81. **[King1]** R.W.P. King, T.T. Wu and L.C. Shen, "The Horizontal Wire Antenna Over a Conducting or Dielectric Half Space: Current and Admittance," Radio Science, vol. 9, pp. 701-709, 1974.

82. **[King2]** R.W.P. King, "The Many Faces of the Insulated Antenna," Proc. IEEE, vol. 64, pp. 228-238, 1976.

83. **[King3]** R.W.P. King and L.C. Shen, "Scattering by Wires Near a Material Half-Space," IEEE-AP, vol. AP-30, pp. 1165-1171, 1982.

84. **[King4]** R.W.P. King, "The Wave Antenna for Transmission and Reception," IEEE Trans. Antennas Prop., vol. AP-31, pp. 956-965, 1983.

85. **[King5]** R.W.P. King, "Electromagnetic Surface Waves: New formulas and Applications," IEEE Trans. Antennas Prop., vol. AP-33, pp. 1204-1212, 1985.

86. **[King6]** R.W.P. King, "Electromagnetic Surface Waves," IEEE Antennas Prop. Newsletter, pp. 5-11, Dec., 1986.

87. **[Kobayashi1]** M. Kobayashi and F. Ando, "Dispersion Characteristics of Open Microstrip Lines," IEEE Trans. Microwave Theory Tech., vol. MTT-35, pp. 101-105, 1987.

88. **[Kobayashi2]** M. Kobayashi, "A Dispersion Formula Satisfying Recent Requirements in Microstrip CAD," IEEE Trans. Microwave Theory Tech., vol. MTT-36, pp. 1246-1250, 1988.

89. **[Kuebler]** W. Kuebler, "A Note Concerning the Evaluation of the Sommerfeld Integral," IEEE Trans. Antennas Prop., vol. AP-27, pp. 254-256, 1979.

90. **[Kuester1]** E.F. Kuester and D.C. Chang, "Propagating Modes Along a Thin Wire Located Above a Grounded Dielectric Slab," IEEE Trans. Microwave Theory Tech., vol. MTT-25, pp. 1065-1069, 1977.

91. **[Kuester2]** E.F. Kuester, D.C. Chang and R.G. Olsen, "Modal Theory of Long Horizontal Wire Structures Above the Earth, 1, Excitation," Radio Science, vol. 13, pp. 605-613, 1978.

92. **[Kuester3]** E.F. Kuester and D.C. Chang, "Evaluation of Sommerfeld Integrals Associated with Dipole Sources Above Earth," Sci. Rep. No. 43, Electromagnetics Laboratory, Dept. of Elect. Eng., Univ. of Colorado, 1979.

93. **[Kuester4]** E.F. Kuester, D.C. Chang and S.W. Plate, "Electromagnetic Wave Propagation Along Horizontal Wire Systems in or Near a Layered Earth," Electromagnetics, vol. 1, pp. 243-266, 1981.

94. **[Lee]** K.S.H. Lee, "EMP Interaction: Principles, Techniques, and Reference Data," Final Report, AFWL-TR-80-402, AFWL, New Mexico, 1980.

95. **[Legro]** J.R. Legro et al., "Study to Assess the Effects of High-Altitude Electromagnetic Pulse on Electrical Power Systems," Phase I Final Report, ORNL/Sub/83-43374/1/V2, Oak Ridge National Lab., Feb. 1986.

96. **[Leung]** T. Leung and C.A. Balanis, "Pulse Dispersion Distortion in Open Microstrips Using the Spectral-Domain Method," IEEE Trans. Microwave Theory Tech., vol. MTT-36, pp. 1223-1226, 1988.

97. **[Leviatan]** Y. Leviatan and A.T. Adams, "The Response of a Two-Wire Transmission Line to Incident Field and Voltage Excitation, Including the Effects of Higher Order Modes," IEEE Trans. Antennas Prop., vol. AP-30, pp. 998-1003, 1982.

98. **[Lindell1]** I.V. Lindell and E. Alanen, "Exact Image Theory for the Sommerfeld Half-Space Problem, Part I: Vertical Magnetic Dipole," IEEE Trans. Antennas Prop., vol. AP-32, pp. 126-133, 1984.

99. **[Lindell2]** I.V. Lindell and E. Alanen, "Exact Image Theory for the Sommerfeld Half-Space Problem, Part II: Vertical Electric Dipole," IEEE Trans. Antennas Prop., vol. AP-32, pp. 841-847, 1984.

100. **[Lindell3]** I.V. Lindell and E. Alanen, "Exact Image Theory for the Sommerfeld Half-Space Problem, Part III: General Formulation," IEEE Trans. Antennas Prop., vol. AP-32, pp. 1027-1032, 1984.

101. **[Mahmoud]** S.F. Mahmoud and A.A. Mohsen, "Assessment of Image Theory for Field Evaluation Over a Multilayer Earth," IEEE Trans. Antennas Prop., vol. AP-33, pp. 1054-1057, 1985.

102. **[Marcuvitz]** N. Marcuvitz, *Waveguide Handbook*, Dover, New York, 1951.

103. **[Michalski]** K.A. Michalski and C.M. Butler, "Evaluation of Sommerfeld Integrals Arising in the Ground Stake Antenna Problem," Proc. IEE, Pt. H, vol. 134, pp. 93-97, 1987.

104. **[Mittra1]** R. Mittra ed., *Computer Techniques for Electromagnetics*, Pergamon Press, New York, 1973.

105. **[Mittra2]** R. Mittra ed., *Numerical and Asymptotic Techniques in Electromagnetics*, Springer-Verlag, New York, 1975.

106. **[Moghram]** I.S. Moghram and D.J. Tylavsky, "Electric Field of a Transmission Line Over Multilayered Media," Proc. IEEE, vol. 75, pp. 170-171, 1987.

107. **[Morse]** P.M. Morse and H. Feshbach, *Methods of Theoretical Physics*, McGraw-Hill, New York, 1953.

108. **[Mosig]** J.R. Mosig and T.K. Sarkar, "Comparison of Quasi-Static and Exact Electromagnetic Fields from a Horizontal Electric Dipole Above a Lossy Dielectric Backed by an Imperfect Ground Plane," IEEE Trans. Microwave Theory Tech., vol. MTT-34, pp. 379-387, 1986.

109. **[Newman1]** E.H. Newman, "The Equivalent Separation(s) for the Self-Impedance of Thin Strips," IEEE Trans. Antennas Prop., vol. AP-35, pp. 110-113, 1987.

110. **[Newman2]** E.H. Newman, "An Overview of the Hybrid MM/Green's Function Method in Electromagnetics," IEEE Proc., vol. 76, pp. 270-282, Mar., 1988.

111. **[Norton]** K.A. Norton, "The Propagation of Radio Waves over the Surface of the Earth and in the Upper Atmosphere," Proc. IRE, vol. 24, Pt. 1, pp. 1367-1387, 1936 and vol. 25, Pt. 2, pp. 1203-1236, 1937.

112. **[Olsen1]** R.G. Olsen and D.C. Chang, "Current Induced by a Plane Wave on a Thin Infinite Wire Near Earth," IEEE Trans. Antennas Prop., vol. AP-22, pp. 586-589, 1974.

113. **[Olsen2]** R.G. Olsen and D.C. Chang, "New Modal Representation of Electromagnetic Waves Supported by a Horizontal Wire Above a Dissipative Earth," Electronics Letters, vol. 10, pp. 92-94, 1974.

114. **[Olsen3]** R.G. Olsen and D.C. Chang, "Propagation of Modes on a Pair of Infinite Wires Above a Conducting Earth," Proc. IEEE-AP/URSI Intl. Symp., Urbana, IL, pp. 427-430, 1975.

115. **[Olsen4]** R.G. Olsen and M.A. Usta, "The Excitation of Current on an Infinite Horizontal Wire Above Earth by a Vertical Electric Dipole," IEEE-AP, vol. AP-25, pp. 560-565, 1977.

116. **[Olsen5]** R.G. Olsen, E.F. Kuester and D.C. Chang, "Modal Theory of Long Horizontal Wire Structures Above the Earth, 2, Properties of Discrete Modes," Radio Science, vol. 13, pp. 615-623, 1978.

117. **[Olsen6]** R.G. Olsen and A. Aburwein, "Current Induced on a Pair of Wires Above Earth by a Vertical Electric Dipole for Grazing Angles of Incidence," Radio Science, vol. 15, pp. 733-742, 1980.

118. **[Olsen7]** R.G. Olsen and T.A. Pankaskie, "On the Exact, Carson and Image Theories for Wires at or Above the Earth's Interface," IEEE Trans. Power Apparatus Systems, vol. PAS-102, pp. 769-776, 1983.

119. **[Olsen8]** R.G. Olsen and B. Stimson, "Predicting VHF/UHF Electromagnetic Noise from Corona on Power-Line Conductors," IEEE Trans. Electromagnetic Compatibility, vol. EMC-30, pp. 13-22, 1988.

120. **[Parhami1]** P. Parhami, Y. Rahmat-Samii, R. Mittra, "An Efficient Approach for Evaluating Sommerfeld Integrals Encountered in the Problem of Current Element Radiating Over a Lossy Ground," IEEE Trans. Antennas Prop., vol. AP-28, pp. 100-104, 1980.

121. **[Parhami2]** P. Parhami and R. Mittra, "Wire Antennas Over a Lossy Half-Space," IEEE Trans. Antennas Prop., vol. AP-28, pp. 397-403, 1980.

122. **[Perel'man]** L.S. Perel'man, "Details of the Theory of Wave Propagation Along Multi-Conductor Transmission Lines in Connection with some Engineering Problems," Izvestiya Naucho-Issledovatel'skii Institut Postoyannogo toka, Leningrad, No. 10, pp. 103-120, 1963; translated by E.F. Kuester, Sci. Rep. No. 27, Electromagnetics Laboratory, Dept. of Elect. Eng., Univ. of Colorado, 1977.

123. **[Pistol'kors]** A.A. Pistol'kors, "On the Theory of a Wire Parallel to the Plane Interface Between Two Media," Radiotekhnika, vol. 8, pp. 8-18, 1953, translated by E.F. Kuester, Sci. Rep. No. 27, Electromagnetics Laboratory, Dept. of Elect. Eng., Univ. of Colorado, 1977.

124. **[Pogorzelski]** R.J. Pogorzelski and D.C. Chang, "On the Validity of the Thin Wire Approximation in Analysis of Wave Propagation Along a Wire Over a Ground," Radio Science, vol. 12, pp. 699-707, 1977.

125. **[Pollaczek]** F. Pollaczek, "Uber des Feld einer unendlich langen weschselstrom-durch flossenen Einfachleitung," Elektr. Nachr. Tech., vol. 3, pp. 339-359, 1926.

126. **[Pozar]** D.M. Pozar, "Input Impedance and Mutual Coupling of Rectangular Microstrip Antennas," IEEE Trans. Antennas Prop., vol. AP-30, pp. 1191-1197, 1982.

127. **[Press]** W.H. Press, B.P. Flannery, S.A. Teukolsky, W.T. Vettering, *Numerical Recipes*, Cambridge University Press, Cambridge, 1986.

128. **[Rahmat-Samii]** Y. Rahmat-Samii, R. Mittra, and P. Parhami, "Evaluation of Sommerfeld Integrals for Lossy Half-Space Problems," Electromagnetics, vol. 1, pp. 1-28, 1981.

129. **[Rana]** I.E. Rana and N.G. Alexopoulos, "Current Distribution and Input Impedance of Printed Dipoles," IEEE-AP, vol. AP-29, pp. 99-105, 1981. IEEE Trans. Antennas Prop., vol. AP-29, pp. 99-105, 1981.

130. **[Scharfman]** W.E. Scharfman, E.F. Vance and K.A. Graf, "EMP Coupling to Power Lines," IEEE Trans. Antennas Prop., vol. AP-26, pp. 129-135, 1978.

131. **[Schelkunoff1]** S.A. Schelkunoff, "Theory of Antennas of Arbitrary Size and Shape," Proc. of IEEE, vol. 72, pp. 1165-1190, 1984. (reprint from Proc. IRE, vol. 29, p.493, 1941)

132. **[Schelkunoff2]** S.A. Schelkunoff, *Electromagnetic Waves*, Van Nostrand, New York, 1943.

133. **[Schelkunoff3]** S.A. Schelkunoff, "Impedance Concept in Waveguides," Quart. Appl. Mathematics, vol. 2, pp. 1-15, 1944.

134. **[Schwinger]** J. Schwinger and D.S. Saxon, *Discontinuities in Waveguides*, Gordon and Breach, New York, 1968.

135. **[Shen1]** L.C. Shen, "Current Distribution on a Long Dipole Antenna," IEEE Trans. Antennas Prop., vol. AP-16, pp. 353-354, 1968.

136. **[Shen2]** L.C. Shen, T.T. Wu, R.W.P. King, "A Simple Formula of Current in Dipole Antennas," IEEE Trans. Antennas Prop., vol. AP-16, pp. 542-547, 1968.

137. **[Shen3]** L.C. Shen, K.M. Lee and R.W.P. King, "Coupled Horizontal-Wire Antennas Over a Conducting or Dielectric Half Space," Radio Science, vol. 12, pp. 687-698, 1977.

138. **[Shih]** Y.C. Shih and T. Itoh, "Analysis of Printed Transmission Lines for Monolithic Integrated Circuits," Electronics Letters, vol. 18, pp. 185-186, 1982.

139. **[Sommerfeld1]** A. Sommerfeld, "Uber die Fortpflanzung electrodynamischer Wellen en einem zylindrischen Leiter," Ann. Phys. un-Chemie, vol. 67, pp. 233-290, 1899.

140. **[Sommerfeld2]** A. Sommerfeld, "Uber die Ausbreitung der Wallen in der drahtlosen Telegraphie," Ann. der Physik, vol. 28, pp. 665-736, 1909. (vol. 81, pp. 1135-1153, 1926, correction of an algebraic sign error)

141. **[Sommerfeld3]** A. Sommerfeld, *Partial Differential Equations in Physics*, vol. 6, Academic Press, New York, 1964.

142. **[Sorbello]** R.M. Sorbello, R.W.P. King, K.M. Lee, L.C. Shen and T.T. Wu, "The Horizontal-Wire Antenna Over a Dissipative Half-Space: Generalized Formula and Measurements," IEEE Trans. Antennas Prop., vol. AP-25, pp. 850-854, 1977.

143. **[Stratton]** J.A. Stratton, *Electromagnetic Theory*, McGraw-Hill, New York, 1941.

144. **[Sunde]** E.D. Sunde, *Earth Conduction Effects in Transmission Systems*, Dover, New York, 1968.

145. **[Tamir1]** T. Tamir and A.A. Oliner, "Guided Complex Waves, Part 1. Fields at a Complex Interface, and Part 2. Relation to Radiation Patterns," Proc. IEE, vol. 110, pp. 310-334, 1963.

146. **[Tamir2]** T. Tamir, "Leaky-Wave Antennas," Ch. 20 in R.E. Collin and F.J. Zucker eds., *Antenna Theory*, McGraw-Hill, New York, 1969.

147. **[Tripathi1]** V.K. Tripathi and J.B. Rettig, "A SPICE Model for Multiple Coupled Microstrips and Other Transmission Lines," IEEE Trans. Microwave Theory Tech., vol. MTT-33, pp. 1513-1518, 1985.

148. **[Tripathi2]** V.K. Tripathi and H. Lee, "Spectral-Domain Computation of Characteristic Impedances and Multiport Parameters of Multiple Coupled Microstrip Lines," IEEE Trans. Microwave Theory Tech., vol. MTT-37, pp. 215-220, 1989.

149. **[Vance]** E.F. Vance, *Coupling to Shielded Cables*, Wiley, New York, 1978.

150. **[vanderPol]** B. Van der Pol, "Theory of the Reflection of the Light from a Point Source by a Finitely Conducting Flat Mirror, with an Application to Radiotelegraphy," Physica, vol. 2, pp. 843-853, 1935.

151. **[Venkataraman]** J. Venkataraman, S.M. Rao, A.R. Djordjevic, T.K. Sarkar, Y. Naiheng, "Analysis of Arbitrary Oriented Microstrip Transmission Lines in Arbitrary Shaped Dielectric Media Over a Finite Ground Plane," IEEE Trans. Microwave Theory Tech., vol. MTT-33, pp. 952-959, 1985.

152. **[Veghte]** R.L. Veghte and C.A. Balanis, "Dispersion of Transient Signals in Microstrip Transmission Lines," IEEE Trans. Microwave Theory Tech., vol. MTT-34, pp. 1427-1436, 1986.

153. **[Walsh]** J. Walsh, "Asymptotic Expansion of a Sommerfeld Integral," Electronics Letters, vol. 20, pp. 746-747, 1984.

154. **[Wait1]** J.R. Wait, "On the Impedance of Long Wire Suspended Over the Ground," Proc. of IRE, vol. 49, p. 1576, 1961.

155. **[Wait2]** J.R. Wait and K.P. Spies, "On the Image Representation of the Quasi-Static Fields of a Line Source Above the Ground," Canadian Journal of Physics, vol. 47, pp. 2731-2733, 1969.

156. **[Wait3]** J.R. Wait, *Electromagnetic Waves in Stratified Media*, Pergamon Press, New York, 1970.

157. **[Wait4]** J.R. Wait and K.P. Spies, "Subsurface Electromagnetic Fields of a Line Source on a Conducting Half-Space," Radio Science, vol. 6, pp. 781-786, 1971.

158. **[Wait5]** J.R. Wait, "Theory of Wave Propagation Along a Thin Wire Parallel to an Interface," Radio Science, vol. 7, pp. 675-679, 1972.

159. **[Wait6]** J.R. Wait, "Comments on 'The Horizontal Wire Antenna Over a Conducting or Dielectric Half-Space: Current and Admittance'," Radio Science, vol. 9, p. 1165, 1974.

160. **[Wait7]** J.R. Wait and D.A. Hill, "Propagation Along a Braided Coaxial Cable in a Circular Tunnel," IEEE Microwave Theory Tech., vol. MTT-23, pp. 401-405, 1975.

161. **[Wait8]** J.R. Wait, "Excitation of a Coaxial Cable or Wire Conductor Located over the Ground by a Dipole Radiator," Arch. Elek. Uberstangungstech., vol. 31, pp. 121-127, 1977.

162. **[Wait9]** J.R. Wait, "Excitation of an Ensemble of Parallel Cables by an External Dipole Over a Layered Ground," Arch. Elek. Uberstrangungstech., vol. 31, pp. 489-493, 1977.

163. **[Wait10]** J.R. Wait, "Reply to Professor R.W.P. King on His Comments on the Exponential Current Modes on an Infinitely Long Wire Over the Earth," Proc. IEEE, vol. 65, pp. 1062-1063, 1977.

164. **[Wait11]** J.R. Wait, "Excitation of an Elevated Cable Over a Stratified Earth by an Overhead Current System," Int. Jour. Electronics, vol. 44, pp. 609-616, 1978.

165. **[Wait12]** J.R. Wait, *Geo-Electromagnetism*, Academic Press, New York, 1982.

166. **[Wait13]** J.R. Wait, *Electromagnetic Wave Theory*, Harper and Row, New York, 1985.

167. **[Wait14]** J.R. Wait, "Comment on 'Electric Field of a Transmission Line Over a Multilayered Media'," Proc. IEEE, vol. 76, p. 284, 1988.

168. **[Wedepohl]** L.M. Wedepohl and A.E. Efthymiadis, "Wave Propagation in Transmission Lines Over Lossy Ground: A New, Complete Field Solution," Proc. of IEE, vol. 125, pp. 505-510, 1978.

169. **[Wei]** C. Wei and R.F. Harrington, "Computation of the Parameters of Multiconductor Transmission Lines in Two Dielectric Layers Above a Ground Plane," Dept. of Electrical Eng., Univ. of Syracuse, Syracuse, N.Y., Tech. Report TR-82-12, Nov., 1982.

170. **[Whitaker]** J.F. Whitaker, T.B. Norris, G. Mourou, T.Y. Hsiang, "Pulse Dispersion and Shaping in Microstrip Lines," IEEE Trans. Microwave Theory Tech., vol. MTT-35, pp. 41-47, 1987.

171. **[Wise]** W.H. Wise, "Propagation of High-Frequency Currents in Ground Return Circuits," Proc. of IRE, vol. 22, pp. 522-527, 1934.

172. **[Wu]** T.T. Wu, L.C. Shen, R.W.P. King, "The Dipole Antenna with Eccentric Coating in a Relatively Dense Medium," IEEE Trans. Antennas Prop., vol. AP-23, pp. 57-62, 1975.

173. **[Xu]** X. Xu and C.M. Butler, "Current Induced by TE Excitation on a Conducting Cylinder Located Near the Planar Interface Between Two Semi-Infinite Half-Spaces," IEEE Trans. Antennas Prop., vol. AP-34, pp. 880-889, 1986.

174. **[Zenneck]** J. Zenneck, "Uber die Fortpflanzung ebener elektomagnetischer Wellen langs einer ebenen Leiterflache und ihre Beziehung zur drahtlosen Telegraphie," Ann. der Physik, vol. 23, pp. 846-866, 1907.

175. **[Zhang]** X. Zhang, J. Fang, K.K. Mei, Y. Liu, "Calculations of the Dispersion Characteristics of Microstrips by the Time-Domain Finite Difference Method," IEEE Trans. Microwave Theory Tech., vol. MTT-36, pp. 263-267, 1988.

Appendix A
Green's Functions for Planar Current Sources Embedded in a Stratified Medium

In this appendix, the potential functions and resulting fields due to an arbitrary two-dimensional planar current source embedded in a stratified medium are developed. This problem has received much attention in both recent and past literature with its applications towards structures above lossy media [Wait3, Felsen, Kuester4, Wait12] and in the analysis of microstrip and semi-conductor devices [Jansen2, Itoh, Das, Bagby]. The problem is initially formulated for an arbitrary source distribution in the plane parallel to the media stratification. A source with a distribution perpendicular to the media stratification can be handled through an integration of the planar sources discussed in this appendix. Special cases, where the planar source is reduced to a line source or to a simple delta function source will also be studied along with some of their applications. The problem presented in this appendix is solved using the usual transform techniques. Thus, the resulting solutions will be in the form of single or double infinite integrals, these sometimes being referred to as Sommerfeld-type integrals due to his solution of the half-space problem in 1909 [Sommerfeld2]. The analytical solution of these infinite integrals, in terms of series expansions or tabulated functions, is available for only some special geometries, with many approximations also having been developed over the past decades. The accurate solution of these integrals, however, usually requires a numerical integration approach. This appendix concentrates on the derivation of the Green's functions in integral form, with an analytical form given for only a few special cases. A discussion of the evaluation techniques for these integrals is left for Appendix B. Further, this appendix concentrates on the formulation of the potential functions and resulting fields for electric sources types $\overline{J}_s$, with the formulation for magnetic sources $\overline{M}_s$ easily derived in a similar manner. The desired Green's functions, required throughout the thesis, can then be developed from these results.

A.1. GREEN'S FUNCTION FORMULATIONS

Consider a planar current source $\overline{J}_s$ (or $\overline{M}_s$) embedded in a stratified media as shown in figure A.1. In this configuration, there are M^+ regions located above the source medium and M^- regions located below the source medium. Each of the

regions, denoted by $-M^- < i < M^+$, has a thickness h_i and electrical properties defined by a permeability μ_i, permittivity ε_i, and conductivity σ_i. The planar source is chosen to be located in the medium $i=0$ at a distance y' above the $y=0$ plane ($0<y'<h_0$). The source is allowed to vary in the $x-z$ plane and is specified as either $\bar{J}_s=\bar{J}_s(x,z)\delta(y-y')$ for an electric source or as $\bar{M}_s=\bar{M}_s(x,z)\delta(y-y')$ for a magnetic source. The source has been chosen to be in the region $i=0$ for convenience, with a simple transformation of the $\hat{y}$ coordinate (changing the subscript i) allowing the problem to be formulated for the source in any desired region.

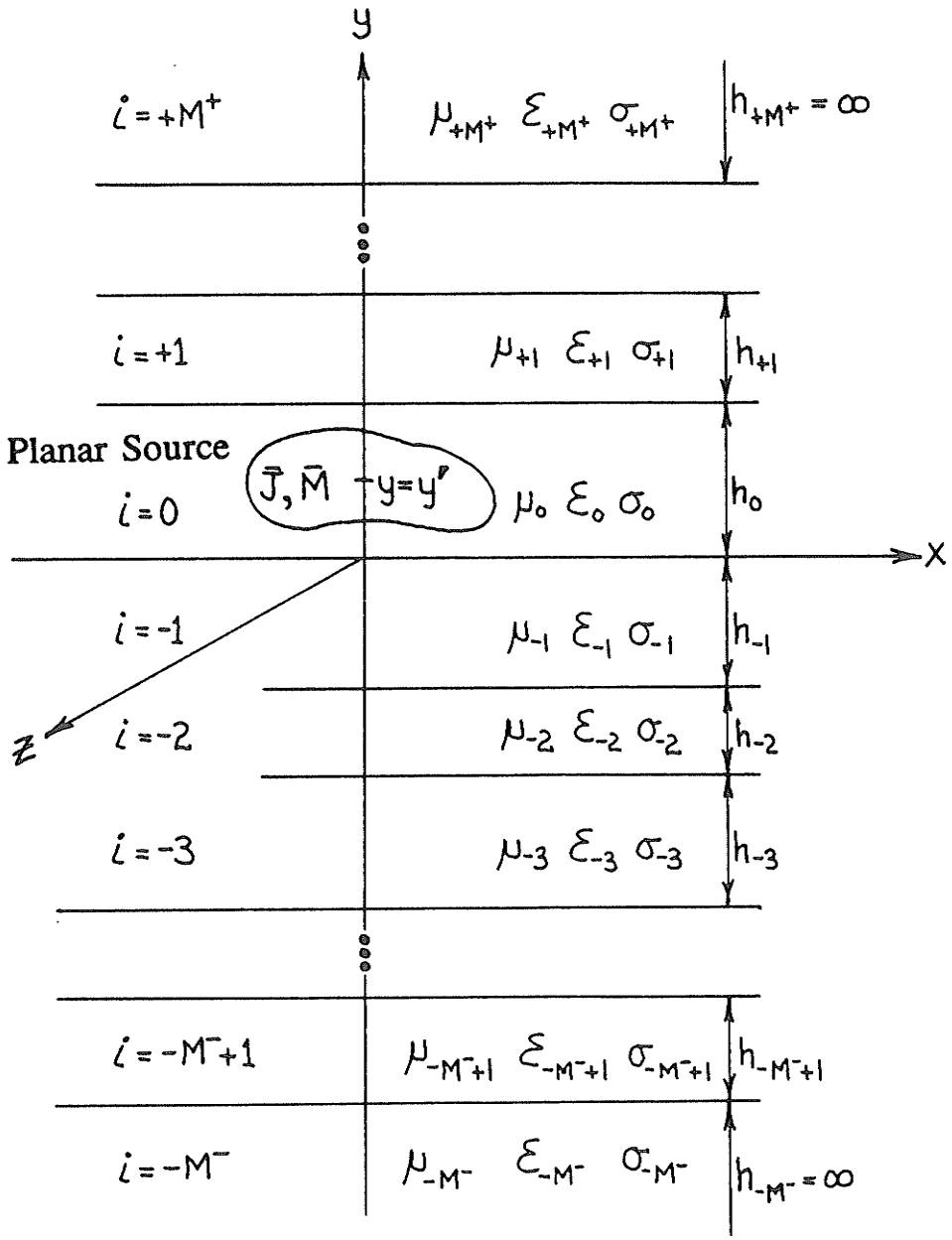

Figure A.1: Planar source embedded in a stratified media.

The goal is to derive the fields in every region i due to the source. Assuming an $e^{-j\omega t}$ time dependence, the fields must be solutions of Maxwell's equations in each region i as [Stratton, Harrington1]

$$\begin{aligned}
\nabla\times \bar{E}^i &= +j\omega\mu_i \bar{H}^i - \bar{M}_s \\
\nabla\times \bar{H}^i &= (\sigma_i - j\omega\varepsilon_i)\bar{E}^i + \bar{J}_s \\
\nabla\cdot\bar{B}^i &= m_s = (1/j\omega)\nabla\cdot\bar{M}_s \\
\nabla\cdot\bar{D}^i &= \rho_s = (1/j\omega)\nabla\cdot\bar{J}_s
\end{aligned} \tag{A.1}$$

where the source terms $\bar{J}_s$ and ρ_s ($\bar{M}_s$ and m_s) are zero except in the region $i=0$. The electric and magnetic Hertz vector potentials $\bar{\Pi}$ and $\bar{\Pi}^*$ are chosen to represent the fields as

$$\begin{aligned}
\bar{E}^i &= \nabla\nabla\cdot\bar{\Pi}^i + k_i^2\bar{\Pi}^i + \frac{k_i^2}{-j\omega\varepsilon_i'}\nabla\times\bar{\Pi}^{*i} \\
\bar{H}^i &= \frac{k_i^2}{j\omega\mu_i}\nabla\times\bar{\Pi}^i + \nabla\nabla\cdot\bar{\Pi}^{*i} + k_i^2\bar{\Pi}^{*i}
\end{aligned} \tag{A.2}$$

$$k_i = \sqrt{\omega^2\mu_i\varepsilon_i + j\omega\mu_i\sigma_i}$$

where the Lorentz gauge $\phi = -\nabla\cdot\bar{\Pi}^i$ and $\psi = -\nabla\cdot\bar{\Pi}^{*i}$ has been used. k_i is the propagation constant in each medium, with $\varepsilon_i' = \varepsilon_i + j\sigma_i/\omega$. Thus, the fields in each region can be described by the corresponding vector potential which are a solution of the Helmholtz wave equations

$$[\nabla^2 + k_i^2]\bar{\Pi}^i = \begin{cases} \dfrac{-j\omega\mu_i}{k_i^2}\bar{J}_s & , i=0 \\ 0 & , i=\pm1, \pm2,\ldots,\pm M^{+/-} \end{cases} \tag{A.3}$$

$$[\nabla^2 + k_i^2]\bar{\Pi}^{*i} = \begin{cases} \dfrac{-j\omega\varepsilon_i'}{k_i^2}\bar{M}_s & , i=0 \\ 0 & , i=\pm1, \pm2,\ldots,\pm M^{+/-} \end{cases} \tag{A.4}$$

To uniquely define (A.3,A.4), continuity of the fields at each interface must be satisfied which are specified as

$$\begin{aligned}
&\text{i)}\ E_x^i = E_x^{i+1} \qquad &&\text{iv)}\ H_x^i = H_x^{i+1} \\
&\text{ii)}\ E_z^i = E_z^{i+1} \qquad &&\text{v)}\ H_z^i = H_z^{i+1} \qquad ; -M^- < i < M^+ - 1 \\
&\text{iii)}\ \varepsilon_i' E_y^i = \varepsilon_{i+1}' E_y^{i+1} \qquad &&\text{vi)}\ \mu_i H_y^i = \mu_{i+1} H_y^{i+1}
\end{aligned} \tag{A.5}$$

The potentials in (A.3,A.4) can be defined in terms of general functions which satisfy the set of differential equations

$$[\nabla^2 + k_i^2]\mathrm{g}^i(x,y,z) = \begin{cases} f(x,z)\delta(y-y') & , i=0 \\ 0 & , i\neq 0 \end{cases} \tag{A.6}$$

These differential equations can be solved by utilizing the two-dimensional Fourier transform pair defined as

$$\begin{aligned} f(k_x,k_z) &= \Gamma_{zx}\{f(x,z)\} = \int_{-\infty}^{\infty}\int_{-\infty}^{\infty} f(x,z)e^{-jk_x x}e^{-jk_z z}\,dk_x\,dk_z \\ f(x,z) &= \Gamma_{zx}^{-1}\{f(k_x,k_z)\} = \frac{1}{4\pi^2}\int_{-\infty}^{\infty}\int_{-\infty}^{\infty} f(k_x,k_z)e^{+jk_x x}e^{+jk_z z}\,dk_x\,dk_z \end{aligned} \tag{A.7}$$

Transforming (A.6) with respect to z-x, then y

$$\left[\frac{\partial^2}{\partial y^2} - (k_x^2+k_z^2-k_i^2)\right]\mathrm{g}^i(k_x,y,k_z) = \begin{cases} f(k_x,k_z)\delta(y-y') & , i=0 \\ 0 & , i\neq 0 \end{cases} \tag{A.8}$$

$$\left[-k_y^2 - U_i^2\right]\mathrm{g}^i(k_x,k_y,k_z) = \begin{cases} f(k_x,k_z)e^{-jk_y y'} & , i=0 \\ 0 & , i\neq 0 \end{cases} \tag{A.9}$$

$$U_i = \sqrt{k_x^2+k_z^2-k_i^2} = \sqrt{k_x^2+\tau_i^2} \quad , \quad \tau_i = \sqrt{k_z^2-k_i^2}$$

The function $\mathrm{g}^i(k_x,k_y,k_z)$ has poles located in the k_y plane at $k_y = \pm jU_i$. Extracting the residues at these poles, the general solution to (A.6) can thus be determined in terms of

$$\begin{aligned} \mathrm{g}^i(k_x,y,k_z) &= \Gamma_y^{-1}\{\mathrm{g}^i(k_x,k_y,k_z)\} \\ &= -f(k_x,k_z)\left[\frac{C^i(k_x,k_z)}{2U_i}e^{+U_i y} + \frac{D^i(k_x,k_z)}{2U_i}e^{-U_i y} + \frac{\delta_i}{2U_i}e^{-U_i|y-y'|}\right] \end{aligned} \tag{A.10}$$

where $C^i(k_x,k_z)$ and $D^i(k_x,k_z)$ are arbitrary constants to be determined by the boundary conditions at each interface. For proper decay of the fields as $|y| \to \infty$ the irrationals U_{-M^-} and U_{+M^+} in the two outer regions are chosen to retain a positive real value on the correct Riemann sheet, $\mathrm{Re}[U_{-M^-},U_{+M^+}]\geq 0$. Thus, the constants $D^{-M^-}=0$ and $C^{+M^+}=0$ are required. Note that the forcing function term in (A.10) is zero if $i\neq 0$. The Green's function for the given source function $f(x,z)\hat{u}_\alpha$; $\alpha\in\{x,y,z\}$ can now be determined from the solution of

$$[\nabla^2 + k_i^2]\overline{\mathrm{G}}^i(x,y,y',z) = \begin{cases} f(x,z)\delta(y-y')\hat{u}_\alpha & , i=0 \\ 0 & , i\neq 0 \end{cases} \tag{A.11}$$

$$\overline{\mathrm{G}}^i(x,y,y',z) = \Gamma_{zx}^{-1}\left\{\overline{\mathrm{G}}^i(k_x,y,y',k_z)\right\} \tag{A.12}$$

A.1.1. Vertical and Horizontal Potential Functions

In this section, the potential functions for a vertically polarized electric source (VES) $J_y(x,z)\delta(y-y')\hat{y}$ and for a horizontally polarized electric source (HES) $J_\alpha(x,z)\delta(y-y')\hat{u}_\alpha$; $\alpha\in\{x,z\}$ will be derived. The fields due to any electric source $\overline{J}_s$ can then be represented in terms of a linear combination of these components. Similarly, any magnetic source $\overline{M}_s$ can be solved in terms of VMS and HMS components. The fields due to the electric sources will be determined from the solution of the wave equation for the Hertz vector potential $\overline{\Pi}$ as defined in (A.2,A.3). Similarly, the fields due to the magnetic sources can be determined through the magnetic Hertz vector potential $\overline{\Pi}^*$. The vector potentials can be written in terms of their scalar components as $\overline{\Pi} = (\mathbf{V}_x,\mathbf{V}_y,\mathbf{V}_z)$ and $\overline{\Pi}^* = (\mathbf{U}_x,\mathbf{U}_y,\mathbf{U}_z)$. For the most general solution, involving both $\overline{J}_s$ and $\overline{M}_s$, all six scalar components are required to represent the source. However, for the case of a HES or HMS, there is one degree of symmetry and only two scalar components are needed for each. For a VES or VMS, there is two degrees of symmetry and only one scalar component is needed for each. Thus, the solution to any source distribution $\overline{J}_s$, $\overline{M}_s$ can be derived in terms of only the scalar potential function components $\mathbf{V}_y\hat{y}$ and $\mathbf{U}_y\hat{y}$. These two components are the conventional TM and TE Debeye potential functions [Wait3, Wait13], respectively, and are specifically chosen since their vertical electric and magnetic fields are uncoupled for a planar geometry, allowing an easier solution of the wave equation. Alternatively, the choice of other scalar components to represent the source can be found through a simple transformation. Thus, the scalar potential functions for the TM and TE cases will be derived next, the potential functions for other source types then being derived in terms of these components.

i) TM case:

For a vertically polarized electric source $J_y(x,z)\delta(y-y')\hat{y}$ located at $y=y'$, the fields are determined from the scalar potential $\mathbf{V}_y^i\hat{y}$ as

$$[\nabla^2+k_i^2]\mathbf{V}_y^i\hat{y} = \begin{cases} \dfrac{-j\omega\mu_i}{k_i^2}J_y(x,z)\delta(y-y')\hat{y} & , i=0 \\ 0 & , i\neq 0 \end{cases} \tag{A.13}$$

$$\overline{E}^i = \nabla\nabla\cdot\mathbf{V}_y^i\hat{y} + k_i^2\mathbf{V}_y^i\hat{y} \tag{A.14}$$

$$\overline{H}^i = \frac{k_i^2}{+j\omega\mu_i}\nabla\times\mathbf{V}_y^i\hat{y} \tag{A.15}$$

The solution to (A.13) is obtained in terms of functions of the type (A.10), where $\overline{\mathbf{G}}^i(k_x,y,k_z) = \mathbf{V}_y^i(k_x,y,k_z)\hat{y}$ and $f(k_x,k_z) = (-j\omega\mu_0/k_0^2)J_y(k_x,k_z)$. The arbitrary coefficients $C^i(k_x,k_z)$ and $D^i(k_x,k_z)$ of (A.10) for the geometry shown in figure A.2

are determined by satisfying the boundary conditions (A.5) at the media interfaces [Kuester4, Wait9, Itoh, Das]. Using the transformed expressions of (A.5), there are $2(M^{+}+M^{-})$ boundary conditions to determine the unknown coefficients (note that the two tangential boundary conditions, x and z, are the same due to symmetry in these dimensions). The transformed potential function $\mathbf{V}_y^i(k_x,y,k_z)$ has a solution

$$\mathbf{V}_y^i(k_x,y,k_z) = \begin{cases} \dfrac{+j\omega\mu_0}{k_0^2} J_y(k_x,k_z)\left[\mathbf{V}_y^{PRIM_0}(k_x,y,k_z) + \mathbf{V}_y^{REF_0}(k_x,y,k_z)\right] & , i=0 \\ \dfrac{+j\omega\mu_0}{k_0^2} J_y(k_x,k_z)\left[\mathbf{V}_y^{TRAN_i}(k_x,y,k_z)\right] & , i\neq 0 \end{cases} \tag{A.16}$$

where in the source region $i=0$ $(0<y<h_0)$

$$\mathbf{V}_y^{PRIM_0}(k_x,y,k_z) = \left[\frac{1}{2U_0} e^{-U_0|y-y'|}\right] \tag{A.17}$$

$$\mathbf{V}_y^{REF_0}(k_x,y,k_z) = \left[\frac{1}{2U_0}\frac{1}{1-R_0^{-e}R_0^{+e}e^{-U_0 2h_0}}\left\{R_0^{-e}e^{-U_0(y+y')} + R_0^{+e}e^{-U_0(2h_0-y-y')} + R_0^{-e}R_0^{+e}e^{-U_0 2h_0}\left[e^{+U_0(y-y')}+e^{-U_0(y-y')}\right]\right\}\right] \tag{A.18}$$

and in the remaining regions $i\neq 0$,

$$\mathbf{V}_y^{TRAN_i}(k_x,y,k_z) = \left[e^{-U_i|y-H_i|} + R_i^{\pm e}e^{-U_i|2h_i-y+H_i|}\right]\frac{T_i^e}{1+R_i^{\pm e}} \tag{A.19}$$

$$T_i^e = \left[\prod_{j=\pm 1}^{i\mp 1}\frac{1+R_j^{\pm e}}{1+R_j^{\mp e}}e^{-U_j h_j}\right]T_{\pm 1}^e \tag{A.20}$$

$$T_{+1}^e = \frac{1}{2U_0}\frac{1+R_0^{+e}}{1-R_0^{-e}R_0^{+e}e^{-U_0 2h_0}}\left[e^{-U_0(h_0-y')} + R_0^{-e}e^{-U_0(h_0+y')}\right] \tag{A.21}$$

$$T_{-1}^e = \frac{1}{2U_0}\frac{1+R_0^{-e}}{1-R_0^{-e}R_0^{+e}e^{-U_0 2h_0}}\left[e^{-U_0(y')} + R_0^{+e}e^{-U_0(2h_0-y')}\right] \tag{A.22}$$

$$H_i = \left\{\sum_{j=0}^{i-1} h_j \;\; ; i>0 \quad , \quad -\sum_{j=-1}^{i+1} h_j \;\; ; i<0\right\} \tag{A.23}$$

where the $\pm$ signs are designated by $i>0$ or $i<0$. The functions R_i^{+e} and R_i^{-e} represent the net reflection from the upper and lower interfaces of medium i, respectively, and are defined recursively as

$$R_i^{\pm e} = \frac{r_{i,i\pm1}^e + R_{i\pm1}^{\pm e} e^{-2h_{i\pm1}U_{i\pm1}}}{1 + r_{i,i\pm1}^e R_{i\pm1}^{\pm e} e^{-2h_{i\pm1}U_{i\pm1}}} \quad ; -M^- < i < +M^+ \tag{A.24}$$

$$R_{\pm M^\pm}^{\pm e} = 0$$

$$r_{i,i\pm1}^e = \frac{n_{i,i\pm1}^2 U_i - U_{i\pm1}}{n_{i,i\pm1}^2 U_i + U_{i\pm1}} \quad ; n_{i,i\pm1}^2 = \frac{\varepsilon_{i\pm1}'}{\varepsilon_i'} \tag{A.25}$$

Here $r_{i,i\pm1}^e$ is the reflection coefficient at the interface between the i and $i\pm1$ media.

ii) TE case:

Similarly, the fields for a vertically polarized magnetic source $M_y(x,z)\delta(y-y')\hat{y}$ located at $y=y'$ are determined from the scalar potential $\mathbf{U}_y^i\hat{y}$ as

$$[\nabla^2 + k_i^2]\mathbf{U}_y^i\hat{y} = \begin{cases} \dfrac{-j\omega\varepsilon_i'}{k_i^2} M_y(x,z)\delta(y-y')\hat{y} & , i=0 \\ 0 & , i\neq 0 \end{cases} \tag{A.26}$$

$$\overline{H}^i = \nabla\nabla\cdot\mathbf{U}_y^i\hat{y} + k_i^2\mathbf{U}_y^i\hat{y} \tag{A.27}$$

$$\overline{E}^i = \frac{k_i^2}{-j\omega\varepsilon_i'}\nabla\times\mathbf{U}_y^i\hat{y} \tag{A.28}$$

The transformed potential $\mathbf{U}_y^i(k_x,y,k_z)$ has a solution

$$\mathbf{U}_y^i(k_x,y,k_z) = \begin{cases} \dfrac{+j\omega\varepsilon_0'}{k_0^2} M_y(k_x,k_z)\left[\mathbf{U}_y^{PRIM_0}(k_x,y,k_z) + \mathbf{U}_y^{REF_0}(k_x,y,k_z)\right] & , i=0 \\ \dfrac{+j\omega\varepsilon_0'}{k_0^2} M_y(k_x,k_z)\left[\mathbf{U}_y^{TRAN_i}(k_x,y,k_z)\right] & , i\neq 0 \end{cases} \tag{A.29}$$

and is equivalent to (A.16) except that all the superscripts e are replaced by m and the reflection coefficients $r_{i,i\pm1}^m$ at the media interfaces are given by

$$r_{i,i\pm1}^m = \frac{m_{i,i\pm1}^2 U_i - U_{i\pm1}}{m_{i,i\pm1}^2 U_i + U_{i\pm1}} \quad ; m_{i,i\pm1}^2 = \frac{\mu_{i\pm1}}{\mu_i} \tag{A.30}$$

Thus, any source $\overline{J}_s$, $\overline{M}_s$, can be decomposed into orthogonal components, and the wave equation solved for each component. An appropriate Green's function can then be derived from the resulting expressions. The Hertz vector potentials $\overline{\Pi}(k_x,y,k_z)$ defined in (A.3) and $\overline{\Pi}^*(k_x,y,k_z)$ defined in (A.4) for each of the electric $J_\alpha\hat{u}_\alpha$ and magnetic $M_\alpha\hat{u}_\alpha$ components $\alpha\in\{x,y,z\}$ can be deduced in terms of the scalar potential functions $\mathbf{V}_y\hat{y}$ and $\mathbf{U}_y\hat{y}$. The two source types considered next are that of a

planar vertically polarized electric source (VES) and that of a planar horizontally polarized electric source (HES). The planar source $\overline{J}_s$ ($\overline{M}_s$) could alternatively be expanded in any other orthogonal coordinate system depending on the problem being studied. A polar coordinate system could alternately be utilized for a loop oriented parallel to the stratification or other circularly symmetric source for example.

A.1.2. Vertically Polarized Electric Source ($\alpha = y$)

The Hertz vector potential $\overline{\Pi}^i$ for a planar vertically polarized electric source $J_y(x,z)\hat{y}$ can be determined in terms of the potential function $\mathbf{V}_y^i\hat{y}$ alone which was derived in the previous section by defining in (A.13-A.15)

$$\overline{\Pi}^i(k_x,y,k_z) = \Pi_y^i(k_x,y,k_z)\hat{y} = \mathbf{V}_y^i(k_x,y,k_z)\hat{y} \tag{A.31}$$

The solution of $\mathbf{V}_y^i\hat{y}$ was previously determined in (A.16), with the corresponding fields found using (A.2).

A.1.3. Horizontally Polarized Electric Source ($\alpha = x,z$)

The Hertz vector potential $\overline{\Pi}^i$ for a planar horizontally polarized electric source requires two scalar components for its representation and thus can be determined in terms of a combination of both the scalar potentials $\mathbf{V}_y^i$ and $\mathbf{U}_y^i$. The horizontal source can be decomposed into the two orthogonal components $\overline{J}_s(x,z)=J_x(x,z)\hat{x}+J_z(x,z)\hat{z}$. Since the analysis is symmetric in the x- and z-dimensions, the fields due to the component J_z only will be determined in detail, with the remaining component J_x found by interchanging the x and z variables.

Considering the source component $J_z(x,z)\hat{z}$, the electric potential vector $\overline{\Pi}^0=\Pi_z^0\hat{z}+\Pi_y^0\hat{y}$ will be chosen for the region containing the source ($i=0$), with the remaining regions $i\neq 0$ using a combination of the scalar potentials $\mathbf{V}_y^i\hat{y}$ and $\mathbf{U}_y^i\hat{y}$. The choice of the components Π_z and Π_y (or Π_x and Π_y for $J_x\hat{x}$) for the vector potential used to represent the fields in the source region is made since the primary contribution of the source is directly identified in the component Π_z (or Π_x) alone. The scattering effect of the layered media is also easily identified and is the only contribution to the component Π_y. Representation of the fields in terms of an alternate choice of vector components, such as directly by $\mathbf{V}_y$ and $\mathbf{U}_y$, would have caused the primary fields to be coupled into both components. The choice of scalar components outside the source region $i\neq 0$ is again arbitrary, and is left in terms of the TM and TE potentials here.

By matching the fields for the various choices of potentials, $\overline{\Pi}^i=\Pi_z^i\hat{z}+\Pi_y^i\hat{y}$ in each medium can be represented in terms of the known potentials $\mathbf{V}_y^i\hat{y}$ and $\mathbf{U}_y^i\hat{y}$ using the transforms

$$\mathbf{U}_y^i \leftarrow \Delta_m^i \Pi_z^i \quad , \quad \Pi_z^i \leftarrow \frac{1}{\Delta_m^i}\mathbf{U}_y^i$$

$$\mathbf{V}_y^i \leftarrow \Pi_y^i + \Delta_e^i \Pi_z^i \quad , \quad \Pi_y^i \leftarrow \mathbf{V}_y^i - \frac{\Delta_e^i}{\Delta_m^i}\mathbf{U}_y^i \tag{A.32}$$

$$\Delta_m^i = j\omega\varepsilon_i' \frac{1}{k_x^2+k_z^2}\frac{\partial}{\partial x} \quad , \quad \Delta_e^i = \frac{1}{k_x^2+k_z^2}\frac{\partial^2}{\partial z\,\partial y}$$

Transforming the primary potential of the source $\overline{\Pi}^{0P}=\Pi_z^{0P}\hat{z}$ to the corresponding TM and TE scalar functions with (A.32), then using the solutions (A.13-A.30), the desired potential functions in each region can be determined. Note that care must be taken in performing the differentiation with respect to y since the sign will depend on $y>y'$ or $y<y'$ for the primary fields. Thus, for the source $J_z(x,z)\hat{z}$, the vector potential $\overline{\Pi}^0(k_x,y,k_z)$ in the source region $i=0$ is given as

$$\overline{\Pi}^0(k_x,y,k_z) = \Pi_z^0(k_x,y,k_z)\hat{z} + \Pi_y^0(k_x,y,k_z)\hat{y} \tag{A.33}$$

$$\Pi_z^0(k_x,y,k_z) = \frac{+j\omega\mu_0}{k_0^2}J_z(k_x,k_z)\left[\frac{e^{-U_0|y-y'|}}{2U_0} + \mathbf{U}_y^{REF_0}\right] \tag{A.34}$$

$$\Pi_y^0(k_x,y,k_z) = \frac{+j\omega\mu_0}{k_0^2}J_z(k_x,k_z)\left[\left(\frac{jk_zU_0}{k_z^2+k_x^2}\right)\left[\mathbf{V}_y^{REF_0} + \mathbf{U}_y^{REF_0}\right]\right] \tag{A.35}$$

with the corresponding fields found using (A.2). The scalar potential functions $\mathbf{V}_y$ and $\mathbf{U}_y$ can be used to find the fields in the remaining regions $i\neq 0$ as

$$\mathbf{V}_y^i(k_x,y,k_z) = \frac{+j\omega\mu_0}{k_0^2}J_z(k_x,k_z)\Delta_e^0\left[\mathbf{V}_y^{TRAN_i}(k_x,y,k_z)\right] \tag{A.36}$$

$$\mathbf{U}_y^i(k_x,y,k_z) = \frac{+j\omega\mu_0}{k_0^2}J_z(k_x,k_z)\Delta_m^0\left[\mathbf{U}_y^{TRAN_i}(k_x,y,k_z)\right] \tag{A.37}$$

with the corresponding fields found using (A.14,A.15,A.27,A.28). The functions $\mathbf{V}_y^{REF_0}$, $\mathbf{V}_y^{TRAN_i}$, $\mathbf{U}_y^{REF_0}$, and $\mathbf{U}_y^{TRAN_i}$ were defined in (A.19-A.23).

By interchanging the $\hat{x}$ and $\hat{z}$ coordinates, the potential functions for the source component $J_x(x,z)\hat{x}$ are given for the source region $i=0$ as

$$\overline{\Pi}^0(k_x,y,k_z) = \Pi_x^0(k_x,y,k_z)\hat{x} + \Pi_y^0(k_x,y,k_z)\hat{y} \tag{A.38}$$

$$\Pi_x^0(k_x,y,k_z) = \frac{+j\omega\mu_0}{k_0^2}J_x(k_x,k_z)\left[\frac{e^{-U_0|y-y'|}}{2U_0} + \mathbf{U}_y^{REF_0}\right] \tag{A.39}$$

$$\Pi_y^0(k_x,y,k_z) = \frac{+j\omega\mu_0}{k_0^2} J_z(k_x,k_z)\left[\left(\frac{jk_x U_0}{k_z^2+k_x^2}\right)\left[\mathbf{V}_y^{REF_0} + \mathbf{U}_y^{REF_0}\right]\right] \qquad (A.40)$$

and in a similar fashion as (A.36,A.37), the potentials in the remaining regions $i \neq 0$ will be found by interchanging the $\hat{x}$ and $\hat{z}$ coordinates.

A.1.4. Horizontal Line Source and Dipole Source

If the planar source distribution is specified in either one or both dimensions, the inverse transform (A.7) defining the potential functions can be performed and even solved in a closed form for some special situations. Two specific cases will be presented.

i) Horizontal Line Source (HLS):

The first case considered is that of an infinite horizontal line source located in the region $i=0$ at a point (x',y'). The source is chosen to vary in the z-dimension and is defined as $\overline{J}_s(x,z)=J_z(z)\delta(x-x')\delta(y-y')\hat{z}$. The vector potential can then be determined by replacing the source term in (A.34,A.35) and performing the inverse transform with respect to the x-dimension as

$$\Pi_z^0(x,y,k_z) = \frac{+j\omega\mu_0}{2\pi k_0^2} J_z(k_z)\int_{-\infty}^{\infty}\left[\frac{e^{-U_0|y-y'|}}{2U_0} + \mathbf{U}_y^{REF_0}\right]e^{+jk_x(x-x')}\,dk_x \qquad (A.41)$$

$$\Pi_y^0(x,y,k_z) = \frac{+j\omega\mu_0}{2\pi k_0^2} J_z(k_z)\int_{-\infty}^{\infty}\left[\left(\frac{jk_z U_0}{k_z^2+k_x^2}\right)\left[\mathbf{V}_y^{REF_0}+\mathbf{U}_y^{REF_0}\right]\right]e^{+jk_x(x-x')}\,dk_x \qquad (A.42)$$

Note that the primary contribution of the source can be identified in the Π_z component as [Abramowitz]

$$\begin{aligned}\overline{\Pi}^P(x,y,k_z) &= \frac{+j\omega\mu_0}{2\pi k_0^2} J_z(k_z)\int_{-\infty}^{\infty}\frac{1}{2U_0}e^{-U_0|y-y'|+jk_x(x-x')}\,dk_x\,\hat{z} \\ &= \frac{+j\omega\mu_0}{2\pi k_0^2} J_z(k_z)K_0(\tau_0\rho)\hat{z} \qquad (A.43)\end{aligned}$$

where $\rho=\sqrt{(x-x')^2+(y-y')^2}$.

ii) Horizontal Electric Dipole (HED):

The second case considered is that of a horizontal electric dipole, polarized in the $\hat{z}$ direction, and located in the region $i=0$ at the point (x',y',z'), where the source function is defined as $\overline{J}_s(x,z)=J_z\delta(x-x')\delta(y-y')\delta(z-z')\hat{z}$. The two-dimensional inverse transform (A.7) defining the potential functions can be evaluated as a single integration using the Bessel function transform [Felsen, Sommerfeld3]. By choosing the appropriate substitutions $\lambda^2=k_x^2+k_z^2$ and $r=\sqrt{(x-x')^2+(z-z')^2}$, the integrals can be

simplified using

$$\Gamma_{zx}^{-1}\left\{ f(k_x^2+k_z^2,y)e^{-jk_x x'}e^{-jk_z z'} \right\}$$

$$= \frac{1}{4\pi^2}\int_{-\infty}^{\infty}\int_{-\infty}^{\infty} f(\lambda^2,y)\frac{-j}{\sqrt{k_z^2-\lambda^2}}e^{-\sqrt{k_z^2-\lambda^2}\,|x-x'|+jk_z(z-z')}\,dk_z\,\lambda d\lambda$$

$$= \frac{1}{4\pi^2}\int_{-\infty}^{\infty} 2f(\lambda^2,y)\,K_0(-j\lambda r)\,(-j\lambda)d\lambda \qquad \text{(A.44)}$$

where the function $f(\lambda^2,y)$ is symmetric about k_x and k_z. Thus, the vector potential functions in the region $i=0$ can be determined as

$$\Pi_z^0(x,y,z) = \frac{+j\omega\mu_0}{2\pi^2 k_0^2}J_z\int_{-\infty}^{\infty}\left[\frac{e^{-U_0|y-y'|}}{2U_0}+\mathbf{U}_y^{REF_0}\right]K_0(-j\lambda r)\,(-j\lambda)d\lambda \qquad \text{(A.45)}$$

$$\Pi_y^0(x,y,z) = \frac{+j\omega\mu_0}{2\pi^2 k_0^2}J_z\frac{(z-z')}{r}\int_{-\infty}^{\infty}U_0\left[\mathbf{V}_y^{REF_0}+\mathbf{U}_y^{REF_0}\right]K_1(-j\lambda r)\,d\lambda \qquad \text{(A.46)}$$

$$U_i = \sqrt{k_x^2+k_z^2-k_i^2} = \sqrt{\lambda^2-k_i^2}$$

Note that the primary contribution of the source can be identified from the Π_z component as [Sommerfeld3]

$$\bar{\Pi}^P(x,y,z) = \frac{+j\omega\mu_0}{2\pi^2 k_0^2}J_z\int_{-\infty}^{\infty}\frac{e^{-U_0|y-y'|}}{2U_0}K_0(-j\lambda r)\,(-j\lambda)d\lambda\,\hat{z}$$

$$= \frac{+j\omega\mu_0}{4\pi k_0^2}\frac{e^{+jk_0R}}{R}J_z\hat{z} \qquad \text{(A.47)}$$

where $R=\sqrt{(x-x')^2+(y-y')^2+(z-z')^2}$. Similarly, for a vertical electric dipole $\bar{J}_s(x,z)=J_y\delta(x-x')\delta(y-y')\delta(z-z')\hat{y}$, the vector potential function in the region $i=0$ is determined as

$$\Pi_y^0(x,y,k_z) = \frac{+j\omega\mu_0}{2\pi k_0^2}J_y\int_{-\infty}^{\infty}\left[\frac{e^{-U_0|y-y'|}}{2U_0}+\mathbf{V}_y^{REF_0}\right]e^{+jk_x(x-x')}\,dk_x \qquad \text{(A.48)}$$

$$\Pi_y^0(x,y,z) = \frac{+j\omega\mu_0}{2\pi^2 k_0^2}J_y\int_{-\infty}^{\infty}\left[\frac{e^{-U_0|y-y'|}}{2U_0}+\mathbf{V}_y^{REF_0}\right]K_0(-j\lambda r)\,(-j\lambda)d\lambda \qquad \text{(A.49)}$$

A.2. SPECIAL CASES

A.2.1. Scattering From a Layered Earth

For remote sensing problems, such as in geological sounding, the scattered fields from dipole and line sources over a stratified earth are desired [Wait3, Wait12, Felsen, Moghram]. Usually, deep penetration into the layered media is desired to adequately characterize the structure's properties. Thus, since the media in remote sensing applications are usually very lossy, low frequency analysis is performed. The potential functions and resulting fields can be determined from the general case of the previous section under the specifications

$$M^+ = 0 \quad , \quad h_{+0} \to \infty \tag{A.50}$$
$$R_0^{+e/m} = 0$$

Here the medium $i=0$ containing the source (usually air) is the upper half-space $y>0$ with the layered earth in the half-space $y<0$. Under the assumption that all the media in the earth are moderately lossy and low frequency probing is desired ($\varepsilon_i \ll \sigma_i/\omega \; ; i<0$)

$$k_i \approx \begin{cases} \omega\sqrt{\mu_0\varepsilon_0} & , i=0 \\ \sqrt{j\omega\mu_i\sigma_i} & , i<0 \end{cases} \tag{A.51}$$

$$m_{i,i-1}^2 = 1 \tag{A.52}$$

where the condition on $m_{i,i-1}$ can be used if the permeabilities of all the media are assumed to be equal $\mu_i=\mu_0$. Thus, the potential functions $\mathbf{V}_y^{REF_0}$ and $\mathbf{U}_y^{REF_0}$ required for the determination of the fields in the medium $i=0$ due to a source located at $(x=x',y=y')$ can be derived as

$$\mathbf{V}_y^{REF_0} = \frac{R_0^{-e}}{2U_0} e^{-U_0(y+y')} \tag{A.53}$$

$$\mathbf{U}_y^{REF_0} = \frac{R_0^{-m}}{2U_0} e^{-U_0(y+y')} \tag{A.54}$$

$$R_i^{-e} = \frac{r_{i,i-1}^e + R_{i-1}^{-e} e^{-2h_{i-1}U_{i-1}}}{1 + r_{i,i-1}^e R_{i-1}^{-e} e^{-2h_{i-1}U_{i-1}}} \quad , \quad r_{i,i-1}^e = \frac{n_{i,i-1}^2 U_i - U_{i-1}}{n_{i,i-1}^2 U_i + U_{i-1}} \tag{A.55}$$

$$R_i^{-m} = \frac{r_{i,i-1}^m + R_{i-1}^{-m} e^{-2h_{i-1}U_{i-1}}}{1 + r_{i,i-1}^m R_{i-1}^{-m} e^{-2h_{i-1}U_{i-1}}} \quad , \quad r_{i,i-1}^m = \frac{U_i - U_{i-1}}{U_i + U_{i-1}} \tag{A.56}$$

$$n_{i,i-1}^2 \approx \begin{cases} j\sigma_{-1}/\omega\varepsilon_0 & , i=0 \\ \sigma_{i-1}/\sigma_i & , i<0 \end{cases}$$

$$U_i \approx \begin{cases} \sqrt{k_x^2+k_z^2-\omega^2\mu_0\varepsilon_0} & , i=0 \\ \sqrt{k_x^2+k_z^2-j\omega\mu_i\sigma_i} & , i<0 \end{cases}$$

The vector potential $\overline{\Pi}^0(k_x,y,k_z)$ for various source types can then be easily obtained using (A.31),(A.33), or (A.38). The specific case examined here are the fields produced by a horizontal line source located above the stratified earth. As discussed above, for most remote sensing applications, very low frequency excitation is required to penetrate the layered structure and thus, a uniform current distribution along the line will be assumed. This is reasonable for situations where:

1. The length of the line is much greater than the depth of all the layers in the structure.
2. End effects on the line can be neglected.
3. Line length is much less than the free space wavelength.
4. All transverse dimensions are much less than the free space wavelength.
5. All the media are assumed to be good conductors at the frequencies of excitation.

The vector potential for a line source carrying a current I_z can be derived from (A.41,A.42) under the axially invariant condition $\partial/\partial z=0$ ($k_z=0$) with

$$J_z(k_z) \rightarrow I_z$$

$$\overline{\Pi}^0(x,y,z) = \frac{+j\omega\mu_0}{2\pi k_0^2} I_z \int_{-\infty}^{\infty} \left[\frac{e^{-U_0|y-y'|}}{2U_0} + R_0^{-m} \frac{e^{-U_0(y+y')}}{2U_0} \right] e^{+jk_x(x-x')} dk_x \hat{z} \qquad \text{(A.57)}$$

The component Π_y in the vector potential is zero since $k_z=0$. The fields in the region above the stratified earth are given using (A.2) as

$$\begin{aligned} \overline{E}^0(x,y,z) &= \nabla\nabla\cdot\overline{\Pi}^0(x,y,z) + k_0^2\overline{\Pi}^0(x,y,z) \\ &= k_0^2\Pi_z^0(x,y,z)\hat{z} \end{aligned} \qquad \text{(A.58)}$$

$$\begin{aligned} \overline{H}^0(x,y,z) &= \frac{k_0^2}{j\omega\mu_0}\nabla\times\overline{\Pi}^0(x,y,z) \\ &= \frac{k_0^2}{j\omega\mu_0}\left[\frac{\partial}{\partial y}\Pi_z^0(x,y,z)\hat{x} - \frac{\partial}{\partial x}\Pi_z^0(x,y,z)\hat{y}\right] \end{aligned} \qquad \text{(A.59)}$$

For remote sensing applications, if the source as well as observation points are located on the surface of the upper half space ($y=y'=0$) and the position of the line is arbitrarily chosen as $x'=0$, then the $\hat{x}$ and $\hat{y}$ components of the magnetic field are given utilizing the Fourier transform as

$$H_y^0(x,y=0,z) = -\frac{I_z}{2\pi}\int_{-\infty}^{\infty}(jk_z)\frac{1+R_0^{-m}}{2U_0}e^{+jk_x x}\,dk_x \tag{A.60}$$

$$H_x^0(x,y=0,z) = -\frac{I_z}{2\pi}\int_{-\infty}^{\infty}\frac{R_0^{-m}}{2}e^{+jk_x x}\,dk_x \tag{A.61}$$

For the single layer earth model series expressions for the fields are available in the literature [Aboul-Atta]. The primary contribution of the source can be found from (A.60) as

$$\overline{H}^P(x,y=0,z) = +\frac{I_z}{2\pi}jk_0K_1(jk_0x)\hat{y} \approx \frac{I_z}{2\pi x}\hat{y} \tag{A.62}$$

Since the primary field has a magnitude which is very large compared to the scattered field from the layered media, the secondary response of the $\hat{y}$ component is masked making accurate analysis difficult. On the other hand, the $\hat{x}$ component of the field is due to only the scattered field and is thus much more applicable to remote sensing analysis [Aboul-Atta].

A.2.2. Two Layered Geometries

For microstrip, MMIC, or printed circuit board applications, a two layered ground structure is usually modeled [Itoh, Jansen2, Rana, Jackson1]. The potential functions and fields for this case can be determined by specifying

$$M^+ = 0\,,\ h_{+0} \to \infty \qquad ;\ R_0^{+e/m} = 0$$

$$M^- = 2\,,\ h_{-2} \to \infty \qquad ;\ R_2^{+e/m} = 0$$

$$\mathbf{V}_y^{REF_0} = \frac{R_0^{-e}}{2U_0}e^{-U_0(y+y')} \tag{A.63}$$

$$\mathbf{U}_y^{REF_0} = \frac{R_0^{-m}}{2U_0}e^{-U_0(y+y')} \tag{A.64}$$

$$R_0^{-e/m} = \frac{r_{-0,-1}^{e/m} + r_{-1,-2}^{e/m}e^{-2h_{-1}U_{-1}}}{1 + r_{-0,-1}^{e/m}r_{-1,-2}^{e/m}e^{-2h_{-1}U_{-1}}} \tag{A.65}$$

For microstrip applications it is usually assumed that the upper region is free space, the permeability of all the substrates is equal to that of the upper half space

$\mu_{-2}=\mu_{-1}=\mu_0$, and that the conductivity of the grounding substrate $i=-2$ can be assumed to be a perfect conductor $\sigma_{-2}\to\infty$. This configuration is shown in figure A.2.

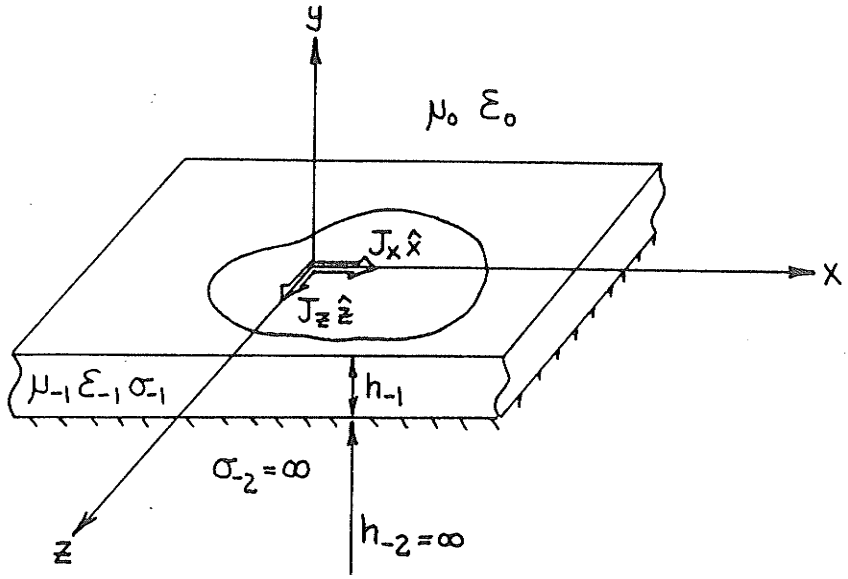

Figure A.2: Two layer microstrip structure.

Under these assumptions

$$\begin{aligned}
&\text{region } 0: \ \mu_0=\mu_{vacuum} \ , \ \varepsilon_0'=\varepsilon_{vacuum} \\
&\text{region } -1: \ \mu_{-1}=\mu_{vacuum} \ , \ \varepsilon_{-1}'=\varepsilon_{rd}\,\varepsilon_{vacuum} \\
&\text{region } -2: \ \mu_{-2}=\mu_{vacuum} \ , \ \sigma_{-2}\to\infty \\
&m^2_{-0,-1} = m^2_{-1,-2} = 1 \\
&r^e_{-1,-2} = +1 \ , \ r^m_{-1,-2} = -1
\end{aligned} \tag{A.66}$$

where the relative dielectric constant ε_{rd} of the supporting substrate can in general be complex. The reflection functions R_0^{-e} and R_0^{-m} can also be determined in the more familiar form in terms of hyperbolic functions as

$$R_0^{-e} = \frac{\varepsilon_{rd}U_0 - U_{-1}\tanh(h_{-1}U_{-1})}{\varepsilon_{rd}U_0 + U_{-1}\tanh(h_{-1}U_{-1})} \tag{A.67}$$

$$R_0^{-m} = \frac{U_0 - U_{-1}\coth(h_{-1}U_{-1})}{U_0 + U_{-1}\coth(h_{-1}U_{-1})} \tag{A.68}$$

$$U_0 = \sqrt{k_x^2+k_z^2+k_0^2} = \sqrt{\lambda^2+k_0^2}$$
$$U_{-1} = \sqrt{k_x^2+k_z^2+\varepsilon_{rd}k_0^2} = \sqrt{\lambda^2+\varepsilon_{rd}k_0^2}$$

Usually the potential functions due to a horizontally polarized source situated on the surface of the substrate are required ($y'=0$). They can be determined for a $\hat{z}$ directed source $J_z(x,z)\hat{z}$ from (A.34,A.35) as

$$\Pi_z^0(k_x,y,k_z) = \frac{+j\omega\mu_0}{k_0^2} J_z(k_x,k_z)\left[\frac{1}{2U_0}(1+R_0^{-m})\right]e^{-U_0 y}$$
$$= \frac{+j\omega\mu_0}{k_0^2} J_z(k_x,k_z)\left[\frac{1}{D_{TE}}\right]e^{-U_0 y} \qquad (A.69)$$

$$\Pi_y^0(k_x,y,k_z) = \frac{+j\omega\mu_0}{k_0^2} J_z(k_x,k_z)\left[\left(\frac{jk_z U_0}{k_z^2+k_x^2}\right)\frac{1}{2U_0}(R_0^{-e}+R_0^{-m})\right]e^{-U_0 y}$$
$$= \frac{+j\omega\mu_0}{k_0^2} J_z(k_x,k_z)\left[\frac{(jk_z)(\varepsilon_{rd}-1)}{D_{TE}D_{TM}}\right]e^{-U_0 y} \qquad (A.70)$$

$$D_{TM} = \varepsilon_{rd}U_0 + U_{-1}\tanh(h_{-1}U_{-1})$$
$$D_{TE} = U_0 + U_{-1}\coth(h_{-1}U_{-1})$$

where D_{TE} is related to the transverse electric modes ($E_y=0$) produced in the substrate and D_{TM} is related to the transverse magnetic modes ($H_y=0$) produced in the substrate. This form, given in term of hyperbolic functions, is the form most often found in the literature.

A.2.3. Homogeneous Half-Space

In this section, the potential functions and fields due to sources located over a homogeneous lossy half-space are considered. The presented results are utilized throughout the thesis. The case has many applications; the propagation of currents along a system of conductors above the earth and associated coupling to external sources [Wait5, Chang3, Kuester2, Wait8, King3], antennas and scattering from finite conducting geometries for problems of radio [King2, King4, Hill], scattering and detection of buried objects and other remote sensing applications [Wait3, Wait12]. For simplicity, the subscripts describing the two media will be denoted as region e for the upper ($i=0$) half-space, and as region g for the lower ($i=-1$) half-space as

$$\text{region } e: \ \mu_e = \mu_{vacuum} \ , \ \varepsilon_e' = \varepsilon_{vacuum}$$
$$\text{region } g: \ \mu_g = \mu_{vacuum} \ , \ \varepsilon_g' = \varepsilon_{rg}\varepsilon_{vacuum} - j\omega\mu_g\sigma_g \qquad (A.71)$$
$$k_e = \sqrt{\omega^2\mu_e\varepsilon_e} \quad , \quad k_g = \sqrt{\omega^2\mu_g\varepsilon_g + j\omega\mu_g\sigma_g}$$

The two specific cases arising in most half-space problems are that of a horizontal line source and that of a vertically or horizontally polarized electric dipole located above a lossy earth.

i) Horizontal Line Source:

The vector potentials $\bar{\Pi}^e$ and $\bar{\Pi}^g$ and resulting fields for an infinite horizontal line source, $\bar{J}_s(x,z)=J_z(z)\delta(x-x')\delta(y-y')\hat{z}$, located at the point (x',y') above earth as

shown in figure A.3 are given using (A.41,A.42) as

$$\Pi_z^e(x,y,k_z) = \frac{+j\omega\mu_e}{2\pi k_e^2} J_z(k_z) \int_{-\infty}^{\infty} \left[\frac{e^{-U_e|y-y'|}}{2U_e} + r_{eg}^m \frac{e^{-U_e(y+y')}}{2U_e} \right] e^{+jk_x(x-x')} dk_x \qquad \text{(A.72)}$$

$$\Pi_y^e(x,y,k_z) = \frac{+j\omega\mu_e}{2\pi k_e^2} J_z(k_z) \int_{-\infty}^{\infty} \left[\left(\frac{jk_z}{k_z^2+k_x^2} \right) \frac{1}{2} [r_{eg}^e + r_{eg}^m] e^{-U_e(y+y')} \right] e^{+jk_x(x-x')} dk_x \qquad \text{(A.73)}$$

$$\Pi_z^g(x,y,k_z) = \frac{+j\omega\mu_e}{2\pi k_e^2} J_z(k_z) \int_{-\infty}^{\infty} \frac{1}{n^2} \left[t_{eg}^m \frac{e^{-U_e y' + U_g y}}{2U_g} \right] e^{+jk_x(x-x')} dk_x \qquad \text{(A.74)}$$

$$\Pi_y^g(x,y,k_z) = \frac{+j\omega\mu_e}{2\pi k_e^2} J_z(k_z) \int_{-\infty}^{\infty} \frac{1}{n^2} \left[\left(\frac{jk_z}{k_z^2+k_x^2} \right) \cdot \left[n^2 U_e t_{eg}^e - U_g t_{eg}^m \right] \frac{e^{-U_e y' + U_g y}}{2U_g} \right] e^{+jk_x(x-x')} dk_x \qquad \text{(A.75)}$$

$$r_{eg}^e = \frac{n^2 U_e - U_g}{n^2 U_e + U_g} \quad , \quad n^2 = \frac{\varepsilon_g'}{\varepsilon_e'}$$

$$r_{eg}^m = \frac{m^2 U_e - U_g}{m^2 U_e + U_g} \quad , \quad m^2 = \frac{\mu_g}{\mu_e}$$

$$t_{eg}^e = 1 - r_{eg}^e = \frac{2U_g}{n^2 U_e + U_g}$$

$$t_{eg}^m = 1 - r_{eg}^m = \frac{2U_g}{m^2 U_e + U_g}$$

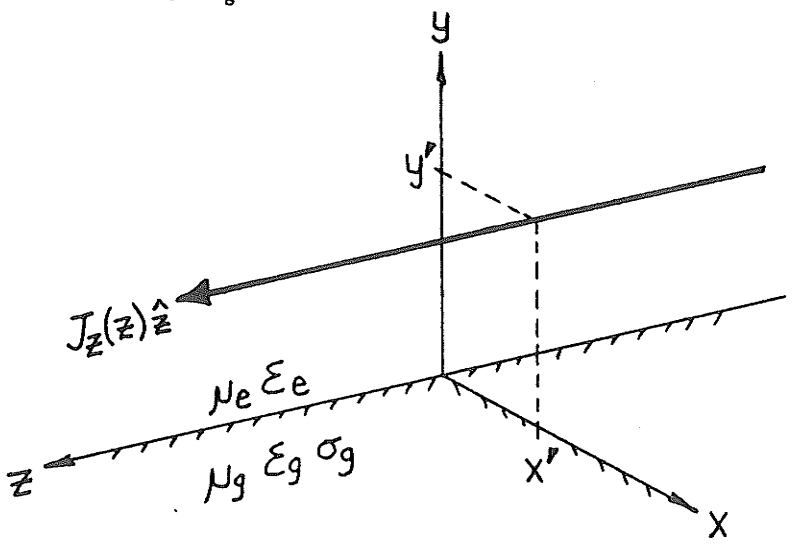

Figure A.3: Line source over homogeneous half-space.

where the fields in each of the regions are found using (A.2). The integrands of

(A.72) and (A.73), for the potential functions in the upper half-space, can be simplified into known forms along with two standard integrals as

$$\Pi_z^e(x,y,k_z) = \frac{+j\omega\mu_e}{2\pi k_e^2} J_z(k_z)\left[K_0(\tau_e \mid \overline{\rho} \mid) - K_0(\tau_e \mid \overline{\rho}^* \mid) + m^2 \mathbf{J}(\tau_e,\overline{\rho}^*)\right] \tag{A.76}$$

$$\Pi_y^e(x,y,k_z) = \frac{+j\omega\mu_e}{2\pi k_e^2} J_z(k_z)\left[(-jk_z)\left(\frac{n^2m^2-1}{n^2-m^2}\right)\int \mathbf{J}(\tau_e,\overline{\rho}^*) - \mathbf{G}(\tau_e,\overline{\rho}^*)dy\right] \tag{A.77}$$

$$\mathbf{J}(\tau_e,\overline{\rho}^*) = \int_{-\infty}^{\infty} \frac{1}{m^2U_e+U_g} e^{-U_e(y+y')+jk_x(x-x')}dk_x \tag{A.78}$$

$$\mathbf{G}(\tau_e,\overline{\rho}^*) = \int_{-\infty}^{\infty} \frac{1}{n^2U_e+U_g} e^{-U_e(y+y')+jk_x(x-x')}dk_x \tag{A.79}$$

$$U_e = \sqrt{k_x^2+k_z^2-k_e^2} = \sqrt{k_x^2+\tau_e^2} \qquad , \mathrm{Re}[U_e]\geq 0$$

$$U_g = \sqrt{k_x^2+k_z^2-k_g^2} = \sqrt{k_x^2+\tau_g^2} \qquad , \mathrm{Re}[U_g]\geq 0$$

$$\mid \overline{\rho} \mid = \sqrt{(x-x')^2+(y-y')^2} \quad , \quad \angle\overline{\rho} = \tan^{-1}\left(\frac{y-y'}{\mid x-x' \mid}\right)$$

$$\mid \overline{\rho}^* \mid = \sqrt{(x-x')^2+(y+y')^2} \quad , \quad \angle\overline{\rho}^* = \tan^{-1}\left(\frac{y+y'}{\mid x-x' \mid}\right)$$

where the parameters $\tau_e=\sqrt{k_z^2-k_e^2}$ and $\tau_g=\sqrt{k_z^2-k_g^2}$ are the transverse wave numbers in the air and earth media, respectively, and $n=k_g/k_e$ is the refractive index of the interface. The real parts of the irrationals $\mathrm{Re}[U_e,U_g]\geq 0$ and $\mathrm{Re}[\tau_e,\tau_g]\geq 0$ have been chosen to retain a positive value on the correct Riemann sheet, these branch cuts being defined to ensure that the currents and fields decay at infinity. $K_0(z)$ is the modified Bessel function of complex argument. In the derivation of (A.76), the term involving $K_0(\tau_e \mid \overline{\rho}_D \mid)$ is due to the primary field of the current source, and the term involving $K_0(\tau_e \mid \overline{\rho}_D^* \mid)$ is due to its image as if the earth were perfectly conducting. The remaining terms in integral form, (A.78) and (A.79), are the corrections due to the imperfectly conducting earth. The evaluation of the infinite integrals **J** and **G** are specifically addressed in appendix B. The fields can be determined using (A.2) for the case when the permeabilities of the earth and air half-spaces are equal $\mu_g=\mu_e$ ($m^2=1$) as

$$\overline{E}^i = \nabla\nabla\cdot\overline{\Pi}^i + k_i^2\overline{\Pi}^i \tag{A.80}$$

$$\overline{H}^i = \frac{k_i^2}{j\omega\mu_i}\nabla\times\overline{\Pi}^i \tag{A.81}$$

$$E_z^e(x,y,k_z) = \frac{-j\omega\mu_e}{2\pi k_e^2} J_z(k_z)\left[\tau_e^2[K_0(\tau_e \mid \bar{\rho} \mid) - K_0(\tau_e \mid \bar{\rho}^* \mid)]\right.$$
$$\left. - k_e^2 \mathbf{J}(\tau_e,\bar{\rho}^*) + k_z^2 \mathbf{G}(\tau_e,\bar{\rho}^*)\right] \quad \text{(A.82)}$$

$$E_x^e(x,y,k_z) = \frac{-j\omega\mu_e}{2\pi k_e^2} J_z(k_z)(+jk_z)\left[\frac{\tau_e(x-x')}{\mid \bar{\rho} \mid} K_1(\tau_e \mid \bar{\rho} \mid) - \frac{\tau_e(x-x')}{\mid \bar{\rho}^* \mid} K_1(\tau_e \mid \bar{\rho}^* \mid)\right.$$
$$\left. - \frac{\partial}{\partial x}\mathbf{G}(\tau_e,\bar{\rho}^*)\right] \quad \text{(A.83)}$$

$$E_y^e(x,y,k_z) = \frac{-j\omega\mu_e}{2\pi k_e^2} J_z(k_z)(+jk_z)\left[\frac{\tau_e(y-y')}{\mid \bar{\rho} \mid} K_1(\tau_e \mid \bar{\rho} \mid) - \frac{\tau_e(y+y')}{\mid \bar{\rho}^* \mid} K_1(\tau_e \mid \bar{\rho}^* \mid)\right.$$
$$\left. - \frac{\partial}{\partial y}\mathbf{G}(\tau_e,\bar{\rho}^*) + k_e^2 \int \mathbf{J}(\tau_e,\bar{\rho}^*) - \mathbf{G}(\tau_e,\bar{\rho}^*) dy\right] \quad \text{(A.84)}$$

$$E_z^g(x,y,k_z) = \frac{-j\omega\mu_e}{2\pi k_e^2} J_z(k_z) \frac{1}{n^2} \int_{-\infty}^{\infty} \left[\frac{1}{k_x^2+k_z^2}\left(\frac{-k_g^2 k_x^2}{U_e+U_g} + \frac{n^2 k_z^2 U_e U_g}{n^2 U_e + U_g}\right)\right]$$
$$\cdot\, e^{-U_e y' + U_g y} e^{+jk_x(x-x')} dk_x \quad \text{(A.85)}$$

Note that when the line source is located at the interface of the two half-spaces ($y' = 0$), the expressions for the $\hat{z}$ components of the fields in the two mediums as given by (A.82) and (A.85), are equivalent when the subscripts $e <-> g$ are interchanged.

ii) Dipole Source:

Similarly, the fields from a dipole source can be determined from the potential functions (A.33-A.40) for a horizontally polarized dipole and from (A.31) for a vertically polarized dipole. Thus, the $\hat{z}$ component of the electric field for the general dipole source $\bar{J}_s = (J_x\hat{x} + J_y\hat{y} + J_z\hat{z})\delta(x-x')\delta(y-y')\delta(z-z')$ is given from

$$E_z^e(x,y,k_z) = \frac{-j\omega\mu_e}{2\pi k_e^2} J_y(+jk_z)\left[\frac{\tau_e(y-y')}{\mid \bar{\rho} \mid} K_1(\tau_e \mid \bar{\rho} \mid) - \frac{\tau_e(y+y')}{\mid \bar{\rho}^* \mid} K_1(\tau_e \mid \bar{\rho}^* \mid)\right.$$
$$\left. - n^2 \frac{\partial}{\partial y}\mathbf{G}(\tau_e,\bar{\rho}^*)\right] e^{-jk_z z'} \quad \text{(A.86)}$$

$$E_z^e(x,y,k_z) = \frac{-j\omega\mu_e}{2\pi k_e^2} J_z\left[\tau_e^2[K_0(\tau_e \mid \bar{\rho} \mid) - K_0(\tau_e \mid \bar{\rho}^* \mid)]\right.$$
$$\left. - k_e^2 \mathbf{J}(\tau_e,\bar{\rho}^*) + k_z^2 \mathbf{G}(\tau_e,\bar{\rho}^*)\right] e^{-jk_z z'} \quad \text{(A.87)}$$

$$E_z^e(x,y,k_z) = \frac{-j\omega\mu_e}{2\pi k_e^2} J_x(+jk_z) \left[\frac{\tau_e(x-x')}{|\bar{\rho}|} K_1(\tau_e |\bar{\rho}|) - \frac{\tau_e(x-x')}{|\bar{\rho}^*|} K_1(\tau_e |\bar{\rho}^*|) - \frac{\partial}{\partial x} \mathbf{G}(\tau_e, \bar{\rho}^*) \right] e^{-jk_z z'} \tag{A.88}$$

As discussed in section A.1.1, any arbitrarily oriented dipole source $\bar{J}_s$ or $\bar{M}_s$ can be formulated in terms of a combination of vertical electric (VED) and vertical magnetic (VMD) dipoles, these representing the TM and TE fields, respectively. The $\hat{z}$ component of the electric field for a VED, $J_y \delta(x-x')\delta(y-y')\delta(z-z')\hat{y}$ was given by (A.86), with the corresponding value for a VMD, $M_y \delta(x-x')\delta(y-y')\delta(z-z')\hat{y}$ given as

$$E_z^e(x,y,k_z) = +\frac{1}{2\pi} M_y \left[\frac{\tau_e(x-x')}{|\bar{\rho}|} K_1(\tau_e |\bar{\rho}|) - \frac{\tau_e(x-x')}{|\bar{\rho}^*|} K_1(\tau_e |\bar{\rho}^*|) - \frac{\partial}{\partial x} \mathbf{J}(\tau_e, \bar{\rho}^*) \right] e^{-jk_z z'} \tag{A.89}$$

Appendix B
Solution of Sommerfeld Type Integrals

In this appendix, the evaluation of the Fourier integrals arising in the solution of the potential functions and fields due to the guiding wave structures studied in this thesis will be discussed. The infinite integrals arise from the transform solution of the Green's functions, satisfying the wave equation for a stratified media, as developed in appendix A. These integrals are often referred to as Sommerfeld type integrals due to his solution of the half-space problem in 1909 [Sommerfeld2]. The integrals requiring evaluation can all be described as a two-dimensional transform of the type

$$F(x,y,z) = \Gamma_z^{-1}\Gamma_x^{-1}\left\{ f(k_x,k_z)e^{-U_i|y|} \right\}$$

$$= \frac{1}{2\pi}\int_{-\infty}^{\infty}\frac{1}{2\pi}\int_{-\infty}^{\infty} f(k_x,k_z)e^{-U_i|y|+jk_x x+jk_z z}\,dk_x\,dk_z \qquad \text{(B.1)}$$

$$U_i = \sqrt{k_x^2+k_z^2-k_i^2} = \sqrt{k_x^2+\tau_i^2}$$

$$\tau_i = \sqrt{k_z^2-k_i^2}$$

where i denotes the medium in which the observation point is located, this being one of the possible layers in the stratified geometry as was shown in figure A.1. Here k_i is the propagation constant in each region, with τ_i the transverse wave number dependent on the axial spectral component k_z. The order of integration in (B.1) is chosen for a geometry where the stratified media is layered in the y-dimension and the guiding wave structure extends in the z-dimension. As described in section A.1, the general problem consists of $-M^- < i < +M^+$ planar regions in total with $i=-M^-$ denoting the lower most layer and $i=+M^+$ denoting the upper most layer. The kernel $f(k_x,k_z)$ is dependent on the geometry and is a function of the irrationals U_i which are defined for each of the layers in the stratified structure. As discussed in section 2.6, there will be two branch cuts $\mathrm{Re}[U_{+M^+},U_{-M^-}]\geq 0$ due to the requirement that the fields decay at $|y|\rightarrow\infty$. These branch cuts are present in both the k_z and k_x spectral domains as shown in figure B.1, and given the order of integration in (B.1), emanate from the branch points $\pm k_{+M^+}$, $\pm k_{-M^-}$ and $\pm j\tau_{+M^+}$, $\pm j\tau_{-M^-}$, respectively. These branch cuts represent the radiated fields into the uppermost and lowermost media. As well as containing the radiation branch cuts, the kernel may also contain a set of poles which occur for a specific combination of the spectral components k_z and k_x. These are

denoted as $\lambda_{Bs}=\sqrt{k_x^2+k_z^2}$; $s=1,2,...,S$, and represent the radial wavenumbers of the possible surface waves which are supported by the layered geometry. They arise from the zeros of the denominators of the TM and TE potential functions $\mathbf{V}_y^{REF}$ and $\mathbf{U}_y^{REF}$ defined in appendix A. Thus, given the order of integration in (B.1), the surface waves result in a set of poles in the k_x domain located at $k_{xBs}=\pm j\sqrt{k_z^2-\lambda_{Bs}^2}$ and a corresponding set of branch cuts in the k_z domain emanating from the branch points $k_{zBs}=\pm\lambda_{Bs}$. The branch cuts arise from the irrationals $\mathrm{Im}[k_{xBs}]\geq 0$ defined so that the surface wave fields decay at $|x|\to\infty$. Finally, a set of poles is also present in the k_z domain only, denoted as $\pm k_z^p; p=1,2,...,P$. These poles represent the contributions of the guided waves supported by the cylindrical structure. Note that if all the media are assumed lossless, the poles and branch cuts would fall on the real axis of integration

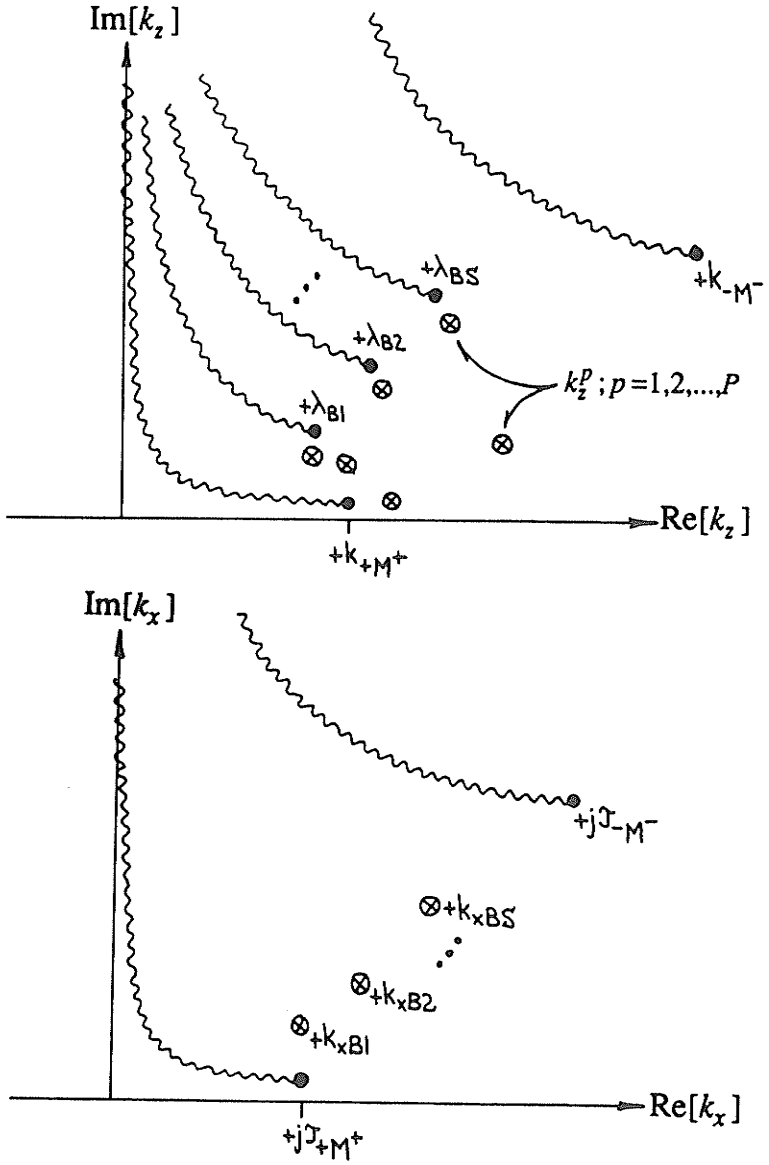

Figure B.1: Radiation and surface wave branch cuts, and guided wave poles in the complex k_z and k_x planes.

(as in cases encountered in the evaluation of lossless dielectric and perfectly conducting structures for example). Also, for the special case of a geometry which is symmetric in both the x- and z-dimensions, as in the case of a dipole source, the double infinite integral can be evaluated as a single integral using the Hankel transform [Sommerfeld3] as described in A.1.4.

Exact analytical solution of integrals of the type (B.1) is difficult due to the presence of the irrationals and singularities. Asymptotic expressions can be developed for the small argument cases and techniques such as the method of steepest descent can be used for the large argument cases. For accurate evaluation of the integrals, and to extract the proper behavior of all the field components (surface waves etc.), numerical techniques must usually be employed. Numerical evaluation is not straightforward, however, due to the possible highly oscillatory nature of the integrals as well as the presence of the singularities. In this appendix, a review of some of the approximation techniques for these integrals is made, and based on these, various expressions commonly available in the literature are derived for the special case of a lossy half-space. Some new closed form expressions are also presented for two of the integrals arising in the half-space problem, and which are consistently utilized throughout the thesis. As well, a technique for the numerical integration of the layered media double infinite integrals is presented. The proposed method has the advantage that it accounts for the possible highly oscillatory nature of the integrand when evaluated in the far field region.

B.1. ANALYTICAL EVALUATION OF THE INTEGRALS J AND G

The evaluation of two of the integrals arising in the study of half-space geometries will be discussed in detail. This special case occurs in many engineering problems involving transmission line structures located above or embedded in a homogeneous lossy media (usually the upper medium is air and the lower medium earth or water). Analytical expressions in terms of series expansions will be developed in the following sections as well as approximate solutions for both the small argument and large argument regions. A discussion of the numerical evaluation of these integrals by referring to the general form (B.1) will be given in the last section. The integrals $\mathbf{J}(\tau_e,\overline{\rho})$ and $\mathbf{G}(\tau_e,\overline{\rho})$ used throughout the thesis are given as a function of the transform variable k_z by defining the kernel in (B.1) as

$$\mathbf{J}(\tau_e=\sqrt{k_z^2-k_e^2},\overline{\rho}): \qquad f(k_x,k_z) = \frac{1}{\sqrt{k_x^2+k_z^2-k_e^2}+\sqrt{k_x^2+k_z^2-k_g^2}} \tag{B.2}$$

$$\mathbf{G}(\tau_e=\sqrt{k_z^2-k_e^2},\overline{\rho}): \qquad f(k_x,k_z) = \frac{1}{n^2\sqrt{k_x^2+k_z^2-k_e^2}+\sqrt{k_x^2+k_z^2-k_g^2}} \tag{B.3}$$

where k_e and k_g are the propagation constants in each of the the upper and lower

mediums, respectively, and $n=k_g/k_e$ is the refractive index at their interface. For a two layer structure there corresponds only the two irrationals, U_e and U_g. The two integrals arise in the formulation of the Green's functions for sources located over a lossy half-space as derived in appendix A (A.78,A.79). Their solution is imperative for the study of transmission line problems above an earth and their evaluation has been studied for decades.

B.1.1. J Function Evaluation

This section presents various methods of evaluating the Fourier integral $\mathbf{J}(\tau_e,\overline{\rho})$ arising in problems of a lossy earth as defined by

$$\mathbf{J}(\tau_e,\overline{\rho}) = \int_{-\infty}^{\infty} \frac{1}{U_e+U_g} e^{-U_e|y|+jk_x x}\, dk_x \tag{B.4}$$

$$U_e = \sqrt{k_x^2+k_z^2-k_e^2} = \sqrt{k_x^2+\tau_e^2} \qquad ; \mathrm{Re}[U_e]\geq 0$$
$$U_g = \sqrt{k_x^2+k_z^2-k_g^2} = \sqrt{k_x^2+\tau_g^2} \qquad ; \mathrm{Re}[U_g]\geq 0$$
$$|\overline{\rho}| = \sqrt{x^2+y^2} \quad , \quad \angle\overline{\rho} = \tan^{-1}(y/x) \qquad , [x,y]\geq 0$$

where k_e and k_g are the propagation constants in the upper and lower media. The parameters τ_e and τ_g, $\mathrm{Re}[\tau_e,\tau_g]\geq 0$, represent the transverse wave numbers in the air and earth media, respectively, and are in general complex. The irrationals U_e, U_g are defined so that the integral decays as $|y|\to\infty$, thus giving the two branch points $\pm j\tau_e$, $\pm j\tau_g$ and associated branch cuts in the complex k_x plane as shown in figure B.2. It is evident that the integrand of (B.4) contains no singularities since $\mathrm{Re}[U_e,U_g]\geq 0$.

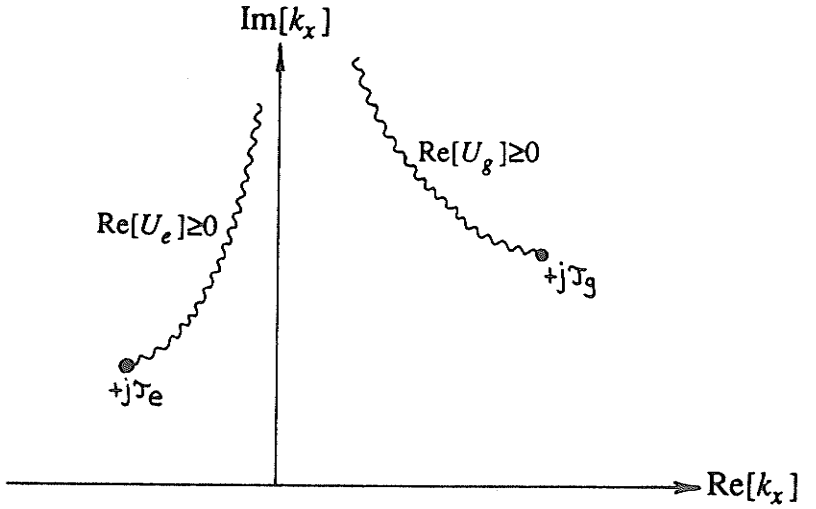

Figure B.2: Branch cuts in the complex k_x plane for $\mathbf{J}(\tau_e,\overline{\rho})$.

The integral $\mathbf{J}(\tau_e,\overline{\rho})$ results from the TE potential function $\mathbf{U}_y^{REF}$, and as it is mainly responsible for conduction losses in the earth, has an appreciable value over

most of the frequency spectrum for typical earth parameters. Various analytical expressions for its evaluation are well documented in the literature. Carson evaluated the integral in the quasi-static region under the assumption $\tau_e = 0$ (the axial propagation constant is equal to the free space value $k_z = k_e$) and gave a solution in terms of a series expansion [Carson]. This formulation has been widely applied at power transmission frequencies, with an improvement found using an effective expression in terms of Struve functions which is valid in the small argument range ($\tau_e \to 0$) [Wait1, Perelman]. Methods utilizing the complex image theory technique of van der Pol are also available in the quasi-static region [vanderPol, Wait2]. For the large argument range (far field), expressions for the integral have also been developed using an asymptotic technique or method of steepest descent [Chiba, Carpentier1]. In the intermediate argument range, expressions which are valid under various restrictions are also available in the literature [Chang3, Olsen5, Kuester4, Aboul-Atta].

A general expression for evaluating $\mathbf{J}(\tau_e, \bar{\rho})$ can be developed for small τ_e by factoring the integrand of (B.4) and evaluating the resulting integral in two parts as

$$\mathbf{J}(\tau_e, \bar{\rho}) = \frac{1}{(n^2-1)k_e^2} \int_{-\infty}^{\infty} [U_e - U_g] e^{-U_e |y| + jk_x x} dk_x = \mathbf{J}_1 + \mathbf{J}_2 \tag{B.5}$$

The solution of the first integral $\mathbf{J}_1$ is straight forward by recognizing the relationship

$$\begin{aligned} \mathbf{J}_1 &= \frac{1}{(n^2-1)k_e^2} \int_{-\infty}^{\infty} U_e e^{-U_e |y| + jk_x x} dk_x \\ &= \frac{2}{(n^2-1)k_e^2} \frac{\partial^2}{\partial y^2} K_0(\tau_e |\bar{\rho}|) \\ &= \frac{-2}{(n^2-1)k_e^2} \left[\frac{(\tau_e |\bar{\rho}|) K_1(\tau_e |\bar{\rho}|) - (\tau_e y)^2 K_2(\tau_e |\bar{\rho}|)}{|\bar{\rho}|^2} \right] \end{aligned} \tag{B.6}$$

The solution of the second integral $\mathbf{J}_2$ is more difficult since the irrationals in the numerator and exponent differ. For $\tau_e \ll 1$, the irrational U_e can be represented using the binomial expansion $\sqrt{k_x^2 + \tau_e^2} = |k_x| (1 + (\tau_e/k_x)^2/2 + \cdots)$, and each of the resulting exponential terms can then be written in a power series. An integratable form for $\mathbf{J}_2$ can then be found by collecting powers of k_x^{-n} to yield

$$\begin{aligned} \mathbf{J}_2 &= \frac{-1}{(n^2-1)k_e^2} \int_{-\infty}^{\infty} U_g e^{-U_e |y| + jk_x x} dk_x \\ &\approx \frac{-1}{(n^2-1)k_e^2} \sum_{n=0}^{\infty} A_n \int_{-\infty}^{\infty} U_g |k_x|^{-n} e^{-|k_x y| + jk_x x} dk_x \end{aligned} \tag{B.7}$$

where

$$A_0 = +1 \qquad A_1 = -\frac{(\tau_e^2 y)}{2}$$

$$A_2 = +\frac{(\tau_e^4 y^2)}{8} \qquad A_3 = -\frac{(\tau_e^6 y^3)}{48} + \frac{(\tau_e^4 y)}{8} \tag{B.8}$$

$$A_4 = +\frac{(\tau_e^8 y^4)}{384} - \frac{(\tau_e^6 y^2)}{16} \qquad A_5 = -\frac{(\tau_e^{10} y^5)}{3840} + \frac{(\tau_e^8 y^3)}{64} \quad \ldots$$

Using appropriate transformations, integrals of the type (B.7) can be identified in terms of recursive integrals of Struve functions $\mathbf{T}_n(z)$ as

$$\mathbf{J}_2 \approx \frac{-1}{(n^2-1)k_e^2} \sum_{n=0}^{\infty} A_n \frac{\tau_g^2}{\tau_g^n} \left[\mathbf{T}_n(z_1) + \mathbf{T}_n(z_2) \right] \tag{B.9}$$

$$z_1 = \tau_g (y+jx) \quad , \quad z_2 = \tau_g (y-jx)$$

$$\mathbf{T}_n(z) = \int_0^{\infty} \sqrt{1+w^2}\, w^{-n} e^{-wz}\, dw = \int_z^{\infty} \mathbf{T}_{n-1}(z)\, dz \tag{B.10}$$

$$\mathbf{T}_0(z) = \int_0^{\infty} \sqrt{1+w^2}\, e^{-wz}\, dw = +\frac{\pi}{2} \left[\frac{\mathbf{H}_1(z) - Y_1(z)}{z} \right] \tag{B.11}$$

where $\mathbf{H}_1(z)$ is the first order Struve function and $Y_1(z)$ is the first order Bessel function of the second kind [Abramowitz]. Series expansions for the recursive integral $\mathbf{T}_n(z)$ can then be developed using the relation (B.10) and expressions for the first order Struve and Bessel functions in (B.11). A first order approximation for $\mathbf{J}(\tau_e, \overline{\rho})$ is given by the $n=0$ term in (B.9) as

$$\mathbf{J}(\tau_e, \overline{\rho}) \approx \frac{-2}{(n^2-1)k_e^2} \left\{ \left[\frac{(\tau_e |\overline{\rho}|) K_1(\tau_e |\overline{\rho}|) - (\tau_e y)^2 K_2(\tau_e |\overline{\rho}|)}{|\overline{\rho}|^2} \right] + \tau_g^2 \frac{\pi}{4} \left[\frac{\mathbf{H}_1(z_1) - Y_1(z_1)}{z_1} + \frac{\mathbf{H}_1(z_2) - Y_1(z_2)}{z_2} \right] \right\} \tag{B.12}$$

This is the form developed by Perel'man [Perelman] and in a similar manner when $\tau_e = 0$ by Wait [Wait1] and Shen [Shen3].

B.1.2. Other Approximations for J

Under the quasi-static assumption, where the axial variation of the fields is assumed to be equal to the free space value $k_z \approx k_e$ ($\tau_e = 0$), the integral $\mathbf{J}(\tau_e = 0, \overline{\rho})$ can be evaluated as

$$\mathbf{J}_c(\overline{\rho}) = \mathbf{J}(\tau_e = 0, \overline{\rho}) = \frac{2}{(n^2-1)k_e^2} \int_0^{\infty} \left[\lambda - \sqrt{\lambda^2 - (n^2-1)k_e^2} \right] e^{-\lambda |y|} \cos(\lambda x)\, d\lambda \tag{B.13}$$

This is the integral form formulated by Carson in 1926 [Carson] in his quasi-static evaluation of the conductor over lossy half-space problem. Assuming $k_g \approx \sqrt{j\omega\mu_g\sigma_g}$, Carson gave a solution to (B.13) through two terms $\mathbf{J}_c = P + jQ$, which were evaluated by an infinite series (known as Carson's series). The convergence of the series has been examined in a number of references [Dommel]. Wise latter improved the series by including the effect of polarization currents (Carson's $k_g \approx \sqrt{j\omega\mu_g\sigma_g}$ was replaced by $k_g = \sqrt{\omega^2\mu_g\varepsilon_g + j\omega\mu_g\sigma_g}$) [Wise]. The evaluation of (B.13) can easily be realized by letting $\tau_e \to 0$ in (B.12) giving

$$\mathbf{J}_c(\bar{\rho}) = \frac{-2}{(n^2-1)k_e^2}\left[\frac{x^2-y^2}{|\bar{\rho}|^4}\right] + \frac{\pi}{2}\left[\frac{\mathbf{H}_1(z_1)-Y_1(z_1)}{z_1} + \frac{\mathbf{H}_1(z_2)-Y_1(z_2)}{z_2}\right] \tag{B.14}$$

$$z_1 = -jk_e\sqrt{n^2-1}(y+jx) \approx -jk_g(y+jx)$$

$$z_2 = -jk_e\sqrt{n^2-1}(y-jx) \approx -jk_g(y-jx)$$

This form was developed by Wait [Wait1] and latter by King, Shen and others [King1, King3, Shen3, Chen], with series expressions also given in [Shen3].

The evaluation of the reflected fields using complex image theory was first introduced by van der Pol in 1935 [vanderPol, Stratton] in connection with the evaluation of the Sommerfeld integrals for a dipole source over a lossy half-space. The theory was latter extensively applied to line source problems for geophysical remote sensing applications [Wait4, Bannister1, bannister2, Bannister3]. Its more recent utilization in the power engineering field was made by Deri and Semlyen [Deri]. As well, an exact image theory for electric and magnetic dipole sources over a lossy half-space has recently been developed by Lindel [Lindell1, Lindell2, Lindell3]. The quasi-static image theory of van der Pol is implemented by subtracting the field due to the source's image as if it was over a perfectly conducting earth from the correction term $\mathbf{J}_c$, which accounts for the finite conductivity. Thus, (B.13) can be formulated [Wait4] by considering

$$\mathbf{J}_c(\bar{\rho}) + \ln(|\bar{\rho}|) = \int_0^\infty \left[\frac{2}{\lambda+\sqrt{\lambda^2-(n^2-1)k_e^2}} - \frac{1}{\lambda}\right] e^{-\lambda|y|}\cos(\lambda x)d\lambda$$

$$= \int_0^\infty \frac{\lambda-U_g}{\lambda+U_g}\frac{e^{-\lambda|y|}}{\lambda}\cos(\lambda x)d\lambda$$

$$\approx -\int_0^\infty \frac{e^{-\lambda(|y|+\alpha)}}{\lambda}\cos(\lambda x)d\lambda \tag{B.15}$$

where $U_g = \sqrt{\lambda^2-(n^2-1)k_e^2}$ and $\alpha = +j2/k_e\sqrt{n^2-1}$. In (B.15), the singular part of the integral $\mathbf{J}_c$ has been removed by adding the logarithmic term. The modified integrand has then been approximated by the first term of its Taylor series expansion. The

remaining integral in (B.15) can then be recognized as

$$J_c(\bar{\rho}) + \ln(|\bar{\rho}|) \approx \ln(|\bar{\rho}'|) \tag{B.16}$$

$$|\bar{\rho}'| = \sqrt{x^2 + (|y|+\alpha)^2} \quad ; \alpha = \frac{+j2}{k_e\sqrt{n^2-1}} \approx \frac{+j2}{\sqrt{j\omega\mu_g\sigma_g}} = (1+j)\delta$$

where $\delta = \sqrt{2/\omega\mu_g\sigma_g}$ is the skin depth in the earth medium. Higher order terms in the expansion of (B.15) can also be included to give a more accurate result [Olsen7].

Chang and Wait [Chang1] have formulated the special case when the source and the observation points are much less than the skin depth in the lossy medium $|\bar{\rho}| \ll \delta$. Noting that both $\mathbf{J}(\tau_e,\bar{\rho})$ and $K_0(\tau_e|\bar{\rho}|)$ possess an order $\mathbf{O}(\ln(\tau_e|\bar{\rho}|))$ singularity as $|\bar{\rho}| \to 0$, the evaluation of (B.4) can be approximated using their integral representations as [Abramowitz]

$$\mathbf{J}(\tau_e,\bar{\rho}) - K_0(\tau_e|\bar{\rho}|) = \int_{-\infty}^{\infty}\left[\frac{1}{U_e+U_g} - \frac{1}{2U_e}\right]e^{-U_e|y|+jk_x x}\,dk_x$$

$$\xrightarrow[x,y\to 0]{} \frac{\tau_g^2}{(n^2-1)k_e^2}\ln\left[\frac{\tau_g}{\tau_e}\right] + \frac{1}{2} \tag{B.17}$$

$$\mathbf{J}(\tau_e,\bar{\rho}) \xrightarrow[|\bar{\rho}|\to 0]{} -\ln\left[\tau_e|\bar{\rho}|\right] + \frac{\tau_g^2}{(n^2-1)k_e^2} + \frac{1}{2} \tag{B.18}$$

B.1.3. G Function Evaluation

This section presents methods of evaluating the Fourier integral $\mathbf{G}(\tau_e,\bar{\rho})$ arising in problems of a lossy earth as defined by

$$\mathbf{G}(\tau_e,\bar{\rho}) = \int_{-\infty}^{\infty}\frac{1}{n^2U_e+U_g}e^{-U_e|y|+jk_x x}\,dk_x \tag{B.19}$$

$$U_e = \sqrt{k_x^2+k_z^2-k_e^2} = \sqrt{k_x^2+\tau_e^2} \qquad ; \mathrm{Re}[U_e]\geq 0$$

$$U_g = \sqrt{k_x^2+k_z^2-k_g^2} = \sqrt{k_x^2+\tau_g^2} \qquad ; \mathrm{Re}[U_g]\geq 0$$

$$|\bar{\rho}| = \sqrt{x^2+y^2} \quad , \quad \angle\bar{\rho} = \tan^{-1}(y/x) \quad , [x,y]\geq 0$$

where k_e and k_g are the propagation constants in the upper and lower media. The parameters τ_e and τ_g, $\mathrm{Re}[\tau_e,\tau_g]\geq 0$, are the transverse wave numbers in the air and earth media, respectively, and $n=k_g/k_e$ is the refractive index at the interface. The irrationals U_e and U_g represent two sets of branch cuts with branch points at $\pm j\tau_e$ and $\pm j\tau_g$ as defined for the function $\mathbf{J}(\tau_e,\bar{\rho})$ in the last section. However, a pair of simple poles located at $\pm k_{xB}$ in the complex k_x plane are also present as shown in figure B.3. The pole locations are defined by setting the denominator of (B.19) to zero yielding

$$k_{xB} = \pm j\tau_e\sqrt{1-s^2} \quad , \; s = \frac{U_{eB}}{\tau_e} = \frac{+jk_e}{\tau_e\sqrt{n^2+1}} \tag{B.20}$$

The location of the poles in the complex k_x plane is dependent on the refractive index n of the interface and on the value of the spectral component k_z. The poles represent a surface wave contribution to the field, a result of the TM potential function $\mathbf{V}_y^{REF}$. The pole k_{xB} is present at all frequencies (has no cut-off) and is defined for a specific radial wavenumber

$$\sqrt{k_{xB}^2+k_z^2} = \lambda_B = \frac{+k_g}{\sqrt{n^2+1}} \tag{B.21}$$

by the electrical properties of the interface alone. Figure B.3 gives possible movement of the pole in the complex k_x plane as a function of frequency for fixed earth parameters. At low frequencies, the pole is located near the branch point $+j\tau_e$. In the high frequency limit, the pole location approaches the imaginary k_x axis $k_{xB} \rightarrow +jk_e/\sqrt{\varepsilon_{rg}+1}$. Note that the pole can cross the real k_x axis for specific values of τ_e, this occurring under the condition $\mathrm{Re}[k_{xB}]=0$ ($\mathrm{Im}[\tau_e^2]=\mathrm{Im}[k_e^2/(n^2+1)]$). This situation arises in the very high frequency region for typical earth parameters. The contribution of the pole to the function $\mathbf{G}(\tau_e,\bar{\rho})$ can be extracted from (B.19) as

$$\mathbf{G}_p = \frac{2n^2}{n^4-1}\left[\frac{\pi s}{\sqrt{1-s^2}}\right] e^{-\sqrt{\tau_e^2-U_{eB}^2}\,|x| - U_{eB}|y|} \tag{B.22}$$

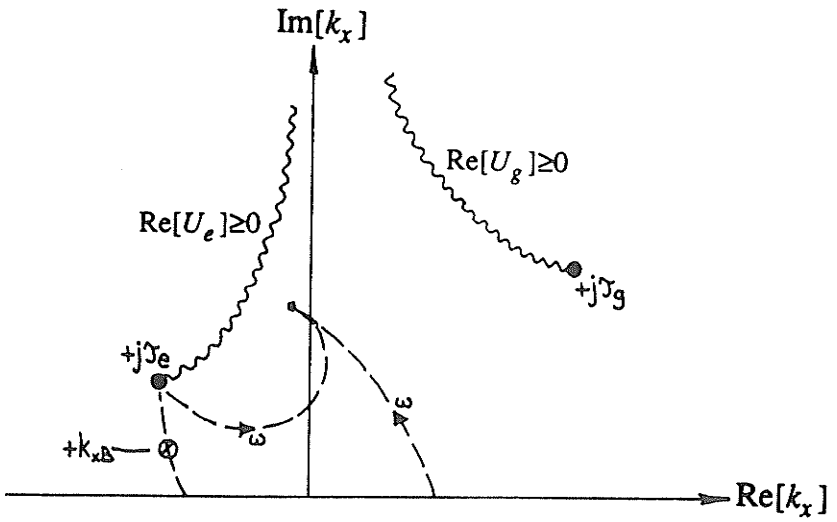

Figure B.3: Branch cuts and surface wave pole in the complex k_x plane for $\mathbf{G}(\tau_e,\bar{\rho})$.

Examination of (B.22) shows it is possible to find a value of τ_e (and thus k_z) which allows the pole contribution to approach infinity. This is given by

$$\tau_e \rightarrow U_{eB} = \frac{+jk_e}{\sqrt{n^2+1}} \quad \text{or alternatively} \quad k_z \rightarrow \lambda_B = \frac{+k_g}{\sqrt{n^2+1}} \tag{B.23}$$

such that $k_z=\lambda_B$ is defined to be the branch point k_{zB}, with U_{eB} being the corresponding propagation constant of the surface wave in the $\hat{y}$ direction (perpendicular to the planar media). The location of the pole U_{eB} in the complex τ_e plane as well as possible paths of the irrational U_e are shown in figure B.4. For given earth parameters, the pole $U_{eB}\rightarrow 0$ for $\omega\rightarrow 0$ and $U_{eB}\rightarrow jk_e/\sqrt{\varepsilon_{rg}+1}$ for $\omega\rightarrow\infty$. It is also possible for the branch cut of U_g to cross the real k_x axis in figure B.3, this occurring under the condition $\mathrm{Im}[\tau_g^2]=0$.

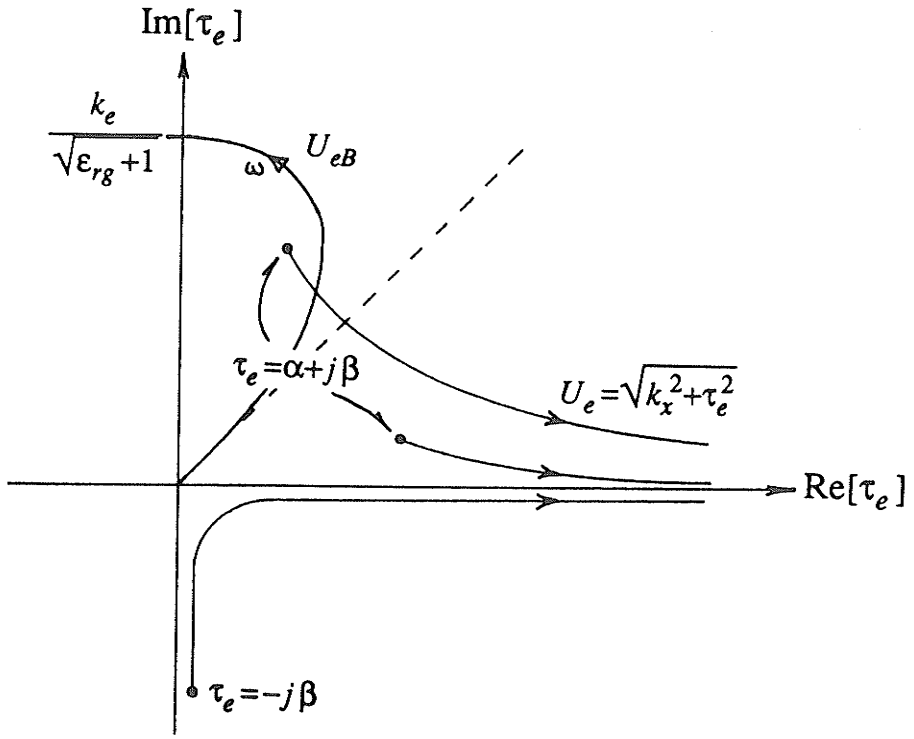

Figure B.4: Complex τ_e plane giving the pole U_{eB} and possible paths of U_e as a finction of τ_e.

The integral $\mathbf{G}(\tau_e,\bar{\rho})$, resulting from the TM potential function $\mathbf{V}_y^{REF}$, is mainly responsible for displacement current losses in the earth. Due to the factor n in the denominator of the integrand, the contribution of the function is small for low frequencies and high earth conductivities, and thus, it is usually completely neglected in quasi-static approximations. However, at higher frequencies, the contribution of $\mathbf{G}(\tau_e,\bar{\rho})$ can not be ignored and in fact may take on an appreciable value if evaluated near the pole $\tau_e\rightarrow U_{eB}$ (the fields then being mainly due to their surface wave contributions).

Various analytical as well as numerical methods can be used to evaluate the $\mathbf{G}(\tau_e,\bar{\rho})$ function. Unlike the function $\mathbf{J}(\tau_e,\bar{\rho})$, it can not be reduced to easily identified integral forms. Instead, an analytical formulation will be developed by factoring the integrand around the pole and then evaluating it in two parts as [Bridges3]

$$\frac{1}{n^2U_e + U_g} = \frac{n^2}{n^4 - 1}\left[\frac{1}{U_e - U_{eB}} - \frac{1}{n^2}\frac{1}{U_g + U_{gB}}\right] \tag{B.24}$$

where $U_{gB} = -n^2U_{eB}$. The integral can now be evaluated as

$$\mathbf{G}(\tau_e,\bar{\rho}) = \mathbf{G}_0(\tau_e,\bar{\rho}) + \mathbf{G}_1(\tau_e,\bar{\rho}) \tag{B.25}$$

$$\mathbf{G}_0(\tau_e,\bar{\rho}) = \frac{n^2}{n^4 - 1}\int_{-\infty}^{\infty}\frac{1}{U_e - U_{eB}}e^{-U_e|y|+jk_x x}\,dk_x \tag{B.26}$$

$$\mathbf{G}_1(\tau_e,\bar{\rho}) = \frac{-1}{n^4 - 1}\int_{-\infty}^{\infty}\frac{1}{U_g + U_{gB}}e^{-U_e|y|+jk_x x}\,dk_x \quad . \tag{B.27}$$

The integral $\mathbf{G}_1$ can usually be neglected when compared to $\mathbf{G}_0$ for large values of refractive index n. For moderate values of n, $\mathbf{G}_1$ can be approximated using the integral form for $K_1(z)$ [Abramowitz] as

$$\mathbf{G}_1(\tau_e,\bar{\rho}) \approx \frac{1}{n^4 - 1}\frac{1}{n^2 s}\left(\frac{|y|}{|\bar{\rho}|}\right)K_1(\tau_e|\bar{\rho}|) \quad . \tag{B.28}$$

To evaluate the remaining integral, note that $\mathbf{G}_0$ is a solution of the homogeneous two-dimensional wave equation as well as a first order differential equation as [Grinberg]

$$\begin{aligned}\left(\frac{\partial^2}{\partial x^2} + \frac{\partial^2}{\partial y^2} - \tau_e^2\right)\mathbf{G}_0(\tau_e,\bar{\rho}) &= 0 \qquad\qquad , \ |\bar{\rho}| \neq 0 ,\\ \left(\frac{\partial}{\partial y} + U_{eB}\right)\mathbf{G}_0(\tau_e,\bar{\rho}) &= \frac{2n^2}{n^4 - 1}\frac{\partial}{\partial y}K_0(\tau_e|\bar{\rho}|) \quad , \ U_e \neq U_{eB} .\end{aligned} \tag{B.29}$$

Accordingly, a general solution can be constructed in terms of an exact particular solution plus a homogeneous part. Now, by rearranging the integrand of (B.26) and by utilizing an appropriate transformation

$$\begin{aligned}\mathbf{G}_0(\tau_e,\bar{\rho}) = \frac{2n^2}{n^4 - 1}\Bigg[&K_0(\tau_e|\bar{\rho}|) + U_{eB}e^{-U_{eB}|y|}\int_{|y|}^{\infty}e^{U_{eB}t}K_0(\tau_e\sqrt{x^2+t^2})\,dt\\ &+ C\left(\frac{\pi s}{\sqrt{1 - s^2}}\right)e^{-\sqrt{\tau_e^2 - U_{eB}^2}|x| - U_{eB}|y|}\Bigg]\end{aligned} \tag{B.30}$$

where the arbitrary constant C defines the residue contribution due to the singularity of the integrand near the pole $U_e = U_{eB}$ and is yet to be determined. This solution, for any value of C, is validated by direct substitution into (B.29). The incomplete integral term present in (B.30) can be evaluated in the uniformly convergent region $\mathrm{Re}[U_{eB}/\tau_e]<1$ by invoking the addition theorem of cylindrical functions [Stratton] to

obtain

$$G_0(\tau_e,\bar{\rho}) = \frac{2n^2}{n^4-1}\left[K_0(\tau_e \mid \bar{\rho} \mid) + I_0(\tau_e x)V_0(z,s) + 2\sum_{m=1}^{\infty}(-1)^m I_{2m}(\tau_e x)V_{2m}(z,s) + C\left(\frac{\pi s}{\sqrt{1-s^2}}\right)e^{-\sqrt{\tau_e^2-U_{eB}^2}\mid x \mid -U_{eB}\mid y \mid}\right] \quad \text{(B.31)}$$

where

$$V_m(z,s) = se^{-sz}\int_z^{\infty} e^{st}K_m(t)\,dt \quad , z = \tau_e \mid y \mid \quad . \quad \text{(B.32)}$$

Here $V_m(z,s)$ is an incomplete integral of the modified Bessel function $K_m(t)$. The choice of expanding the series with $K_m(t)$ in the integrand in (B.30) was made since the series convergence is more rapid under the condition $\mid y \mid > x$. This situation is the one most often encountered in transmission line above earth problems. A reciprocal form of (B.30) can alternatively be developed in terms of incomplete integrals of the modified Bessel function $I_m(t)$ for situations where $x > \mid y \mid$. $V_m(z,s)$ can be solved in terms of a recursion relation for $m>0$ as

$$\begin{aligned} V_1(z,s) &= s[K_0(z) + V_0(z,s)] \\ V_m(z,s) &= 2s[K_{m-1}(z) + V_{m-1}(z,s)] - V_{m-2}(z,s) \quad . \end{aligned} \quad \text{(B.33)}$$

Thus, only the term $V_0(z,s)$ requires evaluation. $V_0(z,s)$ is of similar form to the incomplete Lipschitz-Hankel integral [Agrest, Kuester3] and can be solved analytically by expanding the exponential function within the integrand. Then, the integration of every term of the resulting series is executable analytically as

$$\begin{aligned} V_0(z,s) &= se^{-sz}\left\{A_0^{\infty}\left[\frac{\pi}{2} - zK_0(z) - \frac{\pi z}{2}[\,\mathbf{L}_0(z)K_1(z) + \mathbf{L}_1(z)K_0(z)\,]\right]\right. \\ &\quad + B_0^{\infty}\left[zK_1(z)\right] + \sum_{k=1}^{\infty}[\,zK_1(z) + (2k-1)K_0(z)\,]z^{2k-1}\left(\frac{2^{2k}(k!)^2}{(2k!)^2}\right)A_k^{\infty} \\ &\quad \left. + \sum_{k=1}^{\infty}[\,zK_1(z) + (2k)K_0(z)\,]z^{2k}\left(\frac{1}{2^{2k}(k!)^2}\right)B_k^{\infty}\right\} \end{aligned} \quad \text{(B.34)}$$

where

$$A_k^{\infty} = \sum_{r=k}^{\infty}\left(\frac{(2r)!}{2^{2r}(r!)^2}\right)s^{2r} \quad , \quad B_k^{\infty} = \sum_{r=k}^{\infty}\left(\frac{2^{2r}(r!)^2}{(2r+1)!}\right)s^{2r+1} \quad \text{(B.35)}$$

with $K_0(z)$, $K_1(z)$ being modified Bessel functions of complex argument and $\mathbf{L}_0(z)$, $\mathbf{L}_1(z)$ being modified Struve functions of complex argument. When s falls in the uniformly convergent region $\mid \mathrm{Re}[s] \mid < 1$ the two series (B.35) converge to the values

$$A_0^{\infty} = \frac{1}{\sqrt{1-s^2}} \quad , \quad B_0^{\infty} = \frac{\sin^{-1}s}{\sqrt{1-s^2}} \quad . \tag{B.36}$$

Note that $\sin^{-1}s$ is a multivalued function differing from the principle value by multiplicity $2n\pi$ and having branch cuts defined by $|\,\mathrm{Re}[s]\,| \geq 1$. This multiplicity then defines the value of the residue contribution given in (B.30) and (B.31). Thus, depending on which region of the complex plane τ_e (and thus s) lies, the arbitrary constant C determining this contribution will be $C \in (0,2)$. The regions in the normalized complex τ_e/k_e plane indicating the appropriate value of C are shown in figure B.5 and are defined by the conditions

$$C = \begin{cases} 2\ , & \mathrm{Im}[\tau_e^2] < \mathrm{Im}[U_{eB}^2]\ ;\ \angle\tau_e > \angle U_{eB} \\ 0\ , & \text{otherwise} \end{cases} \quad . \tag{B.37}$$

The condition that $\angle\tau_e > \angle U_{eB}$ defines the branch cut $|\,\mathrm{Re}[s]\,| > 1$ when $U_{eB} > \tau_e$ and the condition $\mathrm{Im}[\tau_e^2] < \mathrm{Im}[U_{eB}^2]$ defines the branch cut where the pole k_{xB} crosses the negative real axis in the complex k_x plane. Other formulations have been presented in the literature for the evaluation of $\mathbf{G}(\tau_e,\bar{\rho})$ [Chang3, Olsen5, Kuester4], but have not directly identified the pole contribution as done in (B.31).

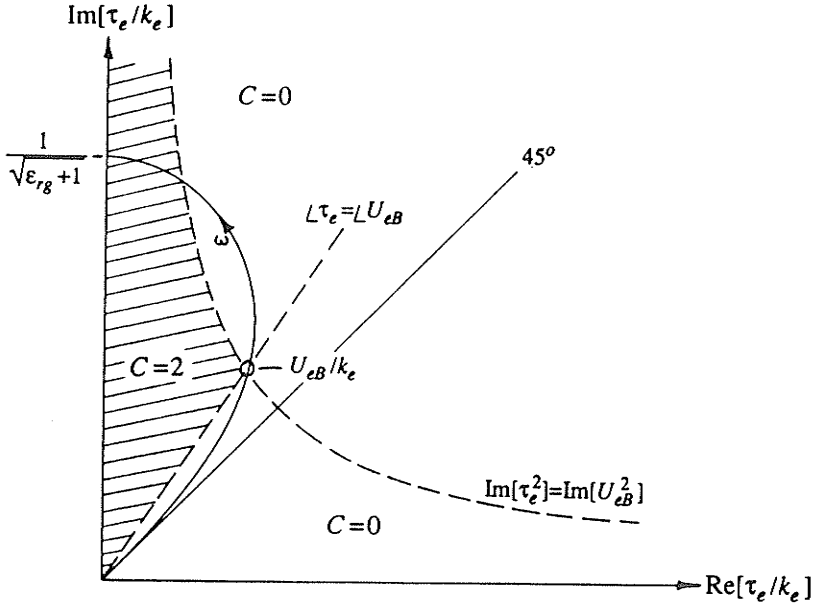

Figure B.5: Value of the constant C as a function of τ_e/k_e for determining the surface wave pole contribution.

For the special case $x=0$, as is only required when matching the fields for single conductor systems, the solution to the integral $\mathbf{G}_0$ becomes

$$\mathbf{G}_0(\tau_e,\bar{\rho}) = \frac{2n^2}{n^4-1}\left[K_0(\tau_e 2h) + se^{-s\tau_e 2h}\int_{\tau_e 2h}^{\infty} e^{st}K_0(t)\,dt + C\,\mathbf{G}_p\right] \tag{B.38}$$

where $\bar{\rho}=2h\hat{y}$ and h is the height of the conductor above the earth, and $\mathbf{G}_p$ is the pole contribution given in (B.22). For the small argument range of $|\tau_e\bar{\rho}|$, the first term of (B.31) is adequate for the evaluation of $\mathbf{G}(\tau_e,\bar{\rho})$ as long as τ_e does not fall near the pole singularity U_{eB}. The validity and convergence of the series solution (B.31) has been examined by comparison to the results generated by numerical integration [Bridges2]. Only in the very large argument range, where the function decays exponentially, is the given expression not adequate due to slow convergence of the series in (B.34). However, accurate asymptotic techniques can alternatively be used in this range.

B.1.4. Small Argument Evaluation of G

The small argument behavior of the integral $\mathbf{G}(\tau_e,\bar{\rho})$ will be determined since it allows a much simpler formulation and is adequate at low frequencies. The integrand of (B.19) can be written in the form

$$\frac{1}{n^2U_e+U_g}=\left[\frac{2}{n^2+1}\right]\frac{1}{2U_e}\left[\frac{1+R}{1+\chi R}\right],\ R=\frac{U_e-U_g}{U_e+U_g},\ \chi=\frac{n^2-1}{n^2+1} \tag{B.39}$$

If $|R|<1$ and $|\chi|<1$, the denominator of (B.39) can be expressed in a binomial expansion and then formed in terms of powers of R as

$$\frac{1}{n^2U_e+U_g}=\left[\frac{2}{n^2+1}\right]\frac{1}{2U_e}\left\{1-\left[\chi-1\right]R+\left[\chi(\chi-1)\right]R^2-\cdots\right\} \tag{B.40}$$

The first order approximation, which was employed by Perel'man [Perelman], can be recognized in terms of the modified Bessel function $K_0(z)$ as

$$\mathbf{G}(\tau_e,\bar{\rho})\approx\frac{2}{n^2+1}K_0(\tau_e|\bar{\rho}|) \tag{B.41}$$

The second order approximation can be identified as containing the integral function $\mathbf{J}(\tau_e,\bar{\rho})$ as

$$\mathbf{G}(\tau_e,\bar{\rho})\approx\frac{2}{n^2+1}\left[\frac{n^2-1}{n^2+1}K_0(\tau_e|\bar{\rho}|)+\frac{2}{n^2+1}\mathbf{J}(\tau_e,\bar{\rho})\right] \tag{B.42}$$

The higher order approximations to $\mathbf{G}(\tau_e,\bar{\rho})$ are not recognized with available functions and involve evaluating integrals containing the kernels $1/U_g$, U_g, U_g^3,... etc. A study of the validity of the small argument approximations (B.41,B.42) is available in the literature [Bridges1].

B.2. FAR FIELD APPROXIMATIONS

In the far field region, The Fourier integrals presented in (B.1,B.4,B.19) can be evaluated using the method of steepest descent. These integrals are of the form

$$F(x,y,z) = \frac{1}{2\pi}\int_{-\infty}^{\infty}\frac{1}{2\pi}\int_{-\infty}^{\infty} f(k_x,k_z)e^{-U_i|y|+jk_x x+jk_z z}\,dk_x\,dk_z \tag{B.43}$$

$$U_i = \sqrt{k_x^2+k_z^2-k_i^2} = \sqrt{k_x^2+\tau_i^2} \quad ; \mathrm{Re}[U_i]\geq 0$$

$$\tau_i = \sqrt{k_z^2-k_i^2} \quad ; \mathrm{Re}[\tau_i]\geq 0$$

$$|\bar{\rho}| = \sqrt{x^2+y^2} \quad , \quad \phi = \angle\bar{\rho} = \tan^{-1}(y/x)$$

$$|\bar{R}| = \sqrt{\rho^2+z^2} = \sqrt{x^2+y^2+z^2} \quad , \quad \gamma = \tan^{-1}(|\bar{\rho}|/z)$$

Each of the integrals in (B.43) can be evaluated individually under the far field condition $|\tau_i\bar{\rho}| \gg 1$ or $|k_i\bar{R}| \gg 1$, in terms of integrals of the general form

$$H(x,y) = \int_{-\infty}^{\infty} h(\lambda)e^{\Phi(\lambda)}d\lambda \tag{B.44}$$

$$\Phi(\lambda) = -\sqrt{\lambda^2+\kappa^2}\,|y| + j\lambda x = -\sqrt{\lambda^2+\kappa^2}\,\rho\sin\phi + j\lambda\rho\cos\phi$$

where $\rho \equiv |\bar{\rho}|$ is assumed. In order to evaluate (B.44) by the saddle point method [Collin], it is convenient to use a transformation of the variable of integration such that

$$\lambda = +j\kappa\sin\Psi \quad <--> \quad \Psi = -j\sinh^{-1}(\lambda/\kappa) = \sigma + j\eta$$

$$\Phi(\Psi) = -\kappa\rho\sin(\Psi+\phi) \tag{B.45}$$

$$= +j(j\kappa\rho)\left[\cos(\sigma+\phi-\frac{\pi}{2})\cosh\eta - j\sin(\sigma+\phi-\frac{\pi}{2})\sinh\eta\right]$$

The transformation allows *both* Riemann sheets in the complex λ plane to be mapped onto adjoining strips in the complex Ψ plane as shown in figure B.6. The proper Riemann sheet $\mathrm{Re}[\sqrt{\lambda^2+\kappa^2}]>0$ is shaded, with the improper Riemann sheet $\mathrm{Re}[\sqrt{\lambda^2+\kappa^2}]<0$ left unshaded. The four quadrants in the complex λ plane are appropriately labeled in the Ψ plane (the quadrant axes are rotated by the angle $\angle(j\kappa)$ from the λ coordinates, this angle approaching zero for lossless media). Noting that the integration contour C can be deformed to any alternate path, as long as poles or branch cuts are not crossed, the most desirable path would be one where the imaginary part of Φ remains constant, and the real part increases as rapidly as possible. The path of steepest descent is thus chosen by specifying

$$\mathrm{Im}[\Phi(\lambda)] = \mathrm{Im}[\Phi(\lambda_S)] = \mathrm{Im}[\Phi(\Psi_S)] = \text{constant}$$

$$\left.\frac{\partial}{\partial\lambda}\Phi(\lambda)\right]_{\lambda=\lambda_s} = \left.\frac{\partial}{\partial\Psi}\Phi(\Psi)\right]_{\Psi=\Psi_s} = 0 \quad \rightarrow \quad \begin{cases} \lambda_S = +j\tau\cos\phi \\ \Psi_S = \dfrac{\pi}{2} - \phi \end{cases} \tag{B.46}$$

where λ_S, Ψ_S define the stationary points (saddle points) in the respective complex planes. The steepest descent paths can be found from (B.45,B.46) by satisfying $\sin(\sigma+\phi)\cosh\eta = +1$.

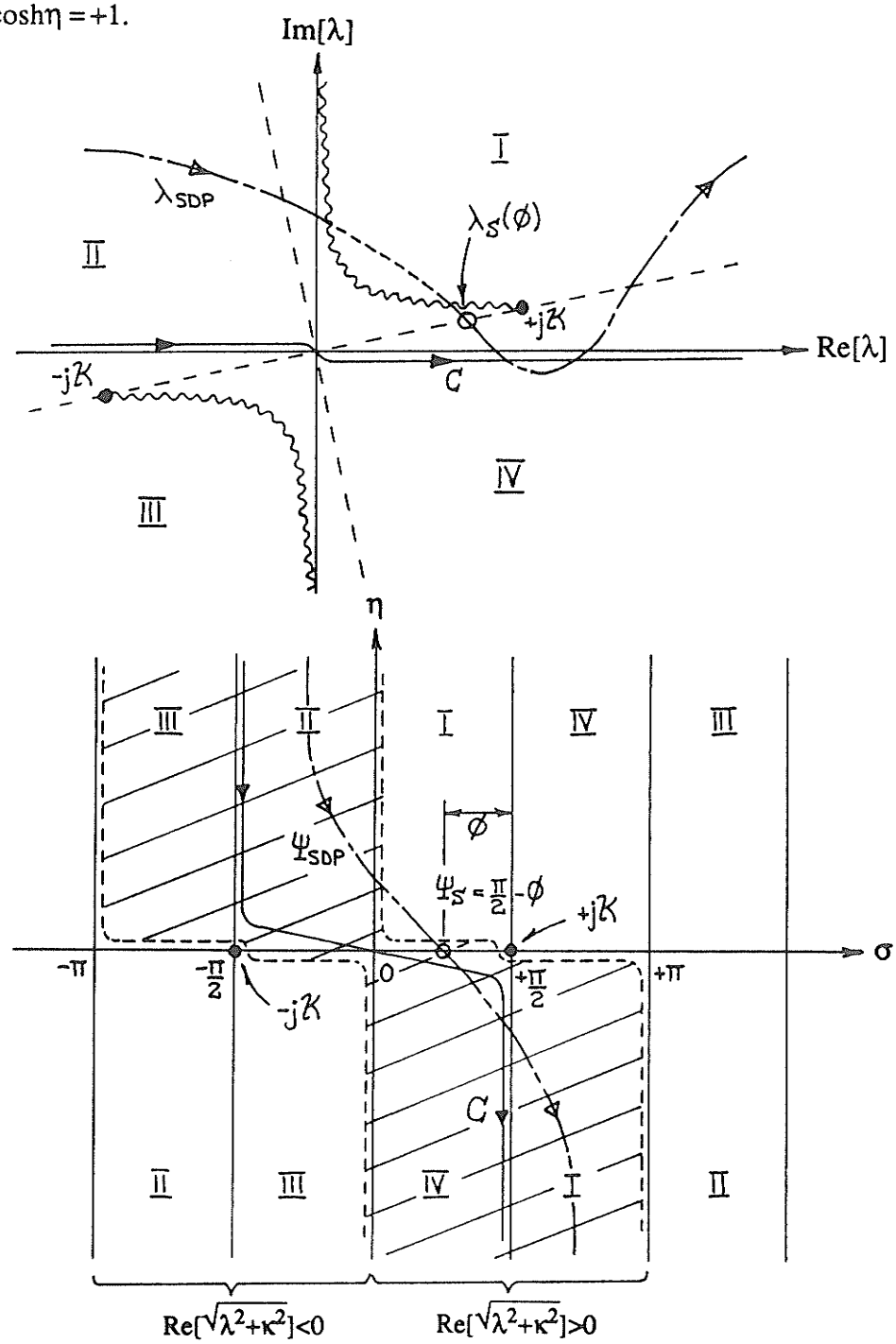

Figure B.6: Steepest descent paths in the complex λ and Ψ planes.

In the far field, the major contribution to the integration along the steepest descent path comes from the neighbourhoud of the saddle point, since at this point the real part of $\Phi(\lambda_S)$ is at a minimum. To determine the contribution from the saddle point region, both the exponent and the kernel $h(\lambda)$ in (B.44) are expanded in a Taylor series about the saddle point, noting that $\Phi'(\lambda_S)=0$ from (B.46), as

$$\Phi(\lambda) = \Phi(\lambda_S) + \Phi''(\lambda_S)(\lambda-\lambda_S)^2/2 + \cdots$$

$$h(\lambda) = \sum_{m=0}^{\infty} \frac{(\lambda-\lambda_S)^m}{m!} \frac{\partial^m}{\partial\lambda^m} h(\lambda) \Bigg]_{\lambda=\lambda_S} \tag{B.47}$$

A first order approximation to the integral (B.44) can then be derived by using the first two terms in (B.47) for the exponent. After bringing the summation outside the integral as

$$H(x,y) = e^{\Phi(\lambda_S)} \sum_{m=0}^{\infty} \frac{1}{m!} \frac{\partial^m}{\partial\lambda^m} h(\lambda) \Bigg]_{\lambda=\lambda_S} \int_{-\infty}^{\infty} (\lambda-\lambda_S)^m e^{\Phi''(\lambda_S)(\lambda-\lambda_S)^2/2}\, d\lambda \tag{B.48}$$

and utilizing an appropriate substitution, the integral term can be transformed into a recognizable form as

$$\int_{-\infty}^{\infty} (\lambda-\lambda_S)^m e^{\Phi''(\lambda_S)(\lambda-\lambda_S)^2/2}\, d\lambda = \left[-\Phi''(\lambda_S)\right]^{-\left(\frac{m+1}{2}\right)} \int_{-\infty}^{\infty} t^m e^{-t^2/2}\, dt \tag{B.49}$$

The kernel of (B.49) is an odd function and thus only the even terms contribute to (B.48), which can then be evaluated in terms of error functions [Abramowitz]. After substitution of λ_S the saddle point contribution is given as

$$H(x,y) = \left\{ h(\lambda_S) + \sum_{m=1}^{\infty} \frac{1}{2^m m!} \left[\frac{\kappa}{\rho}\sin^2\phi\right]^m \frac{\partial^{2m}}{\partial\lambda^{2m}} h(\lambda) \Bigg]_{\lambda=\lambda_S} \right\} \sqrt{\frac{2\pi\kappa}{\rho}} \sin\phi e^{-\kappa\rho} \tag{B.50}$$

with the first term approximation to (B.50) given as

$$H(x,y) = h(\lambda_S) \sqrt{\frac{2\pi\kappa}{\rho}} \sin\phi e^{-\kappa\rho} \tag{B.51}$$

Using the method of steepest descent, integrals of the type (B.43) can now be evaluated in two steps, under the conditions $|\tau_i \bar{\rho}| \gg 1$, $|k_i \bar{R}| \gg 1$, using the form (B.51) as

$$F(x,y,z) = \frac{1}{2\pi} \int_{-\infty}^{\infty} f(k_{xS}, k_z) \sqrt{\frac{\tau_i \sin^2\phi}{2\pi|\bar{\rho}|}} e^{-\sqrt{k_z^2-k_i^2}\,|\bar{\rho}| + jk_z z} dk_z$$

$$= f(k_{xS}, k_{zS}) \frac{+jk_i \sin\phi\sin\gamma}{2\pi|\bar{R}|} e^{+jk_i|\bar{R}|} \tag{B.52}$$

$$k_{zS} = +k_i \cos\gamma$$

$$k_{xS} = +j\tau_i \cos\phi \Big]_{k_z=k_{zS}} = +k_i \sin\gamma\cos\phi$$

For the special case of considering only the primary contribution to the Green's function (a solution of the homogeneous space wave equation $(\nabla^2+k_i^2)F=+\delta(\bar{r})$) the kernel in (B.43) is defined as

$$f(k_x,y,k_z) = f(k_x,k_z)e^{-U_i|y|} = -\frac{e^{-U_i|y|}}{2U_i} = -\frac{e^{-\sqrt{k_x^2+k_z^2-k_i^2}\,|y|}}{2\sqrt{k_x^2+k_z^2-k_i^2}} \quad \text{(B.53)}$$

The homogeneous space Green's function can then be derived through (B.52) as

$$F(x,y,z) = -\frac{e^{+jk_i|\bar{R}|}}{4\pi|\bar{R}|} \quad \text{(B.54)}$$

In the steepest descent evaluation of integrals of the type (B.43), only the saddle point contribution has been considered. In the general case of more complex media, such as layered or cylindrical geometries, the integrand may contain branch cuts as well as poles in the complex plane of integration. In deforming the integration contour to the steepest descent path, these branch cuts or poles (including the poles on any improper Riemann sheet) may be crossed, and their contribution to the integral must also be included. These situations and their method of solution are discussed in many sources for various geometry types [Felsen, Collin, Tamir1].

B.2.1. Steepest Descent Evaluation of J and G

When studying high frequency interaction with transmission lines, the steepest descent technique can be employed to determine the coupling between conductors as well as the radiated fields. The technique is appropriate when the electrical distances considered are large and interaction at grazing angles of incidence is not required. This technique has been used to determine the discrete modes supported by a wire above a lossy earth [Chiba], the radiated fields of a transmission line excited by a delta function source [Olsen4, Carpentier3], and the fields of corona discharge sources along conductors [Olsen8]. The integrals $\mathbf{J}(\tau_e,\bar{\rho})$ and $\mathbf{G}(\tau_e,\bar{\rho})$ in (B.4) and (B.19) can be evaluated in the far field $|\tau_e\bar{\rho}| \gg 1$, by appropriately specifying the kernel $h(\lambda)$ in (B.44). Expressions based on the first two terms of (B.50) are given as

$$\mathbf{J}(\tau_e,\bar{\rho}) \approx \left\{ h_J(\lambda_S) + \frac{\tau_e}{2|\bar{\rho}|}\sin^2\phi\,\frac{\partial^2}{\partial\lambda^2}h_J(\lambda)\Big]_{\lambda=\lambda_S} \right\} \left[\frac{2\pi\tau_e}{|\bar{\rho}|}\right]^{1/2} \sin\phi\, e^{-\tau_e|\bar{\rho}|} \quad \text{(B.55)}$$

$$\mathbf{G}(\tau_e,\bar{\rho}) \approx \left\{ h_G(\lambda_S) + \frac{\tau_e}{2|\bar{\rho}|}\sin^2\phi\,\frac{\partial^2}{\partial\lambda^2}h_G(\lambda)\Big]_{\lambda=\lambda_S} \right\} \left[\frac{2\pi\tau_e}{|\bar{\rho}|}\right]^{1/2} \sin\phi\, e^{-\tau_e|\bar{\rho}|} \quad \text{(B.56)}$$

$$h_J(\lambda_S) = \frac{1}{\tau_e \sin\phi + \sqrt{\tau_e^2 \sin^2\phi + (k_e^2 - k_g^2)}}$$

$$h_G(\lambda_S) = \frac{1}{n^2\tau_e \sin\phi + \sqrt{\tau_e^2 \sin^2\phi + (k_e^2 - k_g^2)}}$$

$$\frac{\partial^2}{\partial\lambda^2} h_J(\lambda)\Big]_{\lambda=\lambda_S} = -h_J(\lambda_s)\chi\left[1 + \tau_e^2\cos^2\phi\,\chi^2 a\right]$$

$$\frac{\partial^2}{\partial\lambda^2} h_G(\lambda)\Big]_{\lambda=\lambda_S} = -h_G^2(\lambda_s)\chi\left[b + \tau_e^2\cos^2\phi\,\chi[\,2b^2 h_G(\lambda_s) + \chi c\,]\right]$$

$$\chi = \frac{1}{\tau_e \sin\phi\sqrt{\tau_e^2 \sin^2\phi + (k_e^2 - k_g^2)}}$$

$$a = 2\tau_e^2 \sin^2\phi + (k_e^2 - k_g^2)$$

$$b = \tau_e \sin\phi + n^2\left[\tau_e^2 \sin^2\phi + (k_e^2 - k_g^2)\right]^{1/2}$$

$$c = \tau_e^3 \sin^3\phi + n^2\left[\tau_e^2 \sin^2\phi + (k_e^2 - k_g^2)\right]^{3/2}$$

The first term approximations, also found in the literature [Chiba], are given as

$$\mathbf{J}(\tau_e, \bar{\rho}) \approx \left[\tau_e \sin\phi + \sqrt{\tau_e^2 \sin^2\phi + (k_e^2 - k_g^2)}\right]^{-1} \left(\frac{2\pi\tau_e}{|\bar{\rho}|}\right)^{1/2} \sin\phi\, e^{-\tau_e |\bar{\rho}|} \qquad \text{(B.57)}$$

$$\mathbf{G}(\tau_e, \bar{\rho}) \approx \left[n^2\tau_e \sin\phi + \sqrt{\tau_e^2 \sin^2\phi + (k_e^2 - k_g^2)}\right]^{-1} \left(\frac{2\pi\tau_e}{|\bar{\rho}|}\right)^{1/2} \sin\phi\, e^{-\tau_e |\bar{\rho}|} \qquad \text{(B.58)}$$

Referring to figures B.3 and B.4 and as discussed in detail in sections 3.3.4 and 3.4.2, the steepest descent paths for the functions **J** and **G** may cross the branch cut $\mathrm{Re}[U_g] \geq 0$ near grazing angles $\phi \rightarrow 0^o$. This branch cut gives the lateral wave contribution to the fields in the region near the interface. At low frequencies the branch point occurs near k_g and thus the contribution is very small when the interface acts as a good conductor ($\sigma_g/\omega\varepsilon_e \gg 1$). As well, the integral **G** possesses a pole at k_{xB} which may also be crossed near grazing angles $\phi \rightarrow 0^o$, this yielding the TM surface wave contribution to the fields. The contributions from both these sources must be incorporated for accurate results in the general case.

B.3. NUMERICAL EVALUATION OF THE FOURIER INTEGRALS

In this section, the numerical evaluation of the Fourier type integrals (B.1) encountered in layered media problems are discussed. Several different techniques have been proposed in the literature. The solution of the integrals required for the solution of dipole sources embedded in microstrip and related geometries has been

solved by direct real-axis integration of the double infinite integrals [Pozar, Burke, Jackson1] as well as through the real-axis integration of the associated Bessel function transform of these [Mosig, Rana, Jackson2]. Various difficulties are encountered in their evaluation, however, one problem being that when the geometry is assumed lossless, the surface wave poles fall on the paths of integration. In the latter case, the problem has been handled by extracting the pole singularities through a folding around the pole technique [Gardiol, Jackson3]. By using a direct integration along the real-axis problems can also arise in the large argument (far field) evaluation of the integrals since the integrands become highly oscillatory. For the case of a dipole source over a lossy half-space, a solution to this has been obtained by deforming the real-axis contour to the steepest descent path [RahmatSamii, Parhami1]. However, even though this produces a very fast converging integral, the possible inclusion of any pole or branch cut contributions, which are crossed during the path deformation, must be constantly monitored. A review of these techniques is given by Michalski [Michalski] along with an alternative integration scheme, also based on a steepest descent path approach.

The method of integration presented in this section is based on a real-axis numerical integration, where the integrand is weighted by an analytically integratable function which damps the oscillation of the integrand. In the non-oscillatory region of the integrand, a segmented Gaussian-quadrature technique is employed where the segmentation is based on a logarithmic scale. In the oscillatory region of the integrand a second order integration is performed, where an exponential weighting proportional to the steepest descent phase variation is directly incorporated. The technique used for the oscillatory region reduces the phase variation of the integrand and thus allows the integrals to be easily evaluated numerically, even in the far field region.

Consider the evaluation of integrals of the general form presented in (B.1), which can be formulated as

$$
\begin{aligned}
F(x,y,z) &= \frac{1}{2\pi}\int_{-\infty}^{\infty}\frac{1}{2\pi}\int_{-\infty}^{\infty} f(k_x,k_z)\,e^{-\sqrt{k_x^2+k_z^2-k_i^2}\,|y|+jk_x x+jk_z z}\,dk_x\,dk_z \\
&= \frac{1}{2\pi}\int_{-\infty}^{\infty}\frac{1}{2\pi}\int_{-\infty}^{\infty} f(k_x,k_z)\,e^{-\sqrt{k_x^2+\tau_i^2}\,|y|+jk_x x}\,dk_x\,e^{+jk_z z}\,dk_z \\
&= \frac{1}{2\pi}\int_{-\infty}^{\infty}\left[f(x,y,k_z)\,e^{+\tau_i \rho}\right]e^{-\sqrt{k_z^2-k_i^2}\,\rho+jk_z z}\,dk_z
\end{aligned}
\qquad \text{(B.59)}
$$

$$
\begin{aligned}
\tau_i &= \sqrt{k_z^2-k_i^2} \\
\rho &= \sqrt{x^2+y^2} \quad , \quad \phi = \tan^{-1}(|y|/x) \\
R &= \sqrt{x^2+y^2+z^2} \quad , \quad \gamma = \tan^{-1}(\rho/z)
\end{aligned}
$$

where the integrands become highly oscillatory for $|k_i y|$, $|k_i x|$, or $|k_i z| \gg 1$.

In section B.2, it was shown that both the infinite integrals in (B.59), one with respect to k_x and one with respect to k_z, can be evaluated in the form

$$H(x,y) = \int_{-\infty}^{\infty} h(\lambda) e^{-\sqrt{\lambda^2+\tau^2}\,|\,y\,|\,+j\lambda x} d\lambda = \int_{-\infty}^{\infty} h(\lambda) e^{\Phi(\lambda)} d\lambda \tag{B.60}$$

Examination of the exponential term in (B.60) shows that their are four possible regions of behaviour of the integrand. These are shown in figure B.7 by plotting the terms $\sqrt{\lambda^2+\tau^2}\,|\,y\,|$ and $j\,|\,\lambda x\,|$ in the complex plane as a function of λ. The path of integration $-\infty < \lambda < +\infty$ will be segmented into these four regions, with a different integral form used for each region.

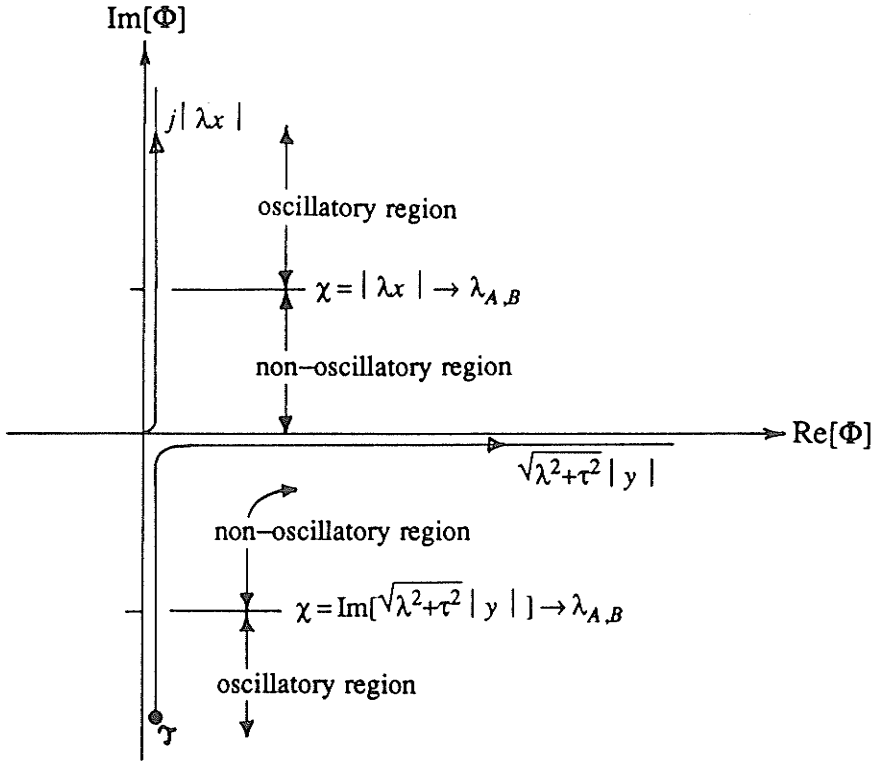

Figure B.7: Four possible oscillatory/non-oscillatory regions of $\Phi(\lambda)$.

The four possible regions depend on the magnitude of the arguments $|\,\tau y\,|$ and $|\,\tau x\,|$ and are defined by the conditions:

1. For $|\,\mathrm{Im}[\sqrt{\lambda^2+\tau^2}\,y]\,| \le \chi$, $|\,\lambda x\,| \le \chi$; the integrand is in the near field region and is evaluated directly in its present form using a gaussian-quadrature technique

$$\int_{\lambda_A}^{\lambda_B} h(\lambda) e^{-\sqrt{\lambda^2+\tau^2}\,|\,y\,|\,+j\lambda x} d\lambda \rightarrow \int_{\lambda_A}^{\lambda_B} \Big[g(\lambda) \Big] d\lambda \tag{B.61}$$

$$g(\lambda) = h(\lambda) e^{-\sqrt{\lambda^2+\tau^2}\,|\,y\,|\,+j\lambda x}$$

where $\lambda_A < \lambda < \lambda_B$ is the region along the real-axis integration path where the above conditions are satisfied. Both exponential terms are incorporated into the

function $g(\lambda)$ since they do not cause a large phase variation, with the dominant contribution to the integral in this region being the behaviour of the kernel $h(\lambda)$. Also, when $\mathrm{Re}[\sqrt{\lambda^2+\tau^2}\,y] \gg 1$, the integrand decays rapidly, this portion of the integrand contributing to the reactive part of the integral. The parameter χ is chosen usually in the range $2 \le \chi \le 10$. Further segmentation of this region, based on a logarithmic scale, is employed for numerical evaluation.

2. For $|\,\mathrm{Im}[\sqrt{\lambda^2+\tau^2}\,y]\,| \le \chi$, $|\,\lambda x\,| > \chi$; the integrand oscillates rapidly with respect to the x-dimension. In this region the integral is evaluated in the form

$$\int_{\lambda_A}^{\lambda_B} h(\lambda) e^{-\sqrt{\lambda^2+\tau^2}\,|y|+j\lambda x}\,d\lambda \;\rightarrow\; \int_{\lambda_A}^{\lambda_B} \Big[g(\lambda)\Big] e^{+j\lambda x}\,d\lambda \qquad \text{(B.62)}$$

$$g(\lambda) = h(\lambda) e^{-\sqrt{\lambda^2+\tau^2}\,|y|}$$

3. For $|\,\mathrm{Im}[\sqrt{\lambda^2+\tau^2}\,y]\,| > \chi$, $|\,\lambda x\,| \le \chi$; the integrand oscillates rapidly with respect to the y-dimension. In this region the integral is evaluated in the form

$$\int_{\lambda_A}^{\lambda_B} h(\lambda) e^{-\sqrt{\lambda^2+\tau^2}\,|y|+j\lambda x}\,d\lambda \;\rightarrow\; \int_{\lambda_A}^{\lambda_B} \Big[g(\lambda)\Big] e^{-\sqrt{\lambda^2+\tau^2}\,|y|}\,d\lambda$$

$$\rightarrow \int_{s_A}^{s_B} \left[g\left(+j\tau \sin(\cos^{-1} s)\right) \frac{-j\tau s}{\sin(\cos^{-1} s)} \right] e^{+j(j\tau|y|)s}\,ds \qquad \text{(B.63)}$$

$$g(\lambda) = h(\lambda) e^{+j\lambda x} \quad , \quad s_{A,B} = \cos\left[\sin^{-1}\frac{\lambda_{A,B}}{j\tau}\right]$$

4. For $|\,\mathrm{Im}[\sqrt{\lambda^2+\tau^2}\,y]\,| > \chi$, $|\,\lambda x\,| > \chi$; the integrand oscillates rapidly with respect to both the x- and y-dimensions. In this region the integral is evaluated in the form

$$\int_{\lambda_A}^{\lambda_B} h(\lambda) e^{-\sqrt{\lambda^2+\tau^2}\,|y|+j\lambda x}\,d\lambda \;\rightarrow\; \int_{\lambda_A}^{\lambda_B} \Big[g(\lambda)\Big] e^{-\sqrt{\lambda^2+\tau^2}\,|y|+j\lambda x}\,d\lambda$$

$$\rightarrow \int_{s_A}^{s_B} \left[g\left(+j\tau \sin(\sin^{-1} s - \phi)\right) \frac{+j\tau \cos(\sin^{-1} s - \phi)}{\cos(\sin^{-1} s)} \right] e^{+j(j\tau\rho)s}\,ds \qquad \text{(B.64)}$$

$$g(\lambda) = h(\lambda) \quad , \quad s_{A,B} = \sin\left[\sin^{-1}\frac{\lambda_{A,B}}{j\tau} + \phi\right]$$

$$\rho = \sqrt{x^2+y^2} \quad , \quad \phi = \tan^{-1}(y/x)$$

The transforms used in regions 2-4 are obtained by multiplying the kernel $h(\lambda)$ by the phase variation of the steepest descent contribution, so that in the new kernels $g(\lambda)$, the phase variation will be minimal. The integral forms given for regions 2,3 are

special cases of the more general form given for region 4. They can be obtained from the transform for region 4 under the limits $\phi \to 0$ and $\phi \to \pi/2$, respectively. Note that the integration does not necessarily pass through all four possible regions.

Each of the integrals (B.61,B.62,B.63,B.64) in the four regions require the evaluation of integrals of the form

$$\mathbf{I} = \int_{\pm s_A}^{\pm s_B} z(s) e^{+j\alpha s} ds = \sum_{n=1}^{N} \mathbf{I}_n = \sum_{n=1}^{N} \int_{s_n}^{s_{n+1}} z(s) e^{+j\alpha s} ds + \int_{-s_{n+1}}^{-s_n} z(s) e^{+j\alpha s} ds \qquad \text{(B.65)}$$

where each region $s_A \to s_B$ (or $\lambda_A \to \lambda_B$) has been divided into N appropriate subregions $\sum(s_n \to s_{n+1})$. Since the conditions defining each region are symmetric for $\pm\lambda$, there are two contributions to the integrals in (B.65), one for $-s_{n+1} < s < -s_n$ and one for $s_n < s < s_{n+1}$. For the case of region 1, the exponential weighting is ignored with $\alpha=0$.

B.3.1. Analytical Evaluation of the Subregion $\mathbf{I}_n$

Each subregion of the integral (B.65) requires the evaluation of integrals of the form

$$\mathbf{I}_n = \int_{\bar{s}-\Delta}^{\bar{s}+\Delta} [\, z(s) e^{+j\alpha s} + z(-s) e^{-j\alpha s} \,] ds \qquad \text{(B.66)}$$

$$\bar{s} = \frac{s_{n+1} + s_n}{2} \quad , \quad \Delta = \frac{s_{n+1} - s_n}{2}$$

For the special case $\alpha=0$, the integral will be evaluated using a gaussian-quadrature formula [Press]. For the case $\alpha \neq 0$, the kernel $z(s)$ will be approximated by a second order polynomial and integrated with the required exponential weighting function. A gaussian-quadrature formula, also weighted by an exponential function could alternatively be used as a more advanced technique. Thus, the kernel in (B.66) will be approximated as

$$z(s) = a^{\pm}(s \mp \bar{s})^2 + b^{\pm}(s \mp \bar{s}) + c^{\pm} \qquad \text{(B.67)}$$

where the $\pm$ signs indicate the range $z(+s)$ and $z(-s)$, respectively. Performing the integration of (B.66) with the approximation (B.67) then yields

$$\begin{aligned} \mathbf{I}_n = \Big[& A(\alpha,\Delta) \left(a^{+} e^{+j\alpha\bar{s}} + a^{-} e^{-j\alpha\bar{s}} \right) \\ & + jB(\alpha,\Delta) \left(b^{+} e^{+j\alpha\bar{s}} - b^{-} e^{-j\alpha\bar{s}} \right) \\ & + C(\alpha,\Delta) \left(c^{+} e^{+j\alpha\bar{s}} + c^{-} e^{-j\alpha\bar{s}} \right) \Big] \end{aligned} \qquad \text{(B.68)}$$

$$a^{\pm} = \frac{z(\pm(\bar{s}+\Delta)) - 2z(\pm\bar{s}) + z(\pm(\bar{s}-\Delta))}{2}$$

$$b^{\pm} = \frac{z(\pm(\bar{s}+\Delta)) - z(\pm(\bar{s}-\Delta))}{2}$$

$$c^{\pm} = z(\bar{s})$$

$$A(\alpha,\Delta) = \frac{2}{\alpha}\sin\alpha\Delta$$

$$B(\alpha,\Delta) = \frac{2}{\alpha}\left(\frac{1}{\alpha\Delta}\sin\alpha\Delta - \cos\alpha\Delta\right)$$

$$C(\alpha,\Delta) = \frac{2}{\alpha}\left(\sin\alpha\Delta + \frac{2}{\alpha\Delta}\cos\alpha\Delta - \frac{2}{\alpha^2\Delta^2}\sin\alpha\Delta\right)$$

For the special case that $z(s)$ is an even function $z(+s)=+z(-s)$, then $a=a^{+}=a^{-}$, $b=b^{+}=b^{-}$, $c=c^{+}=c^{-}$, and

$$\mathbf{I}_n = 2\left[A(\alpha,\Delta)a\cos\alpha\bar{s} - B(\alpha,\Delta)b\sin\alpha\bar{s} + C(\alpha,\Delta)c\cos\alpha\bar{s}\right] \tag{B.69}$$

Similarly, for the special case that $z(s)$ is an odd function $z(+s)=-z(-s)$, then $a=a^{+}=-a^{-}$, $b=b^{+}=-b^{-}$, $c=c^{+}=-c^{-}$, and

$$\mathbf{I}_n = 2j\left[A(\alpha,\Delta)a\sin\alpha\bar{s} + B(\alpha,\Delta)b\cos\alpha\bar{s} + C(\alpha,\Delta)c\sin\alpha\bar{s}\right] \tag{B.70}$$

Appendix C
Axial Power Flow Calculation for Guided Wave Structures

In this appendix, the axially directed power for the discrete modes supported by a conducting strip located above a lossy half-space is derived. As shown in figure C.1, the guiding structure consists of an infinitely thin, perfectly conducting strip of width w oriented horizontally above a single planar interface and located at $(x=0, y=y')$. The upper half-space $y>0$ is considered to be free space, characterized by a permittivity ε_e and a permeability μ_e. The lower half-space $y<0$ is designated as the lossy medium, characterized by a permittivity ε_g, a permeability μ_g, and a conductivity σ_g. The current on the strip is assumed to have a specified axially directed current distribution of the form

$$\overline{J}^p(x,y,z) = \begin{cases} J_z^p(x)\delta(y-y')e^{+jk_z^p z}\hat{z} & ; -w/2 < x < +w/2 \\ 0 & ; x<-w/2\ ,\ x>+w/2 \end{cases} \tag{C.1}$$

where k_z^p is the axial propagation constant of one of the possible guided wave modes, and $J_z^p(x)$ is the corresponding current distribution for that mode. The current and the resulting fields for all the discrete modes have an exponential axial variation of this form. The formulation presented here is similar to the method used to determine the axially directed power for microstrip structures, where Jansen [Jansen2] presented closed form resulted for the shielded case and Hashimoto [Hashimoto] developed formulations for the unbounded case.

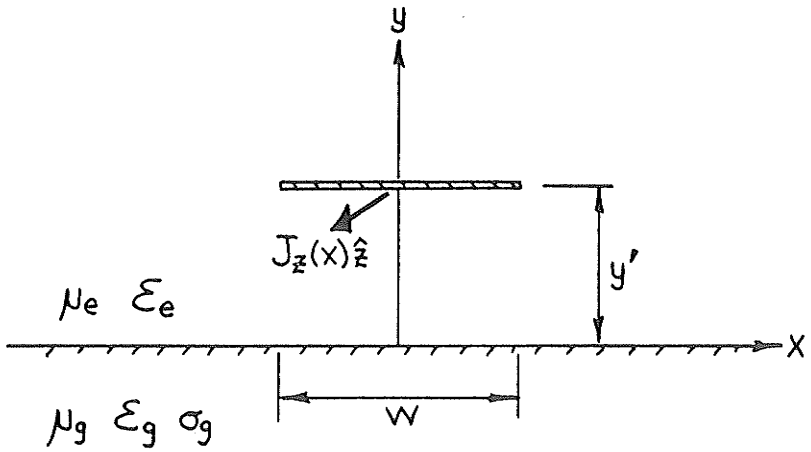

Figure C.1: Infinitely thin conducting strip located over a lossy half-space.

As discussed in section 4.5, the axially directed power for the pth mode can be evaluated as an integration of the $\hat{z}$ component of the Poynting vector in the upper and lower half-spaces as

$$P_p = \left[\int_{0}^{\infty}\int_{-\infty}^{\infty} [\overline{E}^e(\overline{\rho})\times\overline{H}^{e^*}(\overline{\rho})]\cdot\hat{z}\, dxdy + \int_{-\infty}^{0}\int_{-\infty}^{\infty} [\overline{E}^g(\overline{\rho})\times\overline{H}^{g^*}(\overline{\rho})]\cdot\hat{z}\, dxdy \right]_{k_z=k_z^p} \tag{C.2}$$

where $\overline{E}^e$, $\overline{H}^e$ and $\overline{E}^g$, $\overline{H}^g$ are the fields in the air and ground media, respectively, due to the strip current. As also discussed in 4.5 (4.49), this formulation can be easily modified to handle an arbitrary number of planar layers, such as in microstrip for example. The required field components in each region can be derived as a weighted integration of the fields from an elementary delta function line source as

$$\begin{aligned} E^i_\alpha / H^i_\alpha(x,y,k_z^p) &= \int_{-w/2}^{+w/2} J_z^p(x')\frac{1}{2\pi}\int_{-\infty}^{\infty} G_{\alpha z}^{ie(e/m)}(k_x,y,y',k_z^p)e^{+jk_x(x-x')}dk_x\, dx' \\ &= \frac{1}{2\pi}\int_{-\infty}^{\infty} j_z^p(k_x)G_{\alpha z}^{ie(e/m)}(k_x,y,y',k_z^p)e^{+jk_x x}dk_x \\ &= \frac{1}{2\pi}\int_{-\infty}^{\infty} e^i_\alpha / h^i_\alpha(k_x,y,k_z^p)\, e^{+jk_x x}dk_x \qquad ;\ \alpha \in x,y,z \end{aligned} \tag{C.3}$$

$$j_z^p(k_x) = \int_{-\infty}^{\infty} J_z^p(x')e^{-jk_x x'}dx' = \int_{-w/2}^{+w/2} J_z^p(x')e^{-jk_x x'}dx' \tag{C.4}$$

where e^i_α / h^i_α is the $\hat{\alpha}$ component of the spectral domain electric/magnetic field in the region i and $j_z^p(k_x)$ is the spectral domain current. Here $G_{\alpha z}^{ie(e/m)}(k_x,y,y',k_z^p)$ is the transformed Green's function giving the $\hat{\alpha}$ component of the electric (e) or magnetic (m) field in the region i due to the $\hat{z}$ directed line source in the region e. Finally, using (4.50), the double infinite integrals determining the power can be evaluated using the transformed field quantities given above as

$$\begin{aligned} P_p &= \frac{1}{2\pi}\int_{-\infty}^{\infty}\int_{0}^{\infty}[e_x^e(k_x)h_y^{e^*}(k_x) - e_y^e(k_x)h_x^{e^*}(k_x)]dy\, dk_x \\ &+ \frac{1}{2\pi}\int_{-\infty}^{\infty}\int_{-\infty}^{0}[e_x^g(k_x)h_y^{g^*}(k_x) - e_y^g(k_x)h_x^{g^*}(k_x)]dy\, dk_x \end{aligned} \tag{C.5}$$

The Green's functions $G_{\alpha z}^{ie(e/m)}(k_x,y,y',k_z)\ ;\alpha\in x,y$ required for the fields in (C.5) can be deduced from the fields of a line source located above a lossy half-space as formulated in Appendix A. Using the vertical electric and magnetic scalar potential forms from appendix A (A.13-A.30), the transformed field quantities in each region due to the strip current , located at $y=y'$, are given from

$$\overline{e^i}(k_x,y,k_z) = \nabla\nabla\cdot\mathbf{V}_y^i + k_i^2\mathbf{V}_y^i + j\omega\mu_i\nabla\times\mathbf{U}_y^i$$
$$\overline{h^i}(k_x,y,k_z) = \nabla\nabla\cdot\mathbf{U}_y^i + k_i^2\mathbf{U}_y^i - j\omega\varepsilon_i'\nabla\times\mathbf{V}_y^i \qquad (C.6)$$

$$\mathbf{V}_y^e(k_x,y,k_z) = \frac{+j\omega\mu_e}{k_e^2} j_z^p(k_x)\left(\frac{+jk_z U_e}{k_x^2+k_z^2}\right)\left[\mp\frac{e^{-U_e|y-y'|}}{2U_e} + R_e\frac{e^{-U_e(y+y')}}{2U_e}\right] \qquad (C.7a)$$

$$\mathbf{U}_y^e(k_x,y,k_z) = \frac{+j\omega\mu_e}{k_e^2} j_z^p(k_x)\left(\frac{+jk_x j\omega\varepsilon_e'}{k_x^2+k_z^2}\right)\left[+\frac{e^{-U_e|y-y'|}}{2U_e} + R_m\frac{e^{-U_e(y+y')}}{2U_e}\right] \qquad (C.7b)$$

$$\mathbf{V}_y^g(k_x,y,k_z) = \frac{+j\omega\mu_e}{k_e^2} j_z^p(k_x)\left(\frac{+jk_z U_e}{k_x^2+k_z^2}\right)\left[T_e e^{-U_e y' + U_g y}\right] \qquad (C.7c)$$

$$\mathbf{U}_y^g(k_x,y,k_z) = \frac{+j\omega\mu_e}{k_e^2} j_z^p(k_x)\left(\frac{+jk_x j\omega\varepsilon_e'}{k_x^2+k_z^2}\right)\left[T_m e^{-U_e y' + U_g y}\right] \qquad (C.7d)$$

$$R_e = \frac{n^2U_e - U_g}{n^2U_e + U_g} \quad , \quad R_m = \frac{m^2U_e - U_g}{m^2U_e + U_g}$$
$$T_e = \frac{1}{n^2U_e + U_g} \quad , \quad T_m = \frac{1}{m^2U_e + U_g} \qquad n^2 = \frac{\varepsilon_g'}{\varepsilon_e'} \quad , \quad m^2 = \frac{\mu_g}{\mu_e}$$

where $\varepsilon_i' = \varepsilon_i + j\sigma_i/\omega$. Considering the upper half-space first ($i=e$), the integration with respect to y in (C.5) can be evaluated analytically as

$$e_y^e(k_x,y,k_z) = (k_x^2+k_z^2)\mathbf{V}_y^e$$
$$e_x^e(k_x,y,k_z) = (+jk_x)\frac{\partial}{\partial y}\mathbf{V}_y^e - j\omega\mu_e(+jk_z)\mathbf{U}_y^e$$
$$h_y^e(k_x,y,k_z) = (k_x^2+k_z^2)\mathbf{U}_y^e$$
$$h_x^e(k_x,y,k_z) = (+jk_x)\frac{\partial}{\partial y}\mathbf{U}_y^e + j\omega\varepsilon_e'(+jk_z)\mathbf{V}_y^e$$

$$\int_0^\infty [e_x^e h_y^{e*} - e_y^e h_x^{e*}]dy = \left\{AA^*\left(\frac{k_x^2k_z}{k_x^2+k_z^2}\right)(\omega\varepsilon_e')^*\int_0^\infty\left[U_e\frac{\partial}{\partial y}\underline{\mathbf{V}}_y^e\underline{\mathbf{U}}_y^{e*} + k_e^2\underline{\mathbf{U}}_y^e\underline{\mathbf{U}}_y^{e*}\right]dy\right.$$
$$\left. + AA^*\left(\frac{k_z}{k_x^2+k_z^{2*}}\right)(\omega\varepsilon_e')^*\int_0^\infty\left[U_e\underline{\mathbf{V}}_y^e k_x^2\frac{\partial}{\partial y}\underline{\mathbf{U}}_y^{e*} + U_e\underline{\mathbf{V}}_y^e k_z^{2*}U_e^*\underline{\mathbf{V}}_y^{e*}\right]dy\right\} \qquad (C.8)$$

$$AA^*k_z(\omega\varepsilon_e')^* = Z_0\frac{k_z}{k_e}|j_z^p(k_x)|^2$$

where $\underline{\mathbf{V}}_y$, $\underline{\mathbf{U}}_y$ are the portions of (C.7a-C.7d) in square brackets only. The axially

directed power in the upper half-space is then given as

$$P_p^e = \frac{Z_0}{2\pi}\int_{-\infty}^{\infty} |\, j_z^p(k_x)\,|^2\, \mathrm{F}_e(k_x,y',k_z^p)\,dk_x \tag{C.9}$$

$$\mathrm{F}_e(k_x,y',k_z) = \left[\frac{k_z}{k_e}\frac{1}{4U_eU_e^*}\right]\cdot$$

$$\left\{\left[\frac{k_x^2}{k_x^2+k_z^2}\right]\left[U_e^2\left[\frac{2}{U_e+U_e^*}-\frac{R_e e^{-U_e 2y'}-R_m^* e^{-U_e^* 2y'}}{U_e+U_e^*}+\frac{R_e e^{-U_e 2y'}+R_m^* e^{-U_e^* 2y'}}{U_e-U_e^*}\right]\right.\right.$$
$$+k_e^2\left[\frac{2}{U_e+U_e^*}+\frac{R_m e^{-U_e 2y'}+R_m^* e^{-U_e^* 2y'}}{U_e+U_e^*}-\frac{R_m e^{-U_e 2y'}-R_m^* e^{-U_e^* 2y'}}{U_e-U_e^*}\right]$$
$$+U_e^2\left[\frac{-1}{U_e+U_e^*}-\frac{R_e+R_m^*}{U_e-U_e^*}-\frac{R_eR_m^*}{U_e+U_e^*}\right]e^{-(U_e+U_e^*)y'}$$
$$\left.+k_e^2\left[\frac{-1}{U_e+U_e^*}+\frac{R_m-R_m^*}{U_e-U_e^*}+\frac{R_mR_m^*}{U_e+U_e^*}\right]e^{-(U_e+U_e^*)y'}\right]$$
$$+\left[\frac{U_eU_e^*}{k_x^2+k_z^{2*}}\right]\left[k_x^2\left[\frac{2}{U_e+U_e^*}-\frac{R_e e^{-U_e 2y'}-R_m^* e^{-U_e^* 2y'}}{U_e+U_e^*}-\frac{R_e e^{-U_e 2y'}+R_m^* e^{-U_e^* 2y'}}{U_e-U_e^*}\right]\right.$$
$$+k_z^{2*}\left[\frac{2}{U_e+U_e^*}-\frac{R_e e^{-U_e 2y'}+R_e^* e^{-U_e^* 2y'}}{U_e+U_e^*}-\frac{R_e e^{-U_e 2y'}-R_e^* e^{-U_e^* 2y'}}{U_e-U_e^*}\right]$$
$$+k_x^2\left[\frac{-1}{U_e+U_e^*}+\frac{R_e+R_m^*}{U_e-U_e^*}-\frac{R_eR_m^*}{U_e+U_e^*}\right]e^{-(U_e+U_e^*)y'}$$
$$\left.\left.+k_z^{2*}\left[\frac{-1}{U_e+U_e^*}+\frac{R_e-R_e^*}{U_e-U_e^*}+\frac{R_eR_e^*}{U_e+U_e^*}\right]e^{-(U_e+U_e^*)y'}\right]\right\} \tag{C.10}$$

Examination of the function $\mathrm{F}_e(k_x,y',k_z)$, shows that the four terms having no exponential factors represent the primary fields of the strip in an unbounded homogeneous medium. The eight terms with the $\exp[-U_e 2y'$ or $U_e^* 2y']$ factors represent the power due to the reflected fields in the upper half-space due to the interface. The remaining terms with the $\exp[-(U_e+U_e^*)y']$ factors represent the power in the lower half-space region which is subtracted.

Similarly, the axially directed power in the lower half-space ($i=g$), can be evaluated using

$$e_y^g(k_x,y,k_z) = (k_x^2+k_z^2)\mathbf{V}_y^g$$

$$e_x^g(k_x,y,k_z) = (+jk_x)\frac{\partial}{\partial y}\mathbf{V}_y^g - j\omega\mu_g(+jk_z)\mathbf{U}_y^g$$

$$h_y^g(k_x,y,k_z) = (k_x^2+k_z^2)\mathbf{U}_y^g$$

$$h_x^g(k_x,y,k_z) = (+jk_x)\frac{\partial}{\partial y}\mathbf{U}_y^g + j\omega\varepsilon_g'(+jk_z)\mathbf{V}_y^g$$

$$\int_0^\infty [e_x^g h_y^{g*} - e_y^g h_x^{g*}]dy = \left\{ AA^* \left(\frac{k_x^2 k_z}{k_x^2+k_z^2} \right) (\omega\varepsilon_e')^* \int_0^\infty \left[U_e \frac{\partial}{\partial y}\underline{\mathbf{V}}_y^g \underline{\mathbf{U}}_y^{g*} + m^2 k_e^2 \underline{\mathbf{U}}_y^g \underline{\mathbf{U}}_y^{g*} \right] dy \right.$$

$$\left. + AA^* \left(\frac{k_z}{k_x^2+k_z^{2*}} \right) (\omega\varepsilon_e')^* \int_0^\infty \left[U_e \underline{\mathbf{V}}_y^g k_x^2 \frac{\partial}{\partial y}\underline{\mathbf{U}}_y^{g*} + U_e \underline{\mathbf{V}}_y^g (n^2 k_z^2)^* U_e^* \underline{\mathbf{V}}_y^{g*} \right] dy \right\} \quad \text{(C.11)}$$

$$P_p^g = \frac{Z_0}{2\pi} \int_{-\infty}^{\infty} |\, j_z^p(k_x) \,|^2 \, \mathrm{F}_g(k_x,y',k_z^p) dk_x \quad \text{(C.12)}$$

$$\mathrm{F}_g(k_x,y',k_z) = \left(\frac{k_z}{k_e} \frac{e^{-(U_e+U_e^*)y'}}{U_g+U_g^*} \right) \left\{ \left(\frac{k_x^2}{k_x^2+k_z^2} \right) \left[U_e U_g T_e T_m^* + m^2 k_e^2 T_m T_m^* \right] \right.$$

$$\left. + \left(\frac{k_x^2}{k_x^2+k_z^{2*}} \right) \left[U_e U_g^* T_e T_m^* + \frac{U_e U_e^*}{k_x^2} (n^2 k_z^2)^* T_e T_e^* \right] \right\} \quad \text{(C.13)}$$

Using the power method, the characteristic impedance of the strip-half-space guided wave structure for the pth mode can be determined as

$$Z_{Cp} = \frac{P_p^e + P_p^g}{|\, I_p \,|^2} \;,\; |\, I_p \,|^2 = \int_{-w/2}^{+w/2} |\, J_z^p(x) \,|^2 dx = \frac{1}{2\pi} \int_{-\infty}^{\infty} |\, j_z^p(k_x) \,|^2 dk_x \quad \text{(C.14)}$$

$$j_z^p(k_x) = \begin{cases} I_p & \text{; for a } \delta \text{ line source} \\ I_p \dfrac{\sin(k_x w/2)}{k_x w/2} & \text{; for a constant current strip of width } w \end{cases} \quad \text{(C.15)}$$

where $j_z^p(k_x)$ has been defined in (C.15) for two common choices of current distribution. In general, the current distribution is a property of the specific mode.

C.1. SPECIAL CASES

For the special case where the lower half-space has the same material properties as the upper half space (the strip is located in a homogeneous space), the total axially directed power is given as

$$n^2 = m^2 = 1 : \quad \begin{cases} R_e = R_m = 0 \\ T_e = T_m = 1/2U_e \end{cases}$$

$$\mathrm{F}_e(k_x,y',k_z) = \frac{k_z}{k_e}\left[\frac{2}{U_e+U_e^*} - \frac{e^{-(U_e+U_e^*)y'}}{U_e+U_e^*}\right]\left[\frac{k_x^2}{4U_eU_e^*} + \frac{1}{4}\right] \tag{C.16}$$

$$\mathrm{F}_g(k_x,y',k_z) = \frac{k_z}{k_e}\left[\frac{e^{-(U_e+U_e^*)y'}}{U_e+U_e^*}\right]\left[\frac{k_x^2}{4U_eU_e^*} + \frac{1}{4}\right] \tag{C.17}$$

$$P_p^e+P_p^g = \frac{Z_0}{2\pi}\int_{-\infty}^{\infty} |\, j_z^p(k_x)\,|^2 \left[\frac{k_z^p}{k_e}\frac{2}{U_e+U_e^*}\right]\left[\frac{k_x^2}{4U_eU_e^*} + \frac{1}{4}\right]dk_x \tag{C.18}$$

When a delta function line source carrying a current I_p is considered, $j_z^p(k_x)=I_p$, the power integral will not converge since the integrand behaves as $1/k_x$ as $k_x\to\infty$. This divergent part of the integrand, representing the axial power in an unbounded homogeneous space, can be identified in the general half-space power integral (C.9) and can be extracted in this form.

Next, for the special case when the lower half-space is assumed perfectly conducting ($\sigma_g\to\infty$), the total axially directed power will be due to the power flow only in the region $y>0$ as

$$k_g\ ,\ n^2\to\infty : \quad \begin{cases} R_e = +1\ ,\ R_m = -1 \\ T_e = T_m = 0 \end{cases}$$

$$\mathrm{F}_e(k_x,y',k_z) = \frac{k_z}{k_e}\left[\frac{2-e^{-U_e2y'}-e^{-U_e^*2y'}}{U_e+U_e^*}\right]\left[\frac{k_x^2}{4U_eU_e^*} + \frac{1}{4}\right] \tag{C.19}$$

$$\mathrm{F}_g(k_x,y',k_z) = 0 \tag{C.20}$$

$$P_p^e+P_p^g = \frac{Z_0}{2\pi}\int_{-\infty}^{\infty} |\, j_z^p(k_x)\,|^2 \left[\frac{k_z^p}{k_e}\frac{2-e^{-U_e2y'}-e^{-U_e^*2y'}}{U_e+U_e^*}\right]\left[\frac{k_x^2}{4U_eU_e^*} + \frac{1}{4}\right]dk_x \tag{C.21}$$

Again considering the case of a perfectly conducting lower half-space, when there are no losses in the conducting strip the modal propagation constant will be equal to the free space value $k_z^p=k_e$. For a delta function line source carrying a current I_p, $j_z^p(k_x)=I_p$, the axially directed power is then given as

$$P_p^e + P_p^g = \frac{Z_0}{2\pi} \mid I_p \mid^2 \int_{-\infty}^{\infty} \frac{1 - e^{-\mid k_x \mid 2y'}}{2 \mid k_x \mid} dk_x$$

$$= \frac{Z_0}{2\pi} \mid I_p \mid^2 \left[\ln(2y') - \lim_{a \to 0} \ln(a) \right] \qquad \text{(C.22)}$$